

# **Investigating the role of PI3-Kinase $\alpha$ in endothelial cell rearrangements during vascular morphogenesis**

**Inauguraldissertation**

zur Erlangung der Würde eines Doktors der Philosophie

vorgelegt der

Philosophisch-Naturwissenschaftlichen Fakultät

der Universität Basel

von

Kathrin Ingeburg Gundel

aus Lebach (Saar), Deutschland

Basel, 2024

Genehmigt von der Philosophisch-Naturwissenschaftlichen Fakultät  
auf Antrag von

Prof. Dr. Markus Affolter

Prof. Dr. Susan Mango

Prof. Dr. Elke Ober

Dr. Heinz-Georg Belting

Basel, den 19.9.2023

Prof. Dr. Marcel Mayor

Dekan



*Für Hugi und Þykkja.*





## List of Abbreviations

apelinr	Apelin Receptor
AVM	arteriovenous malformation
BAC	Bacterial artificial Chromosome
BMP	Bone Morphogenic Protein
bp	base pair
cdh5	Cadherin-5 / VE-cadherin
CDS	coding sequence without introns
Cre	Causes Recombination
CRISPR	clustered regularly interspaced short palindromic repeats
CV	cardinal vein
CVP	caudal vein plexus
DA	Dorsal Aorta
ddH <sub>2</sub> O	double distilled water
DLAV	dorsal longitudinal anastomotic vessel
dll4	delta-like 4
dNTP	desoxy-nucleotide-triphosphate
dpf	days post fertilization
EC	Endothelial cell
Esam	Endothelial-specific adhesion molecule
EST	Expressed sequence tag
fli	Friend Leukemia Integration 1 Transcription Factor
flt1	FMS related receptor tyrosine kinase 1
Galk	Galactokinase
GFP	Green Fluorescent Protein
HHT	Hemorrhagic Hereditary Telangiectasia
hpf	hours post fertilization
ISV	Intersegmental Vessel
JAIL	Junction-Associated Intermittent Lamellipodia
JBL	Junction-based lamellipodia
kdrl	kinase insert domain receptor-like/VEGFR2 (gene)
LMA	low gelling temperature agarose
loxP	Locus of crossing over from coliphage P1
MLCP2	Myosin Light Chain Phosphatase 2

## List of Abbreviations

nls	nuclear localisation signal
NUAK	Novel (nua) Kinase
ORF	open reading frame
PCR	Polymerase Chain Reaction
PCV	posterior cardinal vein
PH-Akt	Pleckstrin Homology domain of Akt
pik3ca	PI3-Kinase $\alpha$ catalytic subunit
PIP2	Phosphoinositol-4,5-bisphosphate
PIP3	Phosphoinositol-3,4,5-trisphosphate
PTEN	Phosphatase and Tensin Homologue
PTU	1-phenyl-2-thiourea
RFP	Red Fluorescent Protein
rpm	rotations per minute
RT-PCR	Reverse-Transcription PCR
SIV	Subintestinal plexus
SHIP	Src2 Homology domain containing Inositol Phosphatase
tE	duration of extension phase in PCR protocols
Tie2	Tunica Interna Endothelial Cell Kinase 2
T <sub>m</sub>	melting temperature of primers
tol2	transposase tol2 from <i>Oryzias melastigma</i>
VE-cad	Vascular Endothelial Cadherin
VEGFA	Vascular Endothelial Growth Factor A
VEGFC	Vascular Endothelial Growth Factor C
VEGFR1	Vascular Endothelial Growth Factor Receptor 1
VEGFR2	Vascular Endothelial Growth Factor Receptor 2
VEGFR3	Vascular Endothelial Growth Factor Receptor 3
VM	Venous malformation

<b>1. Abstract</b>	1
<b>2. Introduction</b>	5
2.1. Tubes and Tubular Organs	6
2.2. Mechanisms of Vascular Development	10
2.2.1 Anatomy of the Cardiovascular System	10
2.2.2. Vasculogenesis - <i>de novo</i> tube formation	12
2.2.3. Angiogenesis – Tube Formation by Sprouting	13
2.2.4. Vascular Remodeling	18
2.3. Signaling Pathways in Vascular Development	27
2.4. Signaling by PI3-Kinases	30
2.4.1. A brief History of PI3-Kinases	30
2.4.2. Classes and Isoforms of PI3-Kinases in Vertebrates	31
2.4.3. PI3-Kinase $\alpha$ and its Role in Vascular Morphogenesis	35
2.4. Aim of this thesis	39
<b>3. Material and Methods</b>	43
3.1. Zebrafish Methods	44
3.1.1. Zebrafish Maintenance	44
3.1.2. Embryo Handling	44
3.1.3. Injection into fertilized zebrafish eggs	45
3.1.4. Founder Identification	45
3.1.5. Preparation of genomic DNA from adult fin clips	46
3.1.6. Preparation of genomic DNA from zebrafish embryos	46
3.1.7. Fish Lines	46
3.2 Materials and Protocols	47
3.2.1. Chemicals, Buffers and Solutions	47
3.2.2. Antibodies	48
3.2.3. Oligonucleotides	48
3.2.4. gRNA sequences for <i>pik3ca-b</i> mutant alleles <i>ubs49</i> and <i>ubs50</i>	49
3.2.5. Chemical Inhibitors	50
3.2.6. Restriction Enzymes	50
3.2.7. Microscopes	50
3.2.8. Genotyping protocol of the <i>pik3ca-a</i> mutant allele <i>sa16936</i>	51
3.2.9. Generation of the <i>ubs49</i> and <i>ubs50</i> alleles using CRISPR	52
3.2.10. Genotyping protocol of the <i>pik3ca-b</i> mutant allele <i>ubs49</i>	52
3.2.11. Genotyping protocol of the <i>pik3ca-b</i> mutant allele <i>ubs50</i>	54
3.2.12. Antibody stainings against VE-cad and ZO-1	55
3.2.13. RT-PCR of <i>pik3ca-b</i>	56
3.3. Imaging procedures and Image analysis	56
3.3.1. Image acquisition	56
3.3.2. Image analysis	57
3.3.3. Statistical Analysis	57
3.3.4. Figures	57

3.4. Materials for the BAC Project (see section VII: Appendix)	58
3.4.1. Buffers, Solutions and Media	58
3.4.2. Antibiotics	59
3.4.3. <i>Escherichia coli</i> strains	59
3.4.4. BACs and Plasmids	60
3.4.5. Fish Lines	60
3.4.6. Oligonucleotides	61
3.4.7. Other PCR reagents and DNA purification kits	62
3.4.8. Microscopes and Binoculars	62
3.4.9. Restriction Enzymes	63
3.4.10. Protocol for BAC recombineering	63
3.4.11. Overlapping PCR sequencing to confirm integrity	71
3.4.12. BAC Restriction Digest	72
3.4.13. <i>In vitro</i> Transcription of <i>tol2</i> mRNA	73
3.4.14. BAC Injections	73
3.4.15. <i>ubs8</i> genotyping	73
<b>4. Results</b>	<b>75</b>
4.1. The zebrafish genome contains two genes encoding <i>Pik3ca</i>	76
4.2. PI3-Kinase $\alpha$ signaling is active in zebrafish trunk primary ISVs and DLAV	76
4.3. <i>pik3ca</i> mutant alleles <i>sa16936</i> , <i>ubs49</i> and <i>ubs50</i>	83
4.4. Cardiovascular Development of <i>pik3ca</i> mutants	87
4.4.1. <i>pik3ca</i> mutants show reduced heartbeat and delayed onset of blood flow in ISVs and DLAV	87
4.4.2. Arteriovenous specification of ISVs is independent of PI3-Kinase $\alpha$ signaling	89
4.4.3. Loss of PI3-Kinase $\alpha$ signaling causes Hyperplasia in the CVP	91
4.4.4. Development of the trunk vasculature in <i>pik3ca</i> mutants	95
4.5. Genetic loss of PI3-Kinase $\alpha$ impairs Endothelial Cell Rearrangements	99
4.5.1. Junction Connectivity in ISVs and DLAV is perturbed upon loss of PI3-Kinase $\alpha$	99
4.5.2. Cell Rearrangements in the DLAV stall in <i>pik3ca</i> mutants	104
4.5.3. The speed of junction elongation is not affected by loss of PI3-Kinase signaling	108
4.5.4. Polarized distribution of junctional VE-cad is unaffected by genetic loss of PI3-Kinase $\alpha$	110
4.6. Loss of PI3-Kinase $\alpha$ signaling results in unstable <i>de novo</i> cellular contacts	112
4.7. Spatiotemporal Resolution of PI3-Kinase $\alpha$ activity at Endothelial Junctions	117
4.8. PI3-Kinase $\alpha$ signaling at Endothelial cell-cell Junctions is independent of canonical VEGFR2/VEGFR3 signaling	123
<b>5. Discussion</b>	<b>127</b>
5.1. A genetic model to study PI3-Kinase $\alpha$ function in zebrafish vascular development	128
5.2. Distinct functions of PI3-Kinase $\alpha$ in different vascular beds	130
5.2.1. General Vascular Development in zebrafish embryos in absence of PI3-Kinase $\alpha$ signaling	130
5.2.2. Differential Regulation of Foxo, a downstream target of PI3-Kinase $\alpha$	135

5.3. PI3-Kinase $\alpha$ signaling in Multicellular Vascular Tube Formation	136
5.3.1 Endothelial Cell Intercalation requires PI3-Kinase $\alpha$ signaling	136
5.3.2 Tricellular Junctions and de novo contact formation during junction mergence require PI3-Kinase $\alpha$ signaling	138
5.4. Local PI3-Kinase $\alpha$ Signaling at Endothelial Cell Junctions and in JBL	143
5.5. Local Activation of PI3-Kinase $\alpha$ signaling at Endothelial Cell Junctions	146
5.6. Summary and Outlook	147
<b>6. Supplementary Data</b>	<b>151</b>
<b>7. Appendix</b>	<b>157</b>
<b>8. References</b>	<b>163</b>
<b>Acknowledgements</b>	<b>193</b>
<b><i>Curriculum vitae</i></b>	<b>196</b>







I

# Abstract

The cardiovascular system is a hierarchically designed network of specialized tubular blood vessels, which is essential for the distribution of nutrients and oxygen throughout the vertebrate body. During cardiovascular development, distinct morphogenetic processes such as sprouting, fusion, vessel growth and remodeling must be coordinated in order to give rise to an elaborate and functional network of vascular tubes. Especially the development of multicellular vessels and the concomitant cell intercalation movements require harmonized cellular behaviors in order to maintain vessel integrity whilst allowing for positional changes. Here, cell adhesion and mobility require a delicate balance, which is coordinated by endothelial cell (EC) junction proteins and the cytoskeleton downstream of signaling pathways (reviewed in Betz *et al.*, 2016, Yin *et al.*, 2021; Phng and Belting, 2021).

Signaling by PI3-Kinases has been implicated in various cell behaviors like cell migration, differentiation, polarization and regulation of the cytoskeleton. In ECs, PI3-Kinase signaling was shown to regulate distinct behaviors such as arteriovenous differentiation and development of lymphatic vessels both *in vitro* and in different model organisms. Specifically the  $\alpha$ -isoform of PI3-Kinases (PI3-Kinase  $\alpha$ ) is essential for development of a functional vasculature. Genetic loss of PI3-Kinase  $\alpha$  signaling in mice leads to severe defects in angiogenic sprouting and vascular remodeling (Graupera *et al.*, 2008), resulting in early embryonic lethality. Recent studies have suggested a role for PI3-Kinase  $\alpha$  in regulating EC rearrangements by acting on cytoskeletal contractility (Angulo-Urarte *et al.*, 2018). However, we still lack a detailed analysis of how exactly PI3-Kinase  $\alpha$  signaling coordinates EC rearrangements and how it functionally integrates into the mechanistic processes during multicellular vascular tube formation.

In this study, I aimed to further elucidate the role of PI3-Kinase  $\alpha$  signaling in vascular development and, in particular, during EC rearrangements in multicellular blood vessel formation. I analyzed vascular morphogenesis in zebrafish embryos mutant for the catalytic subunit of PI3-Kinase  $\alpha$  (*pik3ca*), thereby making use of the highly advanced possibilities of live microscopy in the zebrafish. Similar to mouse mutants, zebrafish embryos homozygous mutant for both *pik3ca* genes were not viable after 6-7 days post fertilization (dpf) and showed defects in vascular morphogenesis and patterning. Interestingly and in agreement with previous studies in mice and human patients, different vascular beds showed distinct effects of loss of PI3-Kinase  $\alpha$  signaling. For example, the caudal vein plexus (CVP) of mutant embryos displayed

ventral hypersprouting and hyperplasia, whereas the dorsal aorta (DA) displayed reduced diameter, indicative of reduced cell number and decreased EC proliferation. Additionally, the transcription factor FOXO downstream of PI3-Kinases showed diverse behaviors upon acute loss of PI3-Kinase  $\alpha$  signaling depending on vessel identity.

In the trunk vasculature, genetic loss of PI3-Kinase  $\alpha$  signaling impaired cell rearrangements, resulting in unicellular vessel architecture. Analysis of EC behaviors during the rearrangement phase in the DLAV in mutant embryos revealed defective cell junction mergence and unstable tricellular junctions, effectively prohibiting cell pairing and intercalation. Furthermore, spatiotemporal analysis of PI3-Kinase  $\alpha$  activity with a lipid product biosensor unveiled local and recurring peaks of activity at the distal ends of endothelial cell-cell junctions. These oscillations overlap in location and frequency with junction-based lamellipodia (JBL, Paatero *et al.*, 2018), which raises the question of a functional or regulatory interplay of local PI3-Kinase  $\alpha$  signaling and JBL in junction elongation during EC intercalation.

Taken together, my results suggest a critical role for PI3-Kinase  $\alpha$  signaling in EC rearrangements and vessel multicellularization by stabilization of tricellular junctions, putatively by local downregulation of contractile actomyosin forces. I showed that PI3-Kinase  $\alpha$  exerts different functions in distinct vascular beds by differential interplay with other signaling pathways. Finally, spatiotemporal resolution uncovered localized and oscillating activity of PI3-Kinase  $\alpha$  at EC junctions, supporting the idea of PI3-Kinase  $\alpha$  signaling being involved in JBL formation and function.



II

# Introduction

## 2.1 Tubes and Tubular organs

Tubular organs can be found in almost all species in both the animal and plant kingdom. This fundamental biological shape comes in different architectures, sizes and appearances, depending on the respective specific function of the organ.

Tubular organs serve as the organisms' plumbing and organize transport of fluids, nutrients, waste products and hormones from their source to the site where they are consumed or excreted. Furthermore, tubes regulate the transport and exchange of gases, as well as providing barrier function between different tissue compartments. Prominent examples of tubular organs in plants are the xylem and phloem, which span throughout the whole organism and are responsible for the distribution of water and nutrients. In metazoans, most organs contain or are composed of tubes (reviewed in Lubarsky and Krasnow, 2003, Baer *et al.*, 2009), such as lungs, kidneys, intestines, and the cardiovascular system.

Tubular organs usually consist of epithelial cells, which enclose an inner luminal space. Epithelial cells differ from the surrounding mesenchymal (also referred to as stromal) cells in the organ by morphology, extracellular matrix (ECM) secretion and strong cell-cell adhesion. This serves to compartmentalize tissues and ensure proper barrier function between the lumen of the tube and the rest of the organ. Moreover, the epithelial cells in tubular organs are polarized. Their apical side faces the lumen, whereas the side facing away from the lumen towards the ECM, basal lamina or stromal cells, is basally polarized.

On the morphogenetic level, tubular organs can be linear (e.g. neural tube and intestines) or branched (e.g. lung and most glands), depending on the function of the respective organ (reviewed in Baer *et al.*, 2009). Branched tubular morphology extends the epithelial surface of the tube, thereby expanding the platform for molecular interactions between the lumen and the organ tissue. Hence, branched tubular networks can be observed in organs specific for gas exchange or nutrient distribution, such as the lung or the cardiovascular system, respectively.

From a cellular perspective, tubes can employ different conformations. In unicellular tubes, only a single cell surrounds the lumen. This single cell can be hollowed out, creating a seamless tube (Fig. 1 A), or wrap around the lumen and form an autocellular junction with itself (Fig. 1 B). Unicellular tubes can be found in the intestine of *Caenorhabditis elegans*, the tracheal system of *Drosophila melanogaster* as well as in some cases of the vertebrate vasculature (reviewed in Baer *et al.*, 2009).

In contrast, multicellular tubes are formed by at least two cells surrounding the luminal space (Fig. 1C). This type of tubes is the most common type found in mature vertebrate organs (reviewed in Baer *et al.*, 2009, also for trachea in Lubarsky and Krasnow, 2003).

Cellular architectures in tubular organs are plastic and cells can reorganize within the epithelial sheet surrounding the lumen. For example, cells in the *Drosophila* tracheal system have been observed to de-intercalate to form unicellular tubes from previously multicellular tubes (Ribeiro *et al.*, 2004), thereby extending the tracheal sprout. In contrast, ECs in the zebrafish trunk vasculature undergo extensive rearrangements to organize into multicellular blood vessels during vascular morphogenesis (reviewed in Kotini *et al.*, 2019, see also chapter 2.2.3). This remodeling process entails considerable cell shape changes and extends the vascular branch in a convergent extension movement.

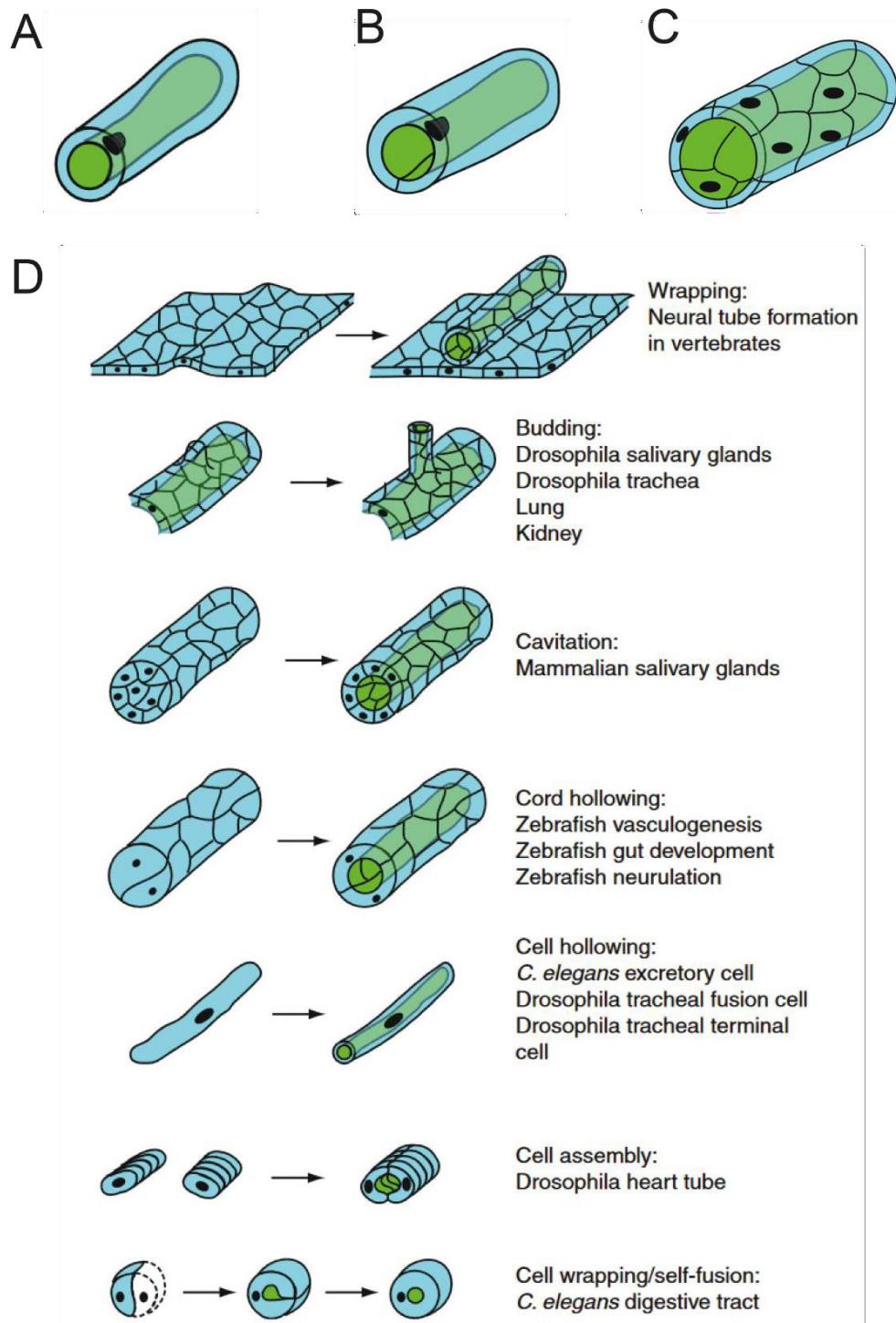


**Fig. 1: Architecture and formation of tubular organs**

**A-C** Different architectures of tubes: **A** Unicellular seamless tube, in which a single hollowed cell encloses the lumen. **B** Unicellular tube with autocellular junction. **C** Multicellular tube with intercalated cells enclosing the lumen. **D** Distinct mechanisms of lumen formation in tubular organs. Adapted from Baer *et al.*, 2009.



The formation of tubular organs can occur via different mechanisms, all of which entail complex cell behaviors and tissue reorganization. Tubes can form based on already polarized tissue sheets by wrapping or budding movements (Fig 1 D). During wrapping, a pre-selected group of cells leaves the tissue sheet and forms a tube on top of it, which is not connected to the parental tissue (e.g. during the formation of the neural tube in most vertebrates). Here, a new lumen must be created. Budding on the other hand describes the outgrowth of cells out of the epithelial tube sheet. In this case, the new tube branch remains connected to the parental sheet, effectively extending the parental lumen and increasing network complexity (e.g. in the mammalian lung and salivary glands).

The formation of a functional lumen in rod-like precursor tissues can occur via distinct mechanisms, including controlled apoptosis and cavitation, cell rearrangements and chord hollowing or hollowing of whole single cells (Fig. 1 D).

Studies in *C. elegans* and *Drosophila* revealed other but rare mechanisms by which tubes can form. The heart of *Drosophila* is formed by cells assembling to a *de novo* tube with a lumen in between them. In the digestive tract of *C. elegans*, tubular structures are formed by epithelial cells wrapping around a luminal space and fusing with themselves (Fig. 1D).

In summary, although tubular organs are so abundant and essential, there is no unifying mechanism by which they develop. Nevertheless, all mechanisms described so far require complex cell behaviors, which depend on cell-cell communication and molecular interactions between and within epithelial cells comprising tubular organs. This is especially true during the formation of multicellular tubes, when cells undergo vast shape changes and intercalation movements within the tube. But how do cells achieve these dynamic movements while retaining overall tissue integrity? Which intercellular interactions are essential during this process and how is this controlled on the intracellular level?

This thesis aims to dissect the molecular regulation and the cell-cell communication events occurring during the formation of multicellular tubular organs. By investigating the formation of multicellular blood vessels in the vasculature of embryonic zebrafish (*Danio rerio*), this work intends to identify essential roles of cell-cell interactions during the morphogenic processes of multicellular vascular tube formation.

## **2.2 Mechanisms of Vascular Development**

Vertebrates employ an intricate network of tubes to distribute oxygen, water and nutrients from their respective source to the sites where they are consumed as well as to remove waste products. This tubular organ is called the cardiovascular system. Its closed network of branched vessels infiltrates all organs and tissues of the body and constantly adapts to meet current requirements of the body, remaining plastic throughout adult life. Its importance is further underlined by the fact that it is the first organ to become functional during embryonic development.

### **2.2.1 Anatomy of the cardiovascular system**

The vertebrate cardiovascular system consists mainly of four different parts, all of which contain and transport blood, a mixture of water, different types of cells, nutrients, hormones and other molecules in need of distribution. First, the heart serves as the pumping engine of the body. Contraction of the hearts' muscular structures creates blood flow, which drives the distribution of blood throughout the vascular network. Vertebrate hearts consist of distinct chambers, namely the atrium (collecting the blood) and ventricle (mainly pumping the blood). Throughout the animal kingdom, different heart architectures can be observed with different numbers of atria and ventricles. Mammals have a four-chambered heart with two atria and two ventricles, as their circulatory system is divided into two parts (pulmonary and systemic circulation) which feed into individual atria and, subsequently, chambers. In contrast, teleost fish including zebrafish have two-chambered hearts with one atrium connecting to a single ventricle. Their hearts pump blood directly into the gills, where it is enriched with oxygen and then distributed throughout the body.

Next to the heart, the tubular vascular system contains three major types of vessels. Arteries transport oxygen enriched blood from the lungs to the heart and into distant tissues. Especially large arteries such as the aorta are surrounded by a number of layers of smooth muscle tissue, which help sustain and regulate artery diameter and

blood pressure within the vessel. Furthermore, arteries are supported by a dense elastin and collagen matrix important for vessel stability under pulsatile flow forces. Big caliber arteries branch into finer arterioles invading tissues and then into capillaries. Capillaries are the main exchange stations between the blood and external tissues. They are usually 8-10  $\mu\text{m}$  in size, which allows them to infiltrate narrow passages within the tissue. Capillaries merge into venules, which again come together to form larger veins.

Veins are valve-containing blood vessels, which transport oxygen depleted blood away from distant tissues and back to the heart and lung (or back to the placenta tissue and away from the embryo). They typically contain lower flow forces, are less muscular and display less complex extracellular matrix (ECM) composition.

At the cellular level, the lumen of all blood vessels including the heart is enclosed by endothelial cells (ECs). They are the building blocks of blood vessels and employ a variety of distinct behaviors and configurations to ensure vessel integrity and functionality. Depending on the vessel type, ECs are coated on the outside with different types and amounts of ECM proteins such as collagens, fibronectin and laminins (Cao *et al.*, 2017). Within vessels, ECs are connected to each other by tight and adherens junctions which maintain vessel integrity and regulate permeability.

In the zebrafish embryo, the first heartbeat can be observed at around 22 hours post fertilization (hpf) and circulation starts shortly after at approximately 24-26 hpf (Isogai *et al.*, 2001). Due to their small size, zebrafish embryos do not rely on functional gills at this stage, but oxygen is absorbed via diffusion from the water medium. This particular feature allows for manipulation of cardiovascular development until 4-5 days post fertilization (dpf), when the larval gills become active, without disrupting tissue oxygenation, as is the case e.g. for mouse embryonic studies.

Additionally, the development of the early blood and blood vessels are highly similar to those of other vertebrate species, supporting zebrafish embryos as a suitable model organism to study vertebrate cardiovascular development.

## 2.2.2 Vasculogenesis – *de novo* tube formation

Studies on mouse, chicken and quail embryos or chimeras of these species discovered two distinct mechanisms by which new blood vessels form (Poole and Coffin, 1988, Poole and Coffin, 1989, Coffin *et al.*, 1991, reviewed in Patan, 2000). The *de novo* generation of a vascular tube from individual ECs is termed vasculogenesis. Here, endothelial precursor cells, so called angioblasts, migrate into an unvascularized tissue, coalesce and arrange themselves into a new functional tube (Risau and Flamme, 1995, Jin *et al.*, 2005).

In zebrafish, the main vessels formed via vasculogenesis are the first axial vessels in developing vertebrate embryos, the dorsal aorta (DA) and the (posterior) caudal vein (CV or PCV). In the zebrafish embryo at around 10hpf, mesodermal angioblasts migrate medially from the lateral sides towards their final position below the notochord (Jin *et al.*, 2005). Here, they coalesce into an axial cord in anterior-posterior direction (Fig 2 A). Arterially-differentiated angioblasts migrate earlier than venous-specified ones, such that the precursory DA cord is formed before the early PCV chord, both in time and space (earlier towards anterior). Additionally, the two cords are at first not completely segregated but arterial ECs reportedly mix with cells in the PCV cord (Herbert *et al.*, 2009). After both DA and PCV are established, they subsequently acquire functionality by lumenization (Fig 2 B, see also section 2.2.2). Together, these two longitudinal vessels form the first vascular loop in the early embryo. The DA transports blood from the heart towards the posterior and distal tissues, whereas the PCV carries blood back from distal tissues to the heart. The vascular network further expands predominantly by angiogenesis.

In general, vasculogenesis is largely restricted to the formation of the first axial and brain vessels during vertebrate embryonic development. However, blood vessel formation by vasculogenesis has been reported in the context of some pathologies like tumor vascularization or endometriosis (reviewed in Drake, 2003, Laschke *et al.*, 2011).

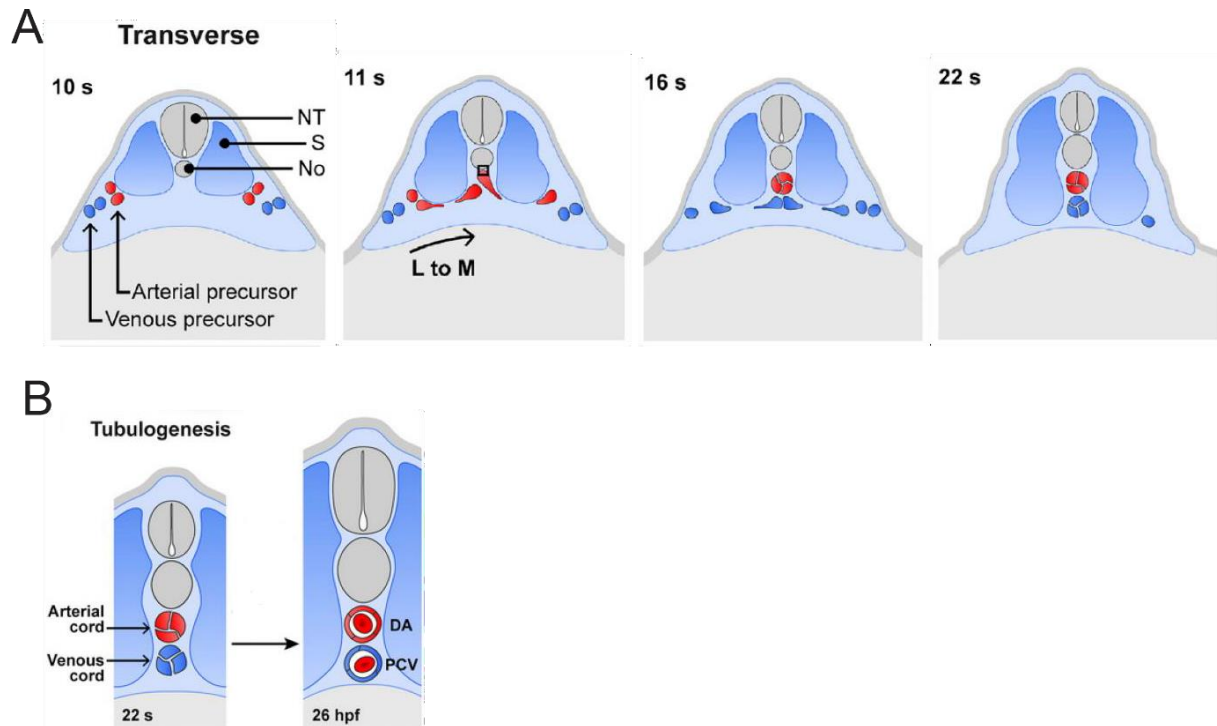


**Fig. 2: Formation of the DA and PCV in the zebrafish embryo by vasculogenesis**

**A** Schematic illustration of transverse views of zebrafish trunk at 10 to 22 somite (s) stage (14-20 hpf). Mesoderm-derived arterial angioblasts (red) migrate medially starting around 10hpf, venous-specified angioblasts (dark blue) follow shortly after. No=Notochord S=Somite NT=Neural Tube L=Lateral m=Medial A=Anterior P=Posterior **B** Schematic transversal section of zebrafish trunk before (left) and after (right) lumenization of the two main axial vessels and onset of blood flow.

Modified from Hogan and Schulte-Merker, 2017.

### 2.2.3 Angiogenesis – Tube formation by sprouting

After the establishment of the first two axial vessels, the vascular network of the embryo further expands in a process termed angiogenesis (Folkman, 1982). Here, new vessels are formed from parental vessels, either by EC outgrowth (sprouting angiogenesis) or by splitting a parental vessel into two (Intussusception). In the last decades, studies in cell culture (e.g. Park *et al.*, 2006), the mouse retina (reviewed in Stahl *et al.*, 2010) or zebrafish embryos (Isogai *et al.*, 2001, Isogai *et al.*, 2003, reviewed in Schuermann *et al.*, 2014 ) have elucidated the cellular mechanisms and molecular principles of angiogenesis.

Angiogenic expansion of the vascular network formed by vasculogenesis occurs during embryonic development and organism growth, tissue regeneration and wound healing, adaptation of muscle tissue to repeated training stimuli, as well as during the female reproductive cycle. Additionally, tumor tissues predominantly vascularize via angiogenesis. Many clinical studies on solid tumor angiogenesis and how to prevent vascularization of tumor tissue have resulted in numerous therapeutic strategies targeting specific aspects of angiogenesis (reviewed in Li *et al.*, 2018).

Angiogenesis entails a sequence of events with distinct cell behaviors and molecular mechanisms, which will be discussed in more detail throughout this chapter.

## **Sprouting**

In order to induce angiogenic vessel growth, the sprouting potential of ECs in already existing vessels needs to be activated by pro-angiogenic extracellular factors (e.g. VEGFA or FGFs) secreted by the surrounding tissue. This process is also influenced by hemodynamic forces, with higher shear stress facilitating EC activation (Song and Munn, 2011). Intracellularly, these extracellular cues trigger a number of responses and activate downstream signaling pathways, changing protein expression in the activated cells.

Within the pool of activated ECs, reciprocal signaling by Notch and its ligand Delta between cells downstream of VEGF mediated activation has been shown to be essential in the final selection of motile cells and induction of migration (Jakobsson *et al.*, 2010, see also chapter 2.3). However, there are also other ways to activate EC sprouting, such as by hypoxia or immune responses and depending on tissue environment.

Angiogenic activation of ECs induces remodeling of cell-cell junctions and secretion of proteases into the ECM, resulting in its local degradation (Senger and Davis, 2011). This local weakening of the ECM facilitates the migration of ECs into the unvascularized tissue following the angiogenic cues by chemotaxis. By doing so, ECs form so-called sprouts or sprouting bodies, which remain connected to the parental vessel at their base. Sprouts contain distinct EC types with different morphology and functions within the sprout. Leading cells, or tip cells, are polarized and motile, and display many filopodia with which they constantly probe the environment for pro- or anti-angiogenic cues, leading the trailing cells in the stalk (stalk cells). Tip cells

employ distinct signaling pathways for their specification, polarization and migration (reviewed in Siekmann *et al.*, 2013, see also section 2.3). Consequently, they differ from trailing stalk cells by protein expression and behavior. Stalk cells can still acquire tip cell identity and exchange their position with the prior tip cell, a process termed tip cell shuffling (Jacobsson *et al.*, 2010).

Endothelial sprouts can extend in length by cell proliferation, thus increasing total cell number in the sprout, and by cell intercalation and convergent extension movements (Blum *et al.*, 2008, Aydogan *et al.*, 2015). The latter entail extensive cell shape changes and elongation of endothelial cell-cell junctions, which will be discussed later in more detail.

Most of our current knowledge of angiogenic sprouting processes stem from studies using postnatal mouse retina or, more commonly, the zebrafish trunk vasculature as a model system. Here, ECs sprout in a regularly interspaced manner from the dorsal aorta (DA) at both sides of the embryo to form primary intersegmental vessels (primary ISVs) starting around 20hpf and in a heterochronic manner (anterior earliest, later towards posterior). Since the embryo absorbs oxygen by osmosis from the water medium and does not show blood flow at this stage, ISV sprouting from the DA is not induced by hypoxic cues from dorsal tissues, but is genetically hardwired (Isogai *et al.*, 2003). In general, sprouting from the DA is induced by VEGFA being secreted by dorsal tissues and binding to VEGFR2 in ECs in the DA (Covassin *et al.*, 2006, see also chapter 2.3).

## **Lumen Formation**

The formation of a functional lumen is a central step in the development of a new blood vessel and has thus been studied in different model systems, sometimes with controversial outcomes. Earlier studies described the generation of a luminal space within new vessels by formation and fusion of intracellular vacuoles, effectively hollowing out ECs (Folkmann & Haudenschild, 1980, Kamei *et al.*, 2006, discussed in Ellertsdottir *et al.*, 2010). However, more recent studies using live imaging in mouse and zebrafish vasculature have shown different morphogenetic pathways to generate a patent lumen, which depend on the morphology of the respective vessel (reviewed in Lammert and Axnick, 2012, Betz *et al.*, 2016, Phng and Belting, 2021).

If blood flow is present, that is, if the expanding lumen is already connected to the lumen of a pre-existing perfused vessel, the lumen can expand transcellularly by hollowing out the ECs and pushing through them (Fig 3 A). This process termed cell hollowing is driven by hemodynamic forces and occurs via inverse blebbing of the EC membrane (Gebala *et al.*, 2016). The incoming transcellular lumen subsequently fuses to local luminal pockets between ECs within the vessel.

ECs in vessels which generate a lumen by cell hollowing generally do not undergo concomitant shape changes or rearrangements, but present a unicellular vessel architecture, with single cells enclosing the lumen in transverse sections. Cells are arranged one after another with circular junctions between them. Such vessels usually transform into multicellular vessels later on by cell elongation and intercalation at some point, with some exceptions of retained unicellular vessel architecture, e.g. in the brain (Bär *et al.*, 1984, discussed in Kotini *et al.*, 2019).

In contrast to cell hollowing, chord hollowing does not rely on hemodynamic forces, but is driven by changes in the cellular architecture of the vessel (Fig. 3 B). During chord hollowing, ECs elongate along each other within the vessel and intercalate (Blum *et al.*, 2008). These cell rearrangements entail elongation of the cell-cell junctions, which contain local luminal pockets subsequently opened by electrostatic repulsive forces between membranes (Strilic *et al.*, 2010). Expansion and coalescence of luminal pockets between ECs generates a single lumen, which is always enclosed by at least two ECs in transverse sections, which is termed multicellular conformation or architecture. Since blood flow forces are absent during chord hollowing mechanisms, EC rearrangements and junctional elongation are solely driven by cytoskeletal forces and junctional remodeling (reviewed in Lammert and Axnick, 2012, Phng and Belting, 2021), which is further discussed in section 2.2.3.

A special case of vascular lumen formation can be observed in the common cardinal veins (CCV) in the anterior trunk of zebrafish embryos. Here, the lumen forms in a process termed lumen ensheathment (Helker *et al.*, 2013), which consists of two distinct phases. In the first vasculogenic phase, ECs on both sides of the embryo migrate ventrally over the yolk syncytial layer, thereby forming an endothelial sheet.



Some ECs within the sheet delaminate and arrange themselves around the future CCV lumen, without closing off it completely. The second angiogenic phase begins with the onset of blood flow and blood cells arriving in the open-ended tube. ECs from the outer sheet migrate collectively towards the heart, enveloping the blood stream and finally meeting the opposing outer sheet ECs on the bottom side (Schuermann, Helker, Herzog, 2014).

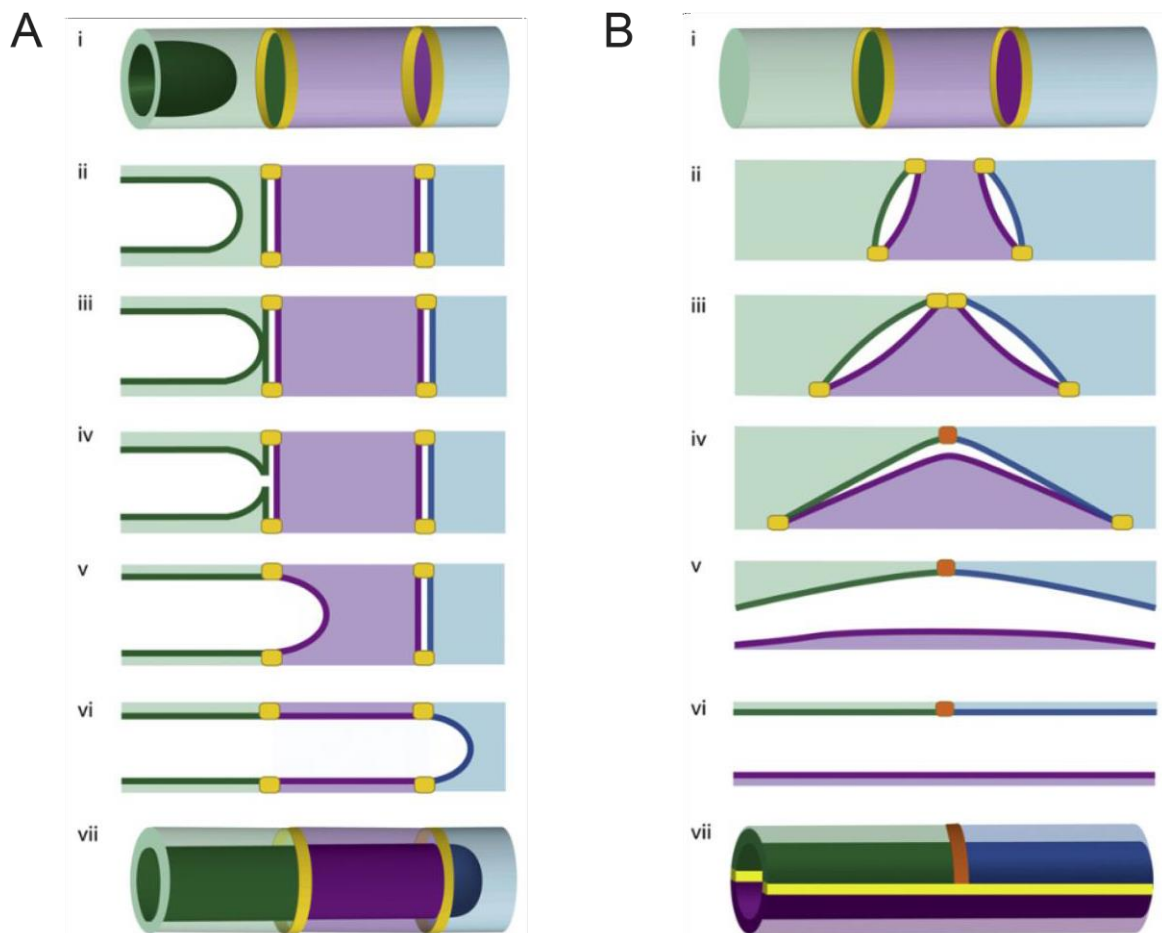


**Fig. 3: Lumen formation in angiogenesis**

**A** Schematic illustration of cell hollowing mechanism resulting in a unicellular tube with single ECs enclosing the lumen. Driven by hemodynamic forces, the lumen pushes through cells and fuses with local lumens inside junctional rings between ECs. **B** Schematic illustration of chord hollowing mechanism. Dynamic cell rearrangements lead to fusion of luminal pockets within junctional rings and formation of a multicellular vessel independent of blood flow.

Adapted from Herwig *et al.*, 2011.

## 2.2.4 Vascular remodeling

A vascular plexus generated by vasculogenesis and angiogenesis must adapt to the current specific needs of the surrounding tissue by changes in cellular conformation, further plexus expansion or vessel branch pruning. Furthermore, dead-ended sprouts must connect to either other sprouts or established vessels to form functional vascular connections. This optimization of the plexus network leads to a functional tissue vasculature with a hierarchical structure of bigger arteries and veins and smaller capillaries between them. In many cases, this process is dependent on blood flow forces, e.g. pruning of the lesser perfused of two parallel branches. Other mechanisms such as cell rearrangements can also occur independent of blood flow in unperfused and non-lumenized branches.

### Intussusceptive Angiogenesis

An alternative mode of angiogenic vessel generation is intussusceptive angiogenesis (sometimes also referred to as splitting angiogenesis). This term describes the gradual segregation of an existing vessel into two functional vascular tubes by extensive remodeling of endothelial cell shapes and progressive parental lumen constriction (de Spiegelaere *et al.*, 2011).

In contrast to sprouting angiogenesis, intussusceptive angiogenesis is much less well studied and understood. This mechanism was only discovered in the late 1980s in postnatal rat pulmonary tissue (Caduff *et al.*, 1986, Burri and Tarek, 1990), but could so far be observed in many other vascular tissues, such as mammary glands, bone tissue or embryonic avian kidney (de Spiegelaere *et al.*, 2011), as well as in pathological contexts (Ali *et al.*, 2019). In zebrafish embryos, intussusception was shown to occur during formation and remodeling of the caudal vein plexus (CVP, Karthik *et al.*, 2018).

Intussusceptive angiogenesis relies on a pre-existing perfused vessel and thus occurs after vasculogenesis and sprouting angiogenesis. Here, ECs flatten out, thereby increasing in size. ECs from opposite walls of the vessel migrate towards each other into the luminal space and tissue pillars are formed within the vessel lumen, effectively segregating the lumen into two compartments. Pillar growth and

subsequent maturation of the two lumens finally completely divide the preexisting vessel until two parallel vascular tubes have been created.

### **Lateral vessel fusion and vessel pruning**

Simplification of a vascular plexus after angiogenesis can occur by either fusion of two parallel vessels or by pruning of smaller vascular tubes. Both mechanisms have similar outcomes and they are both influenced by the amount of local shear stress on ECs caused by blood flow or by arteriovenous identity of new connections and blood flow direction.

Vessel fusion describes the simplification of a vascular plexus by joining of parallel branches within the plexus into bigger vessels, similar to a reversion of intussusception. This process is less well studied than pruning and it was first observed in the 1990s in the dorsal aorta of avian embryos (Drake and Little, 1995), but was later also described in the vitelline vein of mouse embryos (Gifre-Renom and Jones, 2021).

The term pruning describes the regression of a vessel branch and incorporation of the ECs into an adjacent vessel. This mechanism often occurs if two parallel vessels differ in blood flow and diameter or if a new vascular connection renders a parallel connection futile, e.g. because of changes in arteriovenous identity. Pruning reduces the number of surplus vascular connections in a plexus and allows for more efficient blood flow patterns (Lenard *et al.*, 2015).

In the first step of vessel pruning, the lumen is interrupted by formation of a local stenosis. Some ECs undergo apoptosis (Zhang *et al.*, 2018) whereas others migrate towards another vessel and away from the stenosis, de-intercalate and narrow the luminal space in the vessel until the lumen is fully disconnected (Lenard *et al.*, 2015, Franco *et al.*, 2015). Eventually, contacts between the last ECs in the previous vascular branch are disrupted and the vessel connection has regressed completely (reviewed in Korn and Augustin, 2015).

## Anastomosis

The vasculature is a highly ramified and branched system of tubes. Especially capillaries form highly complex and ramified networks to cover the entirety of the infused tissue. Interestingly, and in contrast to many other tubular organs, the vasculature does not contain blind-ended tubes, but consists of an intricate system of closed circulatory loops, ensuring blood flow.

Endothelial sprouts generated during sprouting angiogenesis are dead-ended protrusions from parental vessels. To functionally extend the present vascular network, sprouts must find and fuse to either other endothelial sprouts (head-to-head, Fig. 4 A) or established vessels (head-to-side, Fig. 4 B) (reviewed in Betz *et al.*, 2016) in a process termed anastomosis.

Anastomosis is readily observed during functional expansion of a vascular plexus across many different model organisms and even in 3D-cell culture (Diaz-Santana *et al.*, 2015). However, most of the current knowledge on the molecular processes during anastomosis stem from observations in the zebrafish trunk or brain vasculature. In the trunk vasculature of the zebrafish embryo, it is even possible to observe both types of anastomosis in two consecutive steps (Fig. 4 A, B).

First, primary ISV sprouts emerge from the DA towards the dorsal side of the embryo starting around 20-22 hpf. Above the neural tube, they extend in both anterior and posterior direction, where they meet and fuse to neighboring sprouts in head-to-head anastomosis, ultimately giving rise to the dorsal longitudinal anastomotic vessel (DLAV). However, these sprouts and the DLAV are initially all of arterial identity. In a second step, secondary venous sprouts emerge from the CV starting around 32hpf (Isogai *et al.*, 2003). Some of these venous sprouts migrate to the horizontal myoseptum and form the trunk lymphatic system, whereas others anastomose to primary ISVs, effectively transforming them from arterial to venous identity and allowing flow back to the CV. Within the trunk vasculature, except for the four most cranial ISVs, arteriovenous identity of ISVs is stochastic and largely alternates (Bussmann *et al.*, 2010, reviewed in Hogan and Schulte-Merker, 2017).

Molecularly, anastomosis is a stereotypical and sequential process, which commences with the leading tip cell of an endothelial sprout making contact to either an established vessel or to another tip cell. Contact initiation is facilitated by the

numerous filopodia tip cells extend, and it was shown that even a single filopodial contact between two tip cells is sufficient to initiate anastomosis (Sauteur *et al.*, 2017, Fig. 4 A,C). Upon formation of a filopodial contact site, junction proteins, such as Vascular Endothelial Cadherin (VE-cad, also termed Cdh5 in zebrafish) and Endothelial Specific Adhesion Molecule (esam) stabilize the new contact and form a junctional patch between the cells within minutes (Lenard *et al.*, 2013). Intracellularly, adhesion junction proteins in the patch engage in tight interplay with the cortical actomyosin cytoskeleton, further strengthening the junctional contact.

Simultaneously, the membranes at the patch side become apically polarized (Herwig *et al.*, 2011). As electrostatic repulsion forces open up a luminal pocket between the cells (Strilic *et al.*, 2010) and junction proteins relocalize away from the center of the contact, the initial junction patch is transformed to a circular junctional ring (Lenard *et al.*, 2013), connecting the two ECs together (Fig. 4 D) and surrounding a local miniature lumen.

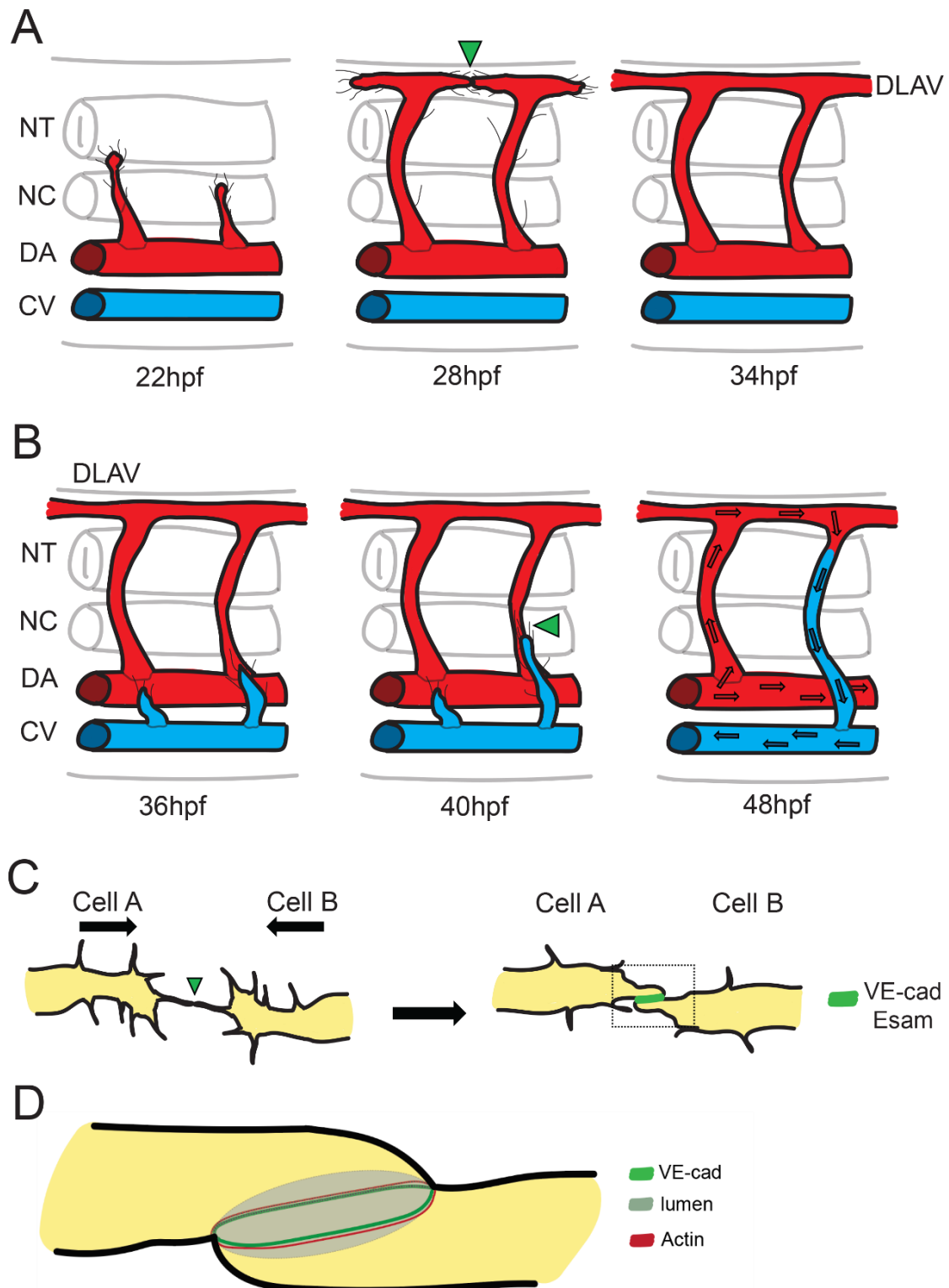


**Fig. 4: Anastomosis in the zebrafish embryo**

**A** Schematic illustration of primary ISV sprouts emerging from the DA and fusing at the dorsal side of the embryo to form the DLAV (head-to-head anastomosis) from 22 to 34 hpf. Green arrowhead

indicates first contact side between ECs. Somite tissue is not shown for simplification. **B** Schematic illustration of secondary ISV sprouting from the CV and fusing to primary ISVs (head-to-side anastomosis) to create venous ISVs and local circulatory loops. Green arrowhead indicates first contact between secondary sprout and established ISV. Red and blue arrows indicate blood flow direction after anastomosis is completed. **C** Contact initiation (green arrowhead) and formation of a junctional patch between two tip cells during head-to-head anastomosis. **D** Junctional ring between two ECs, consisting of adhesion junction proteins and cortical actin enclosing a local luminal pocket. The center of the ring is devoid of junction proteins and contains apical membrane.

### Cell rearrangements and Junction-Based Lamellipodia

Most vessels in the vertebrate body are multicellular, meaning that in transverse sections of the vessel, there is more than a single EC surrounding the vessel lumen. Interestingly, this is true not only for large caliber vessels, but also for most of the smaller capillaries in the microvasculature. Multicellular vessels form and lumenize in a chord hollowing mechanism, which entails dynamic cell shape changes and cell intercalation within the vessel and fusion of local lumens (Blum *et al.*, 2008, Sauteur *et al.*, 2014, Paatero *et al.*, 2018, reviewed in Phng and Belting 2021). Cells move and stretch over each other in a paired manner and using each other as a substrate, elongating the vessel by convergent extension. Dynamic cell rearrangements are represented by changes in the junctional patterns of cells in the vessel, which undergo a transition from circular to ellipsoid as the cells elongate their mutual surfaces (Sauteur *et al.*, 2014), until the junctions appear as long lines outlining the entirety of the vessel in a fully multicellular tube.

However, during the dynamic cell movements that these rearrangements bring about, contacts between ECs must not be disrupted in order to maintain vessel integrity. But how do EC junctions allow mobility during cell rearrangements while keeping contact?

In the past decade and using the zebrafish trunk vasculature as a model system, our group has uncovered a molecular mechanism driving EC junction elongation during cell rearrangements. Originating from a stable endothelial cell-cell junction, cells extend actin-filled protrusions into the direction of migration. This protrusion is stabilized at the distal tip by recruitment of new adhesion junction proteins such as

VE-cad and ZO-1 and binding to junction proteins on the surface of the partnering cell. An intermediate doubled junction is formed with a “new” distal junction and an “old” junction more proximal. This double junction is subsequently resolved by the merging of the two junctions. The resulting singular junction is located more distal than the previous. In this way, the cell has elongated and extended its surface contact with the partnering cell without ever detaching from it. Using each other as a substrate, ECs employ repeated cycles of these so-called Junction-based lamellipodia (JBL) and, like a ratchet, each JBL cycle advances the cell further into its direction of migration (Paatero *et al.*, 2018).

A central role in JBL formation is taken by VE-cad. This adhesion protein is distributed in a polarized manner in elongating junctional rings, with more VE-cad in the distal sides (referring to the elongation direction), which makes junctions appear “thicker” at these sides in antibody stainings or with fluorescent constructs (Paatero *et al.*, 2018). VE-cad engages in homotypic interactions with VE-cad on the surface of the partnering cell, linking the cells tightly together. Intracellularly, VE-cad is attached to cytoskeletal F-actin fibers via  $\beta$ - and  $\alpha$ -catenin and serves as transmitter of forces generated by the cytoskeleton to the partnering cell. Loss of VE-cad disrupts JBL formation and disturbs cortical F-actin localization (Sauteur *et al.*, 2014, Paatero *et al.*, 2018), impeding cell rearrangements and multicellular tube formation. JBL have been best studied during cell rearrangements in the zebrafish trunk in ISVs and during DLAV formation, as well as in the PCeV in the head. Interestingly, they can also be observed in established large caliber vessels like the DA (C. Wiesner, Doctoral Thesis, 2020). It is thus likely that JBL are not restricted to cell rearrangements in nascent vessels, but pose as the general mechanism of dynamic EC maneuverability without disrupting vascular integrity and vessel impermeability.



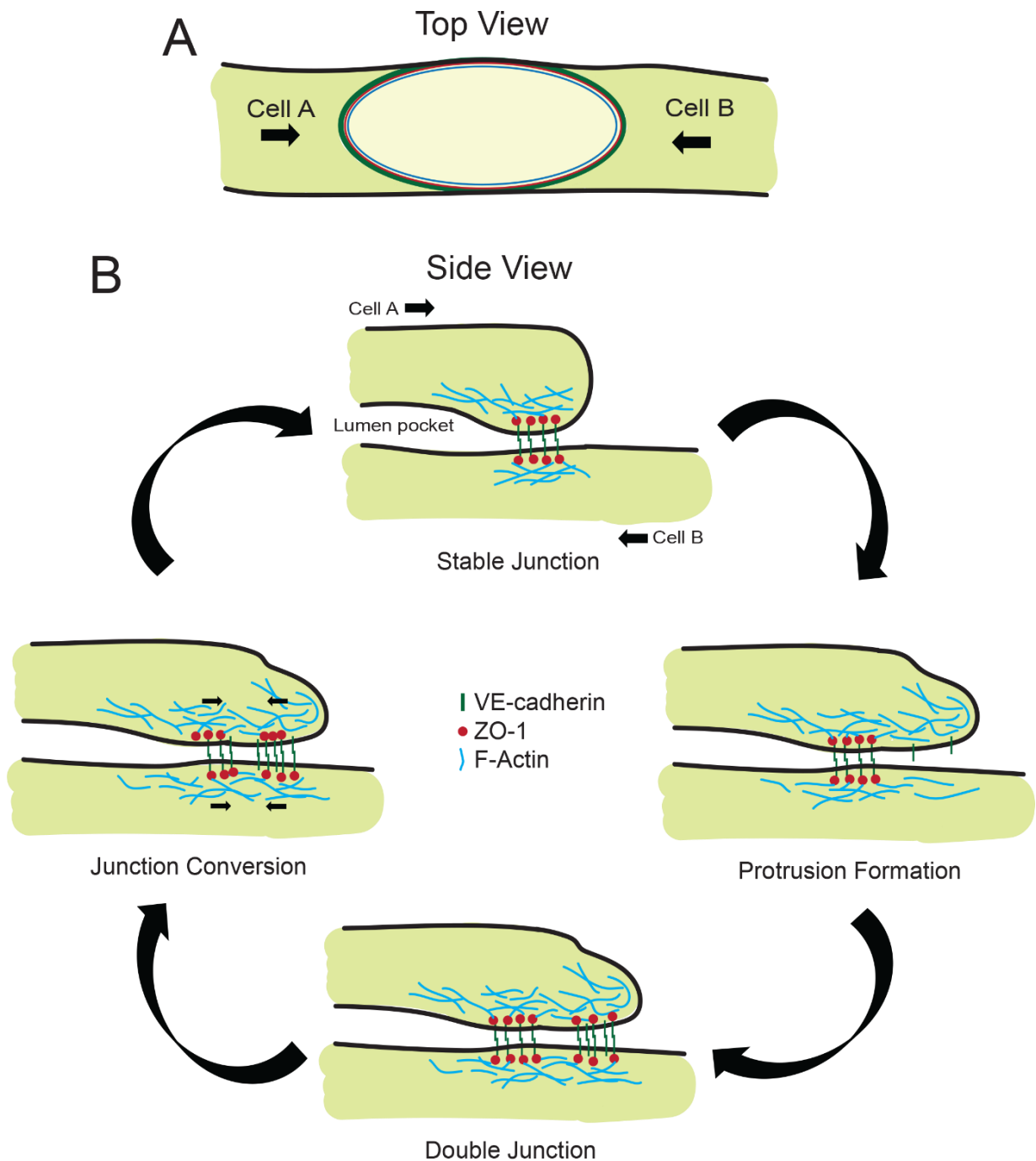


**Fig.5: Junction-Based Lamellipodia (JBL)**

**A** Schematic illustration of the top view of a junctional ring between two ECs migrating over each other. The ring-shaped junction consists of adhesion proteins such as VE-cad (Green), which binds intracellularly to cortical F-actin (Blue) by adapter proteins such as ZO-1 (red).

**B** Schematic illustration of the cyclic JBL mechanism: Based on a stable junction, an F-actin filled membrane protrusion forms in the direction of migration. This protrusion is stabilized by recruitment of adhesion junction proteins to the distal end, which leads to formation of a second distal junction with

the partnering cell. Cytoskeletal contraction forces lead to conversion movement of the two junctions, until only a single stable junction is present, which is positioned more distal than the original junction and the cell has advanced in the direction of migration.

A related mechanism by which ECs can rearrange was observed *in vitro* in subconfluent HUVEC cells. Here, formation of lamellipodia anchored at stable junctions commence by local disassembly of junctional contacts via the removal of VE-cad. At these sites, actin-containing membrane protrusions, so-called Junction-associated Intermittent Lamellipodia (JAIL), develop in an Arp2/3 controlled manner. Subsequently, VE-cad accumulates inside the JAIL, which is accompanied by dissociation of the Arp2/3 complex and disassembly of F-actin fibers, effectively terminating JAIL extension. Clustered VE-cad is then incorporated into the EC junction (Cao *et al.*, 2017). However, in contrast to JBL, JAIL do not advance the cell in the direction of migration and do not lead to elongation of the cell-cell interfaces. Determining to what extent they represent *in vivo* mechanisms of multicellular tube formation requires further analysis in future research.

## 2.3 Signaling pathways in vascular development

The formation of functional vascular tubes requires concerted cell behaviors which are regulated by distinct signaling pathways that cells use to communicate with each other. In the past decades, many inter- and intracellular signaling cascades have been shown to be essential for various aspects of vascular development such as EC proliferation, migration, angiogenic sprouting, tip cell guidance or arteriovenous identity. The following table provides an overview over the main signaling pathways involved in EC communication and regulation during vascular morphogenesis. Furthermore, it contains the respective phenotypes when abrogated in zebrafish embryos as reported in the current literature.

Receptor (zebrafish gene name)	Ligand	Cellular function in ECs and downstream targets	Loss of function phenotype in zebrafish vasculature	References
VEGFR1 ( <i>flt1</i> )	VEGFA or VEGFB	Decoy receptor: Tunes VEGF levels and VEGFR signal activation to regulate sprouting and proliferation by reducing unbound VEGF	Angiogenic hypersprouting in ISVs caused by overactivation of VEGFR2 and VEGFR3 signaling  Increased EC number in DA and DLAV	Krueger <i>et al.</i> , 2011  Wild <i>et al.</i> , 2017
VEGFR2 ( <i>kdr</i> and <i>kdr1</i> )	VEGFA	Induces angiogenic sprouting and promotes tip cell identity  Induces EC proliferation and survival  Activates a number of downstream signals including ERK and PI3-Kinase $\alpha$	Sprouting defects, e.g. no ISV sprouts from DA, no formation of DLAV (VEGFR2)  Reduced number of central arteries in hindbrain (VEGFA)	Gerhardt <i>et al.</i> , 2003  Covassin <i>et al.</i> , 2006  Carmeliet <i>et al.</i> , 1996

		VEGFA KO is haploinsufficient in mouse and zebrafish		Lange <i>et al.</i> , 2022
VEGFR3 ( <i>flt4</i> )	VEGFC	Induces (venous) sprouting and lymphangiogenesis by activating Prox1  Expressed in tip cells in ISVs, repressed by high Notch signaling  Activates a number of downstream signals including ERK and PI3-Kinase $\alpha$ signaling	Defects in secondary sprouting from PCV  Defective lymphatic sprouting in the trunk	Covassin <i>et al.</i> , 2006  Srinivasan <i>et al.</i> , 2014  Shin <i>et al.</i> , 2016-2  Siekmann and Lawson, 2007  Tammela <i>et al.</i> , 2008
Notch	Dll4	Generates heterogeneity within angiogenic sprouts: Tip cells express more dll4 which activates Notch signaling in stalk cells  Notch activity reduces sensitivity to VEGFA by downregulating VEGFR2 expression	Increased number of tip cells  EC hyperproliferation  Dense angiogenic sprouting front in vascular plexi caused by hypersensitivity to VEGFR2 signaling	Hellström <i>et al.</i> , 2007
BMP2 a and b	BMP2b	Promotes EC activation, sprouting and venous identity through activation of EphrinB4  Zebrafish embryos specifically express ligand and receptor in the CVP	Abrogation: prevents ventral venous sprouting, prohibits CVP formation  Overexpression: Induces aberrant sprouting from the CV towards dorsal	Neal <i>et al.</i> , 2019  Wiley <i>et al.</i> , 2011  Ola <i>et al.</i> , 2016

		Aberrant signaling is involved in formation of AVMs and VMs by elevating VEGFA and PI3-Kinase signaling		
tie1 and tie2	Angiopoetin 1-4	<p>Important for plexus organization and vessel branching</p> <p>Induces EC activation, sprouting and migration</p> <p>Important for EC junction integrity and vascular permeability</p> <p>Downstream targets include PI3-Kinases, MAPK/ERK and Rho/Rac</p>	<p>Tie1: defective facial lymphatic vessels</p> <p>Tie2: no aberrant phenotype, negligible for cardiovascular development in zebrafish</p>	<p>Suri <i>et al.</i>, 1996</p> <p>Signaling reviewed in Thomas and Augustin, 2009</p> <p>Jiang <i>et al.</i>, 2020</p> <p>Hußmann <i>et al.</i>, 2023</p>
apelinr	Apelin or elabela	<p>Regulates angioblast migration to the embryonic midline during vasculogenesis of DA and CV</p> <p>Couples EC polarity to flow direction <i>in vitro</i></p> <p>Promotes angiogenic sprouting downstream of Notch signaling</p> <p>Activates MAP-Kinases, ERK and PI3-Kinases/Akt/mTOR</p>	<p>Aberrant positioning of angioblasts along the sides of the embryo, no formation of DA and CV</p> <p>Defective EC polarity against flow forces</p> <p>Defects in ISV sprouting from DA (apelinr and Apelin)</p>	<p>Helker <i>et al.</i>, 2015</p> <p>Kwon <i>et al.</i>, 2016</p> <p>Helker <i>et al.</i>, 2020</p> <p>Dagamajalu <i>et al.</i>, 2022</p>

## 2.4 Signaling by PI3-Kinases

PI3-Kinases are signaling lipid kinases that catalyze the addition of a phosphate group to the 3'-hydroxyl group of the inositol ring of phosphatidylinositols (PIs) at cellular membranes. They are critical mediators of extracellular stimuli (e.g. cytokines or growth factors) and have implications in cellular responses such as cell proliferation, polarization and migration, autophagy and endocytosis. Their importance is further highlighted by their association with various pathological conditions and cancer variants.

### 2.4.1 A brief history of PI3-Kinases

Kinases capable of 3'-OH- phosphorylation of PIs were first discovered by Lewis Cantley and colleagues in the 1980s (Whitman *et al.*, 1985) and subsequently termed PI3-Kinases (PI3Ks). Cantley *et al.* discovered a particular lipid kinase activity of the polyoma virus middle-T antigen and showed that PI phosphorylation by this kinase induced viral transformation *in vitro*. Further studies revealed that activation of this PI3-Kinase prevents cell death, that it can act as an oncogen and, with the discovery of PI3Ks in other model organisms, that certain mutations in the PI3K encoding genes prolong the life span of *C. elegans* (Morris *et al.*, 1996).

Since their discovery, PI3-Kinases have been shown to regulate manifold cellular responses to extracellular stimuli in many different model organisms and tissues in both vertebrates and non-vertebrates. Fundamental aspects of PI3-Kinase signaling were found in studies using the slime mold *Dictyostelium discoideum*. Here, signaling by PI3-Kinases was demonstrated to establish front-rear polarity of migrating cells during chemotaxis (Parent *et al.*, 1998) and to play an essential role in micropinocytosis in this organism (Li *et al.*, 2021).

Findings made in *Dictyostelium* were quickly transferred to migrating vertebrate cells, such as T-cells or neutrophils in culture, and PI3-Kinases being important in cell migration were confirmed there (Turner *et al.*, 1995; Knall *et al.*, 1997). Furthermore, essential roles of PI3-Kinases in cell proliferation and survival were identified in cell culture as well as *Drosophila* and murine models. These were found to be dependent

on PI3K activation of its downstream target Akt, an established pro-mitotic oncogene. It was thus not surprising when advances in screening of cancer patients revealed elevated levels of PI3-Kinase signaling in different hyperproliferative tissues such as breast cancer, colon carcinoma or arteriovenous malformations. Today, signaling by PI3-Kinases (and Akt) is established in many pathologies and is a common target in diverse cancer therapies.

### **2.4.2 Classes and isoforms of PI3-Kinases in vertebrates**

In vertebrates, 3 different classes of PI3-Kinases have been identified, which contain a total of 8 different isoforms. PI3-Kinase classes and isoforms are structurally and functionally different and expressed in distinct patterns in various organs.

Biochemically, both classes and isoforms differ in their respective substrates and products as well as binding to different regulatory subunits as heterodimers, an overview over which is provided in Figure 7. Some protein features are shared between all isoforms, such as the highly conserved catalytic domain, whereas other domains are class- or isoform-specific (reviewed in Vanhaesebroeck *et al.*, 2010). However, they all produce different types of lipid second messenger molecules at membranes. The biological functions of the second messenger lipids include a variety of essential cellular responses, such as proliferation and survival, cytoskeletal rearrangements, endocytosis or metabolic changes.

This thesis focuses on the specific function of the class Ia isoform PI3-Kinase  $\alpha$ . In the following, I will thus concentrate on class I PI3-Kinases and only give a short overview on the other classes and isoforms.

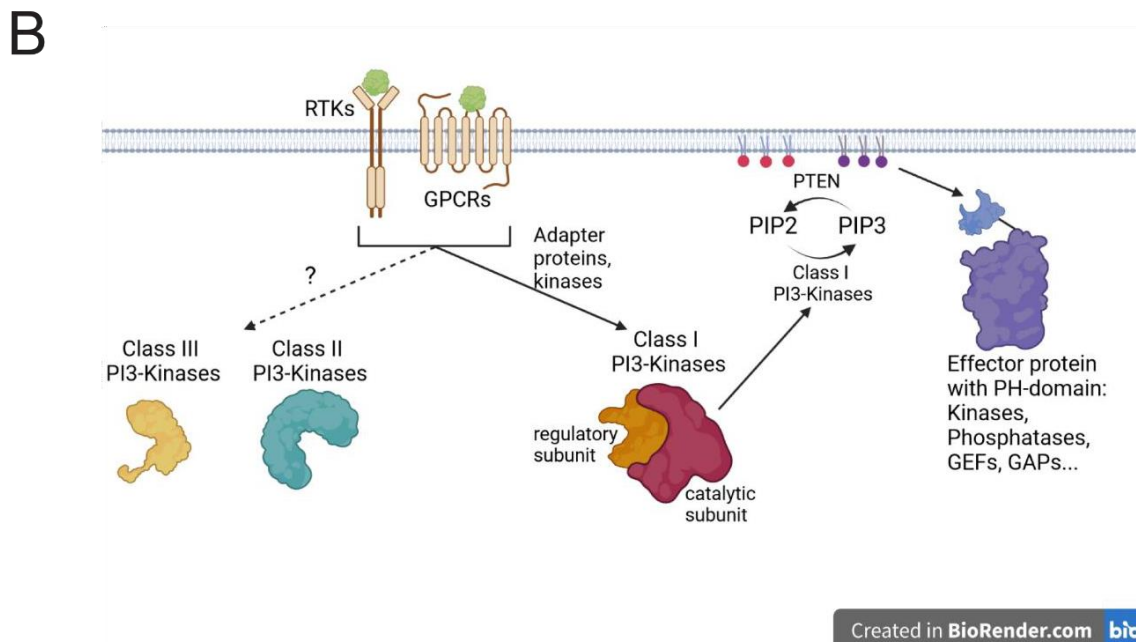
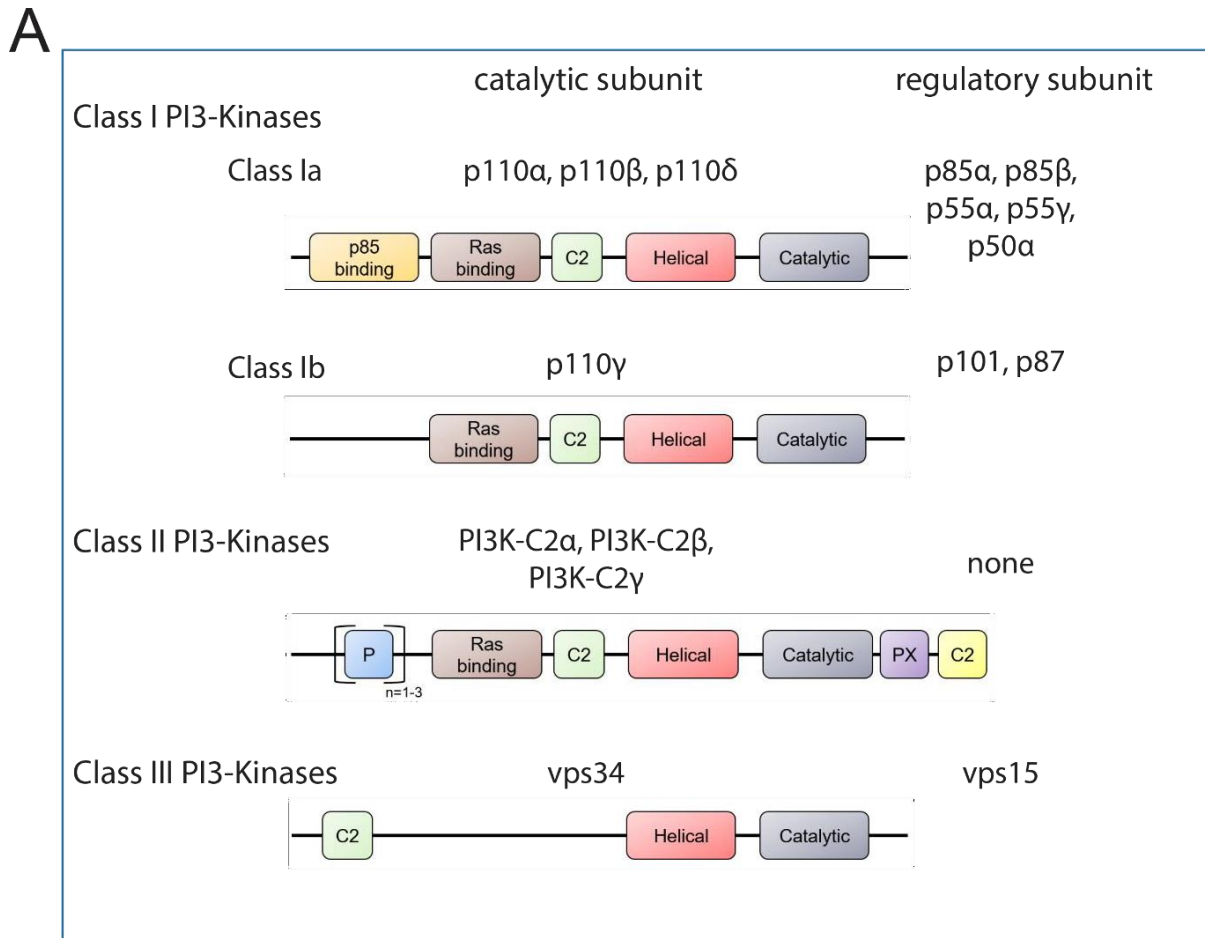


**Fig. 7: Classes and isoforms of vertebrate PI3-Kinases**

**A** Overview over the three classes and their respective catalytic and regulatory isoforms as well as schematic illustration of the protein domains the different PI3-Kinase isoforms contain.

**B** Activation of class I PI3-Kinases by RTK and GPCR signaling at the membrane and conversion of PIP2 to PIP3 (second messenger). Figure B created with Biorender.



## Class I PI3-Kinases

Class I PI3-Kinases are by far the best studied PI3-Kinases. In their active state, Class I PI3-Kinases convert phosphatidylinositol-4,5-bisphosphate (PtdIn(4,5)P<sub>2</sub> or PIP<sub>2</sub>) to phosphatidylinositol-3,4,5-trisphosphate (PtdIn(3,4,5)P<sub>3</sub> or PIP<sub>3</sub>). The Class Ia catalytic subunits p110 $\alpha$ , p110 $\beta$  and p110 $\delta$  are structurally very similar to each other and contain 5 distinct protein domains, namely the p85-binding, Ras-binding, C2, helical PIK-specific and kinase domain (Fig. 7a). They bind to regulatory subunits p85 $\alpha$  (and its splice variants p55 $\alpha$  and p50 $\alpha$ ), p85 $\beta$  and p55 $\gamma$ . p110 $\gamma$  is the only member of Class Ib and differs from other class I members since it lacks the N-terminal p85 binding domain and interacts with a different set of regulatory subunits, namely p101 and p87.

The regulatory subunits of Class I heterodimers bind to active RTKs (Class Ia isoforms) or G-protein coupled receptors (GPCRs) via their Src homology (SH2) domains. This binding can occur both directly or via adaptor proteins, such as Src, depending on the respective RTK/GPCR (reviewed in Engelmann, 2006). The binding of the regulatory subunit to a specific receptor induces a conformational change in the regulatory subunit, thereby activating the kinase domain in the catalytic subunit and the whole PI3-Kinase complex (Panayotou *et al.*, 1992).

The product of Class I PI3-Kinases is the second messenger lipid PIP<sub>3</sub>. PIP<sub>3</sub> controls localization and activation of a number of effector proteins, which bind to PIP<sub>3</sub> via their Pleckstrin Homology-domain (PH-domain, Klarlund *et al.*, 1997).

Among the most prominent effectors of Class I PI3-Kinases is the protein kinase Akt (Klippel *et al.*, 1997), promoting cell proliferation and survival and increasing cell metabolism via signaling to mTOR. Other downstream targets of Class I P3-Kinases include Rac, Ras and Arf GTPase families as well as CyclinD (reviewed in Vanhaesebroeck *et al.*, 2001).

Signaling by Class I PI3-Kinases is counteracted by Phosphatase and Tensin Homologue (PTEN) (Maehema and Dixon, 1998, Stambolic *et al.*, 1998). PTEN dephosphorylates PIP<sub>3</sub> at the 3'-hydroxyl group of the inositol ring and produces PIP<sub>2</sub>, effectively terminating signaling by Class I PI3-Kinases.

Class I PI3-Kinases display distinct expression patterns in vertebrates. In mice, p110 $\alpha$  and p110 $\beta$  are expressed ubiquitously, whereas p110 $\gamma$  and p110 $\delta$  are almost exclusively expressed in leukocytes.

The biological functions of Class I PI3-Kinases are highly diverse and context-

dependent. Global knockout of the p110 $\alpha$  and p110 $\beta$  encoding genes *Pik3ca* and *Pik3cb*, respectively, both resulted in early embryonic lethality in mice (Bi *et al.*, 1999 and Bi *et al.*, 2002), with *Pik3ca* mutants displaying proliferative defects and large hemorrhages and *Pik3cb* mutant embryos not developing beyond blastocyst stage. A later study using tissue-specific knockouts showed that the p110 $\alpha$  isoform is selectively required during angiogenesis and that, in contrast, abrogating neither p110 $\beta$  nor p110 $\delta$  in the endothelium resulted in defective embryonic vascular patterning (Graupera *et al.*, 2008). The role of the p110 $\alpha$  isoform in vascular biology will be further discussed in chapter 2.4.4.

P110 $\delta$  and p110 $\gamma$  are both enriched in leukocytes where they reportedly control lymphocyte activation and migration, respectively (Newman and Turner, 2015, Thomas *et al.*, 2008).

## **Class II PI3-Kinases**

Class II PI3-Kinases encompass three members, namely PI3K-C2 $\alpha$ , PI3K-C2 $\beta$  and PI3K-C2 $\gamma$ . These kinases contain Ras-binding, C2, helical PIK and catalytic kinase domains analogous to class I PI3-Kinases. However, all three class II members also have C-terminal PX domains using which they probably recognize and bind their substrate (Chen *et al.*, 2018). Furthermore, class II PI3-Kinases contain additional proline-rich motifs at the N-terminus, which are thought to play a role in directing the kinases to their respective target structures in the cell.

Class II PI3-Kinases do not bind to regulatory domains, but are directly activated by changing conformation upon binding to their respective substrates (Chen *et al.*, 2018). It is now commonly accepted that they convert PI and PI(4)P to PI(3)P and PI(3,4)P (PIP2) at endosomes, the trans-Golgi network and clathrin-coated endocytic vesicles. Here, signaling by class II PI3-Kinases recruits cytoskeletal effectors such as Arp2/3 to the clathrin lattice of forming vesicles (Yoshioka, 2021), leading to vesicles being pinched off of the membrane.

Both PI3K-C2 $\alpha$  and PI3K-C2 $\beta$  are expressed ubiquitously, whereas PI3K-C2 $\gamma$  is mainly expressed in hepatocytes. Interestingly, PI3K-C2 $\alpha$  was shown to be essential in angiogenesis and vascular barrier function. Endothelial-specific loss of *Pik3c2a* in mice resulted in reduced angiogenic sprouting in postnatal retina vasculature, increased levels of apoptotic ECs in general as well as vascular hyperpermeability

and hemorrhages. The latter were caused by defects in endocytic shuttling and recycling of VE-cadherin and weakened EC junctions in absence of PI3K-C2 $\alpha$  signaling (Yoshioka *et al.*, 2012).

### **Class III PI3-Kinases**

The third class of PI3-Kinases contains only Vacuolar Protein Sorting-34 (Vps34). This isoform was first described in yeast (Herman and Emr, 1990), however it was later found to be expressed in all eukaryotic cells.

Vps34 binds to the protein kinase Vps15, which often is considered its regulatory subunit. However, the exact regulatory interplay between the two kinases is not fully understood (reviewed in Backer, 2008). Vps34 shares considerable similarities to other PI3-Kinases in its protein domain structure and mechanism of action, but lacks the Ras-binding and SH2 domains.

It is now widely accepted that Vps34 converts PI to PI(3)P at early and late endosomes. Downstream targets of Vps34 signaling contain sorting Nexins, t-SNARES and a set of protein kinases. Common to these proteins are FYVE and PX domains, through which they bind to PI(3)P at endosomal membranes.

Vps34 activity plays an essential role in the endosomal system, as well as in autophagy and in phagocytosis. Furthermore, Vps34 is involved in the regulation of the mTOR pathway, controlling metabolic changes as a reaction to incoming extracellular signals.

### **2.4.3 PI3-Kinase $\alpha$ and its role in vascular morphogenesis**

Signaling by PI3-Kinases has various functions in cellular responses such as proliferation, migration, cytoskeletal remodeling, metabolic changes or vesicular trafficking. All of these mechanisms are essential for vascular development and homeostasis. However, one isoform has the strongest implications in vascular morphogenesis and tubular organ development. This particular isoform is the class Ia member PI3-Kinase  $\alpha$ .

In ECs, PI3-Kinase  $\alpha$  is a well-established downstream mediator of signaling by VEGFR2, VEGFR3, Apelinr or Tie2 (Fig. 8 A). In the canonical activation pathway, binding of the ligand VEGFA to VEGFR2 induces receptor dimerization, autophosphorylation and recruitment and binding of Src. With the help of the small transmembrane kinase Axl (Ruan and Kazlaukas, 2012), Src in turn phosphorylates p85, the regulatory subunit of PI3-Kinase  $\alpha$ . Phosphorylated p85 undergoes a conformational change, thereby unmasking the catalytic pocket of p110 $\alpha$ , the catalytic subunit, and switching on kinase activity (Panayotou *et al.*, 1992). At the membrane, PI3-Kinase  $\alpha$  converts PIP2 to PIP3, which acts as a second messenger by binding to various PH-domain containing proteins. Among the most prominent downstream effectors of PI3-Kinase  $\alpha$  signaling are the protein kinase Akt, cytoskeletal effectors RhoA and Rac1, as well as FOXO transcription factors and mTOR via Akt (reviewed in Kobialka and Graupera, 2019).

PI3-Kinase  $\alpha$  signaling is terminated by PTEN and SHIP, which dephosphorylate PIP3 to PI(4,5)P and PI(3,4)P, respectively. Whereas the exact function and regulation of SHIP remains unclear, PTEN is nowadays recognized as the main regulator of signaling by PI3-Kinase  $\alpha$  in ECs (reviewed in Graupera and Potente, 2013).

Global deletion of PI3-Kinase  $\alpha$  in mouse embryos causes major proliferative defects and early lethality (Bi *et al.*, 1999). Interestingly, deficient embryos also displayed impaired angiogenesis and hemorrhages. A later study from 2008 used EC-specific loss of PI3-Kinase  $\alpha$  to circumvent early embryonic lethality and to analyze later aspects of angiogenesis and vascular plexus remodeling. Here, abrogation of PI3-Kinase  $\alpha$  signaling in the endothelium resulted in reduced angiogenic sprouting and impaired EC migration and proliferation (Graupera *et al.*, 2008), which was also confirmed *in vitro*.

The importance of PI3-Kinase  $\alpha$  signaling in EC proliferation was later also confirmed in zebrafish embryos. Pharmacological inhibition of PI3-Kinase  $\alpha$  signaling either with the pan-class I isoform Inhibitor LY294002 or with the  $\alpha$ -isoform specific inhibitor GDC-0326 resulted in reduced cell number in zebrafish trunk ISVs and DLAV (Lange *et al.*, 2022, Angulo-Urarte *et al.*, 2018). Interestingly, EC migration during angiogenic sprouting of primary ISVs was not affected by loss of PI3-Kinase  $\alpha$  signaling in zebrafish trunk vasculature. This could be explained by parallel ERK signaling being primarily responsible for EC migration in the zebrafish trunk, which is also

downstream of VEGFA/VEGFR2 signaling (Shin *et al.*, 2016-1).

Next to EC migration and proliferation, signaling by PI3-Kinase  $\alpha$  is involved in arteriovenous differentiation and development of the lymphatic system from venous precursor cells. It was shown in zebrafish embryos, that arterial versus venous cell fate is regulated by an equilibrium of opposing signaling levels of PI3-Kinases and MAPK/ERK (Hong *et al.*, 2006), with ERK signaling promoting arterial fate and PI3-Kinase downregulating ERK. In contrast, zebrafish embryos mutant for Akt downstream of PI3-Kinase signaling displayed reduced numbers of arterial cells in the DA and impaired arteriovenous segregation of DA and CV without altering ERK signaling levels, suggestive of a more complex regulatory mechanism between PI3-Kinase and ERK signaling in arteriovenous differentiation of angioblasts (Zhou *et al.*, 2020).

In the lymphatic system, interaction of VEGFC with VEGFR3 reportedly activates PI3-Kinase signaling and promotes lymphatic endothelial cell (LEC) proliferation and migration (Coso *et al.*, 2012). Loss of PI3-Kinase signaling impairs LEC sprouting and lymphangiogenesis, whereas hyperactive PI3-Kinase signaling is often associated with pathologies involving lymphatic hyperplasia (Coso *et al.*, 2014).

In the vasculature, the oncogenic potential of PI3-Kinase  $\alpha$  signaling is reflected in its involvement in arteriovenous and venous malformations (AVMs and VMs) in a wide range of human vascular pathologies. In a mouse model of hereditary hemorrhagic telangiectasia entailing AVM development, PI3-Kinase signaling was shown to be upregulated (Ola *et al.*, 2016) downstream of abrogated BMP signaling. Furthermore, inhibition of PI3-Kinases in this model reduced AVM formation and improved therapeutic outcome. The exact function of PI3-Kinase  $\alpha$  in the formation of AVMs and VMs is not clear, because the driving processes underlying AVM formation are only little understood. It is possible that hyperactive PI3-Kinase  $\alpha$  signaling promotes either local EC hyperproliferation, arteriovenous differentiation defects or hypermigratory EC behavior, or combinations of these.

A recent study focused on the role of PI3-Kinase  $\alpha$  on the cytoskeletal changes involved in endothelial cell rearrangements during vessel morphogenesis. Genetic

abrogation of PI3-Kinase  $\alpha$  signaling in both mouse retina as well as inhibitor treatments in zebrafish resulted in impaired EC intercalation and anastomosis defects (Fig. 8 B, Angulo-Urarte *et al.*, 2018). Phosphoproteomic analysis revealed elevated levels of phosphorylated Myosin in murine ECs devoid of PI3-Kinase  $\alpha$  signaling, caused by defects in regulation of Myosin Light Chain Phosphatase 2 (MLCP2). Enhanced Myosin phosphorylation increases actomyosin tension in the cytoskeleton, which prohibits junction elongation and cell intercalation.

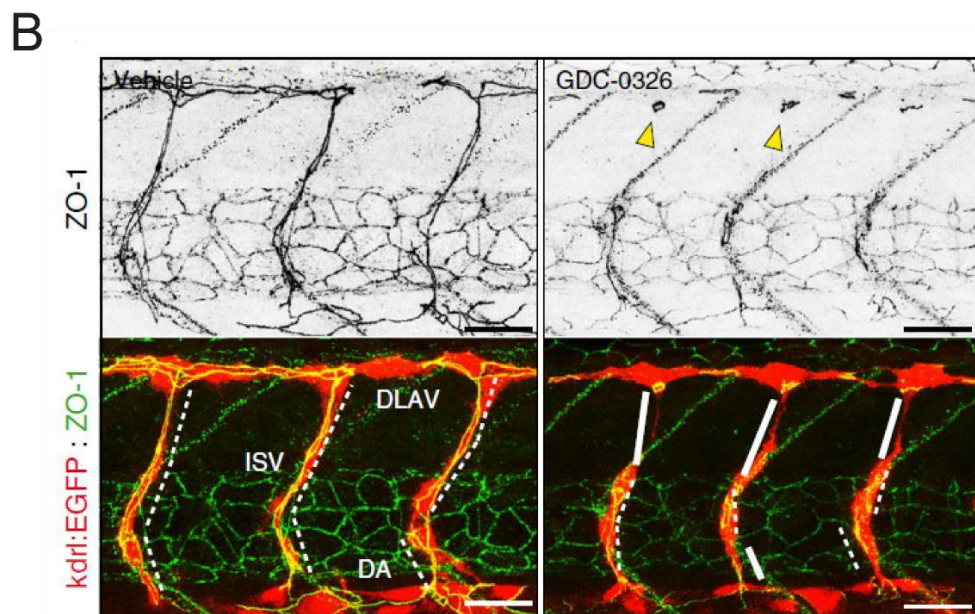
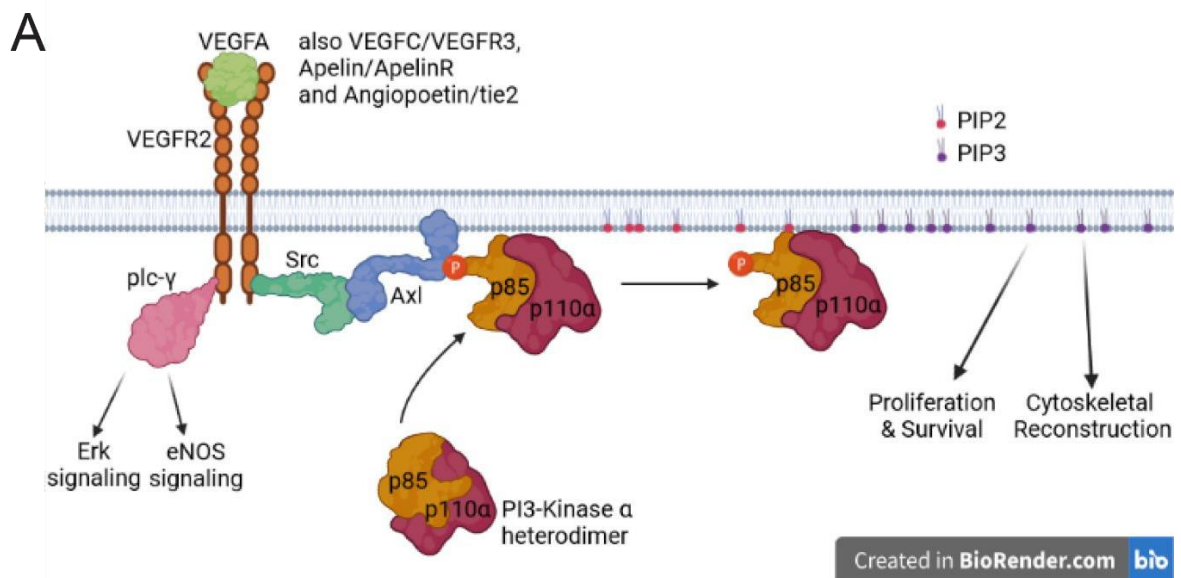


**Fig. 8: PI3-Kinase  $\alpha$  signaling in endothelial cells and its role in cell rearrangements**

**A** Schematic illustration of activation of PI3-Kinase  $\alpha$  signaling by VEGFR2 and its interaction with Src and Axl at the membrane of ECs. **B** Junctional patterns in ISV and DLAV in transgenic *Tg(kdrl:EGFP)<sup>s843</sup>* zebrafish embryos shown by anti-ZO1 staining at 33hpf. Embryos were treated with either DMSO (left panels) or GDC-0326 (PI3-Kinase  $\alpha$  isoform specific inhibitor, right panels). Yellow arrowheads point towards small junctional rings between ECs, white lines indicate gaps between junctions in unicellular vessel devoid of ZO1 staining, punctuated white lines indicate elongated junctions. Scale bar is 30 $\mu$ m, adapted from Angulo-Urarte *et al.*, 2018.

Despite beautifully highlighting the importance of PI3-Kinase  $\alpha$  in EC rearrangements during vascular morphogenesis, the study was limited to *ex vivo*, *in vitro* and pharmacological approaches. A genetic model to study the role of PI3-Kinase  $\alpha$  signaling in a model organism permitting more dynamic analyses was unavailable at the time. Thus, at present, we only have a crude snapshot analysis of a highly dynamic process depending on PI3-Kinase  $\alpha$  signaling.

In this thesis, I aim to elucidate exactly this gap in our understanding of how signaling by PI3-Kinase  $\alpha$  influences vascular development, with special emphasis on PI3-Kinase  $\alpha$  regulating cytoskeletal forces and junctional elongation during multicellular vascular tube formation.

## 2.5 Aim of this thesis

In tubular organs such as the vasculature, lumen formation by chord hollowing depends on dynamic cell rearrangements and cell-cell junction elongation. Our lab has previously identified JBL to be the central mechanism by which cells in the endothelium elongate their mutual interfaces during cell intercalation. Whereas central mechanistic players of JBL (namely VE-cad, ZO1, F-Actin, and myosin) have been identified, the regulatory aspects of this mechanism have not been studied so far. Furthermore, a study in which our lab participated demonstrated an essential role of signaling by PI3-Kinase  $\alpha$  in EC rearrangement during multicellular tube formation, possibly via regulating JBL at junctions. However, this study was limited to *ex vivo* and *in vitro* approaches as well as inhibitor treatments of zebrafish embryos due to

unavailability of a genetic model to study dynamic PI3-Kinase  $\alpha$  signaling in zebrafish.

This thesis aims to combine our current knowledge about EC rearrangements with the role of PI3-Kinase  $\alpha$  signaling in multicellular vascular tube formation by analyzing the particular function of this signaling hub during EC junction elongation and JBL. First, I will describe the generation of a genetic model to study PI3-Kinase  $\alpha$  function in zebrafish and validate this model referring to known functions of PI3-Kinase  $\alpha$  signaling in the vasculature. Using the broad spectrum of available fluorescent reporters, I will then use this model to better define the molecular function of PI3-Kinase  $\alpha$  during junction elongation processes by analyzing the different aspects of cell-cell junction elongation our group has discovered and described so far. My work aims to put signaling by PI3-Kinase  $\alpha$  into the current framework and our understanding of how cell-cell junctions elongate and how cells rearrange in the vasculature and tubular organs in general.







# III

## Materials and Methods

## 3.1 Zebrafish methods

### 3.1.1. Zebrafish maintenance

Zebrafish (*Danio rerio*) were raised and maintained under standardized conditions with controlled pH, conductivity and water temperature according to “The zebrafish book” (Westerfield, 2000). All animal husbandry and experimentation was performed in accordance with federal guidance and approved by the Kantonales Veterinäramt of Kanton Basel-Stadt under licenses 1014H and 1014G1.

Eggs were obtained by natural spawning in the morning.

### 3.1.2. Embryo handling

Zebrafish embryos were kept in 1x E3 embryonic medium at 28.5°C and staged by hours post fertilization (hpf) according to Kimmel *et al.*, 1995.

50x E3 embryonic medium stock solution was prepared as the following:

component	Concentration
NaCl	250 mM
CaCl <sub>2</sub>	8.5 mM
MgSO <sub>4</sub>	16.5 mM
Na <sub>2</sub> CO <sub>3</sub>	To adjust pH to 7.0

To inhibit pigmentation, embryos were incubated in 1-phenyl-2-thiourea (PTU) in embryo medium starting approximately at 24hpf.

Embryos older than 20hpf were exclusively dechorionated manually using forceps (Dumont #5F).

### 3.1.3. Injection into fertilized zebrafish eggs

To obtain zebrafish egg injection needles, borosilicate capillaries (outer diameter 1.0mm, inner diameter 0.5 mm, 10cm length; Sutter Instruments) were pulled in a needle puller (Sutter Instruments) using the following parameters:

Heat = 501

Pull=60

Velocity=80

Time=200

Freshly laid eggs were mounted into grooves of an agarose mold (2% agarose in 1x E3 in petri dishes and eggs covered in 1x E3 medium. Injection needles were loaded with 3µl injection mix using Micro Loader tips (Eppendorf) and needles broken at the very tip using forceps. Injection needles were connected to a pneumatic Pico Pump (SYS-PV820) from WPI. Injection volume was set to approximately 2-3nl by adjusting injection pressure and duration to the respective needle. Zebrafish eggs were injected at the 1-cell-stage either directly into the first cell or into the plasma stream beneath it. Injected eggs were incubated at 28.5°C in E3 medium supplied with low amounts of methylene-blue (Sigma-Aldrich).

### 3.1.4. Founder Identification

Injected embryos (G0) were raised to adulthood and outcrossed against wild-type AB/TU fish as single pairs. The resulting embryos (F1) were screened for fluorescent reporters (BAC and fli:PHAkt-EGFP/fli:PHAkt-mclav) at 30hpf or for genetic alterations by PCR and restriction digest and sequencing (CRISPR mutants).

Identified founders were crossed again to wild-type fish or directly to desired reporter lines and their F1 raised as the first stable line of the particular allele.

### 3.1.5. Preparation of genomic DNA for PCR from adult fin clips

Juvenile (2 month old) or adult zebrafish were anesthetized in 1:1000 diluted 2-phenoxyethanol (Koi Med Sleep, Schönbach-Apotheke, D-35614 Aßlar, Swissmedic Nr. 59'040; ATCvet code: QNO1AA). A small piece of tail fin tissue was cut off using a, EtOH disinfected razor blade. Fish were recovered in single tanks provided with clean system water and methylene-blue solution (Sigma-Aldrich). Tail fin tissue was solved in 50mM NaOH at 95°C for 20min. After cooling down to 4°C, samples were neutralized with 1:10 volume 1M Tris-HCl (pH=8). Samples were subsequently digested with proteinase K at 50°C for 1h and proteinase K inactivated at 95°C for 20min. This protocol yields highly concentrated and relatively clean genomic DNA suitable for PCR and sequencing.

### 3.1.6. Preparation of genomic DNA from zebrafish embryos

Embryos were solved in 15µl 50mM NaOH per embryo at 95°C for 20min. After cooling to 4°C, 1.5 µl 1M Tris-HCl pH=8 was added to neutralize the samples. Proteinase K was added to a final concentration of 5ng/ul and samples incubated at 50°C for 1hour. Proteinase K was inactivated by incubating the sample at 95°C for 15min and subsequently debris in the sample was pelleted by centrifuging at 15000rpm for 30sec. The supernatant was used for PCR analysis.

### 3.1.7. Fish lines

Name	Allele designation	Type	Reference
<b>ABC</b>	wild-type	wild-type	ZIRC, Oregon
<b>TU</b>	wild-type	wild-type	ZIRC, Oregon
<b><i>pik3ca-a</i></b>	sa16936	Mutation	European Zebrafish Resource Centre, Karlsruhe, Germany
<b><i>pik3ca-b</i> allele 1</b>	ubs49	Mutation	This study
<b><i>pik3ca-b</i> allele 2</b>	ubs50	Mutation	This study and Tschudin 2022, Master Thesis
<b>kdrl:EGFP</b>	s843	Transgene	Jin <i>et al.</i> , 2005

<b>fli1a:EGFP</b>	y1	Transgene	Lawson and Weinstein, 2002
<b>fli:GFF</b>	ubs3	Transgene	Herwig <i>et al.</i> , 2011
<b>UAS:RFP</b>		Transgene	Asakawa and Kawakami, 2008
<b>cdh5:cdh5-TS</b>	uq11bh	Transgene (BAC)	Lagendijk <i>et al.</i> , 2017
<b>-0.8flt1:RFP</b>	hu5333	Transgene	Bussmann, Bos <i>et al.</i> , 2010
<b>gata1:dsRed</b>	sd2	Transgene	Traver <i>et al.</i> , 2003
<b>ZO1-tdTomato</b>	pd1224	Knock-In	Bagnat group, unpublished
<b>fli:PH-Akt-EGFP</b>	ubs55	Transgene	Tschudin, 2022, Master Thesis
<b>fli:iRFP-UCHD</b>		Transgene	Wiesner, 2020, Doctoral Thesis
<b>fli:FOXO1b-EGFP</b>	bns515	Transgene	Potente group, unpublished
<b>kdrl:nls-mcherry</b>	is4	Transgene	Wang <i>et al.</i> , 2010

## 3.2. Materials and Protocols

### 3.2.1. Chemicals, Buffers and Solutions

<b>Buffer/Medium/Solution</b>	<b>Composition/Provider</b>
<b>10x PBS</b>	1.37 M NaCl 27mM KCl 100mM Na <sub>2</sub> HPO <sub>4</sub> 18mM KH <sub>2</sub> PO <sub>4</sub> in ddH <sub>2</sub> O, autoclaved
<b>50x TAE (TRIS-Acetic-EDTA)</b>	2M TRIS-Base 5.71% glacial acetic acid 50mM EDTA in ddH <sub>2</sub> O
<b>Agarose</b>	Sigma-Aldrich
<b>Blocking Solution</b>	10% normal goat serum 1% BSA 0.1% TritonX-100 0.01% Sodium Azide in 1x PBST
<b>Dimethylsulfoxide (DMSO)</b>	Sigma-Aldrich

<b>dNTPs 10mM each</b>	oligonucleotides (BioFlux)
<b>Fixing Solution</b>	2% Paraformaldehyde in PBST
<b>Low gelling temperature agarose (LMA)</b>	Carl Roth Chemicals
<b>PBST</b>	1x PBS 0.1% Tween-20
<b>PBST&amp;T</b>	1x PBS 0.1% Tween-20 0.5% TritonX-100
<b>RedSafe</b>	DNA staining agent for electrophoresis (Intron Biotechnology)
<b>TitaniumTaq buffer 10x</b>	TakaraBio
<b>TitaniumTaq Polymerase</b>	TakaraBio
<b>25x Tricaine (Tricainemesylate, MS-222)</b>	Sigma-Aldrich 0.4% w/v in ddH <sub>2</sub> O, pH=7 adjusted with 1M Tris-HCl Stored at -20°C

### 3.2.2. Antibodies

<b>Name</b>	<b>Type</b>	<b>Dilution used</b>	<b>Host species</b>	<b>Reference</b>
<b>α-VE-cadherin</b>	primary	1:500	Rabbit	Blum <i>et al.</i> , 2008
<b>α-hZO1</b>	primary	1:100	Mouse	Invitrogen
<b>α-rabbit F(AB)<sub>2</sub> Alexa 568</b>	secondary	1:1000	Goat	Invitrogen
<b>α-mouse F(AB)<sub>2</sub> Alexa 633</b>	secondary	1:1000	Goat	Invitrogen

### 3.2.3. Oligonucleotides

<b>Name</b>	<b>Sequence 5'-3'</b>
<b>sa16936 P1</b>	ACTCCCTGACAGCTTCATTCCG
<b>sa16936 P2</b>	GGTACTTTTCCAAAAGTT
<b>sa16936 P3</b>	TTTAATTAGGCCTACTGGTAGCC



<b>sa16936 P4</b>	CGGCTGTGACGAGTATC
<b>CRISPR gRNA pik3ca-b exon 3 fw</b>	TAATACGACTCACTATAGGCTCGATGACCTTCAGGATGTTT TAGAGCTAGAAATAGCAAG
<b>CRISPR gRNA pik3ca-b exon 4 fw</b>	TAATACGACTCACTATAGGGCCTTCAACACACACCTGGTTT TAGAGCTAGAAATAGCAAG
<b>CRISPR gRNA constant rev</b>	AAAAGCACCGACTCGGTGCCACTTTTTCAAGTTGATAACGG ACTAGCCTTATTTAACTTGCTATTTCTAGCTCTAAAAC
<b>ubs49 P1</b>	CCCTTAAGCAGTATTTGTGTCTCCAG
<b>ubs49 P2</b>	GGGCCATCTGCTGTATAACACTAG
<b>ubs49 P3</b>	ACGTACAGTGCCTGTGT
<b>ubs49 P4</b>	GCGAGGGTGGAGGCA
<b>ubs50 P1</b>	CAGATCACTAAAGTCACTGTTTGCCTTG
<b>ubs50 P2</b>	ACCGTTTGATATTGTA CTCTAAAA
<b>ubs50 P3</b>	GTCTTTTTTCACCCCATGAC
<b>ubs 50 P4</b>	CTCGATGACCTTCAGGAT
<b>pik3ca-b gene cDNA prep</b>	ATTAAGATAATGGTCATTAGTGC
<b>RT-PCR fw</b>	GAGCCATTGATTTATTCACGC
<b>RT-PCR rev</b>	CCAGTGTTTTCCGCAGATACG

### 3.2.4. gRNA sequences for *pik3ca-b* mutant alleles *ubs49* and *ubs50*

gRNA sequences were selected based on highest predicted efficiency and lowest predicted off-target effects using the CHOPCHOP algorithm at (<https://chopchop.cbu.uib.no/>).

Sequences used were (in 5'-3' direction):

For Exon 4 to generate *ubs49*: GTGGAGGGGCGCACACAC

For Exon 3 to generate *ubs50*: CTCGATGACCTTCAGGAT

### 3.2.5. Chemical Inhibitors

Name	Inhibition Target	Concentration used	Provider
<b>Alpelisib</b>	PI3-Kinase $\alpha$	50-100 $\mu$ M	Lubio Science
<b>GDC-0326</b>	PI3-Kinase $\alpha$	20 – 100 $\mu$ M	Genetech
<b>LY294002</b>	PI3-Kinases all isoforms	10 - 50 $\mu$ M	Merck
<b>SU5416</b>	VEGFR2	0.5-2 $\mu$ M	Selleckchem
<b>SAR131675</b>	VEGFR3	5-10 $\mu$ M	LubioScience

### 3.2.6. Restriction Enzymes

Enzyme name	Manufacturer	Stock concentration
<b>AlwNI</b>	NEB	10000 U/ml
<b>FokI</b>	NEB	5000 U/ml

### 3.2.7. Microscopes

Microscope	Manufacturer	Information	Objectives
<b>Leica M205 FA with Lumencor Sola FISH Light engine</b>	Leica Lumencor	Fluorescence equipped binocular	
<b>SP5-II-Matrix</b>	Leica	Confocal Microscope	HC PL Fluotar 10x air HCX PLAN APO CS 40x water
<b>SpinSR</b>	Olympus	Spinning disk Confocal Microscope	UPL X 4x air UPL APO 60x silicone oil

### 3.2.8. Genotyping of the *pik3ca-a* mutant allele *sa16936*

The *sa16936* allele was created by treating adult zebrafish males with ENU and first identified during the Zebrafish Mutation project in the group of Dirk Stemple at Sanger Institutes. It consists of a T to A conversion in exon 6 of the gene on Chromosome 11, which transforms the affected codon from encoding tyrosine to a Stop codon (HGVSC: c.780T>A) .

To genotype embryos or adult zebrafish for the *pik3ca-a* mutant allele *sa16936*, genomic DNA was prepared from either finclips or embryos as described in chapter 2.1. A multiplex PCR with 4 primers was set up using TitaniumTaq Polymerase as the following:

Component per sample	quantity
H <sub>2</sub> O	To 20µl
10x Titanium Taq buffer	2 µl
Primer 10µM each (4 in total)	1 µl (4 µl total)
dNTPs	1 µl
Titanium Taq enzyme	0.1 µl
Genomic DNA	0.3-0.5 µl

The PCR was performed as the following:

Reaction step	Temperature	Duration
Initial denaturation	95°C	2 min
Denaturation	95°C	30 sec
Primer annealing	56°C	30 sec
Polymerization	68°C	1 min
Final Hold	8°C	hold

30 cycles

This PCR will yield three different products, depending on the genotype of the used DNA sample:

- A control product of 578bp size (P1 and P2), independent of the genotype
- A wild-type product of 214bp (P2 and P3), which appears only if a wild-type allele is present

- A mutant product of 391bp (P1 and P4), which appears only if a mutant allele is present

### 3.2.9. Generation of the *ubs49* and *ubs50* alleles using CRISPR

The two *pik3ca-b* mutant alleles *ubs49* and *ubs50* were created according to the protocol published in Heutschi, 2015 (Master dissertation).

In short, two self-annealing primers, one containing the variant gRNA sequence, were used for a PCR producing a product of around 120 bp length. This product also contained a T7 promoter, which was subsequently used to transcribe the gRNA sequence *in vitro* into RNA using MEGASCRIP T7 Transcription Kit (Ambion). RNA was purified with LiCL precipitation.

gRNAs were co-injected into fertilized zebrafish eggs at one-cell stage with 0.6 ng/ $\mu$ l Cas9 protein (prepared by D. Heutschi) at a concentration of 100-300ng/ $\mu$ l. Efficiency of genetic editing was confirmed by isolation of genomic DNA of some of the injected embryos, PCR of the targeted locus and restriction digest or sequencing. Injected embryos were raised to adulthood and their F1 screened for mutant alleles by PCR and restriction digest and sequencing.

### 3.2.10. Genotyping of the *pik3ca-b* mutant allele *ubs49*

The *ubs49* allele consists of a 14bp deletion in exon 4 of *pik3ca-b* on Chromosome 23 (HGVS: c.429\_443del). To genotype embryos or adult zebrafish, genomic DNA was prepared according to chapter 2.1.

The *ubs49* allele eliminates a restriction cut site for AlwNI, which was used to identify the allele in the first F1 generation. A PCR using primers “*ubs49* P1” and “*ubs49* P2” using TitaniumTaq Polymerase was set up as the following:

Component per sample	quantity
H <sub>2</sub> O	To 20µl
10x Titanium Taq buffer	2 µl
Primer 10µM each	1 µl
dNTPs	1 µl
Titanium Taq enzyme	0.1 µl
Genomic DNA	0.3-0.5 µl

The PCR was performed as the following:

Reaction step	Temperature	Duration
Initial denaturation	95°C	2 min
Denaturation	95°C	30 sec
Primer annealing	54°C	30 sec
Polymerization	68°C	20 sec
Final Hold	8°C	hold

30 cycles

This PCR produces a 509 bp (495 bp for *ubs49*) fragment, which was digested with AlwNI (0.3 µl enzyme per 10µl PCR mix) by adding the enzyme directly to the reaction mix, incubation at 37°C for 30min and subsequent inactivation and denaturation of enzyme-DNA complexes at 80°C for 15min. This results in the wild-type product being cut to 342bp and 167bp whereas the mutant product can not be cut. Analysis of fragments was performed via gel electrophoresis and comparison to uncut control.

The *ubs49* allele can also be genotyped by multiplex PCR. Here, a PCR with 4 primers (“ubs49 P1-P4”) was set up using TitaniumTaq as the following:

Component per sample	quantity
H <sub>2</sub> O	To 20µl
10x Titanium Taq buffer	2 µl
Primer 10µM each (4 in total)	1 µl (4 µl total)
dNTPs	1 µl
Titanium Taq enzyme	0.1 µl
Genomic DNA	0.3-0.5 µl

The PCR was performed as the following:

Reaction step	Temperature	Duration	
<b>Initial denaturation</b>	95°C	2 min	
<b>Denaturation</b>	95°C	30 sec	
<b>Primer annealing</b>	68°C	30 sec	10 cycles
<b>Polymerization</b>	68°C	40 sec	Touchdown: T <sub>M</sub> lowered for 1°C every cycle
<b>Denaturation</b>	95°C	30 sec	
<b>Primer annealing</b>	58°C	30 sec	20 cycles
<b>Polymerization</b>	68°C	40 sec	
<b>Final Hold</b>	8°C	hold	

This PCR produces the 509 bp (495bp) control fragment, a 350 bp wild-type allele fragment and a 182 bp mutant allele fragment.

### 3.2.11. Genotyping of the *pik3ca-b* mutant allele *ubs50*

The *ubs50* allele consists of a 1bp insertion (HGVS c.294CdelinsGA) in exon 3 of *pik3ca-b* on Chromosome 23. To genotype adult zebrafish or embryos, genomic DNA was prepared according to chapter 2.1.

The *ubs50* allele eliminates a FokI restriction cut site, which was used to identify the allele in the first F1 generation. A PCR using primers “ubs50 P1” and “ubs50 P2” using TitaniumTaq Polymerase was set up as the following:

Component per sample	quantity
<b>H<sub>2</sub>O</b>	To 20µl
<b>10x Titanium Taq buffer</b>	2 µl
<b>Primer 10µM each</b>	1 µl
<b>dNTPs</b>	1 µl
<b>Titanium Taq enzyme</b>	0.1 µl
<b>Genomic DNA</b>	0.3-0.5 µl

The PCR was performed as the following:

Reaction step	Temperature	Duration
<b>Initial denaturation</b>	95°C	2 min
<b>Denaturation</b>	95°C	30 sec
<b>Primer annealing</b>	52°C	30 sec
<b>Polymerization</b>	68°C	30 sec
<b>Final Hold</b>	8°C	hold

30 cycles

This PCR produces a 551 bp fragment (552 bp for *ubs50*) which was digested with FokI by directly adding the enzyme to the reaction mix (0.3µl enzyme per 10µl PCR mix), incubation at 37°C for 40 min and subsequent inactivation and denaturation of enzyme-DNA complexes at 65°C for 15min. This results in the wild-type product being cut to 345 bp and 206 bp whereas the mutant product can not be cut. Analysis of fragments was performed via gel electrophoresis and comparison to uncut control.

The *ubs50* allele can also be genotyped by multiplex PCR. A detailed protocol using primers “ubs50 P1-P4” is available in Tschudin, 2021 (Master dissertation).

### 3.2.12. Antibody stainings against VE-cad and ZO-1

Antibody stainings were performed according to the protocol published in Blum *et al.*, 2008. Stained embryos were decapitated using forceps and trunk tissue mounted in 0.3% LMA in PBS in glass bottom dishes (MatTek) for microscopy.

Step	Reagent	Temperature/Duration
<b>Fixation</b>	Fixing Solution	4°C o/n
<b>Wash</b>	4x PBST	RT, 5-10 min each
<b>Permeabilization</b>	PBST&T	RT, 30 min
<b>Blocking</b>	Blocking Solution	4°C o/n
<b>1° Antibody</b>	1° AB in Blocking Solution	4°C o/n
<b>Wash</b>	6x PBST	4°C, 1 h each
<b>2° Antibody</b>	2° AB in Blocking Solution	4°C o/n

<b>Wash</b>	6x PBST	4°C 1h each, last wash o/n
-------------	---------	-------------------------------

### 3.2.13. RT-PCR of *pik3ca-b*

RNA was isolated from 48hpf wild-type embryos using RNeasy Plus Mini Kit (Qiagen) according to the manufacturer's protocol.

cDNA was transcribed using SuperScript III Reverse Transcriptase (Invitrogen) according to the manufacturer's protocol. Both oligo-dTT and a gene-specific primer were compared in two separate samples. For *pik3ca-b*, only the reverse transcription reaction using the gene specific primer resulted in amplification of the desired DNA fragment in the subsequent PCR.

Using the cDNA, a PCR was performed amplifying a 405bp fragment spanning exon 20, 21 and 22 of the published sequence. The fragment was purified using NucleoSpin Gel and PCR Clean-Up Kit and subsequently sent for sequencing at Microsynth AG (Allschwil, CH). Additionally, the fragment was cloned into a TOPO vector using the TOPO TA Cloning Kit from Invitrogen.

## 3.3. Imaging procedures and analysis

### 3.3.1. Image acquisition

Zebrafish embryos selected for the desired transgene and developmental stage were dechorionated manually and anesthetized in 1x E3 with 1x tricaine. Embryos were mounted in 0.7% LMA with 1x tricaine and PTU on glass bottom dishes (MatTek).

For inhibitor treatments, embryos were mounted in 0.3% agarose in E3 and PTU on glass bottom dishes (MatTek). The agarose drop was hardened by placing the dish



on a cooled ice block for 10-15 sec for three times with a rewarming interval of 1 min at room temperature in between.

Live imaging was generally performed in incubation chambers set to 28.5°C. Laser intensities were adjusted to obtain single saturated pixels. Z-step size was determined automatically and adapted to the needs of the experiment. Image acquisition at the SP5 confocal was performed employing bidirectional scanning at 400-700 Hz, with doubled pinhole size for the VE-cad-venus line.

Laser intensities at the Olympus SpinSR were adjusted to 35-50% depending on the expression level of the respective transgene. For imaging of the ZO1-tdTomato line, acquisition time was reduced to 35 milliseconds to avoid excess bleaching.

### **3.3.2. Image analysis**

Image analysis in general was performed using Fiji (free software). Unless stated otherwise, maximum projections of acquired stacks were used. If necessary, background was subtracted and brightness and contrast adjusted.

For data acquired with the SpinSR microscope (Olympus), Gaussian Blur Filter with radius 0.5-1 was applied whenever necessary.

The sizes of the vascular loops in the caudal vein plexus were analysed using the nucleus detection function in QuPath 0.2.3 (free software). Maximum projections of CVP tissue were used.

### **3.3.3. Statistical analysis**

Analysis of statistical significance of acquired data was performed using Prism Graphpad V6 and Microsoft Excel.

### **3.3.4. Figures**

Figures were designed and illustrated using the free version of BioRender ([www.biorender.com](http://www.biorender.com)), Adobe Illustrator and Microsoft PowerPoint.

### 3.4. Materials for BAC Project (Section VII: Appendix)

#### 3.4.1. Buffers, Solutions and Media

<b>Medium</b>	<b>Composition</b>
<b>Agar for microbiology</b>	agar powder for preparation of bacterial plates provided by Applichem
<b>Biotin</b>	0.2 mg/ml d-Biotin in ddH <sub>2</sub> O source: Sigma-Aldrich sterile filtered stored at 4°C up to 2 months
<b>2-Deoxy-Galactose</b>	20% w/v 2-deoxy-Galactose in ddH <sub>2</sub> O sterile filtered stored at -20°C up to 1 year
<b>DNA loading dye</b>	30% w/v glycerol 20% w/v Orange G in ddH <sub>2</sub> O stored at -20°C
<b>Glycerol</b>	20% w/v glycerol in ddH <sub>2</sub> O source: Roth autoclaved
<b>LB medium</b>	1% w/v tryptone 0.5% w/v yeast extract 1% w/v NaCl in ddH <sub>2</sub> O autoclaved
<b>Leucin</b>	10 mg/ml L-Leucin in ddH <sub>2</sub> O source: Roth heated, cooled and sterile filtered
<b>Magnesium sulfate</b>	1 M MgSO <sub>4</sub> • 7 H <sub>2</sub> O
<b>1x M9 medium</b>	42 mM Na <sub>2</sub> HPO <sub>4</sub> 22 mM KH <sub>2</sub> PO <sub>4</sub> 18.5 mM NH <sub>4</sub> Cl 8.5 mM NaCl in ddH <sub>2</sub> O autoclaved
<b>5x M63 medium</b>	75.5 mM (NH <sub>4</sub> ) <sub>2</sub> SO <sub>4</sub> 500mM KH <sub>2</sub> PO <sub>4</sub> 9 µM FeSO <sub>4</sub> • 7 H <sub>2</sub> O in ddH <sub>2</sub> O

	autoclaved
<b>50x TAE</b>	2M TRIS-Base 5.71% v/v glacial acetic acid 50mM EDTA in ddH <sub>2</sub> O
<b>25x Tricaine (Tricainemesylate, MS-222)</b>	Sigma-Aldrich 0.4% w/v in ddH <sub>2</sub> O, pH=7 adjusted with 1M Tris-HCl Stored at -20°C

### 3.4.2. Antibiotics

Antibiotic	Stock concentration	Working concentration
Ampicillin	100 mg/ml	100 µg/ml
Chloramphenicol	34 mg/ul	12.5 µg/ml

### 3.4.3. *Escherichia coli* Strains

Strain	Genotype	Source
<b>DH10β</b>	<i>F- mcrA Δ(mrr-hsdRMS-mcrBC) Φ80dlacZΔM15 ΔlacX74 endA1 recA1 deoR Δ(ara,leu)7697 araD139 galU galK nupG rpsL λ--</i>	NEB
<b>SW102</b>	<i>F- mcrA Δ(mrr-hsdRMS-mcrBC) Φ80dlacZΔM15 ΔlacX74 deoR recA1 endA1 araD139 Δ(ara, leu)7649 galU galK rpsL nupG [λcl857 (cro-bioA) &lt;&gt; tet]</i>	NCI- Frederick
<b>Top10</b>	<i>F- mcrA Δ(mrr-hsdRMS-mcrBC) φ80lacZΔM15 ΔlacX74 nupG recA1 araD139 Δ(ara-leu)7697 galE15 galK16 rpsL(Str<sup>R</sup>) endA1 λ-</i>	Invitrogen

### 3.4.4. BACs and plasmids

Name	Description	Antibiotic resistance marker	Reference
<b>pTARBAC2(CH73-357K2) NS</b>	Modified pTARBAC2, contains zebrafish endogenous <i>cdh5</i> locus exon 3 was removed tol2 sites and $\beta$ -chrystalline:mkate marker added	Chloramphenicol	Original BAC from BACPAC Resources Center  Modified by Niels Schellinx
<b>pGalK</b>	E.coli <i>GalK</i> gene used for 2-step BAC recombineering	Ampicillin	Warming <i>et al.</i> , 2005
<b>pC1(loxP-cdh5-tagRFP-loxP-mcherry-nls)</b>	Plasmid containing <i>cdh5</i> CDS tagged with RFP, flanked with loxP sites and followed by mcherry-nls	Ampicillin	This study  Synthesized by ATG:biosynthetics GmbH
<b>pC2(loxP-cdh5-tagRFP-loxP-mcherry-nls)</b>	Plasmid containing <i>cdh5</i> CDS tagged with RFP, flanked with loxP sites and followed by mcherry-nls	Ampicillin	This study  Synthesized by ATG:biosynthetics GmbH
<b>pCS2FA-tol2</b>	Plasmid containing <i>tol2</i> transposase gene with SP6 promoter	Ampicillin	Addgene.org (Mackey <i>et al.</i> , 2020)

### 3.4.5. Fish lines

Name	Allele designation	Reference
<b>ABC</b>	Wild-type	ZIRC, Oregon
<b>TU</b>	Wild-type	ZIRC, Oregon
<b>VE-cadherin 4bp deletion</b>	Ubs8	Sauteur <i>et al.</i> , 2014

### 3.4.6. Oligonucleotides

<b>Name</b>	<b>Sequence 5' – 3'</b>
<b>C1 galK fw</b>	TAGGGATTTTCCAATCAGGGAAAACGACTGTTGAAGAGACCAAACCTC TGCCTGTTGACAATTAATCATCGGCA
<b>C1 galK rev</b>	CATAAAATATGATAAGAAATACACAATTATATATAAAAACGATCGCATA CTCAGCACTGTCCTGCTCCTT
<b>C2 galK fw</b>	CTACAAGGCATGAATTATCATACAGATATTTGTTTTGTTGTTTTCTGCA GCCTGTTGACAATTAATCATCGGCA
<b>C2 galK rev</b>	CGGATCTCTCCAAATTAAGTGTGATCCATTTGTTTACAAGACCGTCT ACTCAGCACTGTCCTGCTCCTT
<b>C1 hom fw</b>	TAGGGATTTTCCAATCAGGGAAAACGACTGTTGAAGAGACCAAACCTC TG
<b>C1 hom rev</b>	CATAAAATATGATAAGAAATACACAATTATATATAAAAACGATCGCATA C
<b>C2 hom fw</b>	CTACAAGGCATGAATTATCATACAGATATTTGTTTTGTTGTTTTCTGCA G
<b>C2 hom rev</b>	CGGATCTCTCCAAATTAAGTGTGATCCATTTGTTTACAAGACCGTCT AC
<b>C1 seq 1 fw</b>	TCTGATTTTCCAGAGAAGGC
<b>C1 seq 1 rev</b>	ACTGGTATCTTTCTTTCTTAAAGG
<b>C1 seq 2 fw</b>	CACCTTTAAGAAAGAAAGATACCAG
<b>C1 seq 2 rev</b>	ACAATGAGGATTACGATTACCAG
<b>C 1 seq 3 fw</b>	TCATTACCATCCTGGTAATCG
<b>C1 seq 3 rev</b>	ACCATTCAACTTATGTCCCAG
<b>C1 seq 4 fw</b>	CAGATATTGTGACCTGCCG

<b>C1 seq 4 rev</b>	CTCATGAATTCCTTAATGATTGC
<b>C1 seq 5 fw</b>	ATGAGGTTCAAGGTTACATG
<b>C1 seq 5 rev</b>	GGTGTCTTTTCACACAGTATCTC
<b>Ubs8 out fw</b>	TTGGTGTAAGTACAATGGGG
<b>Ubs8 out rev</b>	ACAGTCTTGGTGTTACCATTGGG
<b>Ubs8 mut</b>	CTGATGGATCCAGATTGGAATC
<b>Ubs8 wt</b>	ATCCCCGTTTTCGATTCTGAC

### 3.4.7. Other PCR reagents and DNA purification kits

<b>Reagent</b>	<b>Manufacturer</b>
dNTP mix 10mM each	Promega
5x Q5 buffer	NEB
Q5 polymerase	NEB
10x Taq Thermopol buffer	NEB
Taq Polymerase	NEB
NucleoSpin Gel and PCR Clean-Up Kit	Macherey-Nagel
NucleoSpin Plasmid Mini Kit	Macherey-Nagel
NucleoBond BAC 100 Kit	Macherey-Nagel

### 3.4.8. Microscopes and Binoculars

<b>Microscope</b>	<b>Manufacturer</b>	<b>Information</b>	<b>Objectives</b>
Leica M205 FA with Lumencor Sola FISH Light engine	Leica Lumencor	Fluorescence equipped binocular	

<b>SP5-II-Matrix</b>	Leica	Confocal Microscope	HC PL Fluotar 10x air  HCX PLAN APO CS 40x water
----------------------	-------	------------------------	--

### 3.4.9. Restriction Enzymes

<b>Enzyme name</b>	<b>Manufacturer</b>	<b>Stock concentration</b>
<b>DpnI</b>	NEB	20000 U/ml
<b>BamHI</b>	NEB	20000 U/ml

### 3.4.10. Protocol for BAC recombineering

The following protocol is based on and optimized from Warming *et al.*, 2005, protocol 3, as well as Schellinx, Niels, *Deciphering cytoskeletal interactions during blood vessel morphogenesis in vivo*, Doctoral thesis, 2018.

BAC recombineering is a method to edit large bacterial artificial chromosomes in order to exchange, insert or delete fragments of up to several kb size at specific loci. This method consists of two successive rounds of recombination reactions and selection for successful editing after each reaction. In this work and following the published protocol of Warming *et al.*, 2005, the *E. coli GalK* gene is first inserted into the desired target sequence of the BAC and colonies selected for surviving on carbon restrictive but galactose containing minimal medium plates. In the second step, the *GalK* gene is exchanged with the actual insert at the target site of the BAC and bacteria selected against expression of *GalK*.

### **Generation of insert fragments**

For each modification of the parental BAC two DNA fragments were designed and synthesized. BAC Recombineering relies on homologous sequences of the insert with the targeted locus on the BAC, which is why homology arms of 50bp were added to both 5' and 3' ends of the inserts. The primers for PCR synthesis of the inserts thus always contain the respective 50bp homologous sequence at their 5' end (forward and reverse primer).

In general, sequence correctness is essential for recombineering. To synthesize the inserts, Q5 Polymerase (NEB) was used as it possesses 5'-3'-endonuclease activity and high fidelity (NEB, 2022).

To synthesize the insert fragment containing the *Galk* gene, a PCR reaction was set up as the following:

<b>Component</b>	<b>Final concentration</b>
H <sub>2</sub> O	To 25 µl
5x Q5 Reaction buffer	1x
Forward primer	0.5 µM
Reverse primer	0.5 µM
dNTPs	200 µM
Q5 Polymerase	0.02 U/µl
pGalk	1-5 ng

The PCR reaction was performed as the following:

<b>Reaction step</b>	<b>Temperature</b>	<b>Duration</b>
<b>Initial denaturation</b>	95°C	1 min
<b>Denaturation</b>	95°C	30 sec
<b>Primer annealing</b>	60°C	30 sec
<b>Polymerization</b>	72°C	30 sec
<b>Final extension</b>	72°C	2 min
<b>Final Hold</b>	8°C	hold

This PCR typically yields a DNA fragment of 1331bp (if 50bp homology arms were used). After completion of the PCR program, methylated plasmid template DNA was



digested using 1µl DpnI per 25µl PCR for 30min at 37°C (removal of template plasmid was found to be essential to avoid false-positives in the selection for *galk* expression). After DpnI digestion, the *galk* DNA fragment was purified from the mix using the Nucleo-Spin Gel and PCR clean-up Kit (Macherey-Nagel).

Similar to the *galk* insert, the target insert was amplified from plasmid p(loxP-cdh5-tagRFP-loxP-mcherry-nls) using homology arm containing primers. Here, again Q5 polymerase was used to ensure sequence reliability. Since cassette 1 and 2 (C1 and C2) only differed in their respective insert locus, their only difference were the homology arms. Duration and temperature of annealing and polymerization steps were adjusted as the following:

Cassette	Annealing duration	Annealing temperature	Polymerization duration	Polymerization temperature	Fragment size
C1	30 sec	66°C	2min 40sec	72°C	4646bp
C2	30 sec	72°C	2min 40sec	72°C	4646bp

Similar to the *galk* product, the insert fragments for the desired modifications were digested with DpnI and subsequently purified using the Nucleo-Spin Gel and PCR clean-up Kit (Macherey-Nagel).

### ***Preparation of minimal medium agar plates***

To obtain restrictive medium plates for bacterial selection during BAC recombineering, the following recipe was used. Each recipe yields 20 plates (1l total and 50ml per plate).

Galactose/2-desoxy-galactose plates:

Component	Quantity	Procedure
ddH <sub>2</sub> O	400 ml	
agar	7.5 g	Mix, autoclave
5x M63 medium	100 ml	Add to medium

<b>1M MgSO<sub>4</sub></b>	500 µl	Add to medium, cool down to 50°C afterwards
<b>Carbon source (galactose <u>or</u> 2-desoxy-galactose)</b>	5 ml	Add to medium
<b>Biotin</b>	2.5 ml	Add to medium
<b>Leucine</b>	2.25 ml	Add to medium
<b>Chloramphenicol</b>	188 µl	Add to medium

The medium was poured into sterile petri dishes while still being fluid and subsequently solidified while cooling down to room temperature. Directly after pouring, any remaining air bubbles were eliminated using a handheld gas burner. Per petri dish, approximately 50ml of medium were used. Solidified plates were stored at 4°C for up to one month.

To obtain 20 McConkey agar plates, the following recipe was used:

<b>Component</b>	<b>Quantity</b>	<b>Procedure</b>
<b>McConkey agar</b>	25g	
<b>ddH<sub>2</sub>O</b>	400ml	Mix, autoclave, cool down to 50°C
<b>Galactose</b>	5 ml	Add to medium
<b>Chloramphenicol</b>	188 µl	Add to medium

Approximately 50ml of medium each were poured into a total of 20 petri dishes and plates allowed to solidify and cool to room temperature. Air bubbles were again eliminated using a handheld gas burner. After cooling, plates were stored at 4°C for up to one month.

### ***BAC Recombineering procedure***

BAC Recombineering is based on usage of the particular *E. coli* strain SW102. This strain expresses a set of λ-prophage derived proteins facilitating DNA recombination relying on sequence homology between inserts and the BAC backbone (backto introduction). Since these genes are controlled by a heat-shock inducible promoter, recombination is easily inducible in laboratory conditions by heat-shocking of

bacterial cultures. Additionally, the SW102 strain lacks the *galK* gene present in other *E.coli* strains, which allow for selection of recombinants using colony growth on medium containing galactose as the only carbon source. Similarly, this feature of SW102 *E.coli* allows for selection against *galK* presence in the second step of recombineering in which the *galK* insert is replaced by the desired modification.

The following protocol was adapted for homologous sequences in the desired insert from “Deciphering cytoskeletal junctional interactions during blood vessel morphogenesis *in vivo*”, the doctoral thesis of Niels Schellinx, a former PhD student in the group.

*a) Transformation of the parental BAC into SW102 E.coli*

30ng of purified parental BAC DNA are transformed into electrocompetent SW102 *E.coli* by electroporation. Bacteria were recovered in 500µl standard LB medium at 32°C for 1 hour shaking at 500 rpm and then plated on LB agar plates containing 12.5 µg/ml chloramphenicol. Plates were incubated at 32°C for approximately 16-20 hours.

*b) Inoculation of BAC containing culture and preparation for recombineering*

BAC transformed SW102 *E.coli* were inoculated in 5ml standard LB medium supplied with 12.5 µg/ml chloramphenicol and incubated for 12-16 hours at 32°C in a shaking incubator.

The following morning 500 µl of the overnight culture were diluted in 25ml standard LB with chloramphenicol in a 200ml Erlenmeyer flask and incubated in a shaking incubator at 32°C. The culture was grown to an OD<sub>600</sub> of approximately 0.6 (2-3 hours).

*c) Heat-shock of SW102 culture to induce expression of recombineering genes*

Once the bacterial culture had reached exponential growth phase at an OD<sub>600</sub> of 0.6, a water bath was set to 42°C. 12ml of the culture were transferred to a fresh

Erlenmeyer flask (induced sample) and placed in the water bath for exactly 15min. The remaining culture was kept at 32°C as un-induced control. Simultaneously, a centrifuge (large enough for 15-50ml falcon tubes) was cooled to 2-3°C. An ice bucket was filled with a mix of water and ice to form a fast-cooling ice-water slurry. A falcon tube filled with 50ml ddH<sub>2</sub>O was placed into the cooling slurry to use for the following washing steps.

*d) Preparation of salt-free SW102 cultures for introduction of insert DNA*

After the 15min of heat-shocking the induced sample, both samples were cooled in the ice-water slurry for 2-3min and then transferred into pre-cooled 10ml falcon tubes with a rounded convex bottom. Both cultures were subsequently pelleted in the cooled centrifuge at 2-3°C for 5min at 4200rpm.

The supernatant was discarded and the pellet re-suspended in 1ml ice-cold ddH<sub>2</sub>O by gently rotating the tubes in the ice-water slurry, before carefully adding another 9ml of ddH<sub>2</sub>O. The suspension was then centrifuged again at 2-3°C for 5min at 4200rpm. The washing process was repeated a total of three times. After the last resuspension, the culture was carefully transferred to a 15ml conical falcon tube allowing for an easier harvest of cells in the following steps.

The supernatant of the now salt-free cultures was ultimately drained by quickly inverting the tubes on a paper towel. The pellets were re-suspended in 100µl ddH<sub>2</sub>O by very gently pipetting with a cut pipette tip.

*e) Electroporation of the galK insert DNA into salt-free SW102 cultures*

Both induced and un-induced cultures were split into two pre-cooled electroporation cuvettes (with or without insert DNA) to obtain 4 samples:

- Induced, with DNA added
- Induced, no DNA added
- Un-induced, with DNA
- Un-induced, no DNA added

To the cultures assigned “with DNA”, a total of 100ng of purified *galK* insert DNA was added. Cultures were then electroporated by pulsing twice with 25µF, 1.75kV and

200Ω.

Directly after electroporation cells were recovered in 1ml standard LB without antibiotics at 32°C for 1hour in a shaking heat block (750rpm).

*f) Preparation of cultures for selection on minimal plates and plating*

All four samples were pelleted quickly in a table top centrifuge at 11,000rpm for 30sec. The supernatant was removed and cells carefully re-suspended in 1ml M9 medium. This washing step was repeated three times to remove all nutrients present in the LB medium but provide essential salts to the cells.

Cultures were now serially diluted 1:10 and 1:100 in M9 medium. A total of 100μl volume of both dilutions and per sample were plated on galactose containing minimal plates. The eight plates total were then incubated at 32°C for 3 days.

*g) Selection on McConkey plates*

After 3-3.5 days the first colonies should become visible on the plates with induced sample and DNA added. No other plate should show any colonies; if they do, I advise to restart the experiment with fresh material and new plates.

When the first colonies became visible, a few of them were carefully picked using a pipette tip and streaked out on McConkey plates with galactose and chloramphenicol. Expression of the *galK* gene leads to fermentation of galactose in the medium which lowers the pH of the surrounding area. This pH change converts the neutral red in the medium from red to pink color and colonies appear as bright pink spots. After streaking, the plates were incubated at 32°C for around 16 hours. This particular step simplifies selection of pure colonies derived from a single *galK* containing cell. However, I recommend to also confirm the presence of the *galK* insert either via colony PCR or by quickly mini-prepping from a culture and doing PCR on the harvested DNA. In my case, presence of *galK* gene was confirmed using colony PCR.

*h) Introduction of insert DNA to the galK containing SW102 culture*

A single bright pink colony (which was preferably also tested for *galK* by PCR) was inoculated in 5ml standard LB with chloramphenicol at 32°C overnight in a shaking incubator.

In order to obtain salt-free SW102 culture, growing until exponential phase, induction via heat-shock, washing and electroporation of the culture was repeated as described in steps *b-e*. This time however, 100ng of the desired insert DNA was added to the DNA receiving samples.

After electroporation, cells were recovered in 10ml standard LB medium without antibiotics in 200ml Erlenmeyer flasks for 4 hours at 32°C in a shaking incubator. Afterwards cells were washed three times in M9 medium similar to step *f*, serially diluted and plated on Desoxy-galactose containing plates. The 8 plates in total were incubated at 32°C for 3-3.5 days.

*i) BAC miniprep to secure the unrecombined insert containing repetitive or homologous sequences (e.g. loxP sites) and transformation of intact BAC into DH10 $\beta$*

Homologous, repetitive DNA sequences in the introduced insert, such as loxP sites, pose the danger of spontaneous recombination in the SW102 bacteria. To circumvent this, the BAC containing these sites should not stay in the SW102 strain for any longer than is absolutely needed.

The evening the first colonies become visible on the 2-desoxy-galactose containing plates (here again only the plates containing induced and DNA added sample should show colonies), 30 colonies were inoculated in 3ml LB medium with chloramphenicol and incubated shaking over night at 32°C. Additionally, native DH10 $\beta$  cells were inoculated in standard LB medium without antibiotics shaking over night at 37°C. In contrast to SW102, they do not contain the genes required for recombination and are thus suitable hosts for BAC with homologous sequences.

The next early morning the cultures were quickly but carefully miniprepped according to Bouvier *et al.*, 2011. BAC DNA was ultimately resuspended in 10 $\mu$ l ddH<sub>2</sub>O.

Following suit and using the BAC DNA, screening PCRs were performed to identify

samples in which the BAC had not spontaneously recombined yet but still contained the intact insert. I recommend using primers at least partially spanning the loxP sites themselves, so a PCR product can only be produced and become visible in the gel if the loxP sites did not spontaneously recombine and are in fact intact. A small product designed to prove integrity is sufficient and time-saving.

Simultaneously, the DH10 $\beta$  cells were pelleted and washed three times in 1ml cold ddH<sub>2</sub>O to eliminate salts. The pellet was ultimately solved in 400 $\mu$ l ddH<sub>2</sub>O and divided into 8 pre-cooled electroporation cuvettes, each cuvette containing 50 $\mu$ l bacteria solution. Cuvettes were kept on ice until electroporation.

Immediately after confirmation of the intact insert in the BAC sample, 2 $\mu$ l of the right BAC DNA samples were transformed into the DH10 $\beta$  cells via electroporation using 25 $\mu$ F, 1.75kV and 200 $\Omega$  and pulsing twice. Cells were recovered in standard LB without antibiotics at 37°C for 1h shaking at 350rpm and then 100 $\mu$ l per sample plated on standard LB plates containing chloramphenicol. Plates were incubated at 37°C for 2-3 days. Colonies were tested for BAC integrity and presence of the desired modification by PCR.

### 3.4.11. Overlapping PCR sequencing to confirm integrity

Whole BAC DNA was isolated from DH10 $\beta$  host cells using Nucleobond BAC100 Kit from Macherey-Nagel.

A series of 5 PCRs on overlapping fragments of the BAC insert were performed, fragments isolated from the gel by using NucleoSpin Gel and PCR Clean-Up Kit (Macherey-Nagel) and fragments were sent for Sanger sequencing at Microsynth company (Balgach, Switzerland). PCRs were performed using Taq Polymerase (NEB), 1x Thermopol buffer, 32 cycles and an initial denaturation step of 2min at 95°C as the following:

Name	Size	Primer	T <sub>m</sub>	Extension	Contained insert region
<b>Check PCR 1</b>	919 bp	C1 seq 1 fw C1 seq 1 rev	43°C	1min	Exon1, homology arm, loxP site, <i>cdh5</i> CDS

<b>Check PCR 2</b>	1162 bp	C1 seq 2 fw C1 seq 2 rev	44°C	1min 10sec	<i>cdh5</i> CDS
<b>Check PCR 3</b>	1022 bp	C1 seq 3 fw C1 seq 3 rev	45°C	1 min	<i>cdh5</i> CDS <i>tagRFP</i>
<b>Check PCR 4</b>	927 bp	C1 seq 4 fw C1 seq 4 rev	43°C	55sec	<i>tagRFP</i> , <i>cdh5</i> CDS Rabbit $\beta$ -Globin PolyA loxP site, <i>nls-mcherry</i>
<b>Check PCR 5</b>	1325 bp	C1 seq 5 fw C1 seq 5 rev	46°C	1min 20sec	<i>nls-mcherry</i> , SV40 PolyA, homology arm, intron 1

### 3.4.12. BAC restriction digest

4 $\mu$ g of purified BAC DNA were digested as the following:

<b>Component</b>	<b>Volume</b>
<b>BAC DNA</b>	to 4 $\mu$ g
<b>10x CutSMart buffer (NEB)</b>	15 $\mu$ l
<b>BamHI</b>	3 $\mu$ l
<b>ddH<sub>2</sub>O</b>	to 150 $\mu$ l

BAC DNA was digested at 37°C for 3 hours. Subsequently, 500 $\mu$ l 100% ethanol were added to the sample and the sample centrifuged at 4°C for 20min at 20000 rpm. The supernatant was removed and the pellet air-dried. The pellet was reconstituted in 20  $\mu$ l ddH<sub>2</sub>O and products separated and analysed in an ethidium bromide containing agarose gel under UV light.



### 3.4.13. *In vitro* transcription of *tol2* mRNA

3µg of pCS2FA-*tol2* plasmid was digested with NotI at 37°C for 1 hour and subsequently purified by isopropanol-precipitation, washed twice in 70% EtOH and the pellet solved in 12µl ddH<sub>2</sub>O. 1µg of linearized vector was used to perform *in vitro* mRNA transcription using mMessage mMachine SP6 Transcription Kit (Ambion) according to the manufacturer's protocol. RNA was precipitated using LiCl and resuspended in ddH<sub>2</sub>O to 200 ng/ul and stored at -80°C until usage.

### 3.4.14. BAC injections

The morning of the injection experiment, the injection mix was prepared on ice as the following:

Component	Quantity/dilution
Fresh purified BAC (Nucleobond BAC100 Kit)	25ng/µl
Tol2 mRNA	20ng/µl
ddH <sub>2</sub> O	To 10µl

Approximately 2-3 nl of injection mix was injected into zebrafish eggs at 1-cell-stage as described in chapter 3.1.3.

### 3.4.15. *ubs8* genotyping

Finclip samples of adult fish were used to genotype for *ubs8* according to Sauteur *et al.*, 2014. DNA samples were prepared as described in chapter 2.1.5.



# IV

## Results

PI3-Kinase  $\alpha$  signaling has been implicated in various conserved cell behaviors such as migration and proliferation across many different vertebrate species. In the vertebrate endothelium, PI3-Kinase  $\alpha$  has been shown to exert essential functions in both mouse and zebrafish models as well as in cell culture. Here, among others, signaling by PI3-Kinase  $\alpha$  is important for EC migration (Graupera *et al.*, 2008), arteriovenous differentiation (Hong *et al.*, 2006) and development of lymphatic vessels (Coso *et al.*, 2014).

Recent studies have implicated a role for PI3-Kinase  $\alpha$  in vascular morphogenesis and dynamic vessel remodeling (Angulo-Urarte *et al.*, 2018). Loss of PI3-Kinase  $\alpha$  signaling by genetic mutation or inhibitor treatment resulted in defective cell rearrangements in mouse retina and zebrafish trunk vasculature, respectively. However, a detailed understanding of the concrete function of PI3-Kinase  $\alpha$  during vascular morphogenesis requires further extensive analyses.

Previous work from our group has described cellular mechanisms underlying EC elongation and intercalation during blood vessel formation and remodeling. Based on this knowledge, this thesis focuses on further elucidating the role of PI3-Kinase  $\alpha$  signaling in EC rearrangements during vascular morphogenesis.

## 4.1. The zebrafish genome contains two genes encoding *Pik3ca*

To investigate the role of PI3-Kinase  $\alpha$  signaling in vascular development, I aimed to use a genetic knockout approach to inactivate this signaling pathway in zebrafish embryos. As a starting point, I investigated the genetic background of PI3-Kinase  $\alpha$  in the zebrafish genome and focused on the gene *pik3ca* (*PI3-Kinase  $\alpha$ -catalytic subunit*, nomenclature derived from mouse genetics), which encodes the catalytic subunit of the kinase. Due to genomic duplication events during teleost evolution, zebrafish often have more than one copy of a particular gene. At the start of this project, only one gene located on chromosome 11 was annotated as *Pik3ca* encoding (ZDB-GENE-130409-1). Fortunately, for this gene, a putative knockout allele *sa16936* (Fig. 8) was commercially available.

To test whether there are other *Pik3ca*-encoding loci in the zebrafish genome, tBLASTn analysis of the known *Pik3ca* protein sequence against translated RNA was performed using the freely available tools at [www.blast.ncbi.nlm.nih.gov](http://www.blast.ncbi.nlm.nih.gov). The BLAST revealed the previously described gene on chromosome 11 as well as a second, undescribed gene on chromosome 23 (ZDB-GENE-070112-492). The two amino acid sequences of the translated cDNAs are almost 80% identical, with more than 90% identical catalytic domains (Fig. 8 A).

Interestingly, an earlier study focusing on the role of ENOX1 in the endothelium performed quantitative RNA sequencing in zebrafish ECs after downregulation of ENOX1 (Venkateswaran *et al.*, 2010). Their data also contained reads of the second *pik3ca* gene on Chromosome 23. The authors already defined the gene as *Pik3ca* encoding, but this annotation had so far not been transcribed into the common databases at zfin.org or ENSEMBL. To validate the expression of this putative second *pik3ca* gene, I performed RT-PCR on RNA derived from 48hpf wild-type embryos. Subsequent sequencing of the obtained fragment confirmed expression of the second gene on chromosome 23 (Fig. 8 C).

In summary, there are two distinct genes encoding *Pik3ca* in the zebrafish genome. A new terminology for these two genes is proposed and is used throughout the rest of this thesis: *pik3ca-a* (Chr.11) and *pik3ca-b* (Chr.23) (Fig. 8).

To investigate the tissue specificity of *pik3ca* expression, mRNA levels of both *pik3ca* genes were compared in ECs vs. non-ECs by using the published database in Lawson *et al.*, 2020. In zebrafish embryos, expression of both genes is detected in both the endothelium as well as non-ECs. Both genes are expressed higher in the endothelium (Fig. 8 B) than in other tissues. Interestingly, *pik3ca-b* seems to be more vascular-specific than *pik3ca-a*, as it is more than 4 times higher expressed in the endothelium than in non-ECs (log2 fold change 2,572).

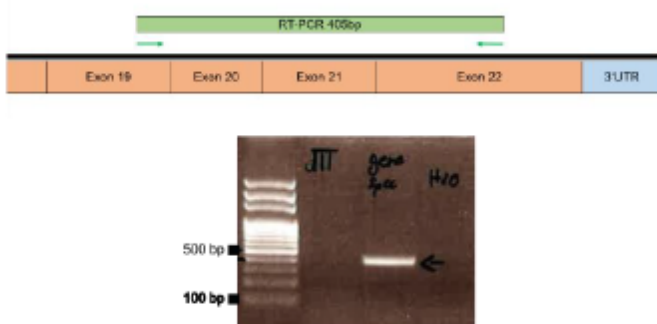
I further compared total RNA levels of both *pik3ca* paralogs during embryonic to larval development using the published zebrafish RNA expression atlas from White *et al.*, 2017. Whereas *pik3ca-b* expression only starts between 25-28 hpf, RNA of *pik3ca-a* can be detected from one-cell stage on and continuously throughout development (Fig. 8 D).



**B**

Gene name	Position in genome	Ensembl ID	ZDB-gene ID	Expression non-EC	Expression Endothelium	Log2 fold change
pik3ca-a	Chr. 11: reverse strand 34,488,869–34,522,249	ENSDARG 00000075456	ZDB-GENE- 130409-1	269,63	646,03	1,261
pik3ca-b	Chr. 23: reverse strand 44,190,852-44,233,410	ENSDARG 00000060597	ZDB-GENE- 070112-492	152,1	904,2	2,572

**C**



**D**

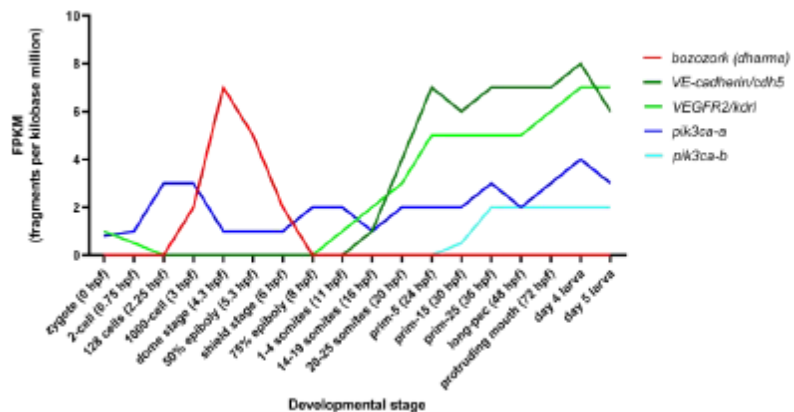


**Fig 8: Pik3ca (p110 $\alpha$ ) is encoded by two paralogs in the zebrafish genome**

**A** Box shade alignment of Pik3ca-a and Pik3ca-b amino acid sequence, red box indicates catalytic domain at the C-terminus of the two isoforms. **B** Tabular summary of *pik3ca-a* and *pik3ca-b* expression profile in ECs vs. non-ECs according to Lawson *et al.*, 2020. Expression measured in arbitrary reference units. **C** RT-PCR on *pik3ca-b* RNA from 2dpf embryos amplifying a 405bp fragment of the 3' region. **D** Expression level of *pik3ca-a* and *pik3ca-b* (blue lines) over developmental stage in the zebrafish embryo. Expression of bozozork (red line) indicates MZT, expression of endothelial specific genes indicated by RNA levels of VE-cadherin/cdh5 (dark green) and VEGFR2/kdrl (bright green). Data according to White *et al.*, 2017.

## 4.2. PI3-Kinase $\alpha$ signaling is active in zebrafish trunk primary ISVs and DLAV

Next, I asked in which vessels PI3-Kinase  $\alpha$  signaling is active in the zebrafish vasculature. Although classical *in situ* hybridization or antibody stainings would show where the kinase is expressed, such analyses are not suited to study the activity of the protein. Therefore, a different way to detect PI3-Kinase  $\alpha$  activity in the zebrafish endothelium was needed.

Active PI3-Kinase  $\alpha$  signaling in ECs results in activation of downstream targets such as Akt. Thus, respective cellular responses can be employed as a way to confirm PI3-Kinase activity. I used the endothelial specific transgenic reporter line *Tg(fli:FOXO1b-EGFP)<sup>bns515</sup>* in combination with an endothelial nuclear marker (*Tg(kdrl:nls-mcherry)<sup>is4</sup>*) to examine the localization of FOXO, a downstream effector of Akt. In homeostatic conditions, the transcription factor FOXO is retained in the cytoplasm due to phosphorylation by active pAkt, ultimately targeting FOXO for proteasomal degradation. Upon loss of PI3-Kinase signaling, Akt is rendered inactive and FOXO translocates to the nucleus (Brunet *et al.*, 1999, Fig 9 A, B).

Consequently, relocalization of fluorescently tagged FOXO in ECs would implicate acute loss of PI3-Kinase signaling and, in turn, imply that signaling had been active in the respective cells before.

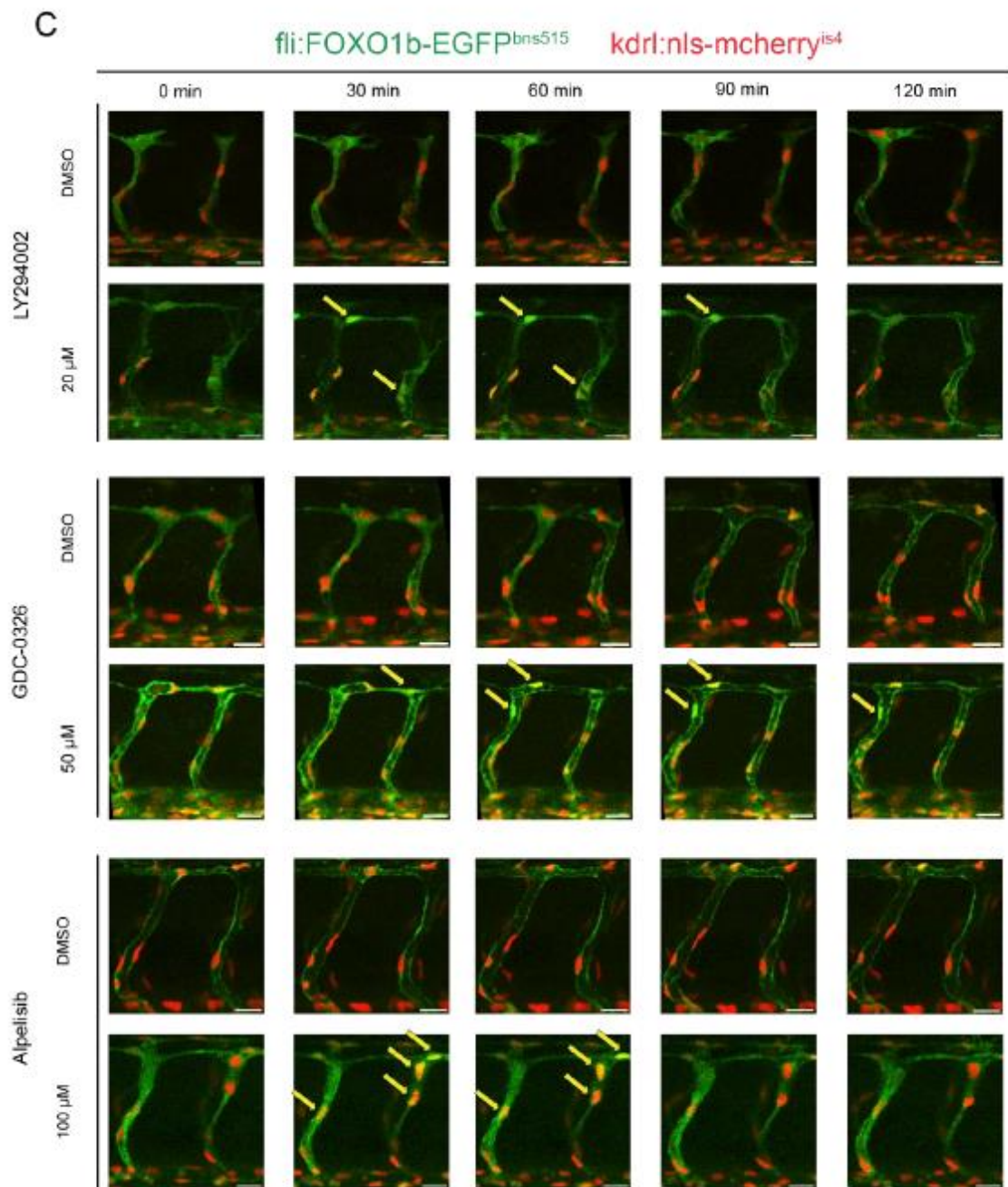
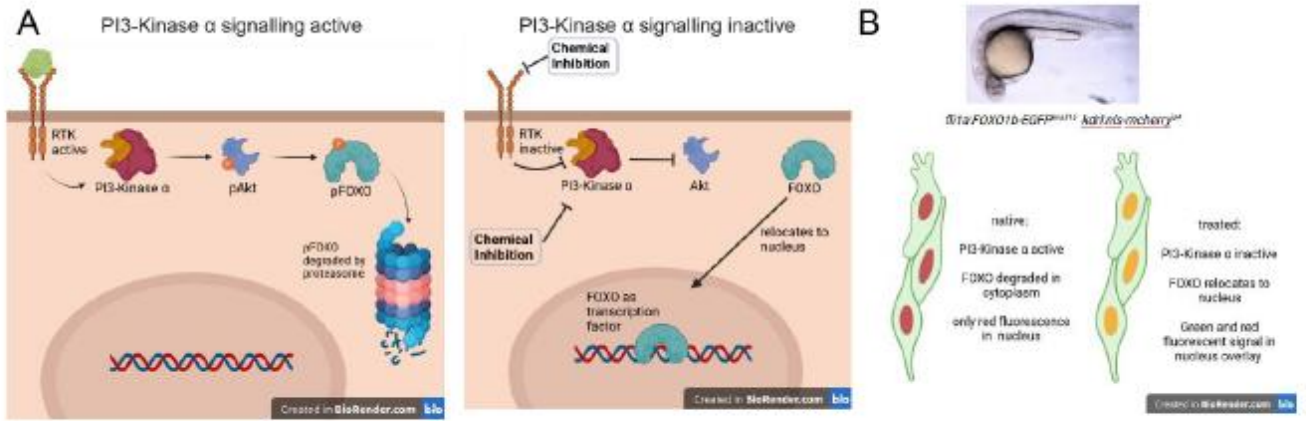




**Fig 9: PI3-Kinase  $\alpha$  signaling is active in primary ISVs and DLAV**

**A** Schematic illustration of regulation of FOXO localization by Akt downstream of PI3-Kinase  $\alpha$  signaling: Active PI3-Kinase  $\alpha$  leads to active Akt which phosphorylates FOXO in the cytoplasm. pFOXO is degraded by the proteasome. Upon inactivation of PI3-Kinase  $\alpha$  signaling via loss of RTK input or by chemical treatment, Akt is inactive and FOXO no longer phosphorylated. FOXO translocates to the nucleus where it acts as a transcription factor. Figure created with Biorender.

**B** Schematic representation of the FOXO assay displayed in the experiment in C: Yellow nuclei serve as readout for inactivated PI3-Kinase in the fluorescence overlay. Figure created with Biorender.

**C** Inactivation of PI3-Kinase  $\alpha$  signaling in DA, primary ISVs and DLAV by chemical treatment in double transgenic zebrafish embryos at 26-29 hpf. FOXO is labelled green, nuclei in red. Yellow arrows indicate yellow nuclei with elevated levels of EGFP signal compared to baseline level. Scale bar 20 $\mu$ m

The dynamic relocalization of FOXO1b-EGFP downstream of PI3-Kinase  $\alpha$  was tested in primary ISVs and in the DLAV of 26-29 hpf zebrafish embryos, which were treated acutely with the pan-PI3-Kinase inhibitor LY294002 or with two inhibitors specifically targeting the  $\alpha$ -isoform (GDC-0326 and Alpelisib). In all three cases, the nuclei of ECs in ISVs and DLAV showed enhanced EGFP signal around 30-60 min after addition of the inhibitor (Fig. 9 C, yellow arrowheads), before EGFP levels gradually returned back to baseline levels after 1.5 to 2 hours after addition of the inhibitor. DMSO treated sibling embryos did not show FOXO-EGFP relocalization at any given time point after DMSO addition. Interestingly, ECs in the DA did not show elevated levels of nuclear EGFP fluorescence during inhibitor treatment. This suggests differential regulation of FOXO and inputs other than PI3-Kinase  $\alpha$  depending on the vessel type.

I also examined the behavior of FOXO-EGFP in the CVP of 30 hpf embryos as a venous endothelial tissue. Here, cells frequently showed enhanced nuclear FOXO-EGFP already without PI3-Kinase inhibition (Fig 10) in a salt-and-pepper distribution. ECs in the CVP also did not show enhanced nuclear FOXO localization after inhibition of PI3-Kinase signaling. In some cases, the nuclear FOXO-EGFP signal even reverted to the cytoplasm after addition of the inhibitor. These results again emphasize that, on the one hand, there is differential regulation of FOXO signaling in different endothelial tissue contexts and, on the other hand, FOXO signaling has other inputs apart from PI3-Kinase signaling.

In summary, I confirmed that PI3-Kinase  $\alpha$  is indeed active in primary ISVs and DLAV



CVP show nuclear FOXO already in native conditions in a salt-and-pepper pattern, which does not react to inhibition of PI3-Kinase  $\alpha$  signaling.

### **4.3. *pik3ca* knockout mutant alleles *sa16936*, *ubs49* and *ubs50***

As mentioned earlier, a mutant allele for *pik3ca-a* (Chr.11) was readily available from Sanger Institutes. This mutation consists of a T to A conversion in exon 6, transforming the tyrosine codon to a premature Stop (Fig. 11 A). The resulting putative protein is truncated and lacks most domains, most importantly the C-terminal kinase domain.

Heterozygous *sa16936* zebrafish embryos are viable and become fertile adults, which are undistinguishable from wild-types (Fig. 12). Zebrafish larvae homozygous for *sa16936* are only viable until 6-7 dpf. They do not develop a functional swim bladder (Fig. 12) and consequently do not start swimming at around 5 dpf.

Since the *pik3ca-b* gene (on Chr.23) had so far scarcely been characterized, no mutant allele was commercially available. Therefore, two new mutant putative knockout alleles were generated using CRISPR, namely *ubs49* and *ubs50* (Fig. 11, D,E, F, Supplementary Fig. 1). Two distinct gRNAs were used in two experiments, one binding in exon 4 (which created the *ubs49* allele) and one binding to exon 3 (which created the *ubs50* allele).

The *ubs49* allele consists of a 14 bp deletion in exon 4, resulting in a frameshift and premature Stop codon in exon 5 (Fig. 11 D). This allele can only produce a severely shortened protein with RAS-binding, C2, PIK and kinase domain missing. Throughout the course of this study, the *ubs49* allele was used as the main *pik3ca-b* mutant allele for functional analyses of PI3-Kinase  $\alpha$  signaling.

The *ubs50* allele is a C to GA transformation in exon 3 (Supplementary Fig. 1). This +1 frameshift results in an early stop codon in exon 4, with the resulting putative protein again lacking Ras-binding, C2, PIK and kinase domains.

When creating a new mutation in the genome using CRISPR, there is always the risk that the gRNA used binds to off-targets and thus produces other mutations in non-targeted genes. It is very important to assess specificity of the observed phenotypes

by comparing different mutant alleles for the same gene to exclude non-target effects. For this study, phenotypes in both *ubs49* and *ubs50* homozygous as well as *ubs49/ubs50* transheterozygous embryos were compared (Supplementary Fig 1). In combination with homozygous mutation of *pik3ca-a*, embryos homozygous for either of the two *pik3ca-b* alleles showed identical phenotypes, indicating they are equally null-alleles for *pik3ca-b*. Furthermore, embryos homozygous mutant for *pik3ca-a* and transheterozygous *ubs49/ubs50* mutant displayed similar phenotypic changes (Supplementary Fig. 1). Therefore, the two alleles do not complement each other and the observed phenotypes are not caused by off-target effects.

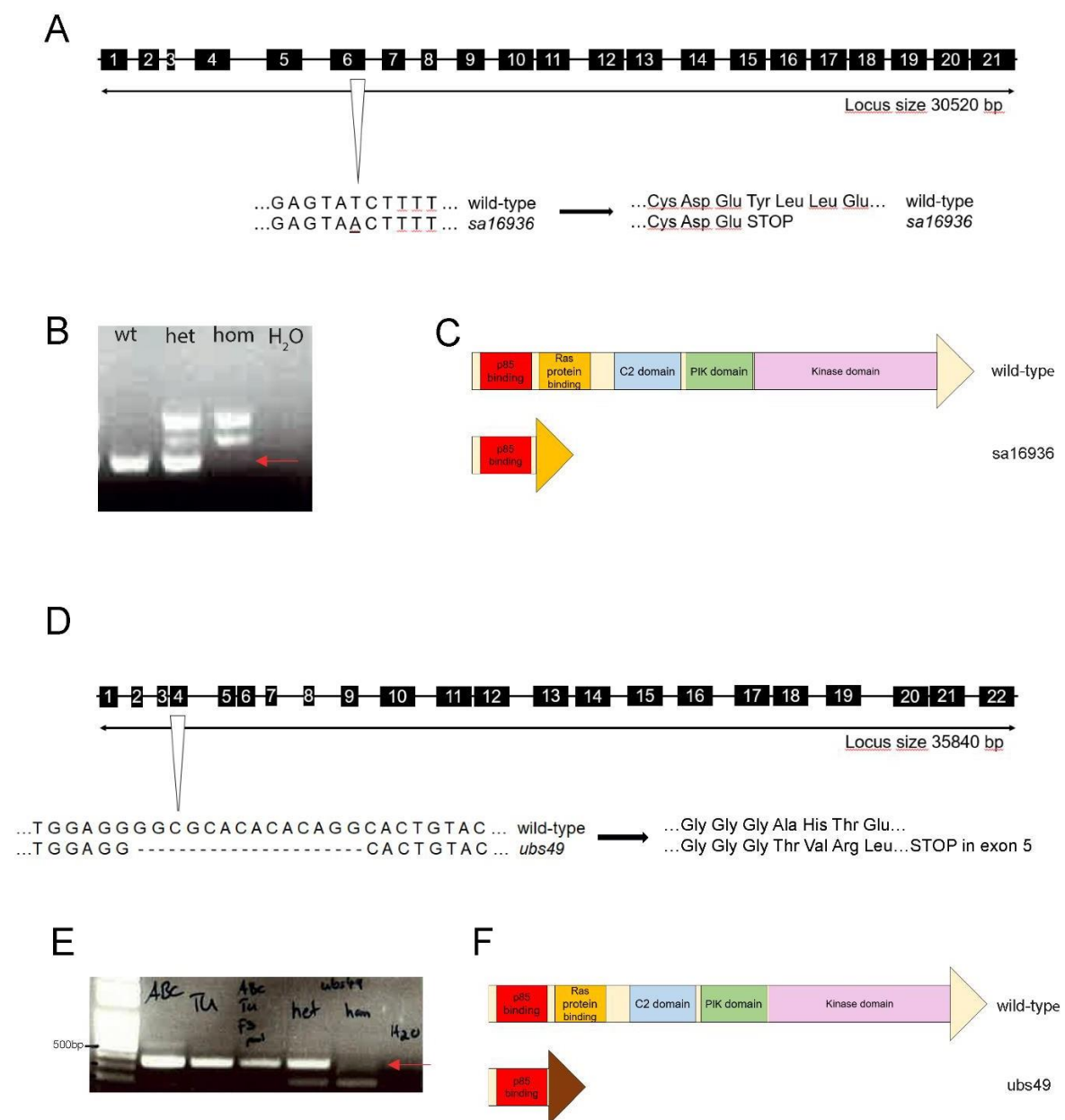


**Fig. 11: Zebrafish mutant *pik3ca* alleles *sa16936* and *ubs49***

**A** *pik3ca-a* mutant allele *sa16936*. **B** Agarose gel image showing genotyping PCR for *sa16936* on isolated genomic zebrafish DNA of wild-type, heterozygous and homozygous samples as well as water control (no DNA). Red arrow indicates missing wild-type band for homozygous sample.

**C** Protein domains of wild-type and *sa16936* Pik3ca-a. **D** *pik3ca-b* mutant allele *ubs49*. **E** Agarose gel image showing genotyping PCR for *ubs49* on isolated genomic zebrafish DNA for different wild-type strains (AB, TU and AB/TU F3 pooled), *ubs49* heterozygous and *ubs49* homozygous samples as well as water control (no DNA). Red arrow indicates missing wild-type band for homozygous sample.

**F** Protein domains of wild-type and *ubs49* Pik3ca-b

Zebrafish heterozygous mutant for *pik3ca-a* (*sa16936 het*) and simultaneously homozygous mutant for *pik3ca-b* (*ubs49 hom*) are viable, fertile and indistinguishable from wild-type siblings. For further functional analysis of PI3-Kinase  $\alpha$  signaling, transgenic reporter lines were kept in a *pik3ca-a* heterozygous/ *pik3ca-b* homozygous (*sa16936 het/ubs49 hom*) double mutant background.

Overall, morphological changes in *pik3ca* double homozygous mutant embryos were subtle and with great variance among them. In most cases, these embryos displayed a smaller hindbrain region (Fig. 12 A, black stars) and general microcephaly starting from approximately 2 dpf, as well as a more beak-like appearance of the upper jaw (yellow arrowhead). Approximately 8-10% of double homozygous mutants displayed severe heart edema from 3 dpf on (Fig. 12 A, lower row). At 4-5 dpf, double homozygous mutant larvae again did not show an inflated swim bladder as had been already described for single homozygous *pik3ca-a* mutants (black arrows).

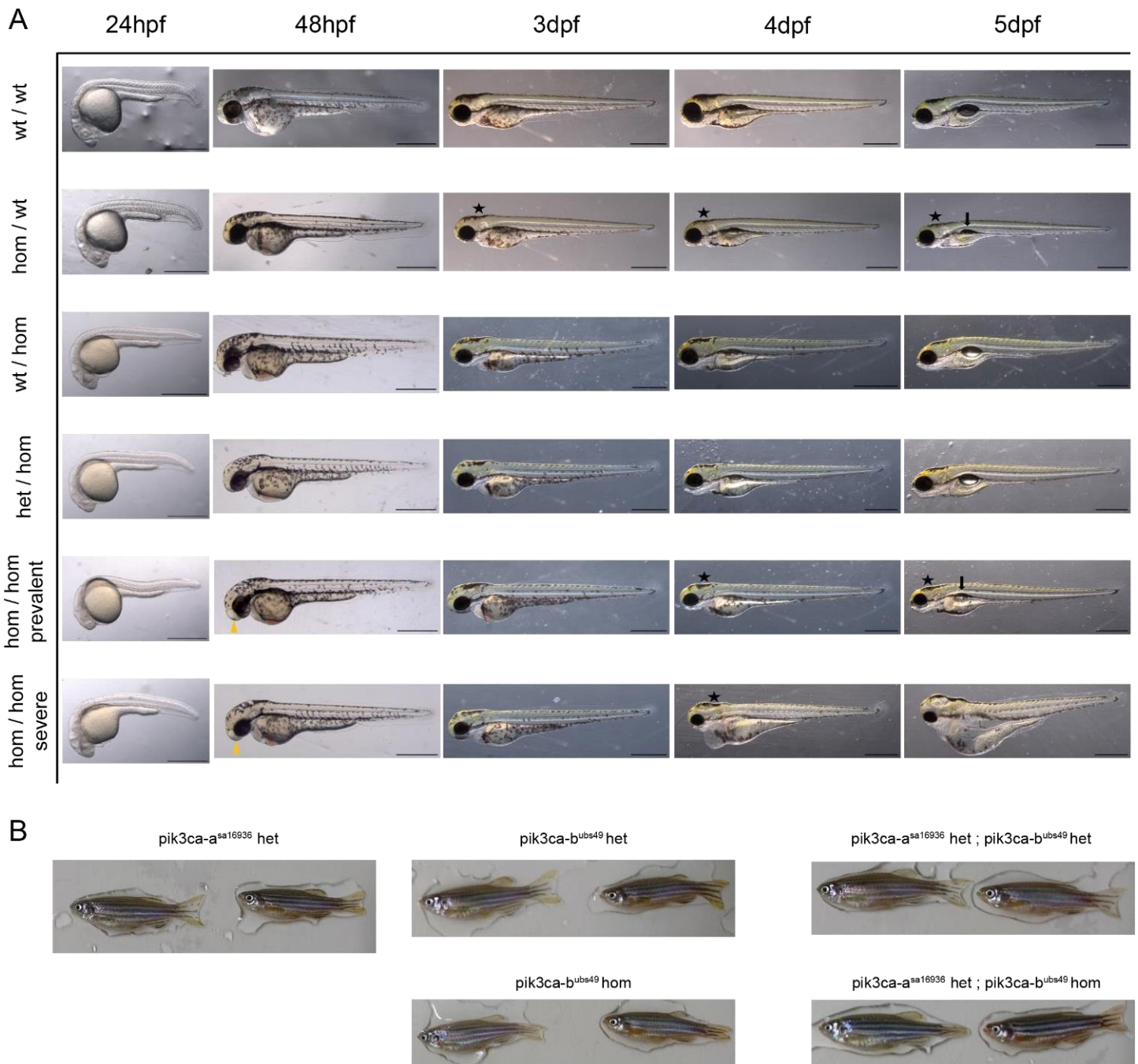


**Fig. 12: Embryonic development of *pik3ca* mutants**

**A** Overview over embryonic habitus of *pik3ca-a/pik3ca-b* mutant zebrafish larvae from 24hpf to 5 dpf, mutant alleles *sa16936* and *uba49* respectively, same embryo shown over time. Homozygous mutation of *pik3ca-a* prevents inflation of a functional swim bladder (black arrows). Black stars indicate microcephaly in double homozygous embryos. Yellow arrowheads show beak-like upper jaw of double mutants. Scale bar 2mm **B** Adult *pik3ca* mutant zebrafish of indicated genotype, female left, male right (anaesthetized). Age varied from 5 to 11 months.



## 4.4. Cardiovascular development of *pik3ca* mutants

### 4.4.1. *pik3ca* mutants show reduced heartbeat and delayed onset of blood flow in ISVs and DLAV

Visual inspection of *pik3ca* mutant embryos under the dissection microscope already implied that blood flow is present in these embryos. In collaboration with Dr. Jianmin Yin, a postdoctoral researcher in the group, we measured blood flow velocity and heartbeat in 2dpf embryos from a *pik3ca-a/pik3ca-b het/hom* incross. Flow velocity in the DA of these embryos was unchanged across all genotypes (Fig. 13 A).

Simultaneously, heartbeat was reduced in double homozygous mutants, albeit not to a statistically significant level (Fig. 13 B).

To analyze vascular patency in ISVs and DLAV of *pik3ca* mutants, time lapse microscopy was performed in mutant embryos fluorescently labelling ECs with EGFP and erythrocytes with dsRed. Onset of blood flow in the first five ISVs behind the yolk extension was observed from 32hpf to 46hpf and compared between *pik3ca* double mutants and control siblings (*wt/hom* and *het/hom*). As shown in Fig. 13 C, ISVs and DLAV became lumenized in double mutants and carried blood flow. However, much fewer red blood cells were observed in these vessels compared to control siblings (not quantified). The time point at which fluorescently labelled erythrocytes appeared in all 5 assessed ISVs in double mutant was delayed about 1.5-2 hours on average compared to control siblings (Fig. 13 D), in line with a general delay in vascular development in the mutants which will be discussed again later. Furthermore, generally fewer erythrocytes could be observed within ISVs.

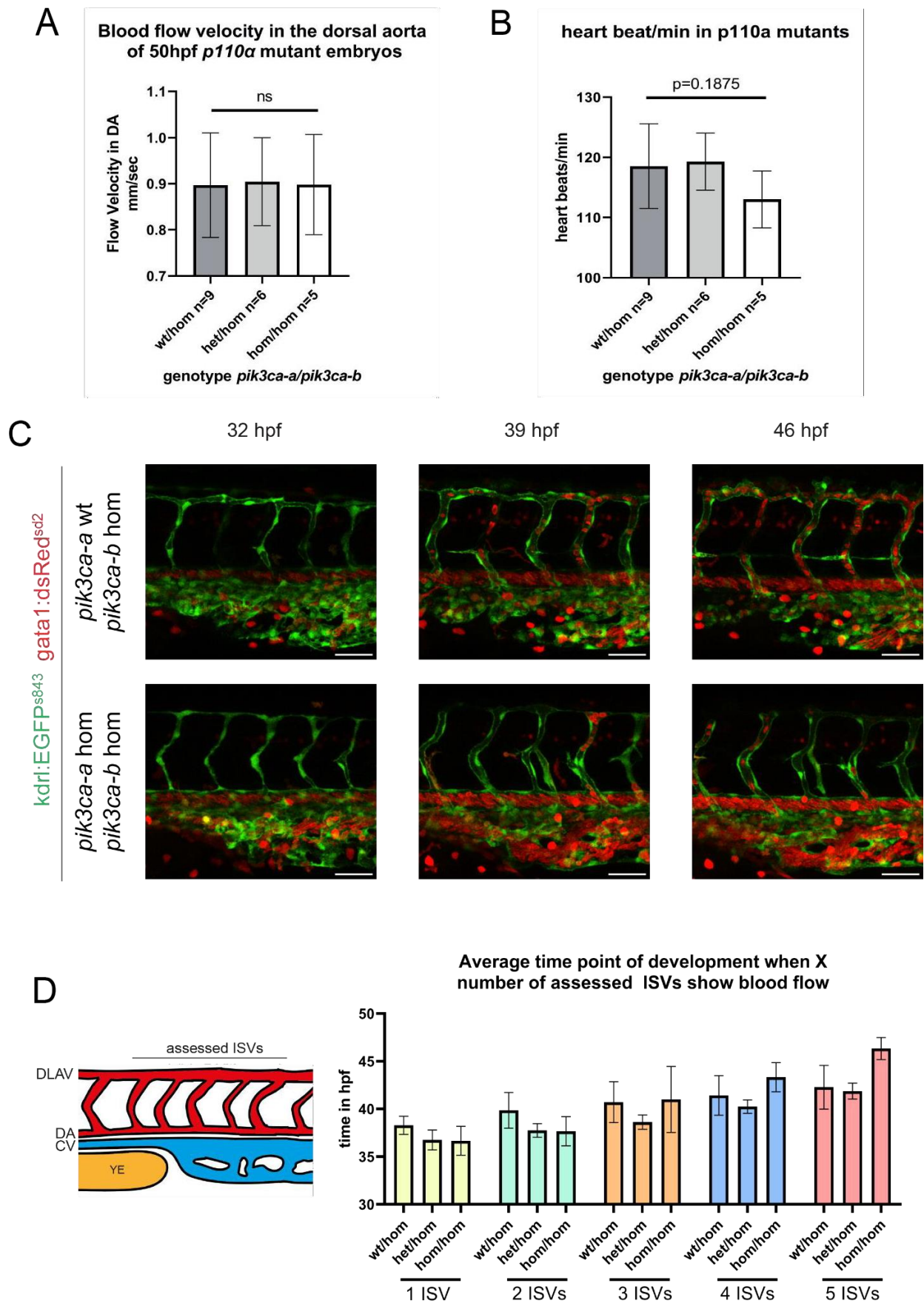




**Fig. 13: Analysis of blood flow in *pik3ca* mutants**

**A** Quantification of blood flow velocity in the DA of 50hpf embryos. Statistical analysis by One-way ANOVA **B** Quantification of heart beats per minute in 50hpf embryos of indicated genotype. Statistical analysis with One-way ANOVA. **C** Time lapse of *pik3ca* mutant embryos, ECs in green, erythrocytes in red. Same region in embryo is displayed. Note that much fewer erythrocytes can be observed within double *hom* mutant ISVs and DLAV compared to single *hom* control. Scale bar 50 $\mu$ m. **D** Quantification of onset of blood flow in the first five ISVs caudal to the YE, bars represent mean time point when the indicated number of ISVs displayed bloodflow per genotype, error bars indicate standard deviation. Sample sizes were n=7 for *wt/hom*, n=8 for *het/hom* and n=3 for *hom/hom* embryos

#### 4.4.2 Arteriovenous specification of ISVs is independent of PI3-Kinase $\alpha$ signaling

Signaling by VEGFR2 in the zebrafish trunk has two major outputs, namely PI3-Kinase signaling and ERK signaling. Both signaling pathways regulate various downstream targets, promoting cell proliferation, migration and other cellular behaviors. Additionally, Akt, which is downstream of PI3-Kinase, is able to inhibit ERK signaling via the phosphorylation of Raf (Zimmermann and Moelling, 1999), creating a regulatory relationship between the two pathways.

Erk signaling reportedly promotes arterial differentiation of ECs in zebrafish embryos (Hong *et al.*, 2006). Based on these findings, I hypothesized that genetic loss of PI3-Kinase signaling and subsequent reduction of Akt activity would result in overactivated ERK signaling, which, in turn, would lead to more vessels acquiring arterial fate.

To test this hypothesis, I used an arterial-specific fluorescent marker (*Tg(flt1:RFP)<sup>hu5333</sup>*) and compared the number of arterial differentiated ISVs in the trunk vasculature between *pik3ca* double mutants and control siblings at 48-50hpf (Fig. 14). Per embryo, I assessed the last seven ISVs over the posterior end of the yolk extension and counted the number of ISVs that showed RFP expression, indicative of arterial EC fate. As shown in Figure 14, no significant changes of the number of arterial ISVs was observed between *pik3ca* double mutants and control siblings. In general, approximately half of the assessed ISVs became arteries and the other half veins, independent of the respective genotype.

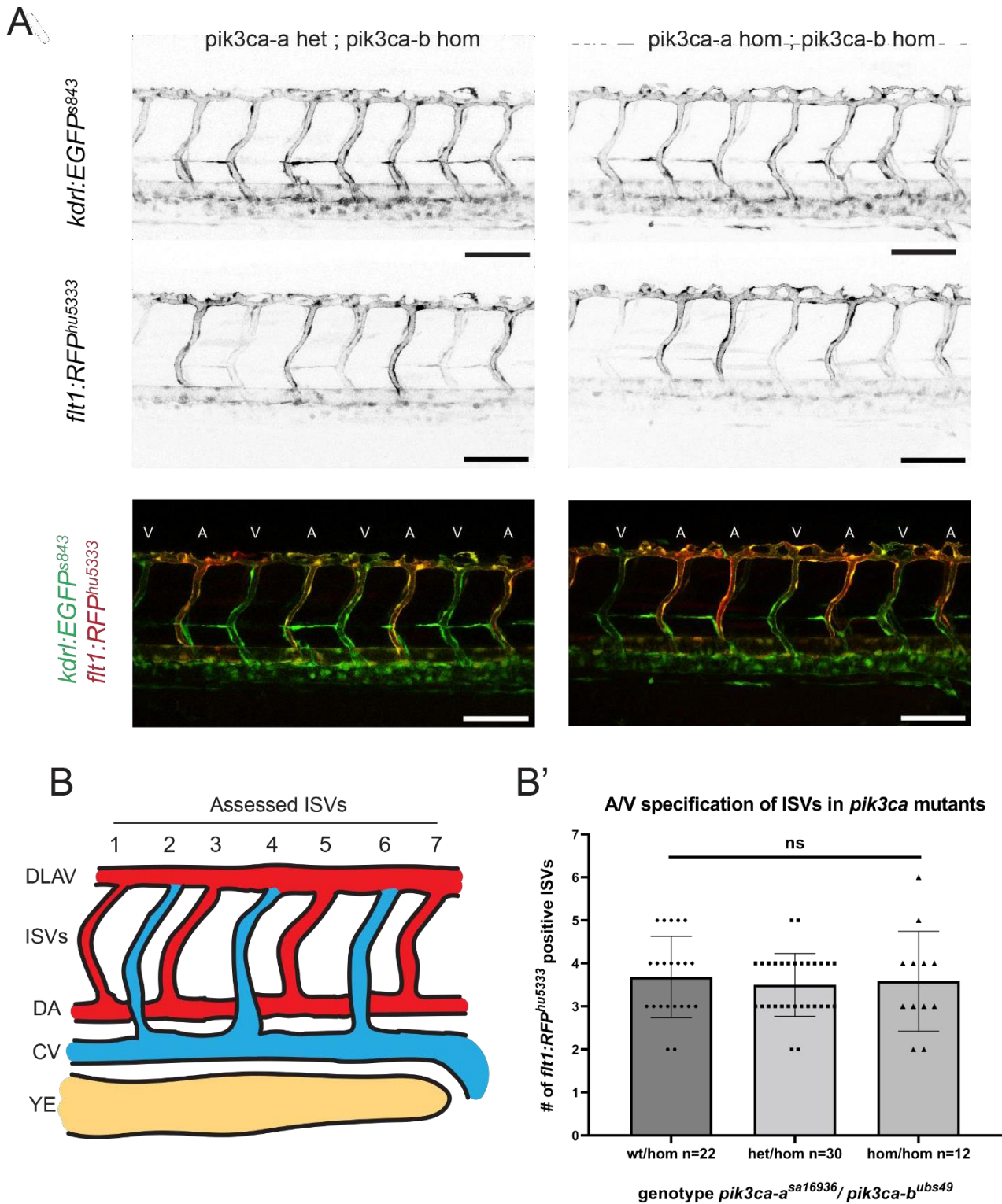


**Fig. 14:** Arteriovenous specification of ISVs is independent of PI3-Kinase  $\alpha$

A representative confocal images of zebrafish embryo trunk vasculature expressing EGFP the whole vasculature and RFP in arterial differentiated ECs. Scale bars 100 $\mu$ m. A=arterial ISV, V=venous ISV.

**B** Schematic illustration of the position of the seven assessed ISVs in the quantification in B'

**C** Quantification of arterial ISVs amongst the ISVs assessed as depicted in B. Bars represent mean number, error bars display standard deviation. Statistical analysis performed with One-way ANOVA.

#### 4.4.3. Loss of PI3-Kinase $\alpha$ signaling causes hyperplasia in the CVP

I compared the overall gross morphology of double homozygous *pik3ca* mutants with their heterozygous and wild-type siblings at 36 hpf when all main embryonic vessels had formed.

As shown in Fig. 15 A, overall vascular anatomy of double homozygous *pik3ca* mutants is unchanged compared to single homozygous or wild-type siblings. DA, CV and the heart develop seemingly normally. In the trunk, ISVs sprout from the DA in a regularly interspaced manner and connect to form the DLAV. However, the CVP is larger than in control siblings with enlarged vascular loops (Fig. 15 A, black arrow, B). Quantification of these loops in the CVP confirmed that double homozygous mutants do not display more, but generally bigger loops in their CVPs (Fig. 15 C, D), leading to the observed overall enlarged tissue phenotype. Moreover, the same observation was made in embryos treated with the PI3-Kinase  $\alpha$  isoform specific inhibitor GDC-0326 (A. Angulo-Urarte, unpublished, Fig. 15 B').

The CVP is a venous plexus which forms via ECs sprouting ventrally from the posterior cardinal vein. The tissue remodels via a honeycomb-like intermediate and segregates into two main veins, namely dorsal and ventral vein, respectively. In *pik3ca* mutants, this honeycomb structure is accentuated by the overall increased size of the tissue, larger ventral sprouts and, in consequence, enlarged vascular loops when the sprouts anastomose (Fig. 15, 16).

Somatic mutations in the mammalian PIK3CA gene cause venous malformations in human patients and mouse models and venous cells are more prone to react to changes in PI3-Kinase  $\alpha$  signaling levels compared to arteries (Limaye *et al.*, 2015, Luks *et al.*, 2015, Castillo *et al.*, 2016, reviewed in Kobialka and Graupera, 2019).

The hyperplasia phenotype in the CVP of *pik3ca* double homozygous mutant zebrafish embryos plays along in this theme and was thus a very encouraging finding.

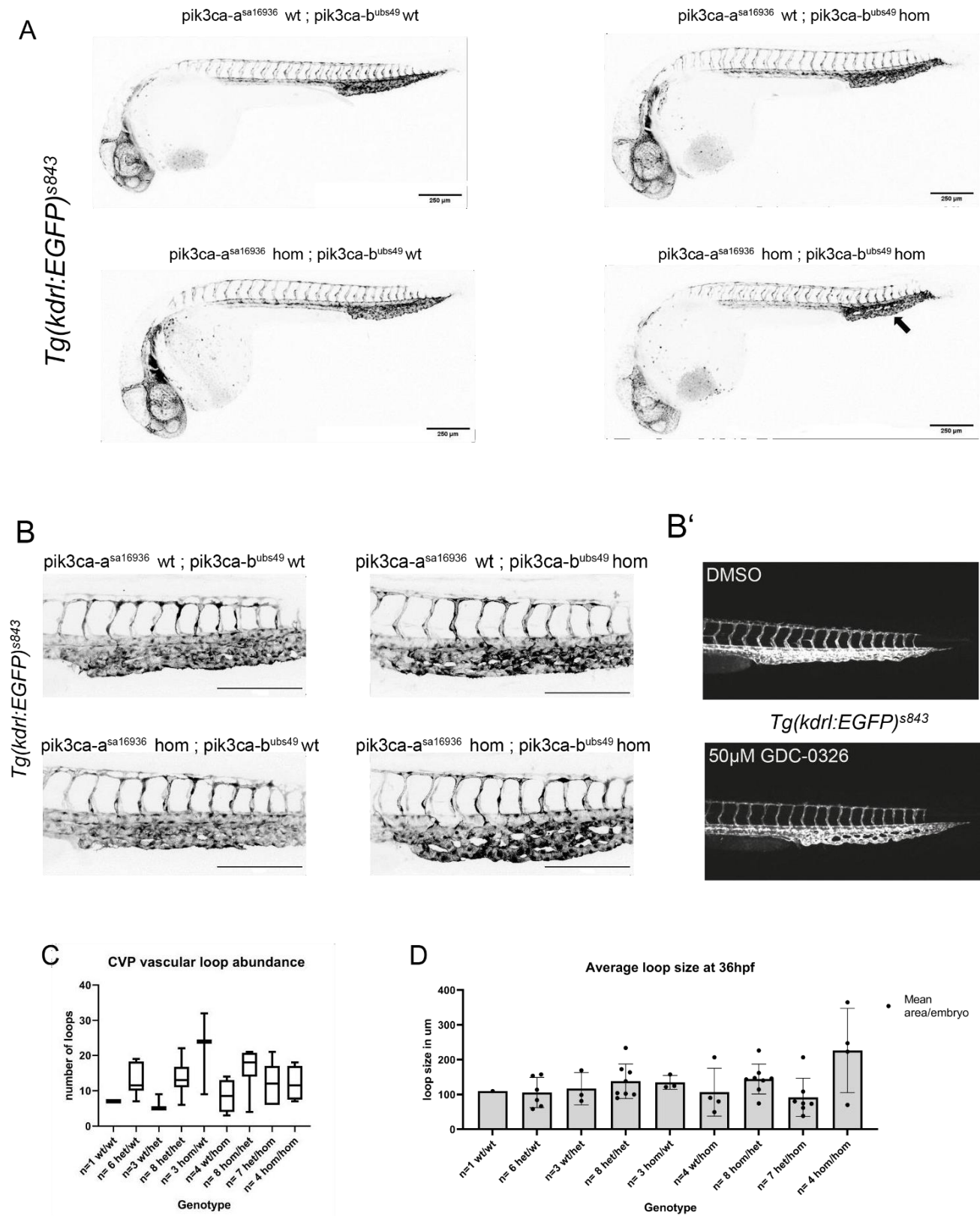


**Fig. 15: Loss of PI3-Kinase  $\alpha$  signaling causes enlarged vascular loops in the zebrafish CVP**

**A** Gross vascular morphology in *pik3ca* wild-type and mutant embryos at 36hpf. Double homozygous embryos display enlarged loops in the CVP (black arrow). Scale bar 250 $\mu$ m. **B** Close-up of CVP in

wild-type and *pik3ca* mutant embryos at 36hpf. Maximum projections of z-stacks are shown. Scale bar 200µm. **B'** CVP region of 38hpf wild-type embryos treated with DMSO (control) or PI3-Kinase  $\alpha$  Inhibitor. Experiment performed by A. Angulo-Urarte and unpublished. **C** Quantification of loop number in CVP of wild-type and *pik3ca* mutant embryos of indicated genotype at 36hpf. **D** Quantification of average loop area in maximum projections of wild-type and *pik3ca* mutant embryos of indicated genotype at 36hpf.

Time-lapse imaging revealed thickened ventral sprouts as the underlying cause of the enlarged vascular loops in the CVP of *pik3ca* double homozygous mutants (Fig. 16 A). Cells migrated as conglomerates rather than single tip cells, and anastomosed in groups, leading to thickened connections and general hyperplasia of the plexus. This ventral hypersprouting could possibly be caused by either a higher number of ECs present in the plexus due to enhanced cell proliferation, or due to ECs becoming larger per se. To distinguish between these possibilities, I have crossed the transgenic reporter *Tg(kdrl:EGFP-nls)<sup>ubs1</sup>* into the *pik3ca* mutant background which fluorescently labels nuclei in the endothelium. Once these fish have reached maturity, I will assess cell numbers over time and compare proliferation in the CVP at different time points during its development.

PI3-Kinase  $\alpha$  signaling has been shown to promote venous identity in ECs (Hong *et al.*, 2006). I thus hypothesized that the ventral hypersprouting phenotype produced by loss of PI3-Kinase  $\alpha$  signaling is part of a general shift of cell identity towards a more artery-like state. To test this, I again used the arterial-specific *Tg(-0.8flt1:RFP<sup>hu5333</sup>)* marker in the *pik3ca* mutant background. I assessed arterial RFP fluorescence intensity in the vasculature of *pik3ca* double homozygous or control sibling embryos with a particular interest of potential elevated levels of RFP signal in the CVP of *pik3ca* double homozygous mutants. Whereas ECs in the DA and arterial ISVs reliably showed strong RFP expression, only very little to no RFP was observed in the PCV and CVP in control siblings (Fig. 16 B). Similarly, no changes in RFP intensity levels were detected in the CVP of double homozygous embryos (Fig. 16 C). Thus, ventral hypersprouting in *pik3ca* mutant CVP is not caused by ECs acquiring arterial cell identity.



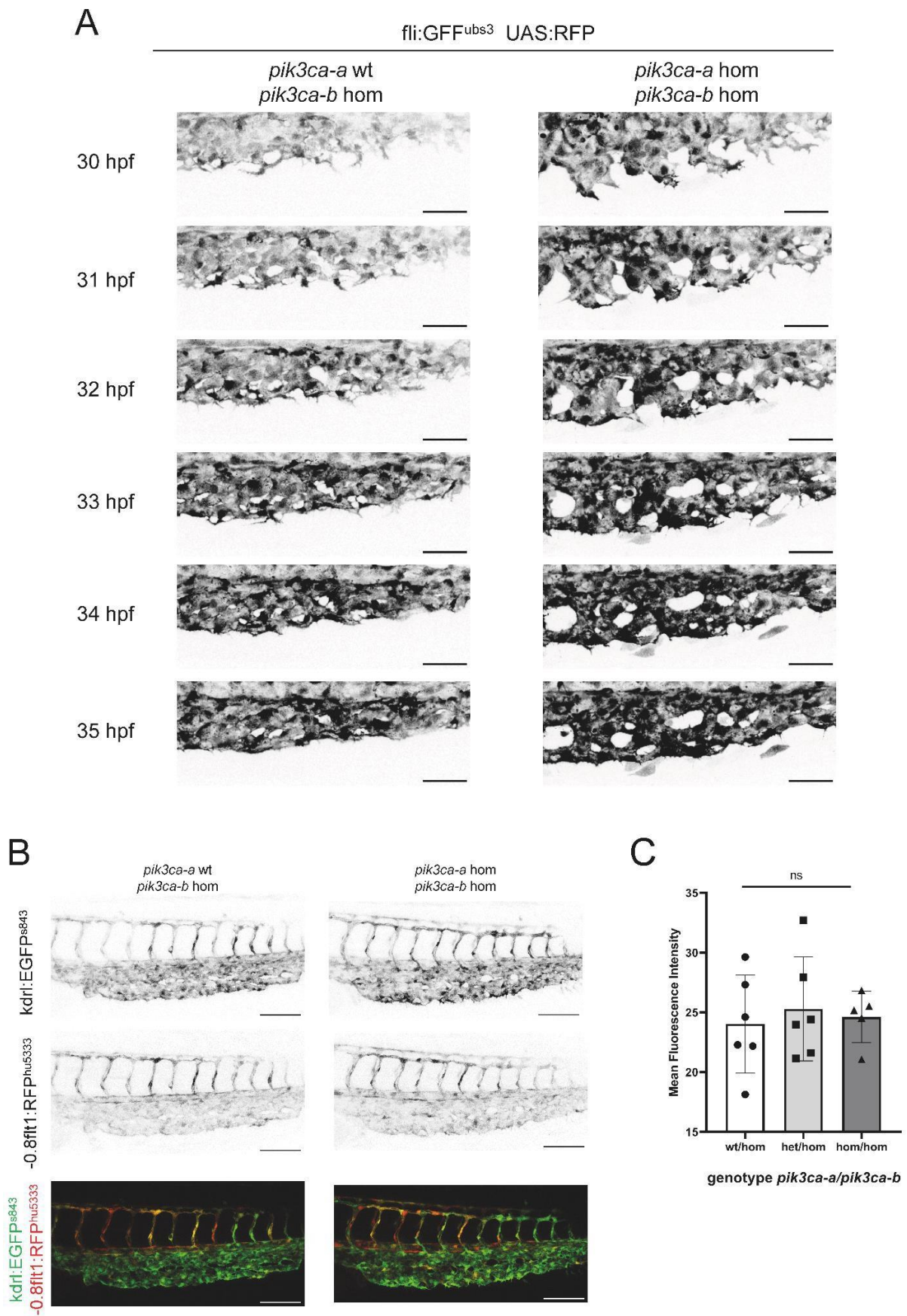


**Fig. 16: Enlarged CVP loops in *pik3ca* double mutants are not caused by arterial identity shift**

**A** Time-lapse live imaging of CVP development in single and double homozygous *pik3ca* mutants from 30 to 35hpf. Scale bar 50 $\mu$ m. **B** Representative images of CVP vasculature expressing EGFP in all ECs and RFP in arterially differentiated cells in *pik3ca* mutants of indicated genotype at 35 hpf. Scale bar 100 $\mu$ m. **C** Quantification of arterial specific RFP fluorescence signal in CVP of *pik3ca* mutant sibling embryos at 35hpf. Statistical analysis performed with One-way ANOVA.

**4.4.4 Development of the trunk vasculature in *pik3ca* mutants**

The main goal of this study was to understand the function of PI3-Kinase  $\alpha$  signaling in complex EC rearrangements during vascular morphogenesis. The zebrafish embryo trunk vasculature has proven a valuable tool to study the mechanisms of vascular remodeling during the development of ISVS and DLAV (e.g. in Sauteur *et al.*, 2014, Paatero *et al.*, 2018).

As a first step, I focused on the development of ISVs and DLAV in *pik3ca* mutants in comparison with wild-type siblings and performed time-lapse analyses of trunk vasculature development. Here, a slight delay of sprouting from the DA was observed (1.5 - 2 hours, not quantified). In *pik3ca* double homozygous mutant embryos, all primary ISV sprouts initially migrated dorsally with uniform velocity. However, once the sprouts reached the embryonic midline, some ISV sprouts halted for some time before resuming migrating dorsally (Fig. 17, black asterisks).

The developing DLAV in *pik3ca* mutants displayed a peculiar webbed appearance, which was caused by tip cells engaging in supernumerary contacts with each other (Fig. 17, red arrowheads). These additional contacts were not observed in heterozygous or wild-type siblings. This was accentuated by tip cells frequently acquiring a bifurcated shape even before reaching the most dorsal point of migration with two or even three forks connecting to the neighboring tip cell. This phenotype could potentially be caused by polarization defects of the tip cells. However, most of these supernumerary contacts were pruned over time and the DLAV acquired a more wild-type appearance until and upon lumenization. In an estimated 10-15% of DLAV segments, connection to the neighboring vessel was lost (Fig. 17, black star, not quantified). Such blunt-ended segments potentially explain why fewer erythrocytes and thus reduced blood flow was observed in ISVs and DLAV but not in the big axial vessels like DA (see Fig. 13).

*fli:GFFubs<sup>3</sup> UAS:RFP*

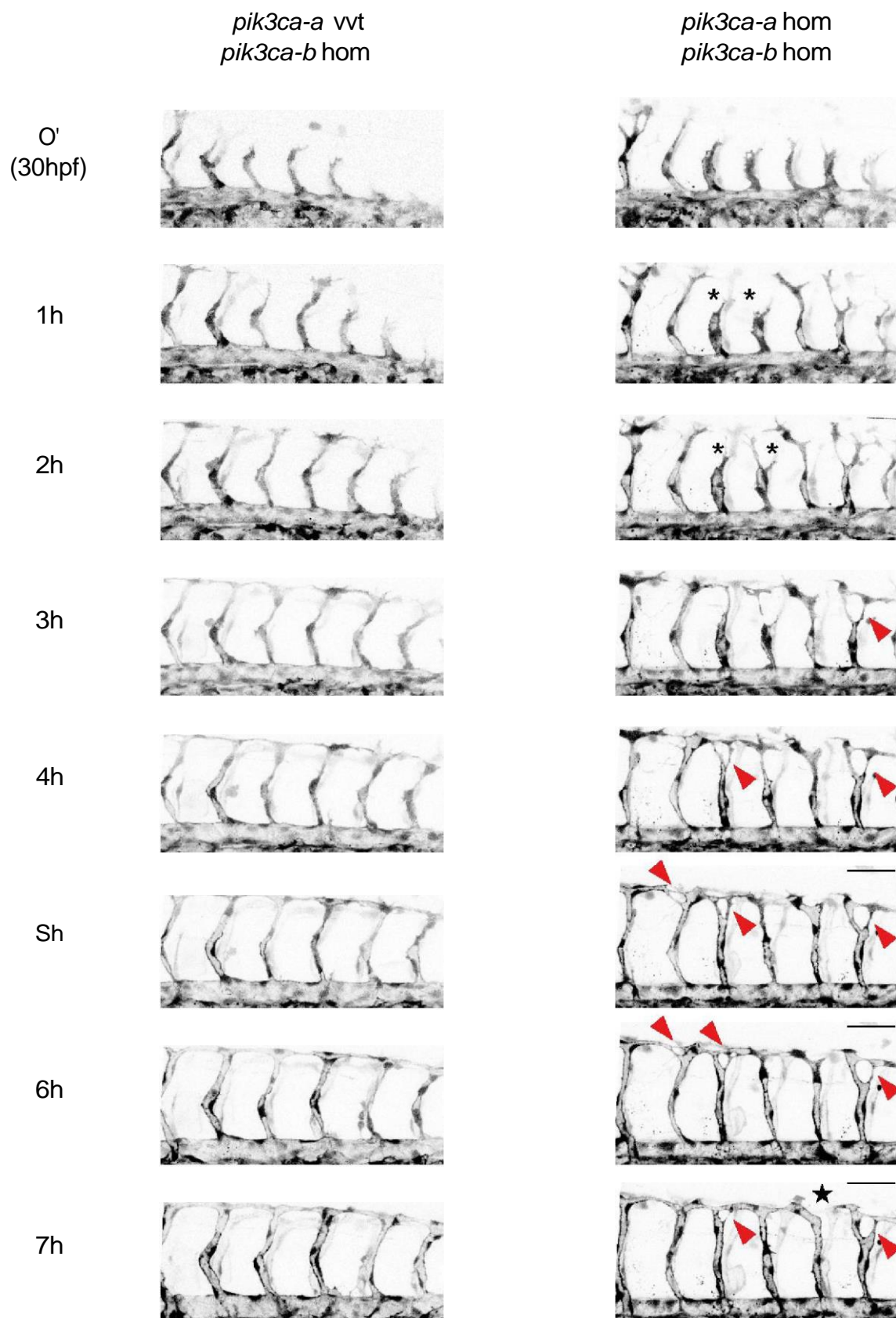




**Fig. 17: Development of primary ISVs and DLAV in *pik3ca* mutants**

Time-lapse imaging of sprouting, anastomosis and lumenization in trunk vasculature of *pik3ca* mutant sibling embryos expressing cytoplasmic RFP in ECs. Black asterisk indicate sprouts stalling at the embryonic midline. Red arrowheads indicate bifurcated tip cells engaging in supernumerary contacts with neighboring tip cells. Black asterisk indicate sprouts stalling at the embryonic midline. Black star indicates unconnected segment in the DLAV. Scale bar 50 $\mu$ m

One of the main outputs of PI3-Kinase  $\alpha$  signaling is the phosphorylation and activation of the protein kinase Akt, which promotes cell proliferation and metabolic changes. A study published in *bioRxiv* reports a reduced diameter of the DA in zebrafish embryos mutant for the three *akt* paralogous genes (Zhou *et al.*, 2020).

Based on this finding I hypothesized that the diameter of the DA in *pik3ca* mutants (which should also show reduced Akt activity) would be similarly decreased.

To investigate this, I measured the diameter of the DA in *pik3ca* mutant embryos at different time points during development using a cytoplasmic endothelial specific reporter. Whilst the DA displayed no changes in diameter in double mutants when compared to control siblings at 28 and 32hpf, DA diameter was significantly reduced from 36hpf onward and remained smaller until at least 56hpf (Fig. 18) upon genetic loss of PI3-Kinase  $\alpha$  signaling.

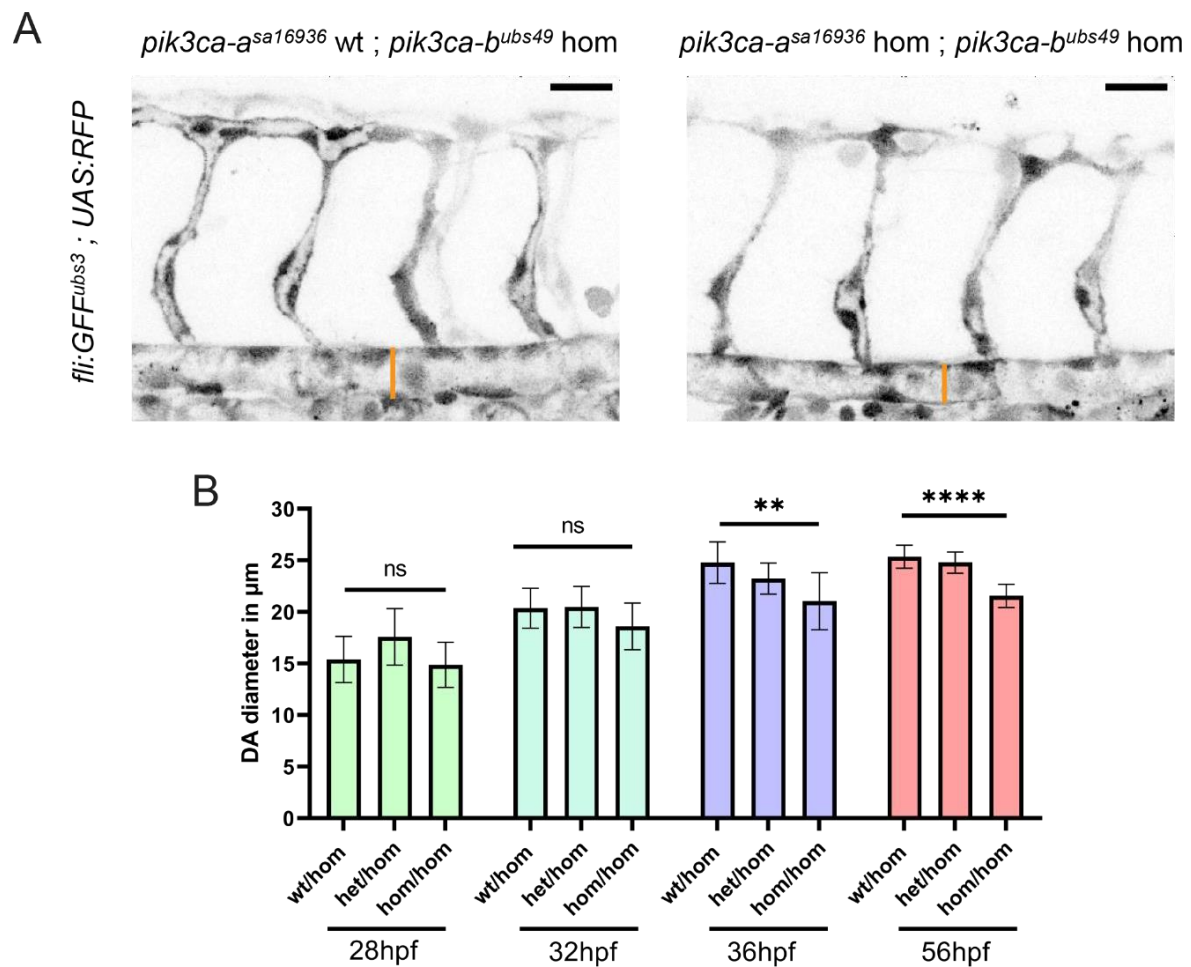


**Fig. 18: Genetic loss of PI3-Kinase  $\alpha$  signaling reduces DA diameter**

**A** Representative images of *pik3ca* double mutant embryo and single mutant control sibling at 32 hpf. ECs labelled with cytoplasmic RFP, scale bar 25 $\mu\text{m}$ . **B** Quantification of DA diameter at indicated time points and in embryos of indicated genotypes.  $n=8$  for all genotypes from 28-36hpf, for 56 hpf  $n=4$  for wt/hom,  $n=9$  for het/hom and  $n=7$  for hom/hom embryos. Statistical analysis performed with One-Way-Anova for each group, error bars indicate standard deviation.

## 4.5. Genetic loss of PI3-Kinase $\alpha$ signaling impairs endothelial cell rearrangements

### 4.5.1. Junction connectivity in ISVs and DLAV is perturbed upon loss of PI3-Kinase $\alpha$ signaling

Following sprouting and anastomosis in the DLAV, ECs in the zebrafish trunk ISVs and DLAV undergo cell shape changes and intercalate within the vessel. These cell rearrangements transform the vessel from a unicellular to a multicellular state (Blum *et al.*, 2008) such that the lumen of the vessel is enclosed by more than one cell in cross sections.

The study of Angulo-Urarte *et al.*, 2018, illustrated how endothelial junction elongation and cell rearrangements become defective under chemical inhibition of PI3-Kinase  $\alpha$  in the zebrafish trunk vasculature. Similar to observations in PIK3CA mutant mouse retina tissue, ECs in ISVs and DLAV failed to rearrange and form a multicellular vessel. Cell pairing and subsequent intercalation was effectively prohibited upon abrogation of PI3-Kinase  $\alpha$  signaling. In wild-type embryos, cell junction elongation during cell rearrangements and multicellular tube formation causes junctions to appear as long lines spanning over the entire vessel. In Angulo-Urarte *et al.*, 2018, chemical inhibition of PI3-Kinase  $\alpha$  signaling caused ECs to remain connected by small and isolated ring-shaped junctions, which did not elongate and were separated by junction gaps along the vessel.

A key aspect in the genetic analysis of PI3-Kinase  $\alpha$  signaling in ECs was the assessment of cell junction elongation in the endothelium of *pik3ca* mutant embryos. As a starting point, I performed antibody stainings against endogenous cell junction proteins VE-cad/Cdh5 and ZO-1 in *pik3ca* mutants fluorescently labelling ECs with cytoplasmic EGFP at 33hpf. Cell rearrangements and junction elongation in ISVs and DLAV was not affected in wild-type, single homozygous, or heterozygous/homozygous mutants (Fig. 19). In contrast, double homozygous mutants displayed large junction gaps in both ISVs and DLAV (green dotted lines), indicative of unicellular architecture and thus impaired EC rearrangements. Quantification of the abundance of such gaps in the last five ISVs over the yolk extension per sample confirmed an increase in gaps from 10-15% in controls to approximately 60% of assessed ISVs in double homozygous embryos (Fig. 19 C).

Furthermore, junctions frequently acquired a smaller, rounded shape compared to heterozygous or single homozygous siblings (red arrows), in which elongated junctions outlined the entire vessel.

Another important observation was that even a single wild-type copy of either *pik3ca-a* or *pik3ca-b* was able to rescue the junction elongation phenotype. This suggests redundant functions between the two isoforms in EC rearrangements and junction elongation. The frequent appearance of unicellular segments not covered with junctions confirmed defective cell rearrangements when PI3-Kinase  $\alpha$  signaling was lost, thereby also confirming the previous results in the inhibitor study. Vice versa, the *pik3ca* double mutants phenocopied the inhibitor treatment, which supports their reliability as a suitable tool to study the function of PI3-Kinase  $\alpha$  signaling in ECs.

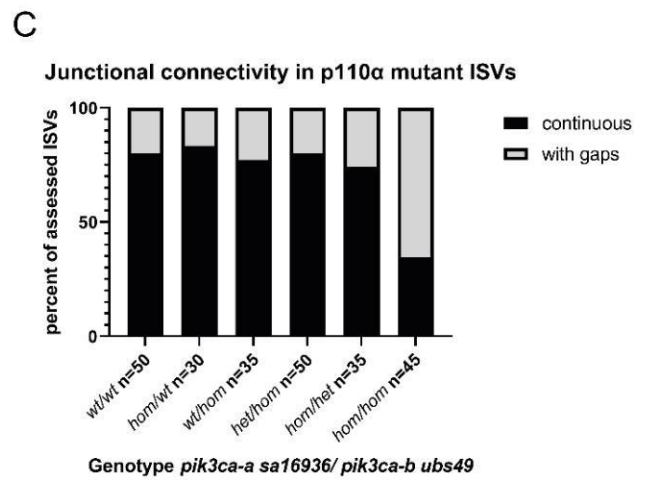
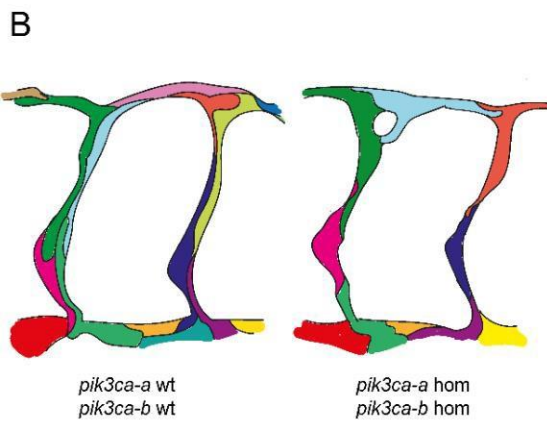
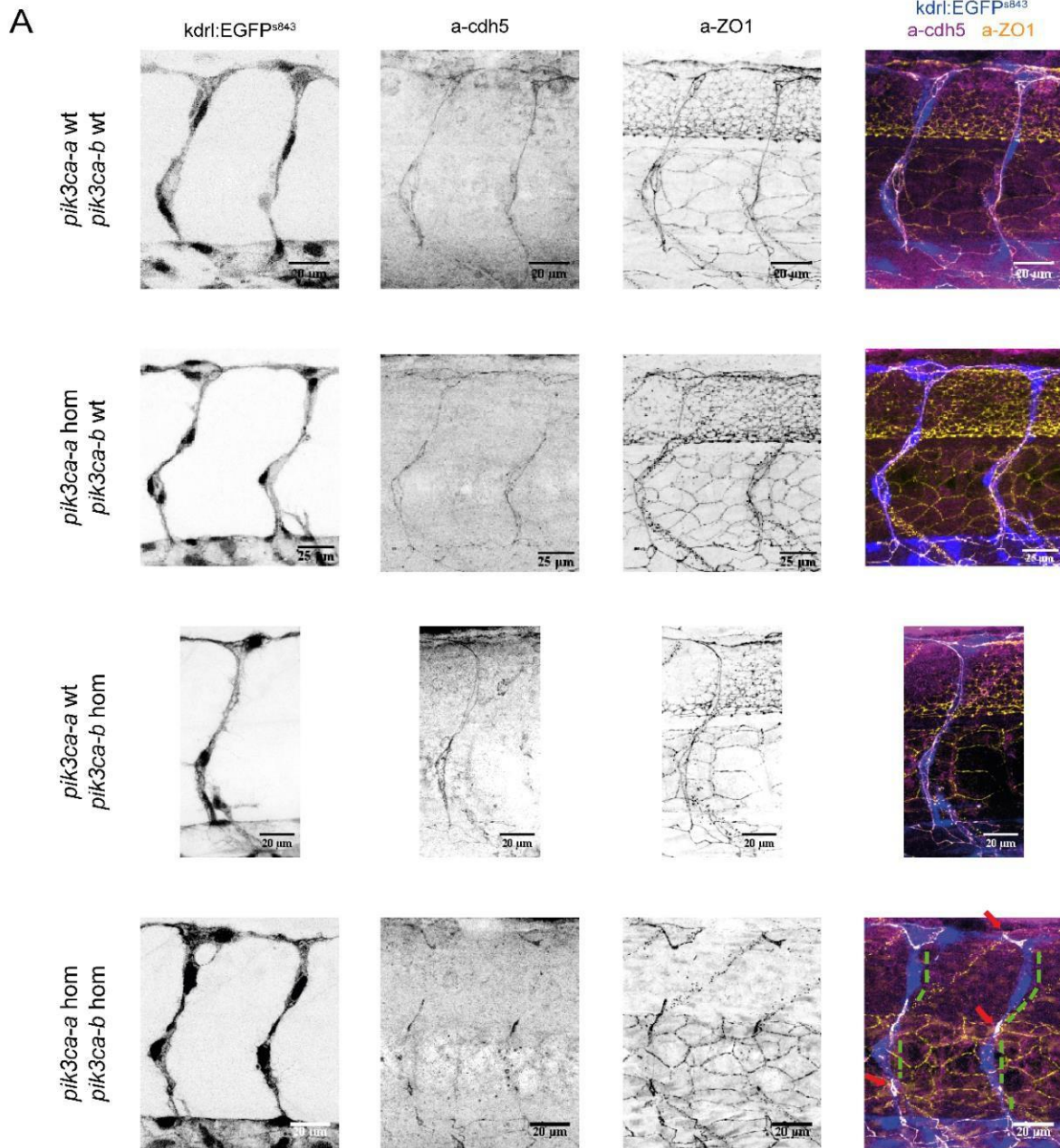


**Fig. 19: Genetic loss of PI3-Kinase  $\alpha$  signaling impairs cell rearrangements in ISVs and DLAV**

**A** Antibody staining against Ve-cad/Cdh5 and ZO1 in wild-type and *pik3ca* mutant embryos expressing EGFP in ECs at 33hpf. Large junction gaps are indicated with green dotted lines, red arrows indicate rounded junctions. **B** Schematic illustration of ISV architecture in wild-type vs. *pik3ca* mutant, drawing according to antibody staining shown in A. **C** Quantification of gap frequency in primary ISVs of 33hpf embryos of indicated genotype.

In addition to the antibody stainings, I also analyzed junction connectivity in the trunk vasculature in *pik3ca* mutant embryos between 28-36 hpf by live imaging. Here, I used fluorescently labelled Ve-cad-venus<sup>uq11bh</sup> to visualize junctions in the trunk vasculature (Fig. 20 A) and focused on junction connections at the base of ISVs to ECs in the DA. In wild-type conditions, the base of an ISV consists of two or more cells with their junctions connecting to cells in the DA, which is visualized by continuous junction lines from the ISV to the DA.

As expected from the earlier results using antibody stainings, the number of ISVs maintaining junctional connection to the DA and thus retaining a multicellular base decreased from approximately 95% in control siblings to around 55% in double homozygous mutant embryos (Fig. 20 B). Furthermore, in the previously acquired antibody stainings at 33hpf, junctional connections were also lost more often in double homozygous mutants compared to controls (Fig. 20 C). The disruption of junctional connection upon genetic loss of PI3-Kinase  $\alpha$  was indicated by a single unpaired stalk cell constituting the base of the ISV, which was connected to the next cell in the DA only by a small circular junction. In some cases, the ISV already did not display a multicellular base from the early sprouting phase on, e.g. the third ISV to the right in Fig. 20 A. Others initially did present a multicellular ISV base, but lost junctional connections over time as the ISV sprouted further and cells became more stretched. The loss of junctional connectivity marked the breaking of multicellular junctions and the loss of contact between formerly connected cells within the vessel. Consequently, the previously connected cells moved apart from each other. The vessel segment now consisted only of the third participating cell which remained placed between and connected to the neighboring cells by bicellular junctions (see also Fig. 26).



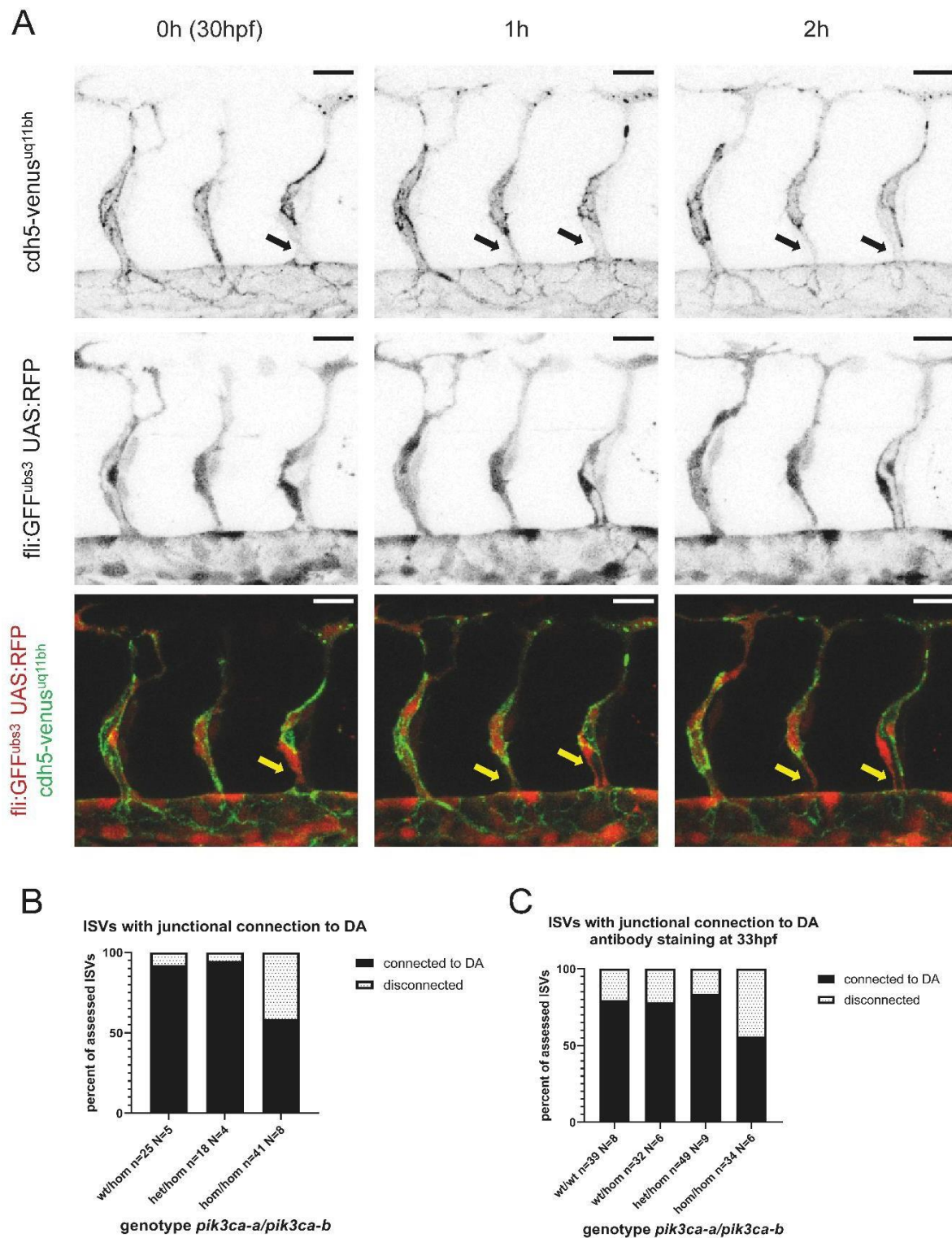


**Fig. 20: Loss of junctional connection to the DA in *pik3ca* mutants**

**A** Time-lapse imaging of trunk vasculature in a *pik3ca* double homozygous mutant embryo expressing cytoplasmic RFP and venus-tagged VE-cad in ECs from 30 to 32hpf. Black and yellow arrows indicate disrupted junctional connection to DA. Scale bar 20 $\mu$ m. **B** Quantification of ISVs with persistent or lost junctional connection to DA from time-lapse data between 28-36hpf in embryos of indicated genotype. n=number of ISVs; N=number of embryos. **D** Quantification of ISVs with persistent or lost junctional

---

connection to DA from antibody stainings at 33hpf in embryos of indicated genotype. n=number of ISVs; N=number of embryos

#### 4.5.2. Cell rearrangements in the DLAV stall in *pik3ca* mutants

Since rearrangements of EC entail cell intercalation and junction elongation, junction coverage can be used as a proxy to assess the ability of cells to rearrange in a specific genetic background. Reduced coverage of the vessel by junctions implies unicellular segments resulting from defective cell intercalation.

Therefore, I measured junction coverage in the DLAV of *pik3ca* double homozygous mutants and control siblings as well as wild-type embryos in antibody stainings for ZO1 at 33hpf. The DLAV segment above the last 5 ISVs over the yolk extension was assessed for this experiment. As shown in Fig. 21, in wild-type and control sibling embryos, around 75-80% of the DLAV segment was covered with endothelial junctions. In contrast, *pik3ca* double homozygous mutants displayed a significant reduction in junction coverage to only around 55%.



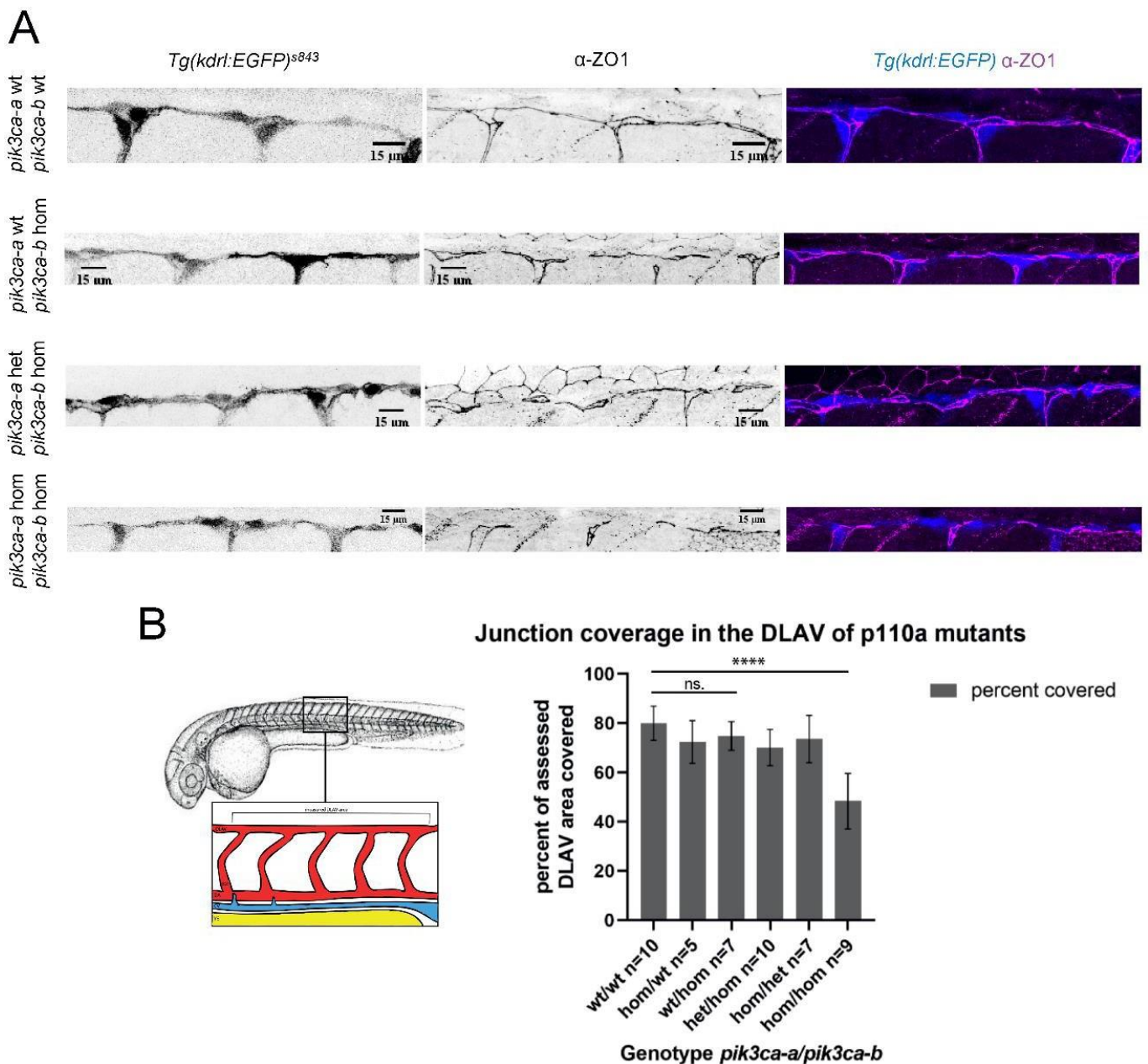


**Fig. 21: Junction coverage in the DLAV is reduced upon genetic loss of PI3-Kinase  $\alpha$  signaling**

**A** Antibody staining against ZO1 in embryos of the indicated genotype at 33hpf expressing cytoplasmic EGFP in ECs. **B** Quantification of junction coverage in the DLAV section depicted left. Statistical analysis performed with One-Way ANOVA for wt. vs single hom, Kruskal-Wallis Test for analysis across all genotypes

Similar to the phenotype at the base of many ISVs in *pik3ca* double homozygous mutants, DLAV segments uncovered by junctions indicate unicellular sections of the

vessel as a consequence of impaired cell intercalation. A possible explanation for this finding could be a general delay in the remodeling of this vessel, since the antibody stainings provide only information about a particular time point during this dynamic process. Therefore, I analyzed how cell intercalation and, subsequently, junction coverage in the DLAV progressed over time. Time-lapse live imaging was performed using fluorescently tagged VE-cad/Cdh5 (*TgBAC(cdh5:cdh5-TS)<sup>uq11bh</sup>*) in the *pik3ca* mutant embryos from 28 to 36hpf. Similar to the measurements performed in the DLAV in the antibody staining experiment, junction coverage over time was measured in the DLAV of *pik3ca* double homozygous and control sibling embryos. In order to normalize against developmental delay, time point zero was defined as the first time when junction material (Cdh5-venus signal) was observed connecting the DLAV segments between at least four consecutive ISVs. From this point onward, junction coverage of the respective DLAV portion was assessed for 6 hours every 30 min.

As expected from wild-type studies, ECs reliably rearranged and formed multicellular DLAVs in control sibling embryos. Junction coverage in the assessed samples grew in a relatively linear manner and most DLAV segments were covered 100% with junctions after 6 hours (Fig. 22 A, red lines, B and B'). In *pik3ca* double homozygous mutants, junctions between tip cells formed and, initially, junction coverage grew linearly over time comparable to control and wild-type embryos. However, the elongation movement stalled at around 60-70% after around 3 hours. Junction rings had elongated until a certain size, but then failed to connect to neighboring junctions and remained isolated. Parts of the DLAV segments in *pik3ca* double homozygous mutants remained uncovered by junctions, again indicative of unicellular architecture.

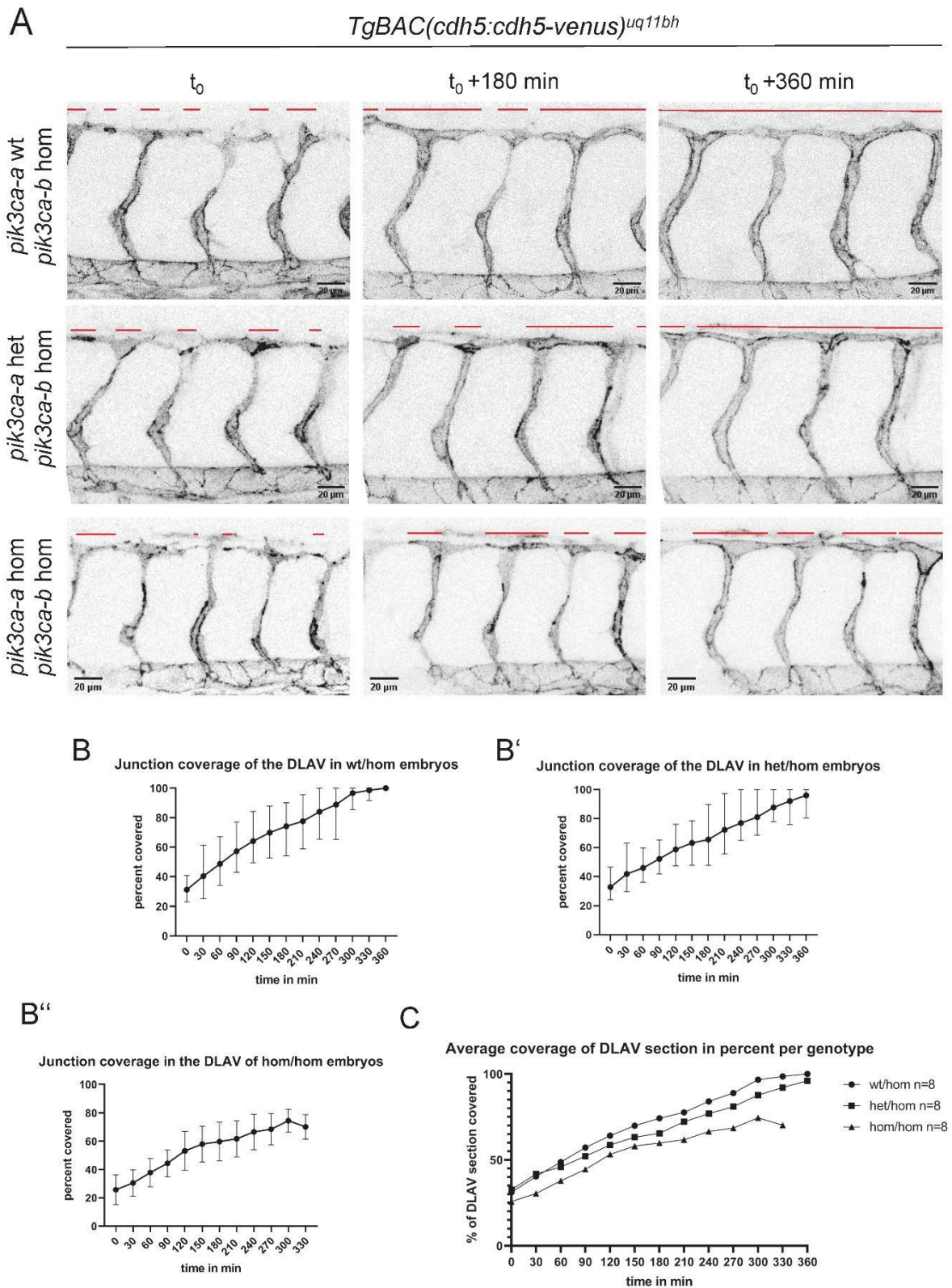


**Fig. 22: Genetic loss of PI3-Kinase  $\alpha$  signaling impairs cell intercalation in the DLAJ**

**A** Time-lapse analysis of junctions in primary ISVs and DLAJ in *pik3ca* mutant embryos expressing Venus-tagged Ve-cad. Red lines indicate DLAJ section covered by junctions. **B-B''** Quantification of junction coverage over time in *pik3ca* single homozygous (**B**), heterozygous/homozygous (**B'**), and

double homozygous (B<sup>''</sup>) sibling embryos. **C** Summarized quantification of DLAV coverage, average of 8 embryos per genotype.

#### **4.5.3. The speed of junction elongation *per se* is not affected by loss of PI3-Kinase $\alpha$ signaling**

So far, I showed that upon genetic loss of PI3-Kinase  $\alpha$  signaling, ECs in ISVs and DLAV lose the ability to efficiently intercalate and form a multicellular vessel. The above results indicate that rearrangements do occur, but they are incomplete which leads to a partially unicellular vessel. Furthermore, I observed that junction rings grow only until a certain size, but then do not elongate any further, suggestive of a defect not only in cell rearrangements but also in junctional elongation.

Our lab has previously described JBL as the main mechanism by which ECs elongate along each other during cell rearrangements (Paatero *et al.*, 2018, see also chapter 2.2.3). I thus asked whether the defects in junction elongation and cell rearrangements in *pik3ca* double homozygous mutants and under PI3-Kinase  $\alpha$  inhibition are caused by defects in JBL.

Each JBL cycle results in elongation of the junction ring by a certain distance along the partnering cell. Effectiveness of JBL can thus be assessed by the speed at which the junctional ring elongates. I measured the speed of junction elongation when inhibiting PI3-Kinases chemically and in *pik3ca* mutants using again VE-cad-Venus as junctional marker. The size of anastomotic tip-tip cell junctions in the DLAV of 28-31 hpf embryos were assessed at two different time points and the speed of junction elongation calculated as shown in Fig. 23 A. Only junctions under 25 $\mu$ m length were assessed in this experiment, because longer and therefore “older” junctions frequently merged with neighboring junctions during the time window of imaging in wild-type and in control conditions, thus prohibiting further measurements.

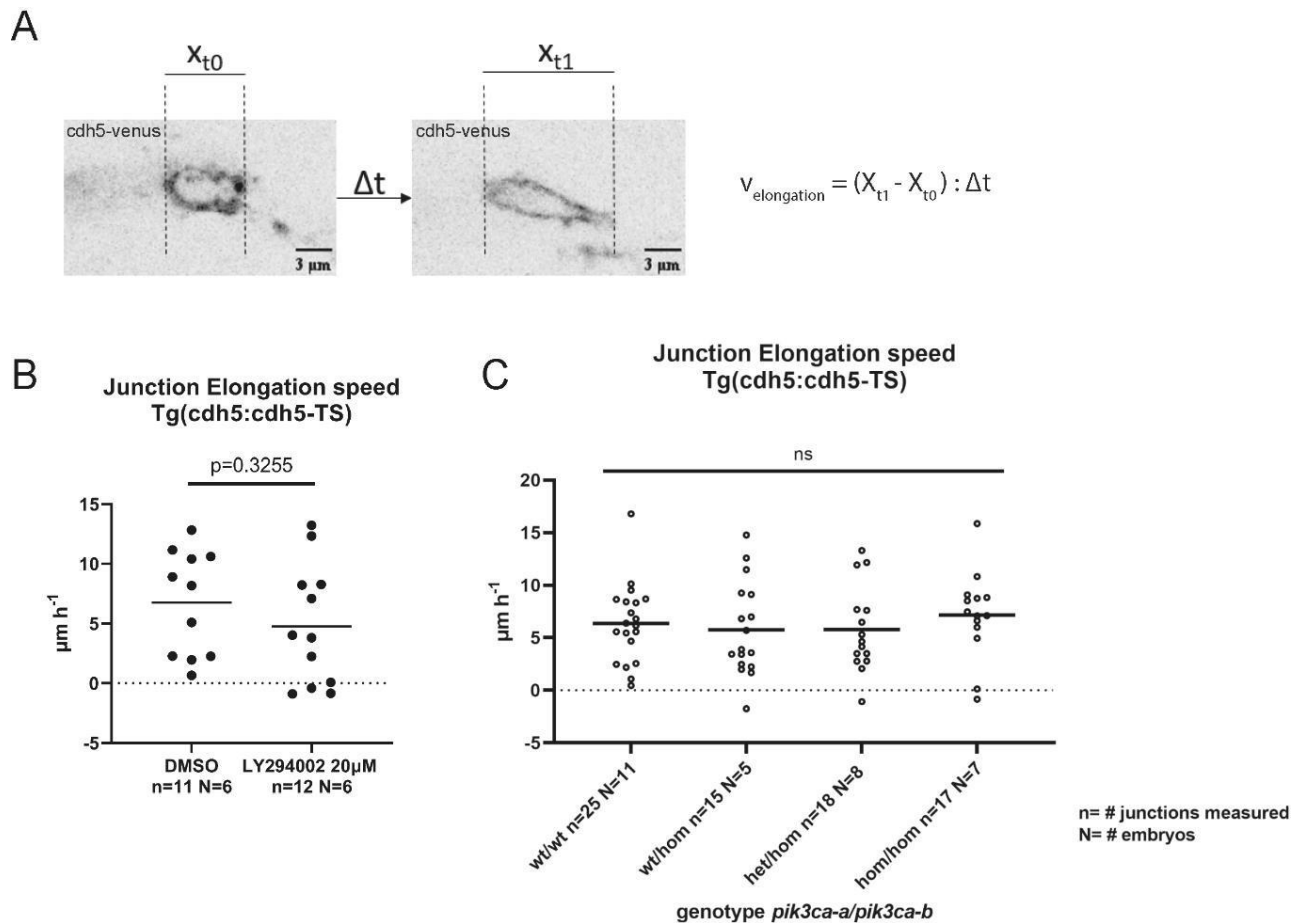


**Fig. 23. The speed of junction elongation is independent of PI3-Kinase  $\alpha$  signaling**

**A** Endothelial cell-cell junctions in the DLAV were imaged at two time points  $t_0$  and  $t_1$ , their size measured and junction elongation per time was calculated as the increase in junction length divided by time. As marker for endothelial junctions, *Ve-cad-venus*<sup>uq11bh</sup> was used in wild-type and *pik3ca* mutant background. **B** Quantification of junction elongation speed in anastomotic tip-tip cell junctions in the DLAV of wild-type embryos at 28-30hpf treated with DMSO or 20 $\mu$ M LY294002, chemical treatment was started 1h prior imaging. Statistical significance determined by unpaired T-test. **C** Quantification of junction elongation speed of anastomotic tip-tip cell junctions in the DLAV of *pik3ca* mutants and wild-type control at 28-30 hpf. Statistical significance determined by One-way ANOVA.

Endothelial cell junction elongation speed in the DLAV at 28-31 hpf was not affected by loss of PI3-Kinase signaling. *pik3ca* double homozygous mutants displayed no change in elongation speed compared to wild-type embryos or control siblings (Fig. 23 C). Similarly, chemical inhibition of PI3-Kinases also did not change elongation speed of junctions (Fig. 23 B). Furthermore, these results validate the observations from the previous experiment, where the incline of junction coverage in the DLAV

was initially the same between *pik3ca* double homozygous mutants and control siblings. In conclusion, the initial speed of endothelial cell-cell junction elongation per se is not affected, but junction elongation comes to a halt after a certain progression.

#### 4.5.4. Polarized distribution of junctional VE-cad is unaffected by genetic loss of PI3-Kinase $\alpha$ signaling

PI3-Kinase  $\alpha$  has been implicated in cell polarization and migration behavior, as well as in actin polymerization via Rac1 (Missy *et al.*, 1998, Vanhaesebroeck *et al.*, 2010). Since JBL consist of polarized, F-actin containing protrusions, it seems highly likely that PI3-Kinase  $\alpha$  would be involved in JBL formation and function. However, since the speed at which anastomotic junctions in the DLAV elongated was not affected by loss of PI3-Kinase signaling, it seems like JBL function is not perturbed when PI3-Kinase signaling is abrogated.

In order to further analyze the functionality of JBL in *pik3ca* mutants, I next assessed polarized distribution of VE-cad in endothelial junctions. VE-cad is thought to be the key regulatory and the mechanistic molecule of JBL, and JBL were first discovered by assessing polarized distribution of VE-cad at medial vs. lateral sides of junctions. Using fluorescently tagged *VE-cad-Venus<sup>uq11bh</sup>*, the medial and lateral thickness of junctions was compared in *pik3ca* double homozygous mutants and control siblings between 28 and 31hpf. Only anastomotic tip-tip cell junctions in the DLAV were included in the analysis. Medial ends generally contained more VE-cadherin and were thus “thicker” than the lateral sides (Fig. 24 A, B) and this feature was independent of the respective *pik3ca* genotype. For a more direct comparison of the degree of polarization across genotypes, a polarization index  $\Delta P$  was calculated by subtracting lateral from medial thickness for each ring. Differences in expression levels in embryos and cells were thereby normalized. No changes in  $\Delta P$  between double homozygous mutants and control siblings were observed (Fig. 24 C).



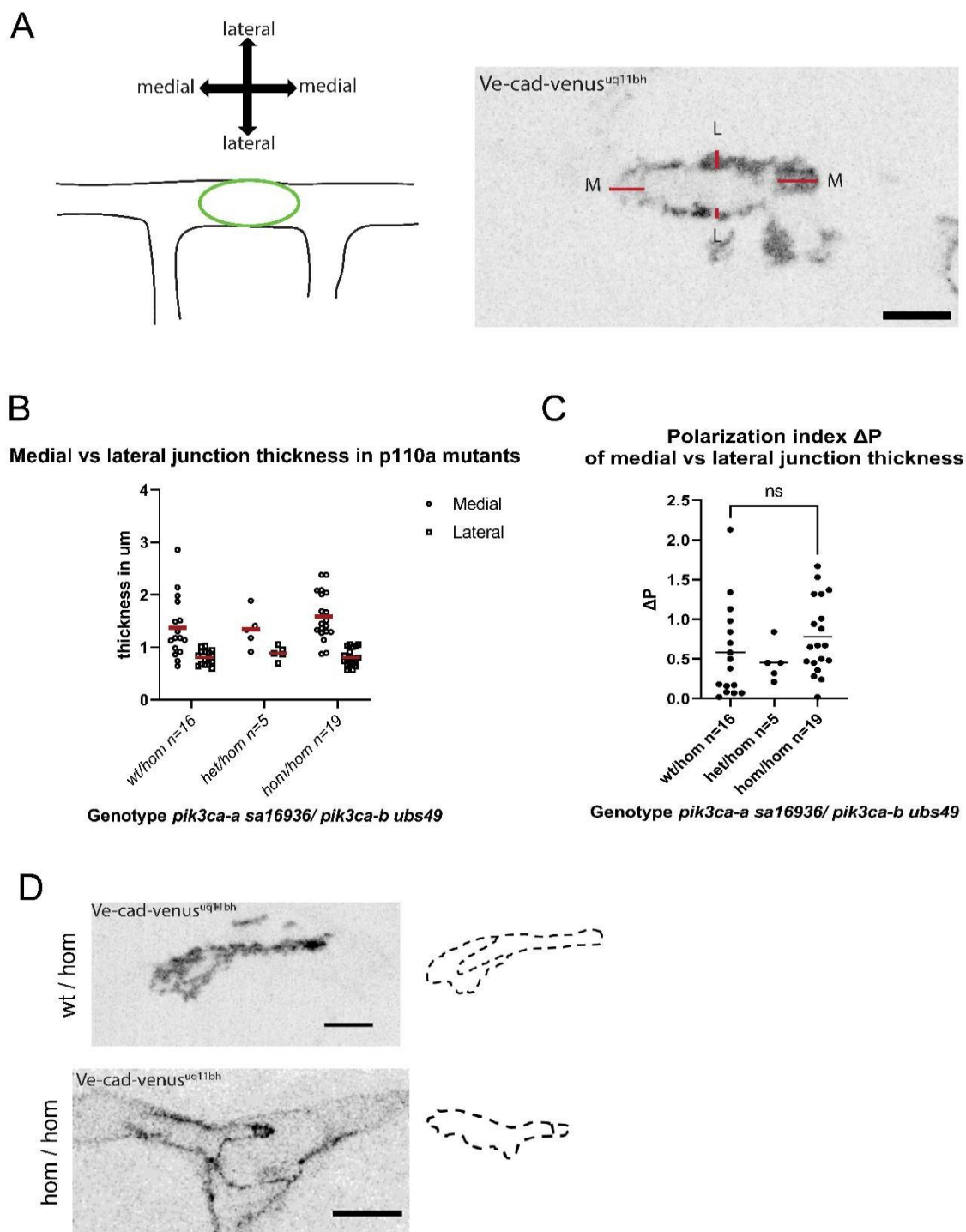


**Fig. 24: Polarized Ve-cad distribution is unchanged in endothelial junctions in *pik3ca* mutants**

**A** Schematic illustration of medial and lateral sides in an elongating junctional ring and exemplified junctional ring in a *pik3ca*<sup>wt/hom</sup> embryo on the right. M=medial, L=lateral. Scale bar is 5 $\mu\text{m}$ .

**B** Medial and lateral junction thickness assessed by signal of Ve-cad-venus in *pik3ca* mutant embryos at 28-31hpf. Only anastomotic junctions in the DLAV were measured. **C** Polarization index  $\Delta P$  for assessed junctions in B.  $\Delta P$  was calculated as medial thickness minus lateral thickness. Statistical analysis performed with Unpaired T-test returned  $p=0,2796$ .

**D** Two examples of double junctions in the DLAV of *pik3ca* heterozygous/homozygous and *pik3ca* double homozygous sibling embryos

labelled with Ve-cad-venus, schematic drawing of corresponding junction ring in right panel. Scale bar is 10 $\mu$ m.

In addition to the unchanged polarization of VE-cad distribution, the formation of double junctions during JBL was observed in both *pik3ca* double homozygous mutants as well as control siblings (Fig. 24 D).

Taken together, these results hint towards JBL being independent of PI3-Kinase  $\alpha$  signaling. However, so far only junctional elongation speed and polarization was analyzed, both of which are an indirect way to quantify JBLs. More thorough examination of the putative connection between JBL and PI3-Kinase  $\alpha$  signaling is needed at this point. Further experiments in *pik3ca* mutants will focus e.g. on JBL frequency over time, their size, duration and appearance in *pik3ca* mutants to fully characterize the impact of PI3-Kinase  $\alpha$  signaling on JBL formation and function.

#### **4.6. Loss of PI3-Kinase $\alpha$ signaling results in unstable *de novo* cellular contacts**

Endothelial cell rearrangements entail formation of new cell-cell contacts, cell junction elongation and subsequent merging of the apical compartments (Herwig *et al.*, 2011). I showed that the process of cell rearrangements is incomplete when signaling by PI3-Kinase  $\alpha$  is abrogated. However, although more precise analysis is needed here, the process of junction elongation via JBL seems to be independent of PI3-Kinase  $\alpha$  signaling. If cell junction elongation is (putatively) normal when PI3-Kinase  $\alpha$  signaling is abrogated, there must be another reason for the incomplete cell rearrangement phenotype. I thus focused on the next step during cell rearrangements and analyzed the formation of new cell-cell contacts and junction mergence during dynamic cell intercalation movements in *pik3ca* mutant embryos. When two junctions between rearranging ECs have elongated far enough, they eventually meet. A new junctional connection between partaking cells must be established in order to connect the junctions. Simultaneously, the third partaking cell must retract in order to give way and allow the fusion of the luminal pockets of the two merging junctions (Fig. 26). Meanwhile, the apical compartments expand and



connect the functional lumen between the three cells outlining the vessel, a process also known as chord hollowing. In summary, junction mergence is the last step by which vessels transform from a unicellular to a multicellular architecture.

To analyze whether the formation of new junction contacts was affected by loss of PI3-Kinase  $\alpha$  signaling, the endothelial cell-cell junction specific VE-cad-Venus reporter was again used in *pik3ca* mutant background to perform time-lapse analyses of junctions in the DLAV from 28-36hpf. In control siblings, junctions reliably elongated and formed new contact sites when meeting another junction, thereby effectively transforming the vessel from a unicellular to multicellular state. This process was repeatedly observed in *pik3ca* single homozygous and heterozygous/homozygous embryos (5 and 4 movies, respectively, Fig. 25 B).

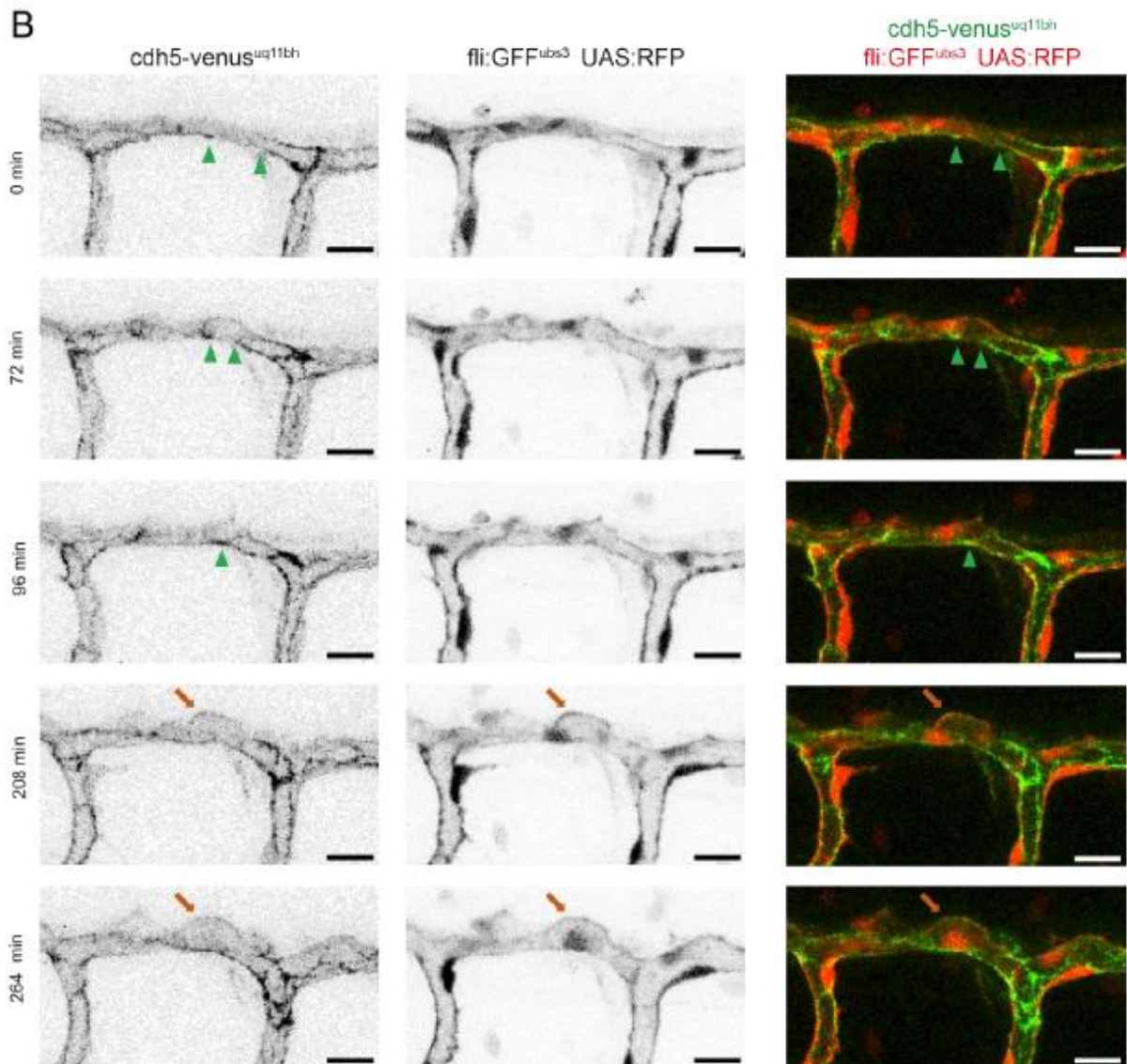
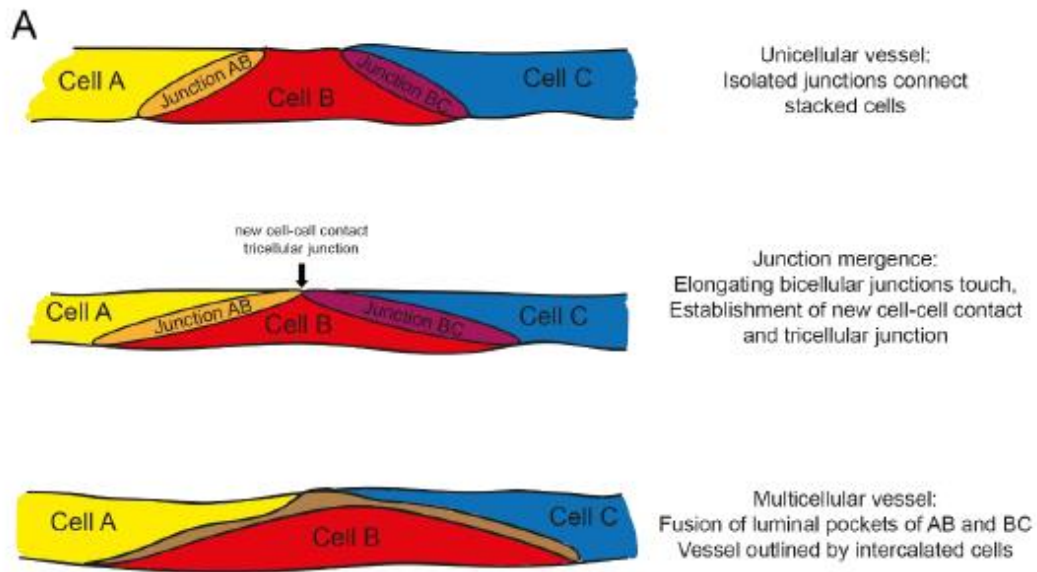


**Fig. 25: Junction mergence as the last step of vessel multicellularization**

**A** Schematic illustration of consecutive steps of junction mergence. **B** Successful junction mergence in the DLAV of a *pik3ca* heterozygous/homozygous mutant embryo at 32-36 hpf. ECs labelled with cytoplasmic RFP (mid panel), junctions are labelled by expression of VE-cad-Venus (left panel). Green arrowheads indicate distal ends of the two partaking junctions. Brown arrows indicate inflating lumen where apical compartments of junctions have merged. Scale bar 15µm.

In contrast to their single homozygous or heterozygous control siblings, *pik3ca* double homozygous mutants showed defects in the merging of two junctions. In at least one incident during 6 out of 8 acquired movies, junctions in the DLAV moved towards each other, but did not successfully form a *de novo* contact site and broke apart again (Fig. 26 A,B). These junctions failed to establish a functional tricellular contact point with a new junctional contact between the previously separated cells. Instead, the new contact sites were unstable, broke apart and cells moved again away from each other, rendering the third participating cell unpaired. At these particular sites, the vessel remained unicellular and was not covered with junctions. Together with a general delay in sprouting, breaking of *de novo* junctional contacts during cell intercalation appears to be the underlying reason why vessels remain partially unicellular in *pik3ca* mutants.

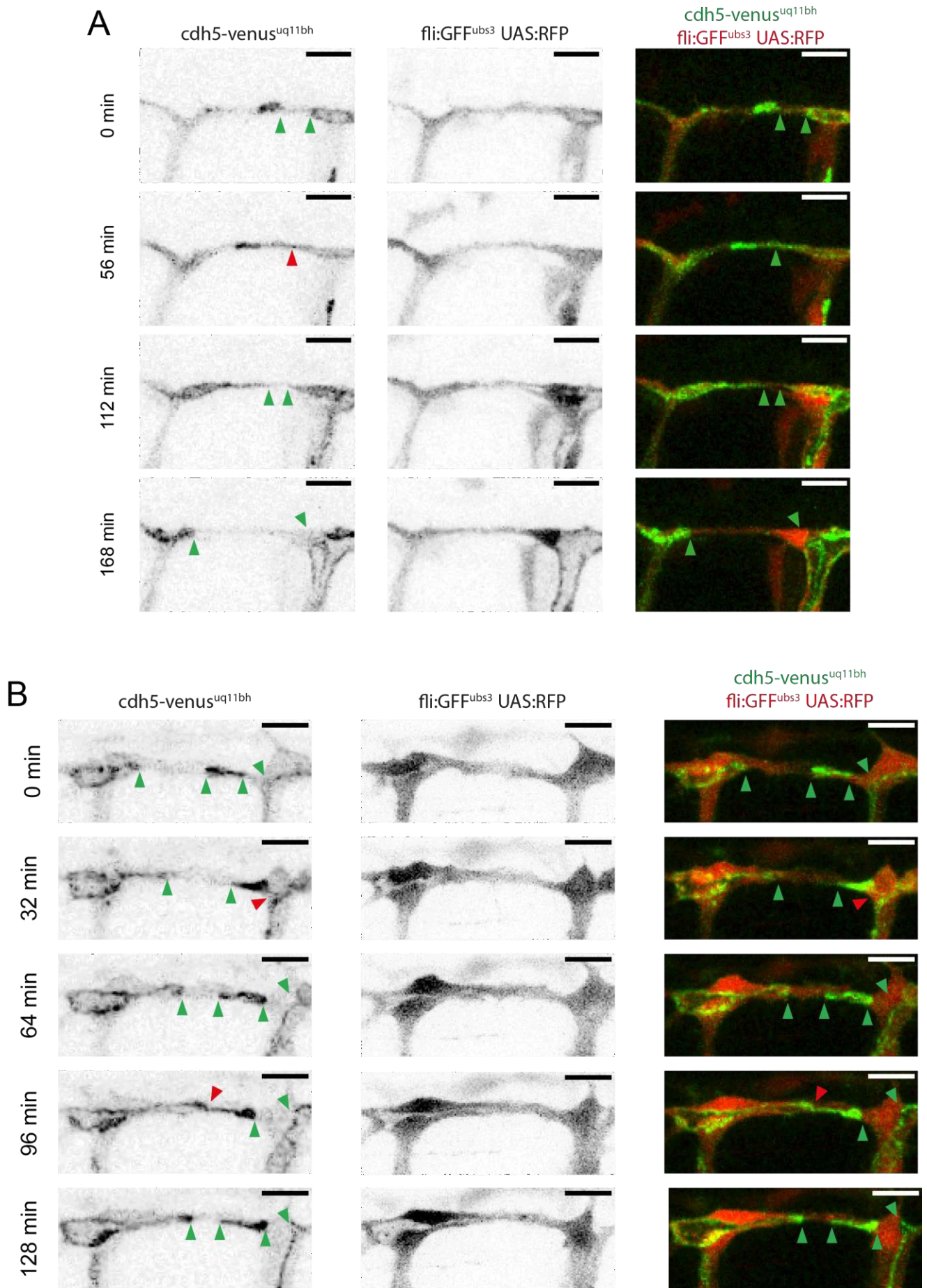


**Fig. 26: Breaking of unstable *de novo* junctional contacts in the DLAV in *pik3ca* double homozygous mutants**

**A and B** Time-lapse analysis in two examples of failed junction mergence due to breaking of tricellular junction in the DLAV at 29-32hpf. Both Embryos were double homozygous mutant for *pik3ca*. Green arrowheads indicate distal ends of elongating junctions in the DLAV. Red arrowheads indicate tricellular junction. Scale bar is 15µm.

## 4.7. Spatiotemporal resolution of PI3-Kinase $\alpha$ activity at endothelial junctions

Endothelial cell intercalation during cell rearrangements entails local and dynamic cell shape changes as a consequence of polarized cell actions. My observations that abrogating PI3-Kinase  $\alpha$  activity leads to defects in cell rearrangements raised the question whether signaling by PI3-Kinase  $\alpha$  is involved in polar cell behavior, e.g. local formation of JBL at junctions.

According to this view, the reception of an external (global) signal would be translated into a local subcellular activation of PI3-Kinase  $\alpha$ . To test this hypothesis, we aimed to resolve PI3-Kinase  $\alpha$  activity at the subcellular level in ECs.

In collaboration with Fabio Tschudin, a master student in the group, we used for this purpose a fluorescent biosensor for local accumulation of PIP3, which is the direct product of PI3-Kinase  $\alpha$  activity. The biosensor consists of the PIP3-binding PH-domain of Akt fused to a fluorophore (EGFP) (Fig. 27 A) and has been verified already in several studies *in vitro* and *in vivo* (e.g. Yoo *et al.*, 2010, Arriemerlou *et al.*, 2005). Exact details on the nature and construction of the sensor construct is described in Tschudin, 2022 (Master dissertation).

We created a zebrafish line expressing the PIP3-sensor in all ECs (*Tg(fli:PH-Akt-EGFP)<sup>ubs55</sup>*). Although stably transgenic, this reporter line shows mosaic expression of the sensor in individual ECs, allowing for identification of the sensor signal from distinct cells.

In the endothelium of transgenic embryos, we observed local EGFP accumulations predominantly at endothelial cell-cell junctions (Fig. 27, 28). When analysed together with a membrane marker (mCherry-CAAX), the local EGFP intensity peaks were independent of the amount of membrane at the analyzed position and occurred specifically at EC interfaces, but not over the cell body (Tschudin, Master dissertation, 2022).

To verify that these intensity peaks were indeed caused by the sensor binding to local high PIP3 levels, I acutely abrogated PI3-Kinase  $\alpha$  signaling using the  $\alpha$ -isoform specific inhibitor GDC-0326. Here, embryos expressing both the PIP3-sensor and ZO1-tdTomato labeling cell junctions were treated with vehicle (DMSO) or inhibitor two hours prior imaging, and EGFP levels at junctions were assessed in the DLAV. In DMSO-treated embryos, local EGFP peaks were still present at endothelial junctions (Fig. 27 B). In contrast, ECs in embryos treated with GDC-0326 displayed evenly distributed EGFP levels without any local intensity peaks (Fig. 27 C).

These results confirm that the observed local EGFP intensity peaks are indeed caused by PIP3 accumulations produced by PI3-Kinases in ECs, thereby validating the sensor as a suitable tool to study subcellular localization of PI3-Kinase activity. Additionally, this shows that PI3-Kinase signaling at endothelial junctions is specifically caused by subcellular activity of PI3-Kinase  $\alpha$  and no other isoform.



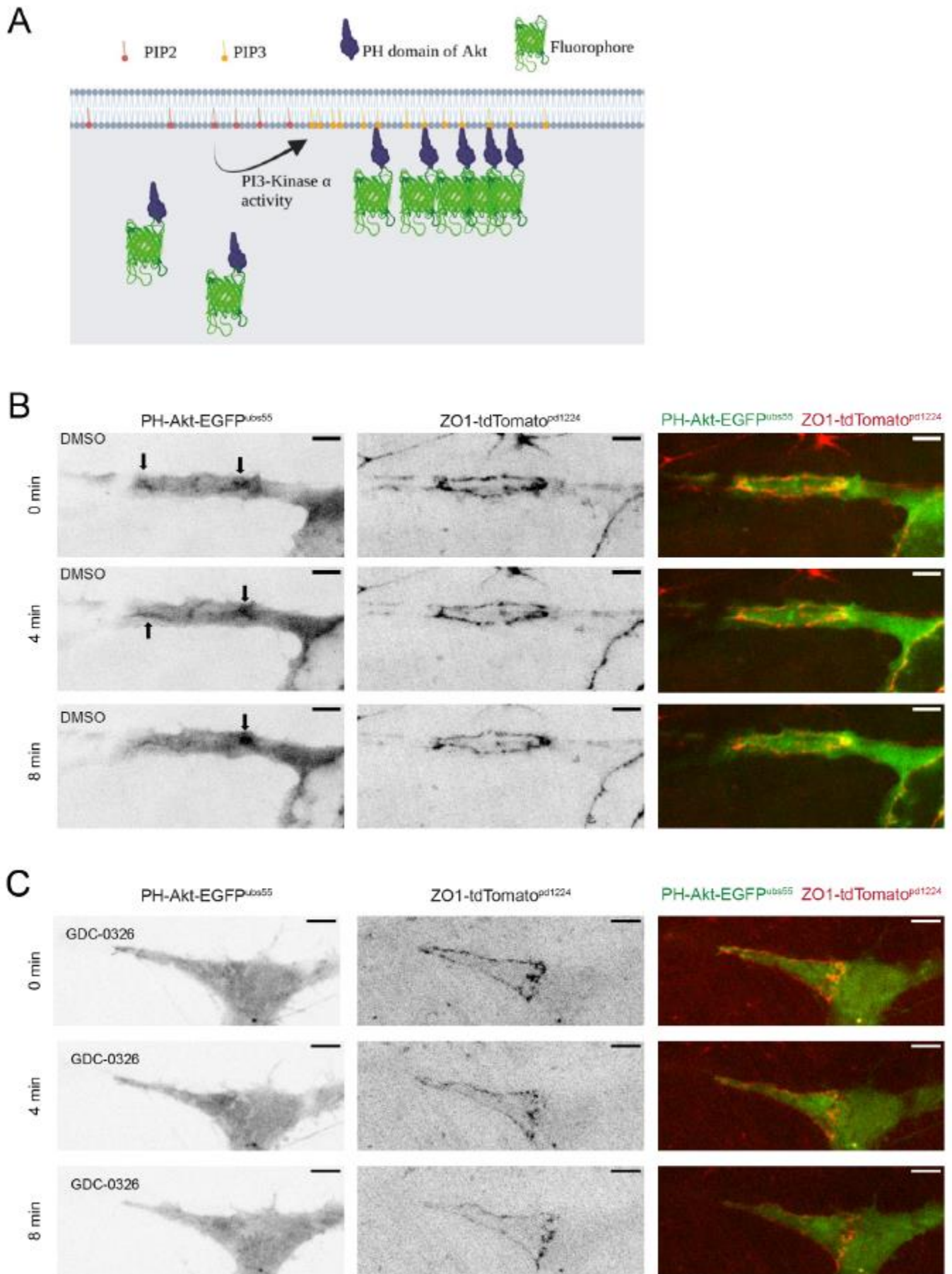


**Fig. 27: PIP3 accumulation at endothelial cell-cell junctions depends on PI3-Kinase  $\alpha$  signaling**

**A** Schematic representation of the PIP3-sensor working mechanism. High local EGFP signal indicates high local PIP3 concentration upon PI3-Kinase activity. **B** Time lapse imaging of PH-Akt-EGFP at an endothelial junction labelled by ZO1-tdTomato in the DLAV at 30hpf. Embryos were treated with 1,8% DMSO in E3 medium two hours prior to imaging. Black arrows indicate high EGFP intensity due to local accumulation of PIP3 at distal ends of the junction. Scale bar is 5 $\mu$ m. **C** Time lapse imaging of PH-Akt-EGFP at an endothelial junction similar to A, but embryo treated with 50 $\mu$ M GDC-0326 in E3 medium two hours prior to imaging. Scale bar is 5 $\mu$ m.

With the validated sensor system, we aimed to connect subcellular PI3-Kinase  $\alpha$  signaling to polarized ECI behaviors such as junction elongation. We transiently expressed the PIP3 sensor in embryos between 28 and 33hpf and assessed the dynamic changes in fluorescence intensity at elongating junctions in the trunk vasculature. As shown in Fig 28 B, local intensity peaks of EGFP at the distal end of EC junctions coincided with the elongation movement marked by forward progression of ZO1 and F-actin. Thus, PI3-Kinase  $\alpha$  exerts polarized activity at elongating endothelial junctions in the direction of movement.



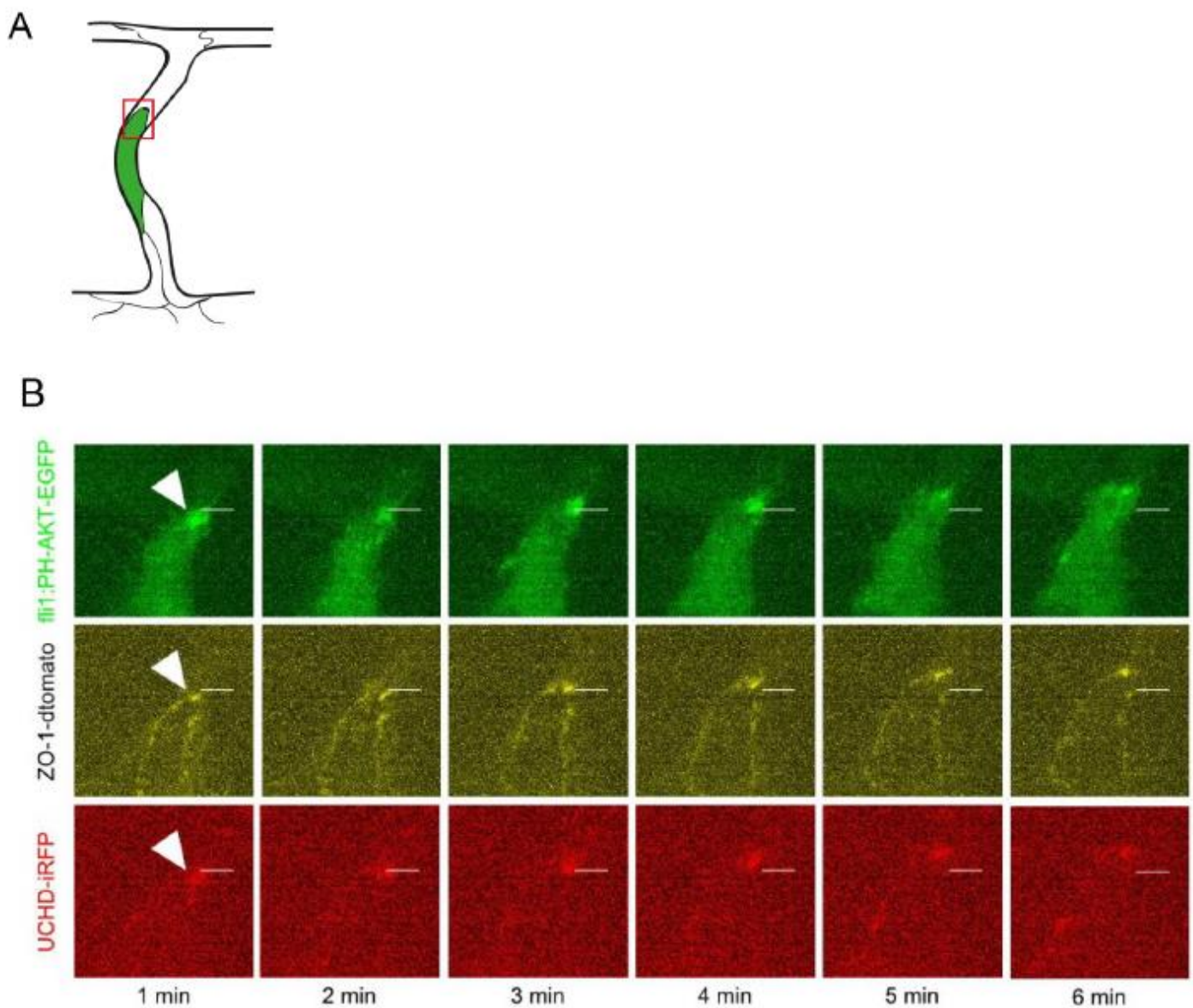


**Fig 28: PI3-Kinase signaling correlates with endothelial junction elongation**

**A** Schematic drawing illustrating the position of close-up panels in C in an ISV stalk cell. **B** Transient expression of the PIP3-sensor in an ISV stalk cell also fluorescently labelling junctions (ZO1) and F-Actin (UCHD). White line as fixed point during elongation movement of the cell. Enhanced local EGFP intensity at the elongating front of the junction indicated by white arrowheads. Figure B from Tschudin, 2022, Master thesis.

When analyzing the time-lapse imaging data of the PIP3-sensor at junctions, two important additional observations were made.

First, when one EC expressed the sensor at much higher levels than the second

(quasi mosaic), the sensor indicated high PIP3 levels on both ends of the junction (Fig. 29 A, black arrows, also in Fig. 27 B). Unfortunately, with the EGFP-tagged sensor, we are currently not able to clearly resolve whether the EGFP peaks come from two individual partaking cells or whether both peaks are inside the same cell. To this end, we have generated a mClav-tagged version of the PIP3-sensor and are planning to use photoconversion experiments to test the contribution of individual cells to the PIP3 accumulations at endothelial junctions.

Secondly, the EGFP intensity peaks at distal ends of elongating junctions showed oscillating intensity with peaks every 6 to 9 minutes (Fig. 29 C). Although more data is needed to thoroughly characterize this behavior, it is interesting to note that this is also the interval at which JBL occur at distal ends of elongating endothelial junctions (Paatero *et al.*, 2018).

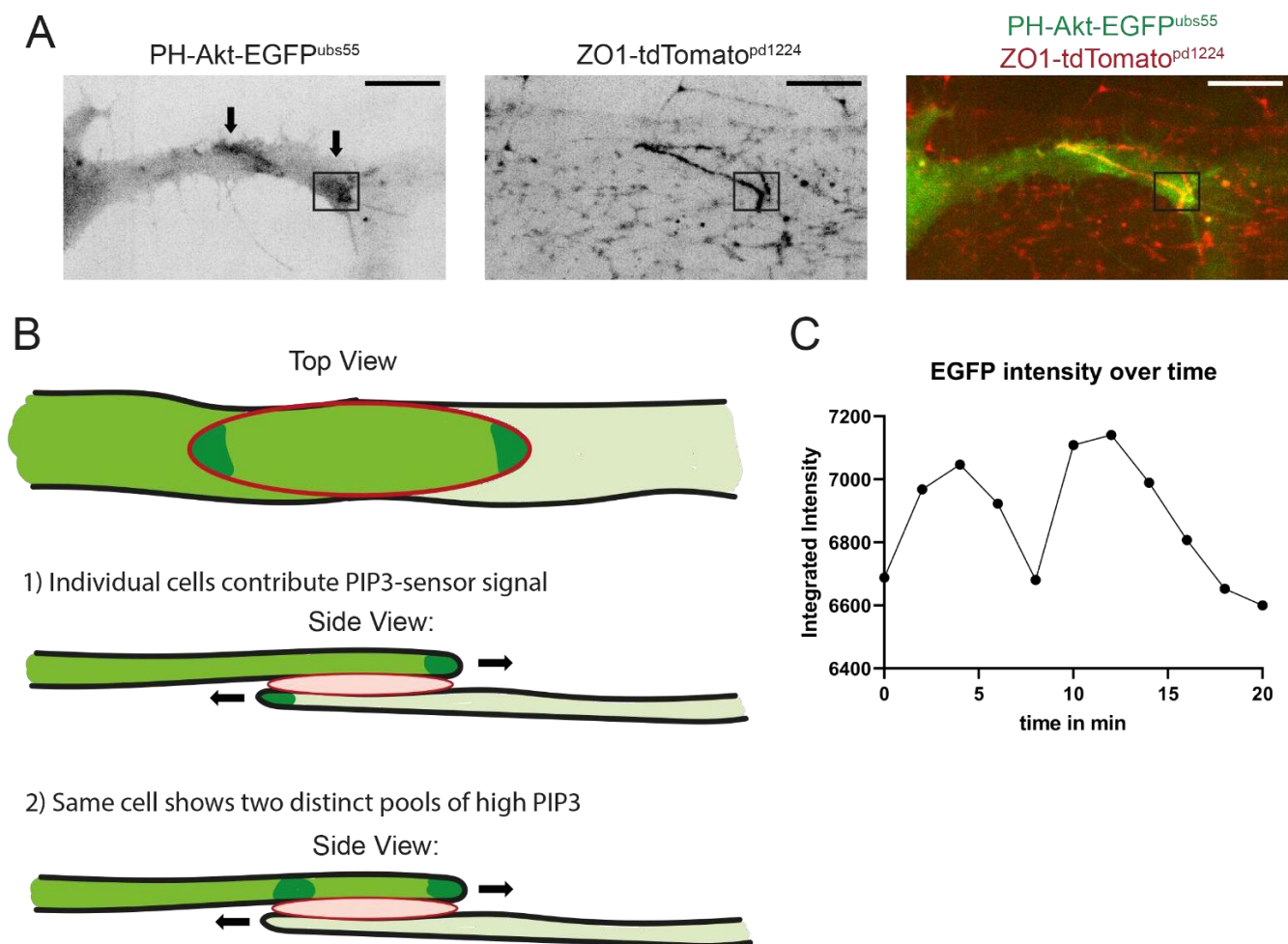


**Fig. 29: Recurring PIP3 accumulations at both ends of elongating endothelial junctions**

**A** Endothelial cell-cell junction in the DLAV (31 hpf) at which the left cell expresses PIP3-sensor at higher levels than right cell (quasi mosaic). Junction labelled with ZO1-tdTomato<sup>Pd1224</sup>. Black arrows indicate local high PIP3 levels at both ends of the junction. Black window depicts ROI quantified in C. Scale bar 10  $\mu$ m. **B** Schematic illustration of top view and two possible side views of setting according to A. Dark green indicates local EGFP signal by accumulation of PIP3 at both ends of the junction. Arrows indicate direction of elongation of the respective cell. **C** Quantification of EGFP signal over time in the ROI depicted in A. Intensity levels acquired by Integrated Intensity Measurement in ImageJ (Fiji).

## 4.8 PI3-Kinase $\alpha$ signaling at endothelial cell junctions is independent of canonical VEGFR2 or VEGFR3 signaling

Canonically, PI3-Kinase  $\alpha$  is activated by VEGFR isoforms 2 and 3 signaling in the vasculature. Since the PIP3-sensor showed distinct localization of PI3-Kinase  $\alpha$  activity at EC junctions, I asked which isoform was responsible for the local activation, or whether they function redundantly.

To address this question, I first tested the potency and necessary concentrations of isoform-specific inhibitors targeting VEGFR2 (SU5416) and VEGFR3 (SAR131675) to fully abrogate the respective signaling pathway (Supplementary Fig. 2). After determining the correct concentrations, I acutely abrogated VEGFR2, VEGFR3 or both simultaneously and assessed fluctuations in the PIP3-sensor signal at EC junctions marked by ZO-1.

In contrast to inhibition of PI3-Kinase  $\alpha$  directly (Fig. 27), the local EGFP intensity peaks marking high local PI3-Kinase  $\alpha$  activity were still detected when VEGFR2, VEGFR3 or both were acutely inhibited. Oscillating PI3-Kinase  $\alpha$  activity at the distal ends of EC junctions was independent of VEGFR2 or VEGFR3 signaling (Fig. 30). Furthermore, combinatory inhibition of both RTKs did also not abrogate the EGFP intensity peaks, excluding redundant functions if the two isoforms in the local activation of PI3-Kinase  $\alpha$ .

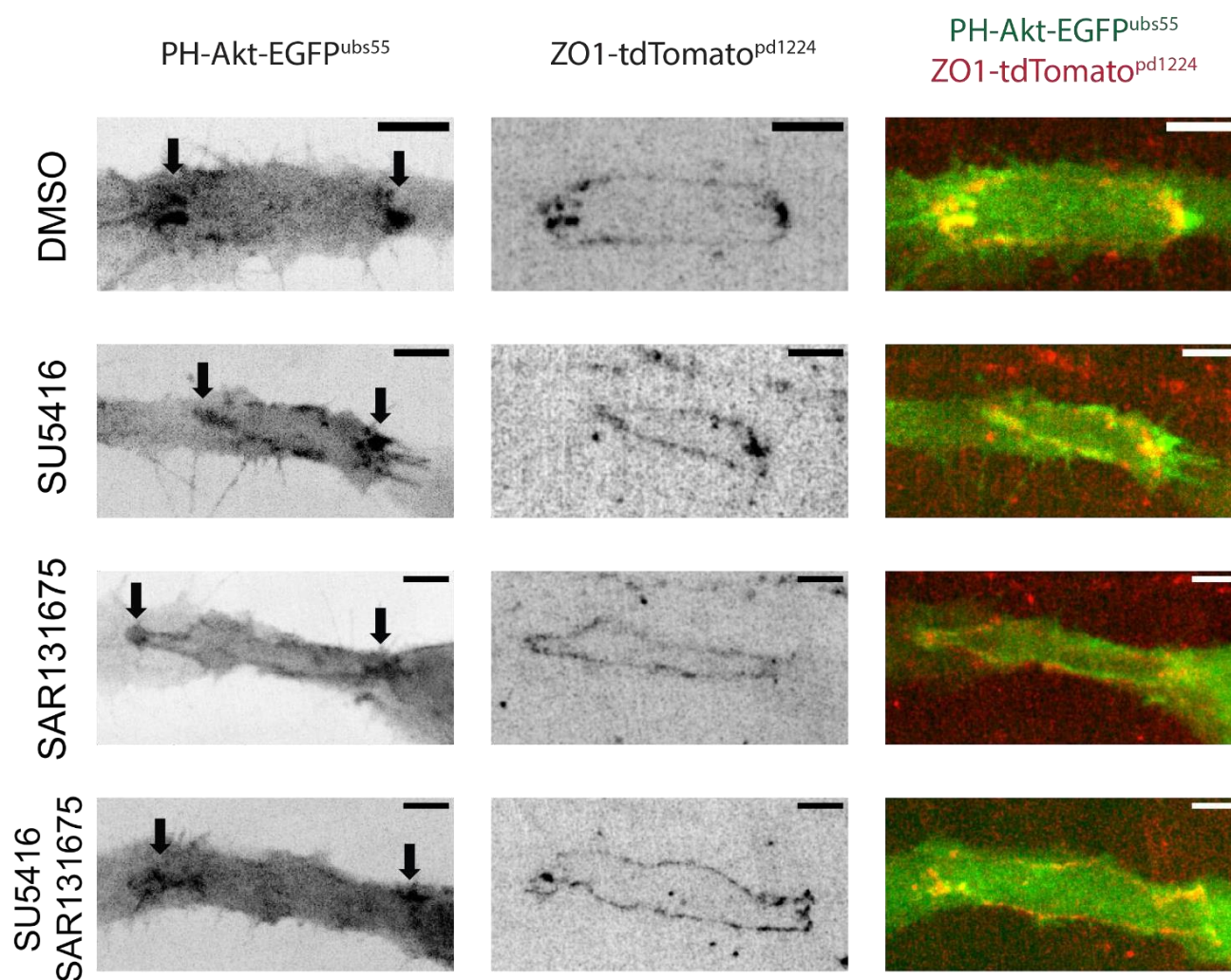


**Fig. 30: Local PI3-Kinase  $\alpha$  activity is independent of canonical VEGFR2/3 signaling**

Representative confocal images of PIP3-sensor signal and fluorescently labelled ZO1 at anastomotic junctions in the DLAV of 28-31 hpf transgenic zebrafish embryos. Inhibition of VEGFR2 (SU5416), VEGFR3 (SAR131675) or both was started approx. 1.5h prior imaging. Black arrows indicate local accumulation of PIP3 at distal ends of the junctions. Scale bar 5 $\mu$ m.





V

## Discussion

---

## 5.1 A genetic model to study PI3-Kinase $\alpha$ function in zebrafish vascular development

Multicellular vascular tube formation relies on dynamic EC rearrangements and cell-cell junction elongation. It was shown already in the study of Angulo-Urarte *et al.*, 2018, that signaling by the lipid kinase PI3-Kinase  $\alpha$  is essential during cell rearrangement processes, as abrogation of PI3-Kinase  $\alpha$  signaling impaired EC junction elongation both in the zebrafish trunk and in the mouse retina vasculature. However, the molecular details of how PI3-Kinase  $\alpha$  promotes dynamic cell intercalation movements and, especially, whether the kinase plays a role in JBL as the driving mechanism junction elongation, was not known at the beginning of my thesis work.

Since a genetic tool in zebrafish was not available at the time, the previous study used chemical inhibition to investigate the role of PI3-Kinase  $\alpha$  in cardiovascular development. Thus, in a first step, I aimed for a genetic approach to abrogate PI3-Kinase  $\alpha$  in zebrafish embryos.

PI3-Kinase  $\alpha$  is a heterodimer consisting of a regulatory subunit (p85) and a catalytic subunit (p110 $\alpha$ ), the latter of which is encoded by the *pik3ca* gene. Genetic analysis of *pik3ca* in the zebrafish genome revealed two distinct *pik3ca* genes, one on chromosome 11 and another on chromosome 23. Since the gene located on chromosome 23 had not been annotated as p110 $\alpha$ -encoding so far, a new nomenclature for the two genes is proposed: *pik3ca-a* and *pik3ca-b* on chromosome 11 and 23, respectively. The two genes encode highly similar proteins and are both expressed during embryonic development according to the common zebrafish RNA expression database.

A putative null allele for *pik3ca-a* was acquired from Sanger Institutes, whereas two putative null alleles for *pik3ca-b* were created using CRISPR/Cas9 genome editing technology.

Embryos homozygous mutant for the *pik3ca-a* mutant allele *sa16936* do not develop a functional swim bladder and are not viable beyond 5-6 dpf. However, I did not observe any vascular defects in these embryos. Apart from the larval lethality, these



---

embryos developed normally and did not show impaired EC rearrangements.

Homozygous knockout of *pik3ca-b* with either of the two created alleles also did not cause vascular defects. Here, embryos are able to develop a functional swim bladder, are viable and become fertile adults.

Interestingly, only embryos double homozygous for both the *pik3ca-a* knockout allele *sa16936* and for one of the two *pik3ca-b* alleles *ubs49* or *ubs50* show impaired cell rearrangements in antibody stainings of the trunk vasculature at 32hpf. The observed phenotypes are highly similar to the phenotypes observed in the earlier inhibitor study, validating its results, but also verifying the acquired alleles as true knockouts. Similarly, only double homozygous mutants show vascular hyperplasia in the CVP (see also chapter 4.2.1), which was also previously observed under chemical PI3-Kinase  $\alpha$  inhibition (A. Angulo-Urarte, unpublished).

Additionally, embryos homozygous mutant for *pik3ca-a* and transheterozygous for the two *pik3ca-b* alleles phenocopy the cell rearrangement defects of double homozygous embryos (Supplementary Fig.1). This further validates the CRISPR-generated alleles as true loss-of-function alleles and confirms the suitability of the acquired alleles as a tool to study PI3-Kinase  $\alpha$  function in multicellular vascular tube formation.

A single wild-type copy of either one of the two *pik3ca* genes was able to rescue cell rearrangements ISVs and DLAV. This means that the two genes have redundant functions during multicellular tube formation and already a single gene copy can rescue the rearrangement phenotype if the others are mutated or lost. Furthermore, the hyperplasia phenotype observed in the CVP was also rescued by a single wild-type allele of either of the genes, suggesting redundancy not only during cell rearrangements, but in the vasculature *per se*. In contrast, the swim bladder defects appeared only in homozygous *pik3ca-a* mutants with 100% penetrance, but not in larvae homozygous for either of the two *pik3ca-b* mutant alleles. Thus, the gene product of *pik3ca-a* is essential for swim bladder development, whereas *pik3ca-b* is dispensable in this process. Since *pik3ca-b* knockout mutants become viable and fertile without any visible defects, any function of this gene can apparently be rescued by *pik3ca-a*, but *pik3ca-b* is not able to rescue the *pik3ca-a* knockout swim bladder phenotype. In conclusion, the two genes fulfil redundant functions in the vasculature, but distinct functions in other tissues, such as the swim bladder.

---

## 5.2 Distinct functions of PI3-Kinase $\alpha$ in different vascular beds

Zebrafish mutant for *pik3ca* displayed different phenotypes in distinct vascular beds, indicating particular roles of the kinase depending on vessel identity and developmental process. Concomitant with careful dissection of PI3-Kinase  $\alpha$  function in the development of DA, CV, CVP and trunk vasculature, I also analyzed dynamic relocalization of FOXO, a downstream target of PI3-Kinase  $\alpha$  signaling, upon acute chemical inhibition of PI3-Kinase  $\alpha$ . Dissimilar behaviors of FOXO in different vascular tissues suggests differential regulation of FOXO in distinct vessel types and, again, separate functions of PI3-Kinase  $\alpha$  signaling in different vascular beds.

### 5.2.1 General cardiovascular development in zebrafish embryos in absence of PI3-Kinase $\alpha$ signaling

Using the genetic model to study PI3-Kinase  $\alpha$  signaling in zebrafish, I started investigating the overall phenotypes produced in the vasculature by genetic loss of PI3-Kinase  $\alpha$ .

#### Development of the DA and CV

The first two axial vessels of the zebrafish embryo, the DA and CV/PCV, develop via vasculogenesis. In *pik3ca* double mutants, both DA and CV formed and blood flow was observed, indicating that the kinase is dispensable for vasculogenesis of the first vessels. The heart rate was slightly reduced in *pik3ca* double mutants, albeit not to a statistically significant level. Furthermore, blood flow velocity in the DA was found normal, indicating normal heart function upon loss of PI3-Kinase  $\alpha$  signaling.

A so far unpublished study (Zhou *et al.*, 2020, *bioRxiv*) reports decreased diameter of the DA and CV as well as ectopic connections between them in zebrafish embryos mutant for *Akt*. Since *Akt* is one of the main downstream targets of PI3-Kinase  $\alpha$ , similar phenotypes could potentially be expected upon loss of PI3-Kinase  $\alpha$ .

However, no ectopic connections between the two axial vessels were observed in

---

*pik3ca* double mutants. I measured the diameter of the DA at different time points during development and, indeed, DA diameter was decreased upon genetic loss of PI3-Kinase  $\alpha$ . This could potentially be caused by reduced EC proliferation downstream of reduced Akt activity, as has been reported for ISVs and DLAV when abrogating PI3-Kinase signaling chemically (Angulo-Urarte *et al.*, 2018, Lange *et al.*, 2022). In turn, this hypothesis would support a specific function for PI3-Kinase  $\alpha$  signaling in promoting EC proliferation in arterial vessels such as DA, primary ISVs and DLAV (see also Fig. 31).

### Development of ISVs and DLAV

In the trunk vasculature of *pik3ca* double mutants, primary sprouts from the DA emerged regularly interspaced and reached their final dorsal position above the neural tube. Although not quantified directly, I observed a delay in sprouting and ISV outgrowth from the DA of approximately about 1.5 to 2 hours. Likewise, the onset of blood flow in ISVs was delayed in *pik3ca* double mutants. Apart from this delay, which could be due to a general delay in embryonic development, sprouting and outgrowth of primary ISVs was not affected by loss of PI3-Kinase  $\alpha$  signaling. This is in line with the finding that of the two main signaling outputs of VEGFR2 signaling, namely PI3-Kinase and ERK, ERK is responsible for induction of ISV sprouting and migration (Shin *et al.*, 2016-1). In contrast, abrogation of class I PI3-Kinases or PI3-Kinase  $\alpha$  specifically was shown to inhibit cell proliferation in ISVs, leading to reduced cell number (Angulo-Urarte *et al.*, 2018, Lange *et al.*, 2022).

In some cases, tip cells of primary ISV sprouts in *pik3ca* double mutants acquired a Y-shaped conformation when growing over the neural tube instead of the wild-type T-conformation once the dorsal side is reached. Furthermore, the DLAV showed supernumerary contacts between tip cells during early development of this vessel, and displayed a webbed intermediate appearance, which was resolved as the surplus contacts were gradually pruned. However, migration *per se* was not affected, as sprouts were able to reach their destined positions and form the DLAV, indicating sprouting induction, EC migration and anastomosis being independent of PI3-Kinase  $\alpha$ .

ERK signaling in the trunk vasculature was shown to regulate arteriovenous identity in ECs, promoting arterial cell fate. PI3-Kinase  $\alpha$  signaling can feedback and finetune

---

ERK signaling levels, potentially interfering with arteriovenous identity of ISVs as well. Quantification of arterial vs. venous ISV fate in the trunk vasculature both by expression of an arterial marker and by blood flow direction showed no changes in the number of arterially fated ISVs between wild-type and PI3-Kinase  $\alpha$  mutant embryos. Thus, arteriovenous specification of ISVs is independent of PI3-Kinase  $\alpha$  signaling regulating ERK levels.

### Development of the CVP

Double homozygous *pik3ca* mutant embryos displayed general hyperplasia and subsequent enlarged vascular loops in the CVP starting around 34-36 hpf. This phenotype was easily recognizable and reproducible in double homozygous mutants, but was rescued by a single wild-type allele of either of the genes (see chapter 4.1). Time-lapse imaging revealed thickened sprouts emerging ventrally from the CV, which anastomosed at the ventral side and formed the observed enlarged loops in the developing plexus. Quantification of these loops showed that the overall abundance of loops during CVP development was unchanged, but their average size almost doubled in *pik3ca* double homozygous mutants. This could be caused by an increase in total EC number in the plexus due to hyperproliferation, hypermigration of ECs towards ventral or by ECs becoming generally larger. Arteriovenous specification of ECs in the CVP was unchanged upon genetic loss of PI3-Kinase  $\alpha$ . In case the hyperplasia in *pik3ca* mutants is indeed caused by elevated EC proliferation, this would be an extremely interesting finding as it opposes the commonly accepted role of PI3-Kinase  $\alpha$  signaling promoting cell proliferation downstream of Akt. Reduced EC number was observed in zebrafish ISVs and DLAV when abrogating PI3-Kinase  $\alpha$  chemically (Angulo-Urarte *et al.*, 2018, Lange *et al.*, 2022) as well as in PIK3CA mutant mouse retinae (Angulo-Urarte *et al.*, 2018). Therefore, loss of PI3-Kinase  $\alpha$  signaling causing increased EC proliferation in the CVP would point towards a tissue-specific role of PI3-Kinase  $\alpha$  and also indicate an interplay with distinct signaling pathways regulating cell proliferation. This notion is, in fact, not new. It was shown before, that venous ECs react differently to changes in the levels of PI3-Kinase signaling than arterial ECs. Gain-of-function mutations in the PIK3CA gene in mice cause spontaneous malformations in veins (Castillo *et al.*, 2016) and in low flow conditions such as during sprouting

---

angiogenesis (Kobialka *et al.*, 2022) but not in big caliber arteries. High flow conditions and arterial identity seem to potentially enhance robustness of ECs to altered PI3-Kinase  $\alpha$  signaling and prevent pathological outcomes. In turn, venous EC identity and low-flow conditions, such as a position at the sprouting front of an angiogenic plexus, enhances sensitivity to PI3-Kinase  $\alpha$ . The phenotypes I described in zebrafish *pik3ca* mutant primary ISVs and DLAV (arterial, but not to low flow) and CVP (venous identity) agree with this hypothesis. To further support this idea, I propose investigating phenotypes in other vessels that fall under these categories, e.g. the developing subintestinal vascular plexus (SIV).

Ventral sprouting in the zebrafish CVP is regulated by Bmp2b signaling via its receptors Bmpr2a and Bmpr2b (Wiley *et al.*, 2011) and abrogation of either ligand or receptors prohibits ventral sprouting and CVP formation. Additionally, mice deficient for the BMP receptor ALK1 displayed elevated levels of PI3-Kinase signaling during the formation of arteriovenous malformations (AVMs, Ola *et al.*, 2016), which are phenotypically similar to the observed CVP hyperplasia in *pik3ca* mutant zebrafish embryos. These findings point towards a regulatory interplay between PI3-Kinase  $\alpha$  signaling and Bmp signaling in the CVP, if not in other venous tissues as well. Generally, PI3-Kinase  $\alpha$  is thought to promote EC proliferation via Akt, which was shown by reduction of cell proliferation in ISVs and DLAV upon chemical inhibition of PI3-Kinase  $\alpha$  (Angulo-Urarte *et al.*, 2018, Lange *et al.*, 2022). In venous tissues such as the CVP, my data suggests a role of PI3-Kinase in inhibiting cell proliferation, possibly by downregulating BMP signaling (Fig. 31).

To investigate this possibility, I plan to assess changes in levels of BMP signaling in the CVP when abrogating PI3-Kinase  $\alpha$  signaling chemically and acutely on transgenic BMP-reporter embryos. Elevated BMP signaling would support reciprocal regulation between the two signaling pathways controlling CVP development. In collaboration with Dr. Jianmin Yin, a postdoc in the group, I plan to perform antibody stainings against phosphorylated Smad (p-Smad) in the CVP in *pik3ca* mutants as a direct readout for active BMP signaling. Lower p-Smad levels upon genetic loss of PI3-Kinase  $\alpha$  would further strengthen the hypothesis of a relationship between signaling by BMP and PI3-Kinase  $\alpha$  in venous ECs.

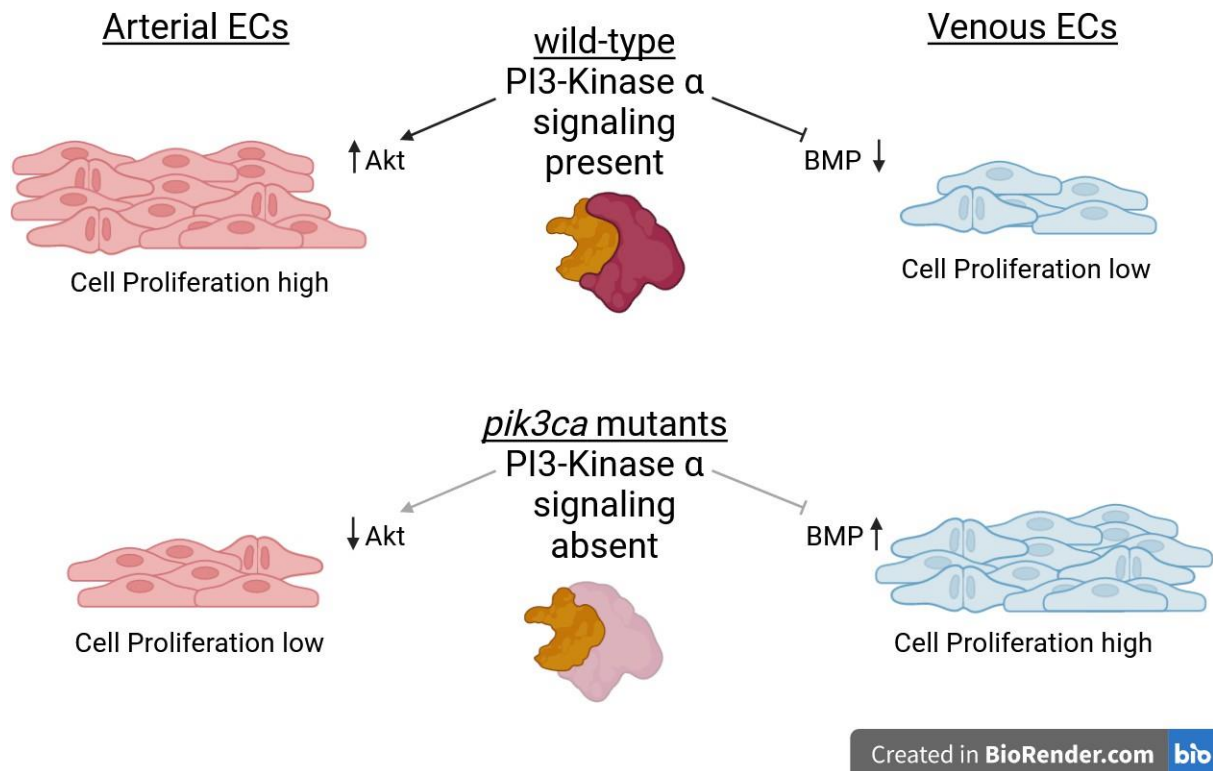


**Fig. 31: Differential regulation of cell proliferation by PI3-Kinase  $\alpha$  in arterial and venous ECs**

Proposed model of PI3-Kinase  $\alpha$  promoting cell proliferation in arterial ECs presumably via Akt, and potentially downregulating cell proliferation by inhibition of BMP signaling in venous ECs. Absence of PI3-Kinase  $\alpha$ , e.g. by genetic loss of *pik3ca*, leads to reduced Akt activity and decreased proliferation in arterial ECs. In contrast, loss of PI3-Kinase  $\alpha$  signaling increases cell proliferation in venous tissues due to overactivation of BMP signaling. Figure created in Biorender.

---

### 5.2.2 Differential regulation of Foxo, a downstream target of PI3-Kinase $\alpha$

An essential step in the analysis of PI3-Kinase  $\alpha$  signaling during vascular development in general was to see in which vessels the kinase is active. Based on the previously described distinct phenotypes in different vascular beds produced by genetic loss of PI3-Kinase  $\alpha$ , I initially assumed that the kinase would e.g. not be active in the DA and CV, but show activity in ISVs, DLAV and CVP.

To investigate this, I used a fluorescent reporter construct of EGFP-tagged Foxo, a transcription factor downstream of PI3-Kinase  $\alpha$ . Dynamic relocalization of Foxo to the nucleus in absence of PI3-Kinase  $\alpha$  signaling is commonly used to show abrogation of previously active PI3-kinase signaling (e.g. in Ola *et al.* 2016).

When inhibiting PI3-Kinase  $\alpha$  acutely via chemical treatment in *Tg(fli1a:Foxo1b-EGFP)<sup>bns515</sup>* embryos, I observed different behaviors dependent on the respective vascular bed.

As expected, upon PI3-Kinase inhibition, Foxo-EGFP relocalized to the nucleus in ISVs and in the DLAV. This dynamic behavior was reproducible between embryos and experiments and was also detected both with a pan-class I PI3-Kinase Inhibitor as well as with a  $\alpha$ -isoform-specific inhibitor, suggesting that in ISVs and DLAV, Foxo localization is regulated by PI3-Kinase  $\alpha$  activity and that the kinase is thus confirmedly active in these vessels.

In contrast, Foxo-EGFP in ECs in the DA did not react to acute abrogation of PI3-Kinase  $\alpha$  and no nuclear signal was observed at any given time point during treatment. This indicates that in these cells, Foxo is not regulated by PI3-Kinase  $\alpha$  signaling, but most likely by other pathways.

In the CV and CVP, some ECs displayed nuclear localization of Foxo-EGFP already prior inhibitor treatment in a salt-and-pepper distribution. Additionally, this localization did not change upon inhibition of all class I PI3-Kinases or PI3-Kinase  $\alpha$  specifically. This is most likely due to other inputs into Foxo signaling in these vessels, which are not affected by inhibitor treatment. In turn, this means that, similar to the DA, PI3-Kinase  $\alpha$  is not responsible for Foxo localization in these vascular tissues, again highlighting distinct functions of the kinase in different vascular beds.

---

## 5.3 PI3-Kinase $\alpha$ signaling in multicellular vascular tube formation

The main goal of this study was to investigate the function of PI3-Kinase  $\alpha$  signaling in the development of multicellular vascular tubes. It was shown already before that loss of PI3-Kinase  $\alpha$  impairs EC pairing and junction elongation underlying multicellular tube formation (Angulo-Urarte *et al.*, 2018). The study further identified a role of PI3-Kinase  $\alpha$  signaling in downregulation of actomyosin tension via activation of Myosin light chain phosphatase (MLCP).

In light of this, I aimed to further characterize the dynamic requirement of PI3-Kinase  $\alpha$  during EC rearrangements in multicellular vascular tube formation. Using the new *pik3ca* knockout alleles in zebrafish, I analyzed EC rearrangement dynamics in the mutant background by assessing the junctional phenotypes in ISVs and DLAV.

### 5.3.1 Endothelial cell intercalation requires PI3-Kinase $\alpha$ signaling

#### ***Pik3ca* mutants phenocopy chemical abrogation of PI3-Kinase $\alpha$ signaling during cell rearrangements in ISVs and DLAV**

I started investigating the effects of genetic loss of PI3-Kinase  $\alpha$  on cell rearrangements during vascular development by analyzing junction phenotypes in ISVs and DLAV in antibody stainings of *pik3ca* mutants at 32hpf. Here, the previously observed junction gap phenotypes under chemical inhibition were phenocopied in double mutants. In ISVs, the incidence of junction gaps was increased from 20-25% in wild-type and sibling control embryos to around 65% in double mutants. In the DLAV stainings, junction elongation was perturbed as well and a decrease in junction coverage of DLAV sections as readout for elongation was observed. Together, these observations validate both the mutants and the inhibitor treatment results. This data again confirms that signaling by PI3-Kinase  $\alpha$  is required during the formation of multicellular vascular tubes in the zebrafish trunk vasculature.



---

### **The DLAV of *pik3ca* mutants fails to become multicellular**

The DLAV is an anastomotic vessel which forms by contacts between and subsequent intercalation of primary ISV sprout tip cells. As the cells intercalate, their mutual interaction surfaces, the junctions, elongate as well. Consequently, junction coverage over time can be used as a readout to actually measure cell intercalation during the formation of the multicellular DLAV. To do so in *pik3ca* mutants, I performed live-imaging of EC rearrangement processes during the formation of the DLAV and measured junction coverage over time. As expected from previous experiments, tip cells were able to anastomose and formed junctional rings between them in both control siblings and double homozygous mutants. Thus, contact formation and anastomosis per se can occur independent of PI3-Kinase  $\alpha$  signaling. During the subsequent intercalation movements, junctional rings in double mutants initially elongated analogous to rings in control siblings. This observation was also confirmed by measuring the initial elongation speed of isolated junctional rings, which again was independent of the *pik3ca* genotype. Additionally, chemical abrogation of class I PI3-Kinases by LY294002 treatment did not change the junction elongation speed, further supporting junction elongation speed being independent of PI3-Kinase  $\alpha$  signaling. However, during live imaging I observed that once a certain ring size was reached, junctional rings in double mutants failed to elongate further, which was represented by the percentage of junction covered area staggering at around 60-70%, even when control siblings had already reached 100% coverage and developed a fully multicellular DLAV. This suggests that the DLAV fails to become multicellular in *pik3ca* mutants, but contains unicellular sections, in which the vessel consists only of a single cell that did not pair and intercalate with a second cell. This phenotype was retained in both ISVs and DLAV until at least 40hpf. However, ISVs and the DLAV became lumenized even in the unicellular parts where the lumen is enclosed only by single EC.

---

### 5.3.2 Tricellular junctions *and de novo* contact formation during junction mergence require PI3-Kinase $\alpha$ signaling

#### Breaking of tricellular junctional contacts in ISVs of *pik3ca* mutants

When analyzing the dynamic behavior of junctions in *pik3ca* mutant ISVs in live movies, I observed disruptions in junction connectivity at the base of ISVs. In some vessels, the base of the ISV never showed a junctional connection to the DA, whereas in others, the junction was disrupted at some point during sprouting. An unconnected ISV base indicates a single cell placed between the DA and the next ISV stalk cell, which is not paired with another cell within the vessel. Furthermore, the observed breaking of junction connectivity effectively de-intercalated cells at the ISV base. In wild-type conditions, the ISV base consists of three cells: One DA cell and two paired ISV stalk cells, which share a tricellular junction. In *pik3ca* mutants, this tricellular contact was unstable and opened up either before or during sprouting movements. Subsequently, one of the ISV stalk cells moved dorsally, thereby de-intercalating with the second cell.

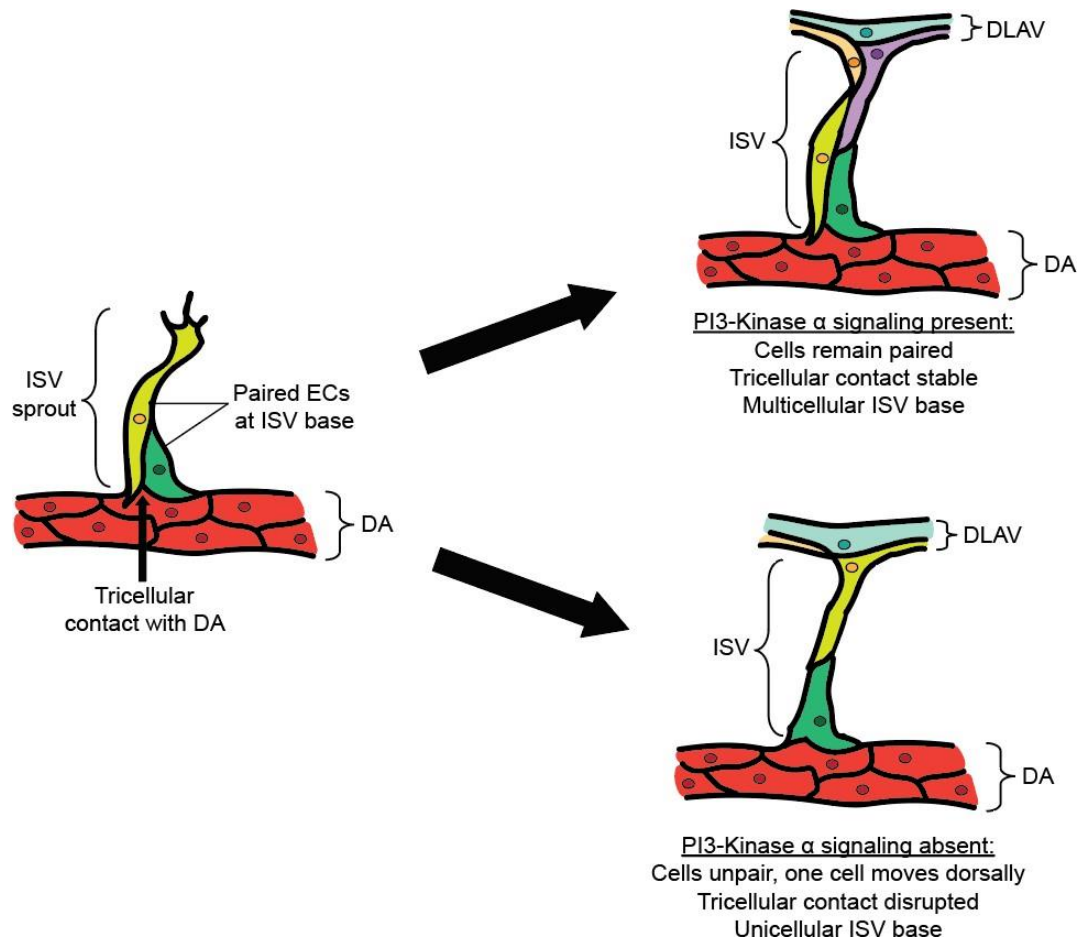


**Fig. 32: Loss of PI3-Kinase  $\alpha$  signaling impairs cell pairing at the ISV base**

Schematic illustration of paired cells at the base of ISVs, where at least two cells are paired and connected to the DA cell by a tricellular contact. In wild-type conditions, this contact is stable, ISV cells remain paired and the base of the ISV remains multicellular. Loss of PI3-Kinase  $\alpha$  causes paired cells to de-intercalate, whereupon one cell moves dorsally and the remaining cell is connected to the DA by a single bicellular junction.

### **Destabilized *de novo* contacts during junction mergence in the DLAV of *pik3ca* mutants**

A phenotype related to the destabilized tricellular junction contacts in ISVs was found in the DLAV of *pik3ca* mutants. Here, junction mergence underlying intercalation was perturbed by genetic loss of PI3-Kinase  $\alpha$  signaling. Junctions did elongate until a certain point and touched during intercalation movements, but then failed to stabilize the novel connection between the previously unconnected cells. Instead, junction rings moved apart again, indicative of cells de-intercalating and the vessel remaining

unicellular.

The formation of *de novo* junctional contacts entails establishment of a stable tricellular contact point (Fig. 33, green arrow). Hence, this phenotype directly connects to the defect in junction connectivity at the base if *pik3ca* mutant ISVs. In summary, loss of PI3-Kinase  $\alpha$  signaling causes defects in the formation and maintenance of tricellular junctional contacts. The breaking of tricellular contacts in turn prohibits stable cell pairing and completion of cell intercalation movements, which are required for multicellular tube formation.

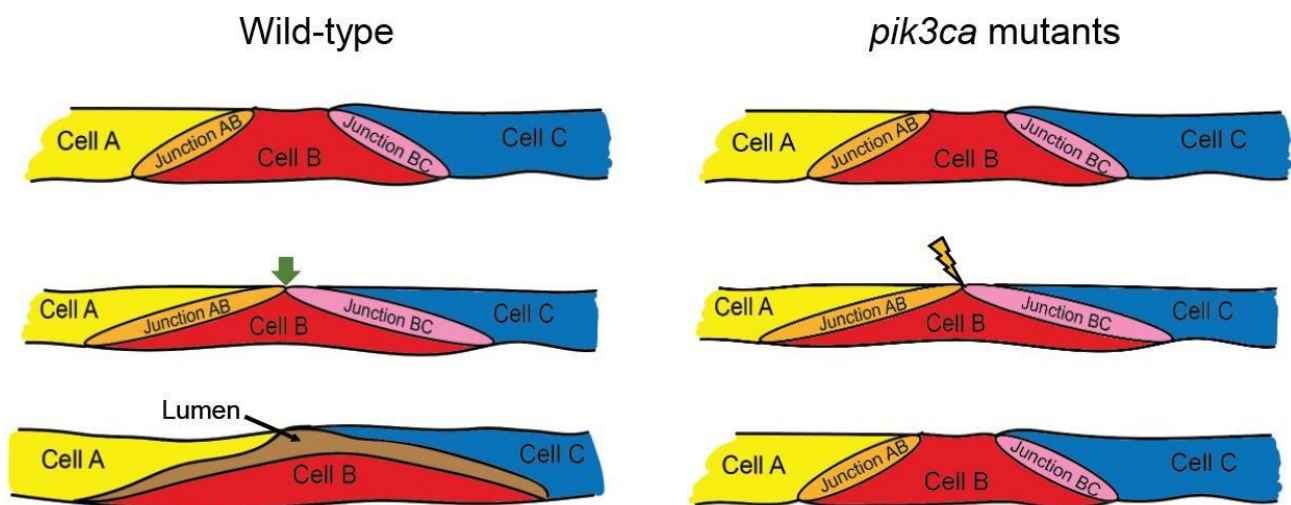


**Figure 33: EC intercalation requires signaling by PI3-Kinase  $\alpha$**

Schematic illustration of three ECs in the DLAV of wild-type and *pik3ca* mutant embryos during cell intercalation. In wild-types (left side), cells elongate their mutual interfaces until formation of novel contacts at tricellular junctions. At these sites, lumen pockets fuse, effectively creating a single lumen, which is always enclosed by at least two cells in cross sections. In contrast, loss of PI3-Kinase  $\alpha$  signaling destabilizes tricellular contact sites and prohibits novel contact formation, which leads to cell de-intercalation within the vessel (right side).

---

### **The role of actomyosin tension in junction elongation and tricellular contact formation between *pik3ca* mutant endothelial cells**

Tricellular junctional contacts are known to be under enhanced actomyosin tension compared to bicellular junctions (reviewed in Higashi and Miller 2017). In order to stabilize them, cells are known to recruit higher levels of adhesive and tight junction proteins, such as ZO1 (*tjp1*) or Vinculin (Higashi *et al.*, 2016).

It was shown in Angulo-Urarte *et al.*, 2018, that loss of PI3-Kinase  $\alpha$  signaling increased actomyosin tension by enhanced myosin light chain phosphorylation. In light of this, defects in junction mergence by unstable tricellular junctions offer a reasonable explanation for the observed cell rearrangement defects. As these points are already under increased cytoskeletal tension in wild-type conditions, further elevation of cortical actomyosin contractility could lead to contact disruption and breaking of junctional contacts, similar to pre-determined breaking points in technical devices. In such a scenario, the contractile force within the junctional ring would also be too high to sustain junction elongation from a certain point onward, which is in agreement with the observation that after a certain phase of elongation junctional rings did not remodel further in *pik3ca* double mutants and remained isolated and circular.

In order to test this hypothesis, I propose to assess actomyosin tension both in wild-type and *pik3ca* mutant conditions, e.g. via antibody stainings against phosphorylated myosin light chain (p-myosin) or by evaluation of junctional F-actin fibers. A more technically challenging but highly elegant way would be FRET-based live-imaging of junctional tension in *pik3ca* mutant embryos using the previously published VE-cad-tension sensor construct (Lagendijk *et al.*, 2017).

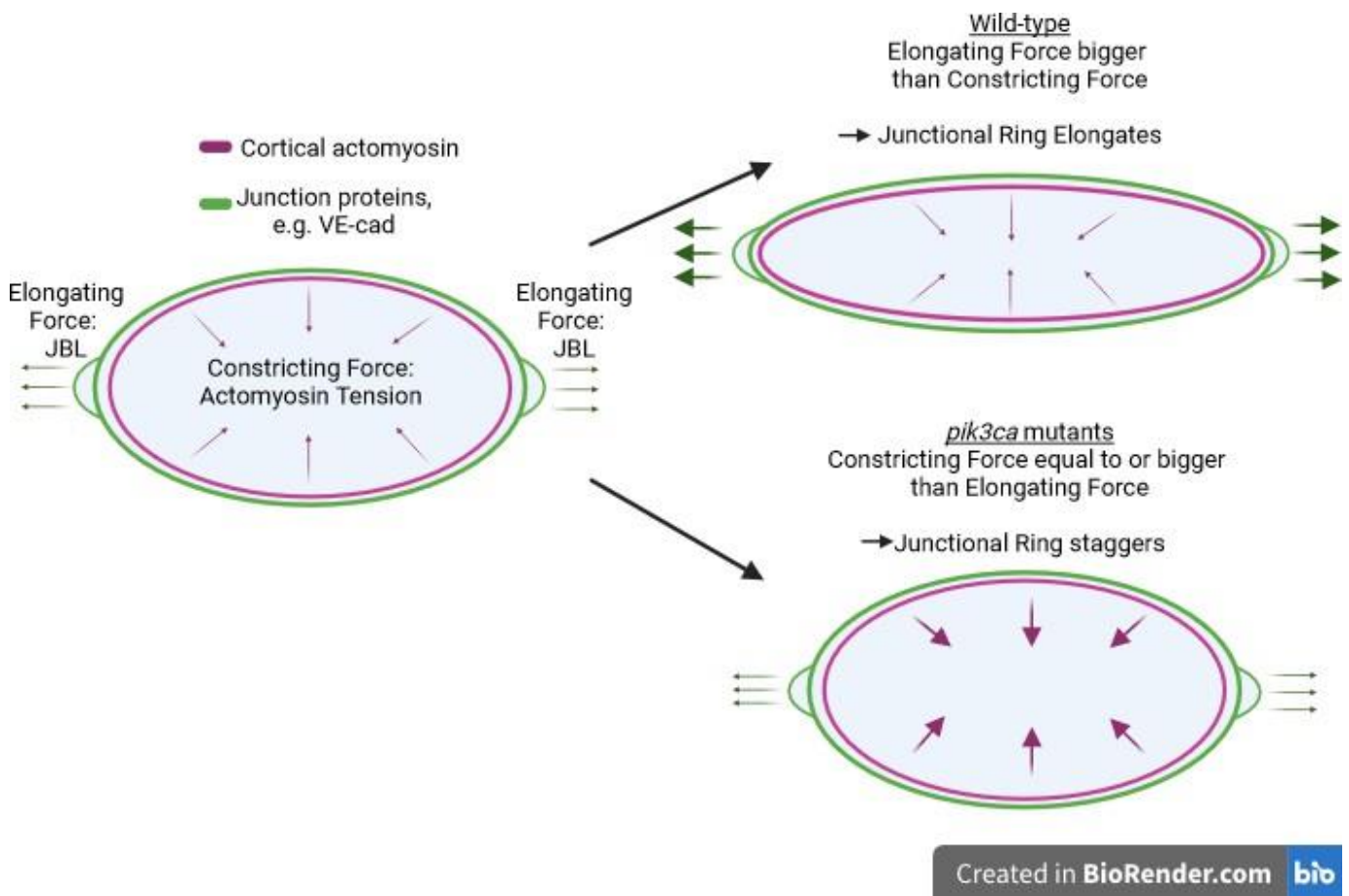


**Figure 34: Junction elongation requires balanced forces within the junctional ring**

Schematic illustration of constricting actomyosin forces and elongating JBL within a junctional ring. In wild-type conditions (upper right), elongating forces created by JBL are stronger than contractile actomyosin forces, causing the ring and cell interfaces to elongate. Loss of PI3-Kinase  $\alpha$  signaling leads to increased actomyosin tension and thus presumably elevated constricting forces within the junctional ring, thereby prohibiting junctional elongation and cell-cell interface extension (lower right). Figure created in BioRender.

---

## 5.4 Local PI3-Kinase $\alpha$ signaling at EC junctions and in JBL

When analyzing the live imaging data obtained in *pik3ca* mutants, I observed that endothelial cell-cell interfaces (junction rings) only elongated until a certain size but not any further and, as a result, ISVs and DLAV remained unicellular. This implies that EC junction elongation, which is driven by JBL, is impaired by loss of PI3-Kinase  $\alpha$  signaling and, in turn, that PI3-Kinase  $\alpha$  could potentially play a role in JBL function. In order to test this hypothesis, I performed spatiotemporal analysis of PI3-Kinase  $\alpha$  activity in ECs using the PIP3-sensor construct PH-Akt-EGFP. This sensor revealed distinct localized peaks of EGFP fluorescence at the distal ends of EC junctions during junction elongation. These local peaks of EGFP intensity were abrogated by isoform-specific inhibition of PI3-Kinase  $\alpha$ , thereby confirming them as the result of specific local activity of PI3-Kinase  $\alpha$  at junctions. Furthermore, the EGFP intensities were uncoupled from local fluctuations in overall membrane material (Tschudin, 2022). Unfortunately, even though the transgenic line expresses the sensor in a mosaic manner in the , it is so far not clear from the imaging data whether the observed oscillations at both ends of the junctional ring originate from single cells or from both partaking cells.

Interestingly, the local intensity maxima oscillated with a period of approximately 6 to 10 minutes (4 out of 6 movies which show two distinct peaks). This period is remarkably similar to the frequency with which JBL oscillations occur (Paatero *et al.*, 2008). From this point, and in combination with the peculiar location of PI3-Kinase  $\alpha$  activity at the distal ends of elongating junctional rings, it seems highly likely that PI3-Kinase  $\alpha$  signaling is indeed involved in JBL function or regulation. However, elongation speed of EC junctions per se was not affected in mutants or by chemical inhibition. Similarly, polarized distribution of VE-cad at distal ends of the junction, measured by polarized thickness of junctions labeled with VE-cad-venus, did not change when interfering with PI3-Kinase  $\alpha$  genetically or chemically. These pieces of evidence speak against a possible function of PI3-Kinase  $\alpha$  in JBL. Nonetheless, the overlap of PI3-Kinase  $\alpha$  signaling and JBL in localization and periodicity strongly suggest PI3-Kinase  $\alpha$  being involved in JBL function or regulation.

---

Molecularly, JBL are the driving mechanism of endothelial cell-cell junction elongation. The cortical cytoskeletal network consisting of actin and myosin plays a central role in the formation function of JBL. Since PI3-Kinase  $\alpha$  signaling has been linked to regulation of both actin (via Rac1, reviewed in Campa *et al.*, 2015) and p-myosin (via Mypt1, Angulo-Urarte *et al.*, 2018), a possible molecular role of PI3-Kinase  $\alpha$  signaling in JBL is highly likely and in agreement with the result showing localized and oscillating activity at junctions. Future experiments will focus on linking specific cytoskeletal behaviors to local PIP3 accumulations at elongating endothelial cell-cell junctions and during cycling JBL. For example it is possible that PI3-Kinase  $\alpha$  promotes actin polymerization via Rac1, leading to the formation of the lamellipodia-like protrusion which commences the JBL cycle. Another possibility could be a role of PI3-Kinase  $\alpha$  in the local release of actomyosin tension by inhibiting Mypt1 in order to regulate distinct steps during the JBL cycle (Fig. 35).



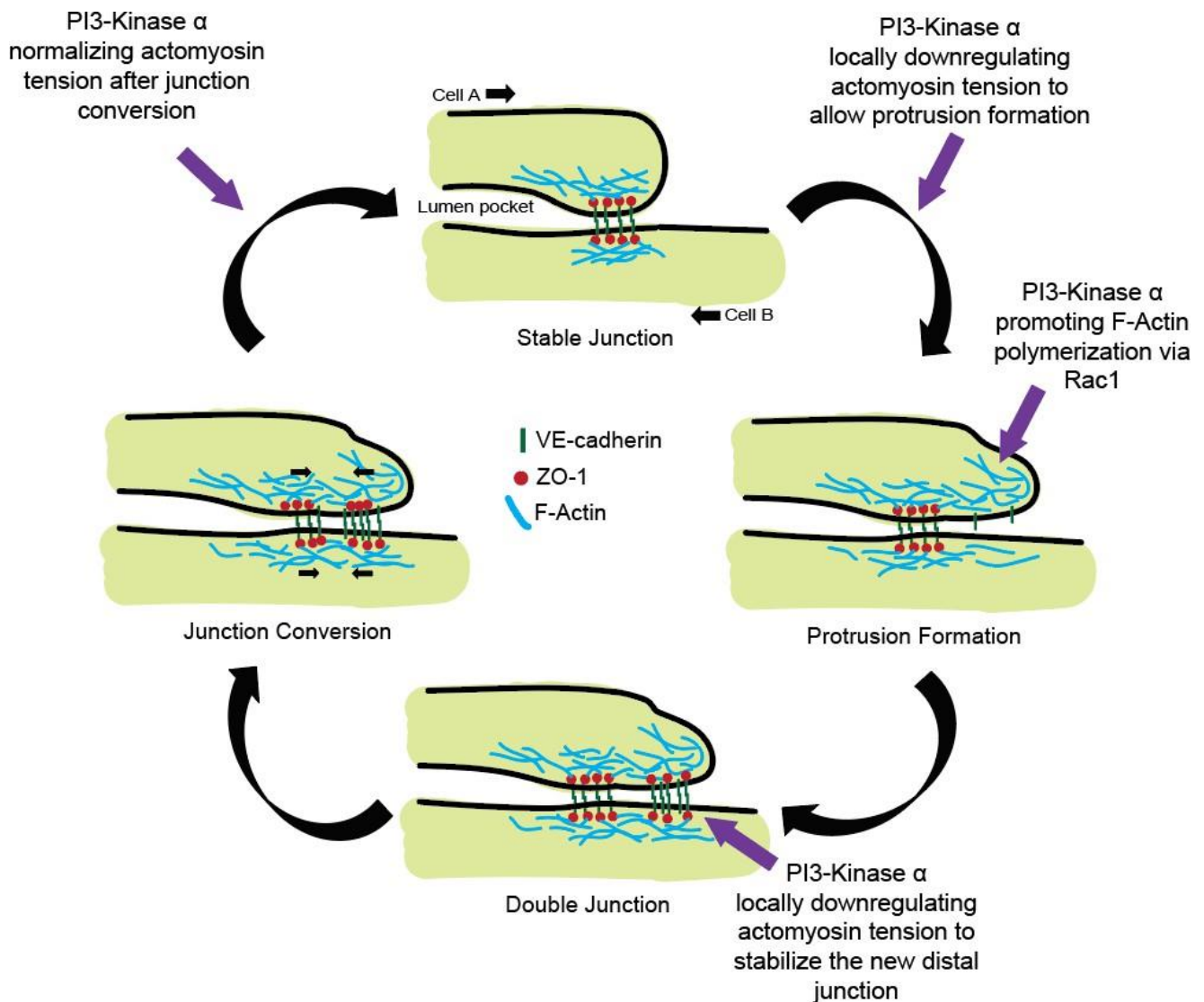


**Fig. 35: Possible functions for PI3-Kinase  $\alpha$  within JBL formation and function**

Localized PI3-Kinase  $\alpha$  signaling could potentially promote F-actin polymerization during protrusion formation, but also downregulate local actomyosin tension via Mypt1 during formation of a stable double junction, to normalize tension after junction conversion or to allow local protrusion formation upstream of the JBL mechanism.

---

## 5.5 Local activation of PI3-Kinase $\alpha$ signaling at endothelial cell junctions

PI3-Kinase  $\alpha$  is a signaling hub, positioned at the interface between extracellular stimuli and intracellular responses. Since I showed that the kinase is specifically active at the distal ends of elongating junctional rings between ECs, analysis of the upstream events which locally lead to the activation of the kinase is an essential aspect in understanding the function of PI3-Kinase  $\alpha$  in junction elongation and cell rearrangements.

Canonically, PI3-Kinase  $\alpha$  is activated downstream of VEGFRs binding to their respective ligands. However, chemical inhibition of neither VEGFR2 or VEGFR3 or both at the same time abrogated the EGFP oscillations of the PIP3-sensor at junctions. Both inhibitors were tested before the experiment for capability to abrogate VEGFR2/VEGFR3 signaling respectively. It is thus possible that:

- a) the inhibitors targeted sites within the receptors that are not essential to activate PI3-Kinase  $\alpha$ . This could be tested by using different inhibitors with other binding sites.
- b) neither VEGFR2 nor VEGFR3 alone is responsible for local activation of PI3-Kinase  $\alpha$  at the distal ends of EC junctions.

In case the latter is true, this poses the question of what else could be responsible for local activation of PI3-Kinase  $\alpha$ . Other factors known to activate PI3-Kinase  $\alpha$  signaling in ECs are Tie2 signaling, Apelinr or Integrins, all of which could be possibly targeted by chemical inhibition. Additionally, it was shown that the formation of an intramembrane complex consisting of PECAM, VEGFR2 and Ve-cadherin can trigger PI3-Kinase signaling *in vitro* in response to shear stress (Tzima *et al.*, 2005). It is possible, that such a complex is also responsible for local activation of PI3-Kinase  $\alpha$  at EC junctions *in vivo*, and that this complex would not be targeted by the inhibitors used in the previous experiment.

---

## 5.6 Summary and outlook

In my thesis work, I have analyzed the role of PI3-Kinase  $\alpha$  signaling in EC rearrangements during cardiovascular development by genetic ablation of the catalytic subunit in zebrafish. Three knockout alleles, two of which I created by CRISPR/Cas9 technology, for the two *pik3ca* encoding genes in the zebrafish genome were successfully established. *pik3ca* double mutants phenocopied the defects in vascular remodeling observed during inhibitor treatment and can therefore be considered as valid knockout alleles.

In *pik3ca* double mutants, I documented a number of distinct phenotypes depending on the respective vascular bed. Whereas the trunk vasculature showed defects in cell rearrangements and junction elongation, the CVP displayed hyperplasia and enlarged vascular loops. The CVP phenotype could possibly be caused by elevated levels of BMP signaling inducing venous sprouting, a scenario which would propose differential regulation of cell proliferation in arterial and venous cells by distinct targets of PI3-Kinase  $\alpha$ . Furthermore, the finding that PI3-Kinase  $\alpha$  signaling fulfils different functions in distinct vascular beds was further corroborated by analysis of Foxo relocalization behavior as a downstream target of PI3-Kinase  $\alpha$ .

Using the *pik3ca* double mutants, I have investigated junction elongation and cell rearrangements in the trunk vasculature upon loss of PI3-Kinase  $\alpha$  signaling. Time-lapse live imaging revealed defects in junction mergence and instability of tricellular contact sites during vessel remodeling. In light of the findings in the study of Angulo-Urarte *et al.*, 2018, these deficiencies could likely be caused by elevated actomyosin tension at junctions upon loss of PI3-Kinase  $\alpha$  signaling. As junction elongation requires integration of constricting and elongating forces, increased actomyosin tension due to abrogated PI3-Kinase  $\alpha$  activity plausibly prohibits junction elongation and cell-cell interface extension, similar to what I observed in *pik3ca* mutants.

Spatiotemporal analysis of PI3-Kinase  $\alpha$  signaling in ECs using the PIP3-sensor showed distinct localization of oscillating PI3-Kinase  $\alpha$  activity at distal ends of elongating junctions. This overlap in localization and the similar period of PI3-Kinase  $\alpha$  signaling and JBL oscillation, combined with the role of PI3-Kinase  $\alpha$  in junction

---

elongation and actomyosin regulation, suggests a function of PI3-Kinase  $\alpha$  in JBL. In contrast, the velocity of junction elongation as well as VE-cadherin distribution was unchanged in *pik3ca* mutants, which points towards JBL functioning independently of PI3-Kinase  $\alpha$  signaling. Future experiments on this aspect of PI3-Kinase  $\alpha$  in vascular remodeling should focus on a careful dissection of the JBL mechanism in PI3-Kinase  $\alpha$  mutants and coincidence of PI3-Kinase  $\alpha$  activity with distinct steps of the JBL mechanism.

Lastly, I asked how PI3-Kinase  $\alpha$  is activated locally at elongating junctions and found that chemical inhibition of the canonical upstream RTKs, VEGFR2 and VEGFR3, did not abrogate localized PI3-Kinase  $\alpha$  activity. A possible explanation for this result is that PI3-Kinase  $\alpha$  is activated by complex formation and interaction of VEGFR2 with Ve-cad at junctions, a scenario which remains to be investigated.

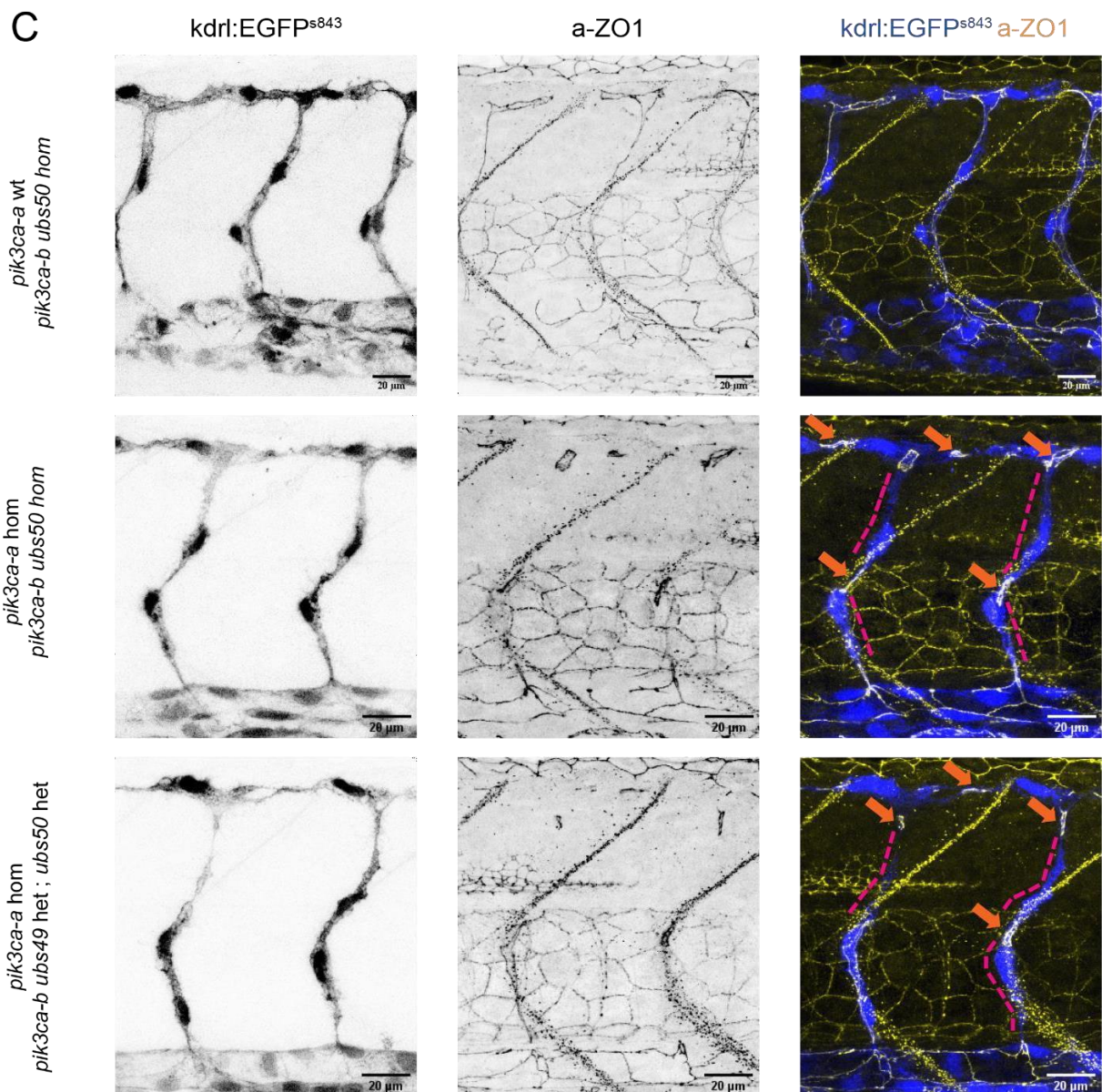
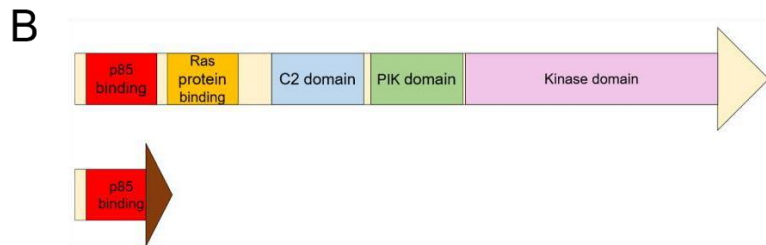
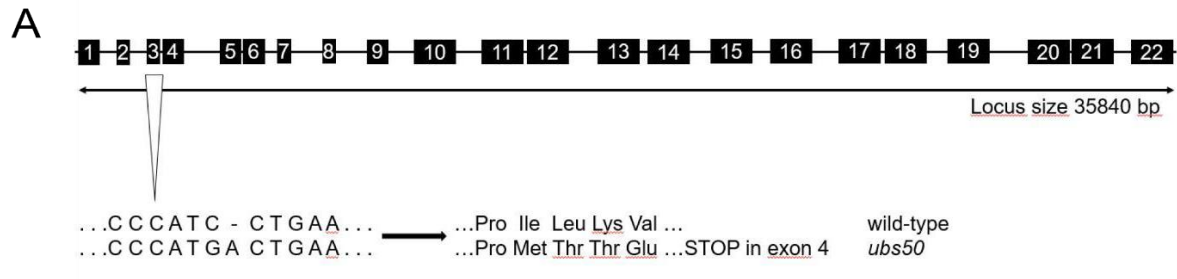
Taken together, my thesis work has paved the way for a detailed molecular analysis of PI3-Kinase  $\alpha$  during junction elongation and cell rearrangements. I have established, verified and thoroughly described a new genetic model to study PI3-Kinase  $\alpha$  in zebrafish. I showed that, in agreement with findings human and mouse vasculature, PI3-Kinase  $\alpha$  fulfils distinct functions in the zebrafish vasculature depending on the respective nature of the vessel and I have proposed distinct regulatory interplays with other signaling pathways depending on vascular identity. Comprehensive analysis of junction behavior during cell rearrangements in the trunk vasculature has shed light on the distinct role of PI3-Kinase  $\alpha$  during this process, especially in the regulation of distinct physical forces during cell-cell interface elongation mechanisms. Future research should focus on assessment of actomyosin tension in the absence of PI3-Kinase  $\alpha$  and correlation of PI3-Kinase  $\alpha$  signaling with JBLs and its potential functional connection in cell rearrangements during vascular morphogenesis.





VI

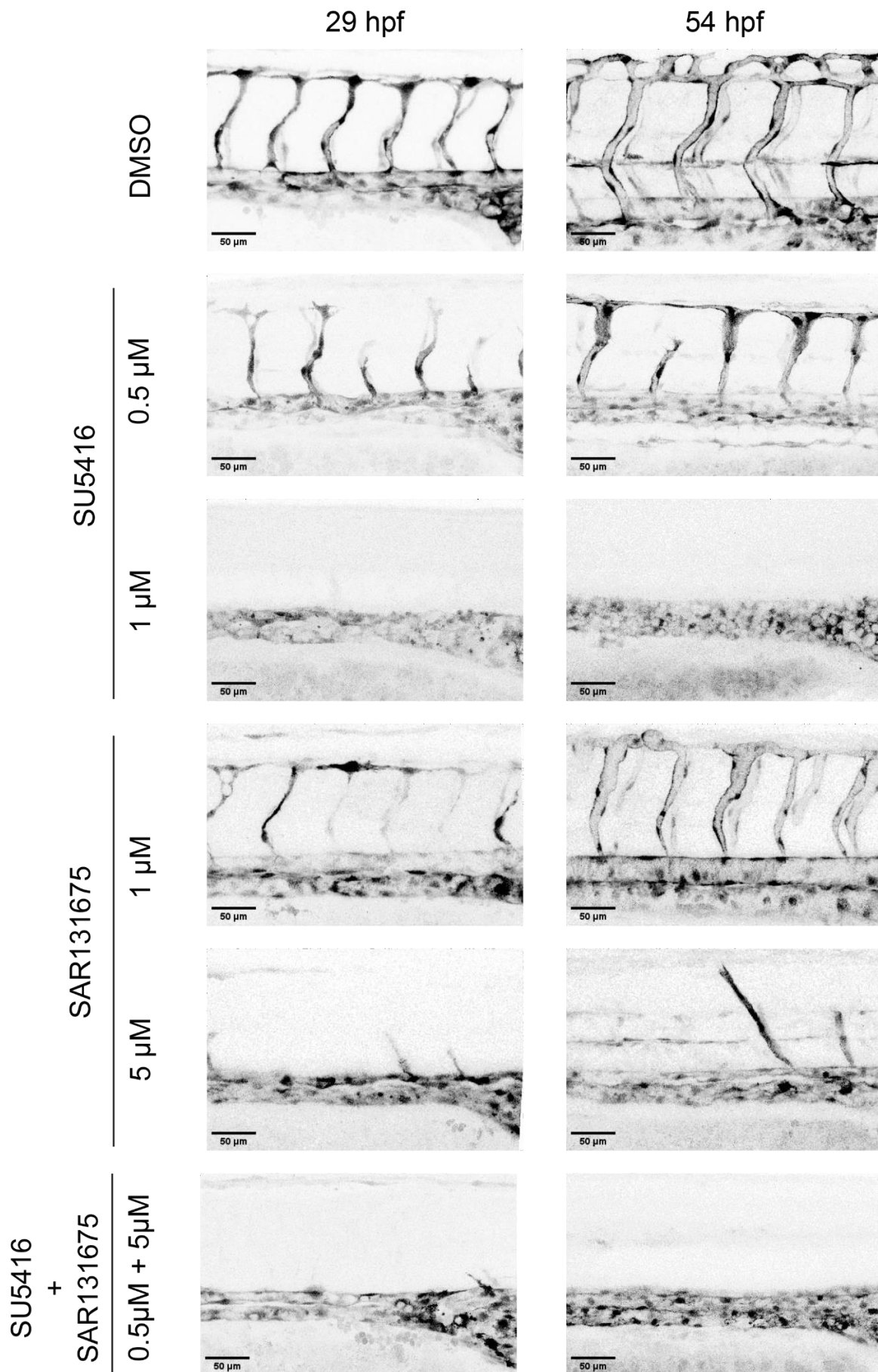
## Supplementary Data





**Supplementary Fig. 1: *ubs50* is a second *pik3ca-b* knockout allele**

**A** The *pik3ca-b* mutant allele *ubs50* is a C7GA insertion in exon 3, and the resulting frameshift creates a STOP codon in exon 4. **B** Putative protein domains of the amino acid sequence encoded by the *ubs50* allele in comparison with the wild-type locus. **C** Antibody staining in ISVs and DLAV against ZO1 in *pik3ca* mutant embryos of the indicated genotype at 32hpf. ECs are labelled by transgenic expression of cytoplasmic EGFP under *kdrl* promoter (*Tg(kdrl:EGFP)<sup>s843</sup>*). Small rounded junctions indicated with orange arrows, red dotted lines indicate gaps between junctions in unicellular ISVs. Scale bar is 20µm.



**Supplementary Fig. 2: Validation of VEGFR2 inhibitors**

Representative confocal images of trunk vasculature at the end of the yolk extension of *pik3ca* wildtype embryos at indicated timepoints and treated with VEGFR2/VEGFR3 inhibitors SU5416/SAR131675 at indicated concentrations. ECs are labelled by expression of cytoplasmic EGFP under *fli1a* promoter (*Tg(fli1a:EGFP)<sup>y1</sup>*). Scale bar is 50µm.



## VII

### Appendix

Creation of a novel genetic tool for the inducible  
*in vivo* mosaic analysis of *VE-cad/cdh5* function  
during blood vessel morphogenesis

VE-cad/Cdh5 plays a central role in endothelial cell rearrangements and junction elongation (Paatero *et al.*, 2018, Sauteur *et al.*, 2014). However, analysis of the exact function of VE-cad in mutant alleles has been limited by adverse side effects of global loss of VE-cad, such as loss of blood flow and early embryonic lethality. To circumvent these, our group aimed to use a mosaic knockout approach in future experiments. Deleting VE-cad in only some of the partaking cells will give us answers to questions like

- What function does VE-cad play in cell-cell recognition during anastomosis? Do the cells still initiate and form contact sites in a mosaic setting?
- Are *VE-cad* knockout cells still able to rearrange in an otherwise wild-type background of the vessel? Is VE-cad required cell-autonomously?
- What is the exact role of VE-cad in JBL? Do cells use each other as substrate via VE-cad? Does VE-cad play an active role in JBL regulation? Can mosaic JBL still form and how functional are they?

These points all target different time points and mechanisms during vascular development. In order to perturb the system only at the times of interest during development, our group aimed for an inducible way to delete VE-cad in a mosaic manner. At the start of my contribution to this project, Dr. Niels Schellinx, a former PhD student in the group, had already designed several different Bacterial Artificial Chromosomes (BACs) to use as a transgene in zebrafish. These BAC constructs contain the whole zebrafish endogenous VE-cad locus, which ensures expression at normal levels. This way, possible overexpression phenotypes are avoided. Furthermore, a transgenesis marker on the constructs backbone (*β-chrys:mKate*) was added to distinguish more easily between transgenic and wild-type embryos prior to experiments.

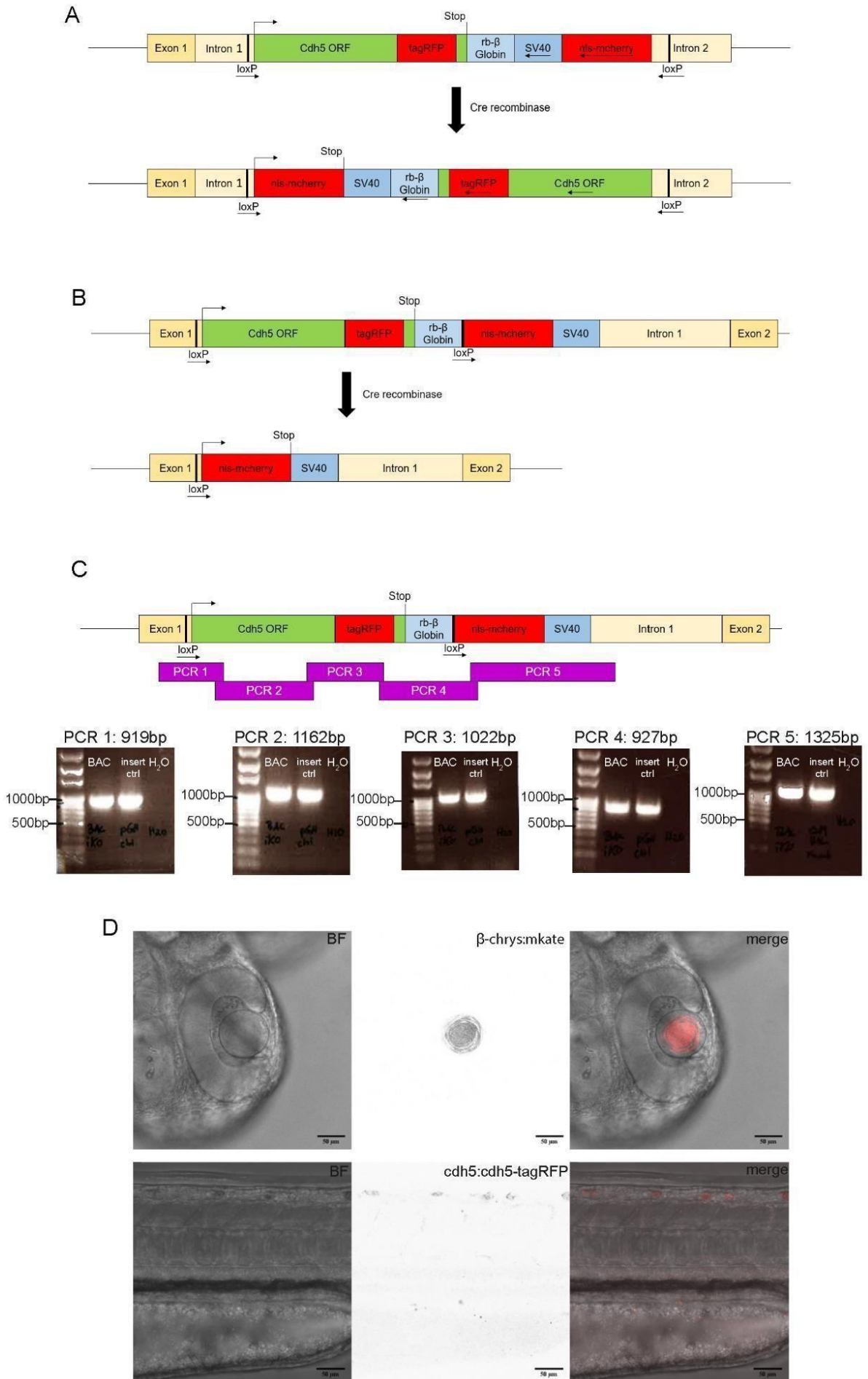


**Fig. 36: Re-design and expression of an inducible knockout construct for *VE-cad/cdh5* A**

Previously used BAC construct. Two facing loxP sites flank the whole insert. The inverted nls-mcherry sequence in 3' is only transcribed once the whole construct is inverted by Cre-based recombination.

**B** Re-designed BAC construct. loxP sites flank only *cdh5*-tagRFP ORF which is deleted upon Crebased recombination. Expression of nls-mcherry occurs only if 5' *cdh5* ORF is lost. **C** Overlapping PCRs on re-designed insert in BAC backbone. All five PCRs resulted in bands of the right size compared to control plasmid containing the original insert. **D** Expression of the BAC construct in an injected 48hpf embryo. Upper row: expression of the transgenesis marker in the eye is readily observed at this stage (mid panel). Lower row: No fluorescent signal of Cdh5-tagRFP can be detected in DA, PCV, trunk ISVs and DLAV (mid panel). Scale bar is 50µm.

Dr. Schellinx BAC cassette is displayed in Fig. 36 A. Here, the insert cassette replaces exon 2 of the *VE-cad* sequence. Since exon 1 is non-coding, the endogenous translation start site was thereby removed and replaced it with a complete ORF encoding fluorescently tagged VE-cad. An inverted nls-mcherry is placed directly in 3' behind, separated by two commonly used polyadenylation signal sequences to stop translation. The whole insertion cassette is flanked by two facing loxP sites for inducible recombination via Cre recombinase.

In its native state of this insert, only the RFP tagged *cdh5* ORF is transcribed and translated, labelling *cdh5* fluorescently in the endothelium. When recombined, the two loxP sites cause an inversion of the construct, such that nls-mcherry is expressed instead of *cdh5*-RFP. Knockout cells for VE-cad can thus easily be identified by means of nuclear red fluorescence.

This construct resulted in expression of both VE-cad-RFP and nuclear mcherry in zebrafish embryos without addition of Cre recombinase (Schellinx N., Doctoral Thesis). Furthermore, the inverted loxP sites would not prohibit inversion of the cassette after the first event, but could potentially initiate more recombination events, each flipping the cassette between native and recombined state.

To tackle these issues, I re-designed the BAC construct, as shown in Fig 36 B. Placed directly behind exon 1 and making use of the transcription initiation site there, only the VE-cad-RFP ORF is flanked by equally oriented loxP sites, ensuring its deletion after Cre recombination. Nls-mcherry is no longer inverted, but is still transcribed only after deletion of the loxP flanked ORF.



Overlapping PCRs on BAC DNA gave bands of the right-size after cloning of the construct inside the BAC. Sequence analysis revealed a 100% true sequence of the desired insert, confirming the successful insertion of the 4733bp insert.

When introduced into zebrafish embryos, I could readily observe expression of the transgenic eye marker on the BAC backbone. However, none of the injected G0 embryos showed any junctional RFP signal. Injected embryos were raised to adulthood and four different alleles were isolated by founder screening for the eye marker. In the F1 generation, again no expression of fluorescently tagged *VE-cad* was detected.

The four different BAC alleles were also crossed into *VE-cad* mutant background (*ubs8 het*). Here, fish heterozygous for one of the four BAC alleles and for *ubs8* were incrossed and 20 BAC positive embryos per BAC allele screened for expression. Following Mendelian heredity, a quarter of these embryos were homozygous mutant for endogenous *VE-cad*. The only functional copy of *VE-cad* in the genome of these embryos was the RFP-tagged BAC construct. Still, no florescent RFP signal could be detected in the endothelium at 52hpf in any of the screened embryos irrespective of the BAC allele.

In summary, the genetic construct to delete *VE-cad* in an inducible and mosaic manner was re-designed and successfully cloned in the BAC backbone. However, expression of RFP-tagged *VE-cad* was not detected across four different alleles in the F1 and F2 generation. Furthermore, homozygous loss of endogenous *VE-cad* did not result in enhanced fluorescent signal upon compensatory expression of the BAC construct.

At this point, I propose to confirm the expression of the construct by isolation of RNA from BAC transgenic embryos and RT-PCR on cDNA derived from them. If the construct is indeed expressed, functionality of the tagged *VE-cad* could be assessed by observing the potential rescue of the *ubs8* phenotype in *ubs8* homozygous, BAC heterozygous embryos. In case the BAC rescues endogenous *VE-cad* loss, the RFP moiety is most likely improperly folded and thus not functional and unsuited to fluorescently tag *VE-cad* with. In this case, I suggest exchanging tagRFP in the construct with another monomeric fluorophore such as mScarlet or mRuby in future approaches.



# VIII

## References

Ali, Zaheer; Mukwaya, Anthony; Biesemeier, Antje; Ntzouni, Maria; Ramsköld, Daniel; Giatrellis, Sarantis et al. (2019): Intussusceptive Vascular Remodeling Precedes Pathological Neovascularization. In *Arteriosclerosis, thrombosis, and vascular biology* 39 (7), pp. 1402–1418. DOI: 10.1161/ATVBAHA.118.312190.

Andrew, Deborah J.; Ewald, Andrew J. (2010): Morphogenesis of epithelial tubes: Insights into tube formation, elongation, and elaboration. In *Developmental biology* 341 (1), pp. 34–55. DOI: 10.1016/j.ydbio.2009.09.024.

Angulo-Urarte, Ana; Casado, Pedro; Castillo, Sandra D.; Kobiakka, Piotr; Kotini, Maria Paraskevi; Figueiredo, Ana M. et al. (2018): Endothelial cell rearrangements during vascular patterning require PI3-kinase-mediated inhibition of actomyosin contractility. In *Nature communications* 9 (1), p. 4826. DOI: 10.1038/s41467-018-07172-3.

Arriemerlou, Cécile; Meyer, Tobias (2005): A local coupling model and compass parameter for eukaryotic chemotaxis. In *Developmental cell* 8 (2), pp. 215–227. DOI: 10.1016/j.devcel.2004.12.007.

Asakawa, Kazuhide; Kawakami, Koichi (2008): Targeted gene expression by the Gal4-UAS system in zebrafish. In *Development, growth & differentiation* 50 (6), pp. 391–399. DOI: 10.1111/j.1440-169X.2008.01044.x.

Aydogan, Vahap; Lenard, Anna; Denes, Alexandru Stefan; Sauter, Loic; Belting, HeinzGeorg; Affolter, Markus (2015): Endothelial cell division in angiogenic sprouts of differing cellular architecture. In *Biology open* 4 (10), pp. 1259–1269. DOI: 10.1242/bio.012740.

Backer, Jonathan M. (2008): The regulation and function of Class III PI3Ks: novel roles for Vps34. In *The Biochemical journal* 410 (1), pp. 1–17. DOI: 10.1042/BJ20071427.

Baer, Magdalena M.; Chanut-Delalande, Helene; Affolter, Markus (2009): Cellular and molecular mechanisms underlying the formation of biological tubes. In *Current topics in developmental biology* 89, pp. 137–162. DOI: 10.1016/S0070-2153(09)89006-6.

Bär, Th.; Güldner, F.-H.; Wolff, J. R. (1984): "Seamless" endothelial cells of blood capillaries. In *Cell Tissue Research* 235, pp. 99–106.

Bart Vanhaesebroeck; Sally J. Leever; Khatereh Ahmadi; John Timms; Roy Katso; Paul C. Driscoll et al. (2001): Synthesis and Function of 3-Phosphorylated Inositol Lipids. In *Annual Reviews in Biochemistry* 70, pp. 535–602.

- Betz, Charles; Lenard, Anna; Belting, Heinz-Georg; Affolter, Markus (2016): Cell behaviors and dynamics during angiogenesis. In *Development (Cambridge, England)* 143 (13), pp. 2249–2260. DOI: 10.1242/dev.135616.
- Bi, L.; Okabe, I.; Bernard, D. J.; Wynshaw-Boris, A.; Nussbaum, R. L. (1999): Proliferative defect and embryonic lethality in mice homozygous for a deletion in the p110 $\alpha$  subunit of phosphoinositide 3-kinase. In *The Journal of biological chemistry* 274 (16), pp. 10963–10968. DOI: 10.1074/jbc.274.16.10963.
- Bi, Lei; Okabe, Ichiro; Bernard, David J.; Nussbaum, Robert L. (2002): Early embryonic lethality in mice deficient in the p110 $\beta$  catalytic subunit of PI 3-kinase. In *Mammalian Genome* 13, pp. 169–172.
- Blum, Yannick; Belting, Heinz-Georg; Ellertsdottir, Elin; Herwig, Lukas; Lüders, Florian; Affolter, Markus (2008): Complex cell rearrangements during intersegmental vessel sprouting and vessel fusion in the zebrafish embryo. In *Developmental biology* 316 (2), pp. 312–322. DOI: 10.1016/j.ydbio.2008.01.038.
- Bouvier, Jason; Cheng, Jr-Gang (2009): Recombineering-based procedure for creating Cre/loxP conditional knockouts in the mouse. In *Current protocols in molecular biology* Chapter 23, Unit 23.13. DOI: 10.1002/0471142727.mb2313s85.
- Brunet, Anna; Bonni, Azad; Zigmond, Michael J.; Lin, Michael Z.; Juo, Peter; Hu, Linda S. et al. (1999): Akt Promotes Cell Survival by Phosphorylating and Inhibiting a Forkhead Transcription Factor. In *Cell* 96, pp. 857–868.
- Burri, P. H.; Tarek, M. R. (1990): A novel mechanism of capillary growth in the rat pulmonary microcirculation. In *The Anatomical Record* 228, pp. 35–45.
- Bussmann, Jeroen; Bos, Frank L.; Urasaki, Akihiro; Kawakami, Koichi; Duckers, Henricus J.; Schulte-Merker, Stefan (2010): Arteries provide essential guidance cues for lymphatic endothelial cells in the zebrafish trunk. In *Development (Cambridge, England)* 137 (16), pp. 2653–2657. DOI: 10.1242/dev.048207.
- Caduff, J. H.; Fischer, L. C.; Burri, P. H. (1986): Scanning electron microscope study of the developing microvasculature in the postnatal rat lung. In *The Anatomical Record* 216, pp. 154–164.
- Campa, Carlo C.; Ciruolo, Elisa; Ghigo, Alessandra; Germena, Giulia; Hirsch, Emilio (2015): Crossroads of PI3K and Rac pathways. In *Small GTPases* 6 (2), pp. 71–80. DOI: 10.4161/21541248.2014.989789.
- Cao, Jiahui; Ehling, Manuel; März, Sigrid; Seebach, Jochen; Tarbashevich, Katsiaryna; Sixta, Tomas et al. (2017): Polarized actin and VE-cadherin dynamics regulate junctional

remodelling and cell migration during sprouting angiogenesis. In *Nature communications* 8 (1), p. 2210. DOI: 10.1038/s41467-017-02373-8.

Cao, Xia; Maharjan, Sushila; Ashfaq, Ramla; Shin, Jane; Zhang, Yu Shrike (2021): Bioprinting of Small-Diameter Blood Vessels. In *Engineering* 7 (6), pp. 832–844. DOI: 10.1016/j.eng.2020.03.019.

Carmeliet, Peter; Ferreira, Valerie; Breier, Georg; Pollefeyt, Saskia; Kieckens, Lena; Gertsenstein, Marina et al. (1996): Abnormal blood vessel development and lethality in embryos lacking a single VEGF allele. In *Nature* 380, pp. 435–439.

Castillo, Sandra D.; Tzouanacou, Elena; Zaw-Thin, May; Berenjano, Inma M.; Parker, Victoria E. R.; Chivite, Inigo et al. (2016): Somatic activating mutations in *Pik3ca* cause sporadic venous malformations in mice and humans. In *Science Translational Medicine* 8 (332).

Chen, Kai-En; Tillu, Vikas A.; Chandra, Mintu; Collins, Brett M. (2018): Molecular Basis for Membrane Recruitment by the PX and C2 Domains of Class II Phosphoinositide 3-Kinase *C2α*. In *Structure (London, England : 1993)* 26 (12), 1612-1625.e4. DOI: 10.1016/j.str.2018.08.010.

Coffin, Douglas; Poole, Thomas J. (1991): Endothelial cell origin and migration in embryonic heart and cranial blood vessel development. In *The Anatomical Record* 231, pp. 383–395.

Coso, Sanja; Bovay, Esther; Petrova, Tatjana (2014): Pressing the right buttons: signaling in lymphangiogenesis. In *BLOOD* 123 (17).

Coso, Sanja; Zeng, Yiping; Opeskin, Kenneth; Williams, Elizabeth D. (2012): Vascular endothelial growth factor receptor-3 directly interacts with phosphatidylinositol 3-kinase to regulate lymphangiogenesis. In *PloS one* 7 (6), e39558. DOI: 10.1371/journal.pone.0039558.

Covassin, L. D.; Villefranc, J. A.; Kacergis, M. C.; Weinstein, B. M.; Lawson N D (2006): Distinct genetic interactions between multiple *Vegf* receptors are required for development of different blood vessel types in zebrafish. In *Proceedings of the National Academy of Sciences of the United States of America* 103, pp. 6554–6559.

Dagamajalu, Shobha; Rex, D. A. B.; Philem, Pushparani Devi; Rainey, Jan K.; Keshava Prasad, T. S. (2022): A network map of apelin-mediated signaling. In *Journal of cell communication and signaling* 16 (1), pp. 137–143. DOI: 10.1007/s12079-021-00614-6.

Diaz-Santana, Anthony; Shan, Mengrou; Stroock, Abraham D. (2015): Endothelial cell dynamics during anastomosis in vitro. In *Integrative biology : quantitative biosciences from nano to macro* 7 (4), pp. 454–466. DOI: 10.1039/c5ib00052a.

Drake, Christopher J. (2003): Embryonic and adult vasculogenesis. In *Birth defects research. Part C, Embryo today : reviews* 69 (1), pp. 73–82. DOI: 10.1002/bdrc.10003.

Drake, Christopher J.; Little, Charles D. (1995): Exogenous vascular endothelial growth factor induces malformed and hyperfused vessels during embryonic neovascularization. In *Proceedings of the National Academy of Sciences of the United States of America* 92, pp. 7657–7661.

Ellertsdóttir, Elín; Lenard, Anna; Blum, Yannick; Krudewig, Alice; Herwig, Lukas; Affolter, Markus; Belting, Heinz-Georg (2010): Vascular morphogenesis in the zebrafish embryo. In *Developmental biology* 341 (1), pp. 56–65. DOI: 10.1016/j.ydbio.2009.10.035.

Engelman, Jeffrey A.; Luo, Ji; Cantley, Lewis C. (2006): The evolution of phosphatidylinositol 3-kinases as regulators of growth and metabolism. In *Nature reviews. Genetics* 7 (8), pp. 606–619. DOI: 10.1038/nrg1879.

Folkman, J. (1982): Angiogenesis: initiation and control. In *Annals of the New York Academy of Sciences* 401, pp. 212–227. DOI: 10.1111/j.1749-6632.1982.tb25720.x.

Folkman, J.; Haudenschild, C. (1980): Angiogenesis in vitro. In *Nature* 288, pp. 551–556.

Franco, Claudio A.; Jones, Martin L.; Bernabeu, Miguel O.; Geudens, Ilse; Mathivet, Thomas; Rosa, Andre et al. (2015): Dynamic endothelial cell rearrangements drive developmental vessel regression. In *PLoS biology* 13 (4), e1002125. DOI: 10.1371/journal.pbio.1002125.

Gebala, Véronique; Collins, Russell; Geudens, Ilse; Phng, Li-Kun; Gerhardt, Holger (2016): Blood flow drives lumen formation by inverse membrane blebbing during angiogenesis in vivo. In *Nature cell biology* 18 (4), pp. 443–450. DOI: 10.1038/ncb3320.

Gerhardt, Holger; Golding, Matthew; Fruttiger, Marcus; Ruhrberg, Christiana; Lundkvist, Andrea; Abramsson, Alexandra et al. (2003): VEGF guides angiogenic sprouting utilizing endothelial tip cell filopodia. In *The Journal of cell biology* 161 (6), pp. 1163–1177. DOI: 10.1083/jcb.200302047.

Gifre-Renom, Laia; Jones, Elizabeth A. V. (2021): Vessel Enlargement in Development and Pathophysiology. In *Frontiers in physiology* 12, p. 639645. DOI: 10.3389/fphys.2021.639645.

Graupera, Mariona; Guillermet-Guibert, Julie; Foukas, Lazaros C.; Phng, Li-Kun; Cain, Robert J.; Salpekar, Ashreena et al. (2008): Angiogenesis selectively requires the p110alpha isoform of PI3K to control endothelial cell migration. In *Nature* 453 (7195), pp. 662–666. DOI: 10.1038/nature06892.

- Graupera, Mariona; Potente, Michael (2013): Regulation of angiogenesis by PI3K signaling networks. In *Experimental cell research* 319 (9), pp. 1348–1355. DOI: 10.1016/j.yexcr.2013.02.021.
- Helker, Christian S. M.; Schuermann, Annika; Karpanen, Terhi; Zeuschner, Dagmar; Belting, Heinz-Georg; Affolter, Markus et al. (2013): The zebrafish common cardinal veins develop by a novel mechanism: lumen ensheathment. In *Development (Cambridge, England)* 140 (13), pp. 2776–2786. DOI: 10.1242/dev.091876.
- Helker, Christian S. M.; Schuermann, Annika; Pollmann, Cathrin; Chng, Serene C.; Kiefer, Friedemann; Reversade, Bruno; Herzog, Wiebke (2015): The hormonal peptide Elabela guides angioblasts to the midline during vasculogenesis. In *eLife*. DOI: 10.7554/eLife.06726.001.
- Helker, Christian Sm; Eberlein, Jean; Wilhelm, Kerstin; Sugino, Toshiya; Malchow, Julian; Schuermann, Annika et al. (2020): Apelin signaling drives vascular endothelial cells toward a pro-angiogenic state. In *eLife* 9. DOI: 10.7554/eLife.55589.
- Hellström, Mats; Phng, Li-Kun; Hofmann, Jennifer J.; Wallgard, Elisabet; Coultas, Leigh; Lindblom, Per et al. (2007): Dll4 signalling through Notch1 regulates formation of tip cells during angiogenesis. In *Nature* 445 (7129), pp. 776–780. DOI: 10.1038/nature05571.
- Herbert, Shane P.; Huisken, Jan; Kim, Tyson N.; Feldman, Morri E.; Houseman, Benjamin T.; Wang, Rong A. et al. (2009): Arterial-venous segregation by selective cell sprouting: an alternative mode of blood vessel formation. In *Science (New York, N.Y.)* 326 (5950), pp. 294–298. DOI: 10.1126/science.1178577.
- Herman, Paul K.; Emr, Scott D. (1990): Characterization of VPS34, a Gene Required for Vacuolar Protein Sorting and Vacuole Segregation in *Saccharomyces cerevisiae*. In *Molecular and Cellular Biology* 10 (12), pp. 6742–6754.
- Herwig, Lukas; Blum, Yannick; Krudewig, Alice; Ellertsdottir, Elin; Lenard, Anna; Belting, Heinz-Georg; Affolter, Markus (2011): Distinct cellular mechanisms of blood vessel fusion in the zebrafish embryo. In *Current biology : CB* 21 (22), pp. 1942–1948. DOI: 10.1016/j.cub.2011.10.016.
- Higashi, Tomohito; Arnold, Torey R.; Stephenson, Rachel E.; Dinshaw, Kayla M.; Miller, Ann L. (2016): Maintenance of the Epithelial Barrier and Remodeling of Cell-Cell Junctions during Cytokinesis. In *Current biology : CB* 26 (14), pp. 1829–1842. DOI: 10.1016/j.cub.2016.05.036.
- Higashi, Tomohito; Miller, Ann L. (2017): Tricellular junctions: how to build junctions at the TRICKiest points of epithelial cells. In *Molecular biology of the cell* 28 (15), pp. 2023–2034. DOI: 10.1091/mbc.E16-10-0697.



Hogan, Benjamin M.; Schulte-Merker, Stefan (2017): How to Plumb a Pisces: Understanding Vascular Development and Disease Using Zebrafish Embryos. In *Developmental cell* 42 (6), pp. 567–583. DOI: 10.1016/j.devcel.2017.08.015.

Hong, Charles C.; Peterson, Quinn P.; Hong, Ji-Young; Peterson, Randall T. (2006): Artery/Vein Specification Is Governed by Opposing Phosphatidylinositol-3 Kinase and MAP Kinase/ERK Signaling. In *Current biology : CB* 16 (13), pp. 1366–1372.

Hußmann, Melina; Schulte, Dörte; Weischer, Sarah; Carlantoni, Claudia; Nakajima, Hiroyuki; Mochizuki, Naoki et al. (2023): Svp1 is a binding ligand of Tie1 and affects specific aspects of facial lymphatic development in a Vegfc-independent manner. In *eLife* 12. DOI: 10.7554/eLife.82969.

Isogai, S.; Horiguchi, M.; Weinstein, B. M. (2001): The vascular anatomy of the developing zebrafish: an atlas of embryonic and early larval development. In *Developmental biology* 230 (2), pp. 278–301. DOI: 10.1006/dbio.2000.9995.

Isogai, Sumio; Lawson, Nathan D.; Torrealday, Saioa; Horiguchi, Masaharu; Weinstein, Brant M. (2003): Angiogenic network formation in the developing vertebrate trunk. In *Development (Cambridge, England)* 130 (21), pp. 5281–5290. DOI: 10.1242/dev.00733.

Jakobsson, Lars; Franco, Claudio A.; Bentley, Katie; Collins, Russell T.; Ponsioen, Bas; Aspalter, Irene M. et al. (2010): Endothelial cells dynamically compete for the tip cell position during angiogenic sprouting. In *Nature cell biology* 12 (10), pp. 943–953. DOI: 10.1038/ncb2103.

Jiang, Zhen; Carlantoni, Claudia; Allanki, Srinivas; Ebersberger, Ingo; Stainier, Didier Y. R. (2020): Tek (Tie2) is not required for cardiovascular development in zebrafish. In *Development (Cambridge, England)* 147 (19). DOI: 10.1242/dev.193029.

Jin, Suk-Won; Beis, Dimitris; Mitchell, Tracy; Chen, Jau-Nian; Stainier, Didier Y. R. (2005): Cellular and molecular analyses of vascular tube and lumen formation in zebrafish. In *Development (Cambridge, England)* 132 (23), pp. 5199–5209. DOI: 10.1242/dev.02087.

Kamei, Makoto; Saunders, W. Brian; Bayless, Kayla J.; Dye, Louis; Davis, George E.; Weinstein, Brant M. (2006): Endothelial tubes assemble from intracellular vacuoles in vivo. In *Nature* 442 (7101), pp. 453–456. DOI: 10.1038/nature04923.

Karthik, Swapna; Djukic, Tijana; Kim, Jun-Dae; Zuber, Benoît; Makanya, Andrew; Odriozola, Adolfo et al. (2018): Synergistic interaction of sprouting and intussusceptive angiogenesis during zebrafish caudal vein plexus development. In *Scientific reports* 8 (1), p. 9840. DOI: 10.1038/s41598-018-27791-6.

Kimmel, C. B.; Ballard, W. W.; Kimmel, S. R.; Ullmann, B.; Schilling, T. F. (1995): Stages of embryonic development of the zebrafish. In *Developmental dynamics : an official publication of the American Association of Anatomists* 203 (3), pp. 253–310. DOI: 10.1002/aja.1002030302.

Klarlund, J. K.; Guilherme, A.; Holik, J. J.; Virbasius, J. V.; Chawla, A.; Czech, M. P. (1997): Signaling by phosphoinositide-3,4,5-trisphosphate through proteins containing pleckstrin and Sec7 homology domains. In *Science (New York, N.Y.)* 275 (5308), pp. 1927–1930. DOI: 10.1126/science.275.5308.1927.

Klippel, Anke; Kavanaugh, Michael; Pot, David; Williams, Lewis T. (1997): A Specific Product of Phosphatidylinositol 3-Kinase Directly Activates the Protein Kinase Akt through Its Pleckstrin Homology Domain. In *Molecular and Cellular Biology* 17 (1), pp. 338–344.

Knall, Cindy; Worthen, G. Scott; Johnson, Gary L. (1997): Interleukin 8-stimulated phosphatidylinositol-3-kinase activity regulates the migration of human neutrophils independent of extracellular signal-regulated kinase and p38 mitogen-activated protein kinases. In *Proceedings of the National Academy of Sciences of the United States of America* 94, pp. 3052–3057.

Kobialka, Piotr; Graupera, Mariona (2019): Revisiting PI3-kinase signalling in angiogenesis. In *Vascular biology (Bristol, England)* 1 (1), H125-H134. DOI: 10.1530/VB-19-0025.

Kobialka, Piotr; Sabata, Helena; Vilalta, Odena; Gouveia, Leonor; Angulo-Urarte, Ana; Muixí, Laia et al. (2022): The onset of PI3K-related vascular malformations occurs during angiogenesis and is prevented by the AKT inhibitor miransertib. In *EMBO molecular medicine* 14 (7), e15619. DOI: 10.15252/emmm.202115619.

Korn, Claudia; Augustin, Hellmut G. (2015): Mechanisms of Vessel Pruning and Regression. In *Developmental cell* 34 (1), pp. 5–17. DOI: 10.1016/j.devcel.2015.06.004.

Kotini, Maria Paraskevi; Mäe, Maarja Andaloussi; Belting, Heinz-Georg; Betsholtz, Christer; Affolter, Markus (2019): Sprouting and anastomosis in the *Drosophila* trachea and the vertebrate vasculature: Similarities and differences in cell behaviour. In *Vascular pharmacology* 112, pp. 8–16. DOI: 10.1016/j.vph.2018.11.002.

Krueger, Janna; Liu, Dong; Scholz, Katja; Zimmer, Anja; Shi, Yu; Klein, Christian et al. (2011): Flt1 acts as a negative regulator of tip cell formation and branching morphogenesis in the zebrafish embryo. In *Development (Cambridge, England)* 138 (10), pp. 2111–2120. DOI: 10.1242/dev.063933.

Kwon, Hyouk-Bum; Wang, Shengpeng; Helker, Christian S. M.; Rasouli, S. Javad; Maischein, Hans-Martin; Offermanns, Stefan et al. (2016): In vivo modulation of endothelial

polarization by Apelin receptor signalling. In *Nature communications* 7, p. 11805. DOI: 10.1038/ncomms11805.

Legendijk AK, Gomez GA, Baek S, Hesselson D, Hughes WE, Paterson S, Conway DE, Belting HG, Affolter M, Smith KA, Schwartz MA, Yap AS, Hogan BM. Live imaging molecular changes in junctional tension upon VE-cadherin in zebrafish. *Nat Commun.* 2017 Nov 10;8(1):1402. doi: 10.1038/s41467-017-01325-6

Lammert, Eckhard; Axnick, Jennifer (2012): Vascular lumen formation. In *Cold Spring Harbor perspectives in medicine* 2 (4), a006619. DOI: 10.1101/cshperspect.a006619.

Lange, Martin; Ohnesorge, Nils; Hoffmann, Dennis; Rocha, Susana F.; Benedito, Rui; Siekmann, Arndt F. (2022): Zebrafish mutants in vegfab can affect endothelial cell proliferation without altering ERK phosphorylation and are phenocopied by loss of PI3K signaling. In *Developmental biology* 486, pp. 26–43. DOI: 10.1016/j.ydbio.2022.03.006.

Laschke, M. W.; Giebels, C.; Menger, M. D. (2011): Vasculogenesis: a new piece of the endometriosis puzzle. In *Human reproduction update* 17 (5), pp. 628–636. DOI: 10.1093/humupd/dmr023.

Lawson N. D.; Weinstein B. M. (2002): In vivo imaging of embryonic vascular development using transgenic zebrafish. In *Developmental Biology*, 248(2):307-18. DOI: 10.1006/dbio.2002.0711.

Lawson, Nathan D.; Li, Rui; Shin, Masahiro; Grosse, Ann; Yukselen, Onur; Stone, Oliver A. et al. (2020): An improved zebrafish transcriptome annotation for sensitive and comprehensive detection of cell type-specific genes. In *eLife* 9. DOI: 10.7554/eLife.55792.

Lenard, Anna; Daetwyler, Stephan; Betz, Charles; Ellertsdottir, Elin; Belting, Heinz-Georg; Huisken, Jan; Affolter, Markus (2015): Endothelial cell self-fusion during vascular pruning. In *PLoS biology* 13 (4), e1002126. DOI: 10.1371/journal.pbio.1002126.

Lenard, Anna; Ellertsdottir, Elin; Herwig, Lukas; Krudewig, Alice; Sauteur, Loïc; Belting, Heinz-Georg; Affolter, Markus (2013): In vivo analysis reveals a highly stereotypic morphogenetic pathway of vascular anastomosis. In *Developmental cell* 25 (5), pp. 492–506. DOI: 10.1016/j.devcel.2013.05.010.

Leslie, Jonathan D.; Ariza-McNaughton, Linda; Bermange, Adam L.; McAdow, Ryan; Johnson, Stephen L.; Lewis, Julian (2007): Endothelial signalling by the Notch ligand Deltalike 4 restricts angiogenesis. In *Development (Cambridge, England)* 134 (5), pp. 839–844. DOI: 10.1242/dev.003244.

Li, Tinglu; Kang, Guangbo; Wang, Tingyue; Huang, He (2018): Tumor angiogenesis and antiangiogenic gene therapy for cancer. In *Oncology letters* 16 (1), pp. 687–702. DOI:

10.3892/ol.2018.8733.

Li, Xiaoguang; Pal, Dhiman Sankar; Biswas, Debojyoti; Iglesias, Pablo A.; Devreotes, Peter N. (2021): Reverse fountain flow of phosphatidylinositol-3,4-bisphosphate polarizes migrating cells. In *The EMBO journal* 40 (4), e105094. DOI: 10.15252/embj.2020105094.

Limaye, Nisha; Kangas, Jaakko; Mendola, Antonella; Godfraind, Catherine; Schlögel, Matthieu J.; Helaers, Raphael et al. (2015): Somatic Activating PIK3CA Mutations Cause Venous Malformation. In *American journal of human genetics* 97 (6), pp. 914–921. DOI: 10.1016/j.ajhg.2015.11.011.

Lubarsky, Berry; Krasnow, Mark A. (2003): Tube Morphogenesis: Making and Shaping Biological Tubes. In *Cell* 112, pp. 19–28.

Luks, Valerie L.; Kamitaki, Nolan; Vivero, Matthew P.; Uller, Wibke; Rab, Rashed; Bovée, Judith V. M. G. et al. (2015): Lymphatic and other vascular malformative/overgrowth disorders are caused by somatic mutations in PIK3CA. In *The Journal of pediatrics* 166 (4), 1048-54.e1-5. DOI: 10.1016/j.jpeds.2014.12.069.

Maehama, T.; Dixon, J. E. (1998): The tumor suppressor, PTEN/MMAC1, dephosphorylates the lipid second messenger, phosphatidylinositol 3,4,5-trisphosphate. In *The Journal of biological chemistry* 273 (22), pp. 13375–13378. DOI: 10.1074/jbc.273.22.13375.

Missy, K.; van Poucke, V.; Raynal, P.; Viala, C.; Mauco, G.; Plantavid, M. et al. (1998): Lipid products of phosphoinositide 3-kinase interact with Rac1 GTPase and stimulate GDP dissociation. In *The Journal of biological chemistry* 273 (46), pp. 30279–30286. DOI: 10.1074/jbc.273.46.30279.

Morris, Jason Z.; Tissenbaum, Heidi A.; Ruvkun, Gary (1996): A phosphatidylinositol-3-OH kinase family member regulating longevity and diapause in *Caenorhabditis elegans*. In *Nature* 382, 536-539.

Neal, Alice; Nornes, Svanhild; Payne, Sophie; Wallace, Marsha D.; Fritzsche, Martin; Louphrasitthiphol, Pakavarin et al. (2019): Venous identity requires BMP signalling through ALK3. In *Nature communications* 10 (1), p. 453. DOI: 10.1038/s41467-019-08315-w.

Newman, Rebecca; Turner, Martin (2015): The Role of p110 $\delta$  in the Development and Activation of B Lymphocytes. In *Advances in experimental medicine and biology* 850, pp. 119–135. DOI: 10.1007/978-3-319-15774-0\_9.

Niklas, Karl J.; Newman, Stuart A. (2013): The origins of multicellular organisms. In *Evolution & development* 15 (1), pp. 41–52. DOI: 10.1111/ede.12013.

- Ola, Roxana; Dubrac, Alexandre; Han, Jinah; Zhang, Feng; Fang, Jennifer S.; Larrivée, Bruno et al. (2016): PI3 kinase inhibition improves vascular malformations in mouse models of hereditary haemorrhagic telangiectasia. In *Nature communications* 7, p. 13650. DOI: 10.1038/ncomms13650.
- Paatero, Ilkka; Sauter, Loïc; Lee, Minkyung; Lagendijk, Anne K.; Heutschi, Daniel; Wiesner, Cora et al. (2018): Junction-based lamellipodia drive endothelial cell rearrangements in vivo via a VE-cadherin-F-actin based oscillatory cell-cell interaction. In *Nature communications* 9 (1), p. 3545. DOI: 10.1038/s41467-018-05851-9.
- Panayotou, G.; Bax, B.; Gout, I.; Federwisch, M.; Wrobelowski, B.; Dhand, R. et al. (1992): Interaction of the p85 subunit of PI 3-kinase and its N-terminal SH2 domain with a PDGF receptor phosphorylation site: structural features and analysis of conformational changes. In *The EMBO journal* 11 (12), pp. 4261–4272.
- Parent, Carole A.; Blacklock, Brenda J.; Froehlich, Wendy M.; Murphy, Douglas B.; Devreotes, Peter N. (1998): G Protein Signaling Events Are Activated at the Leading Edge of Chemotactic Cells. In *Cell* 95, pp. 81–91.
- Park, Ho-Jin; Zhang, Yali; Georgescu, Serban P.; Johnson Kristin L; Kong, Dequon; Galper, Jonas B. (2006): Human Umbilical Vein Endothelial Cells and Human Dermal Microvascular Endothelial Cells Offer New Insights Into the Relationship Between Lipid Metabolism and Angiogenesis. In *Stem Cell Reviews*.
- Patan, Sybill (2000): Vasculogenesis and Angiogenesis as Mechanisms of Vascular Network Formation, Growth and Remodeling. In *Journal of Neuro-Oncology* 50, pp. 1–15.
- Phng, Li-Kun; Belting, Heinz-Georg (2021): Endothelial cell mechanics and blood flow forces in vascular morphogenesis. In *Seminars in cell & developmental biology* 120, pp. 32–43. DOI: 10.1016/j.semcd.2021.06.005.
- Pontes-Quero, Samuel; Fernández-Chacón, Macarena; Luo, Wen; Lunella, Federica Francesca; Casquero-Garcia, Verónica; Garcia-Gonzalez, Irene et al. (2019): High mitogenic stimulation arrests angiogenesis. In *Nature communications* 10 (1), p. 2016. DOI: 10.1038/s41467-019-09875-7.
- Poole, Thomas J.; Coffin, Douglas (1989): Vasculogenesis and angiogenesis: Two distinct morphogenetic mechanisms establish embryonic vascular pattern. In *The Journal of Experimental Zoology* 251, pp. 224–231.
- Poole, Thomas J.; Coffin, Douglas (1998): Developmental angiogenesis: Quail Embryonic Vasculature. In *Scanning Microscopy* 2 (1), pp. 443–448.

- Pudliszewski, Michel; Pardanaud, Luc (2005): Vasculogenesis and angiogenesis in the mouse embryo studied using quail/mouse chimeras. In *The International journal of developmental biology* 49 (2-3), pp. 355–361. DOI: 10.1387/ijdb.041956mp.
- Ribeiro, Carlos; Neumann, Marc; Affolter, Markus (2004): Genetic control of cell intercalation during tracheal morphogenesis in *Drosophila*. In *Current biology : CB* 14 (24), pp. 2197–2207. DOI: 10.1016/j.cub.2004.11.056.
- Richard J White; John E Collins; Ian M Sealy; Neha Wali; Christopher M Dooley; Zsofia Digby et al. (2017): A high-resolution mRNA expression time course of embryonic development in zebrafish. In *eLife*. DOI: 10.7554/eLife.30860.001.
- Ruan, Guo-Xiang; Kazlauskas, Andrius (2012): Axl is essential for VEGF-A-dependent activation of PI3K/Akt. In *The EMBO journal* 31 (7), pp. 1692–1703. DOI: 10.1038/emboj.2012.21.
- Sauteur, Loïc; Affolter, Markus; Belting, Heinz-Georg (2017): Distinct and redundant functions of Esama and VE-cadherin during vascular morphogenesis. In *Development (Cambridge, England)* 144 (8), pp. 1554–1565. DOI: 10.1242/dev.140038.
- Sauteur, Loïc; Krudewig, Alice; Herwig, Lukas; Ehrenfeuchter, Nikolaus; Lenard, Anna; Affolter, Markus; Belting, Heinz-Georg (2014): Cdh5/VE-cadherin promotes endothelial cell interface elongation via cortical actin polymerization during angiogenic sprouting. In *Cell reports* 9 (2), pp. 504–513. DOI: 10.1016/j.celrep.2014.09.024.
- Schellinx, N. (2018): Deciphering cytoskeletal junctional interactions during blood vessel morphogenesis in vivo: Introduction of novel genetic tools for mosaic analysis of Cdh5/VEcadherin regulation and function & phenotypic analysis of RadilB function in sprouting angiogenesis, Doctoral Thesis, Faculty of Science, University of Basel
- Schuermann, Annika; Helker, Christian S. M.; Herzog, Wiebke (2014): Angiogenesis in zebrafish. In *Seminars in cell & developmental biology* 31, pp. 106–114. DOI: 10.1016/j.semcdb.2014.04.037.
- Senger, Donald R.; Davis, George E. (2011): Angiogenesis. In *Cold Spring Harbor perspectives in biology* 3 (8), a005090. DOI: 10.1101/cshperspect.a005090.
- Shin, Masahiro; Beane, Timothy J.; Quillien, Aurelie; Male, Ira; Zhu, Lihua J.; Lawson, Nathan D. (2016): Vegfa signals through ERK to promote angiogenesis, but not artery differentiation. In *Development (Cambridge, England)* 143 (20), pp. 3796–3805. DOI: 10.1242/dev.137919.

Shin, Masahiro; Male, Ira; Beane, Timothy J.; Villefranc, Jacques A.; Kok, Fatma O.; Zhu, Lihua J.; Lawson, Nathan D. (2017): Correction: Vegfc acts through ERK to induce sprouting and differentiation of trunk lymphatic progenitors. In *Development (Cambridge, England)* 144 (3), p. 531. DOI: 10.1242/dev.148569.

Siekmann, Arndt F.; Affolter, Markus; Belting, Heinz-Georg (2013): The tip cell concept 10 years after: new players tune in for a common theme. In *Experimental cell research* 319 (9), pp. 1255–1263. DOI: 10.1016/j.yexcr.2013.01.019.

Song, Jonathan W.; Munn, Lance L. (2011): Fluid forces control endothelial sprouting. In *Proceedings of the National Academy of Sciences of the United States of America* 108 (37), pp. 15342–15347. DOI: 10.1073/pnas.1105316108.

Spiegelaere, Ward de; Casteleyn, Christophe; van den Broeck, Wim; Plendl, Johanna; Bahramsoltani, Mahtab; Simoens, Paul et al. (2012): Intussusceptive angiogenesis: a biologically relevant form of angiogenesis. In *Journal of vascular research* 49 (5), pp. 390–404. DOI: 10.1159/000338278.

Srinivasan, R. Sathish; Escobedo, Noelia; Yang, Ying; Interiano, Ashley; Dillard, Miriam E.; Finkelstein, David et al. (2014): The Prox1-Vegfr3 feedback loop maintains the identity and the number of lymphatic endothelial cell progenitors. In *Genes & development* 28 (19), pp. 2175–2187. DOI: 10.1101/gad.216226.113.

Stahl, Andreas; Connor, Kip M.; Sapielha, Przemyslaw; Chen, Jing; Dennison, Roberta J.; Krahl, Nathan M. et al. (2010): The mouse retina as an angiogenesis model. In *Investigative ophthalmology & visual science* 51 (6), pp. 2813–2826. DOI: 10.1167/iovs.10-5176.

Stambolic, Vuc; Suzuki, Akira; La Pompa, José Lois de; Brothers, Greg M.; Mirtsos, Christine; Sasaki, Takehiko et al. (1998): Negative Regulation of PKB/Akt-Dependent Cell Survival by the Tumor Suppressor PTEN. In *Cell* 95, pp. 29–39.

Strilić, Boris; Eglinger, Jan; Krieg, Michael; Zeeb, Martin; Axnick, Jennifer; Babál, Pavel et al. (2010): Electrostatic cell-surface repulsion initiates lumen formation in developing blood vessels. In *Current biology : CB* 20 (22), pp. 2003–2009. DOI: 10.1016/j.cub.2010.09.061.

Suri, C.; Jones, P. F.; Patan, S.; Bartunkova, S.; Maisonpierre, P. C.; Davis, S. et al. (1996): Requisite role of angiopoietin-1, a ligand for the TIE2 receptor, during embryonic angiogenesis. In *Cell* 87 (7), pp. 1171–1180. DOI: 10.1016/s0092-8674(00)81813-9.

Szymborska, Anna; Gerhardt, Holger (2018): Hold Me, but Not Too Tight-Endothelial CellCell Junctions in Angiogenesis. In *Cold Spring Harbor perspectives in biology* 10 (8). DOI: 10.1101/cshperspect.a029223.

- Tammela, Tuomas; Zarkada, Georgia; Wallgard, Elisabet; Murtomäki, Aino; Suchting, Steven; Wirzenius, Maria et al. (2008): Blocking VEGFR-3 suppresses angiogenic sprouting and vascular network formation. In *Nature* 454 (7204), pp. 656–660. DOI: 10.1038/nature07083.
- Thomas, Markus; Augustin, Hellmut G. (2009): The role of the Angiopoietins in vascular morphogenesis. In *Angiogenesis* 12 (2), pp. 125–137. DOI: 10.1007/s10456-009-9147-3.
- Thomas, Molly S.; Mitchell, Jason S.; DeNucci, Christopher C.; Martin, Amanda L.; Shimizu, Yoji (2008): The p110gamma isoform of phosphatidylinositol 3-kinase regulates migration of effector CD4 T lymphocytes into peripheral inflammatory sites. In *Journal of leukocyte biology* 84 (3), pp. 814–823. DOI: 10.1189/jlb.0807561.
- Thorpe, Lauren M.; Yuzugullu, Haluk; Zhao, Jean J. (2015): PI3K in cancer: divergent roles of isoforms, modes of activation and therapeutic targeting. In *Nature reviews. Cancer* 15 (1), pp. 7–24. DOI: 10.1038/nrc3860.
- Traver, David; Paw, Barry H.; Poss, Kenneth D.; Penberthy, W. Todd; Lin, Shuo; Zon, Leonard I. (2003): Transplantation and in vivo imaging of multilineage engraftment in zebrafish bloodless mutants. In *Nature immunology* 4 (12), pp. 1238–1246. DOI: 10.1038/ni1007.
- Tschudin, F. (2022): The role and function of PI3-Kinase  $\alpha$  signaling during blood vessel morphogenesis in the zebrafish embryo. Master thesis, Faculty of Science, University of Basel
- Turner, L.; Ward, S. G.; Westwick, J. (1995): RANTES-activated human T-lymphocytes- a role for phosphoinositide-3-kinase. In *Journal of Immunology* 155 (5), pp. 2437–2444.
- Tzima, Eleni; Irani-Tehrani, Mohamed; Kiosses, William B.; Dejana, Elizabetta; Schultz, David A.; Engelhardt, Britta et al. (2005): A mechanosensory complex that mediates the endothelial cell response to fluid shear stress. In *Nature* 437 (7057), pp. 426–431. DOI: 10.1038/nature03952.
- Vanhaesebroeck, Bart; Guillermet-Guibert, Julie; Graupera, Mariona; Bilanges, Benoit (2010): The emerging mechanisms of isoform-specific PI3K signalling. In *Nature reviews. Molecular cell biology* 11 (5), pp. 329–341. DOI: 10.1038/nrm2882.
- Venkateswaran, Amudhan; Sekhar, Konjeti R.; Levic, Daniel S.; Melville, David B.; Clark, Travis A.; Rybski, Witold M. et al. (2014): The NADH oxidase ENOX1, a critical mediator of endothelial cell radiosensitization, is crucial for vascular development. In *Cancer research* 74 (1), pp. 38–43. DOI: 10.1158/0008-5472.CAN-13-1981.



- Wang, Ying; Kaiser, Mark S.; Larson, Jon D.; Nasevicius, Aidas; Clark, Karl J.; Wadman, Shannon A. et al. (2010): Moesin1 and Ve-cadherin are required in endothelial cells during in vivo tubulogenesis. In *Development (Cambridge, England)* 137 (18), pp. 3119–3128. DOI: 10.1242/dev.048785.
- Weijts, Bart; Shaked, Iftach; Ginsberg, Mark; Kleinfeld, David; Robin, Catherine; Traver, David (2021): Endothelial struts enable the generation of large lumenized blood vessels de novo. In *Nature cell biology* 23 (4), pp. 322–329. DOI: 10.1038/s41556-021-00664-3.
- Werner Risau and Ingo Flamme (1995): Vasculogenesis. In *Annual Reviews in Cell and Developmental Biology* 11, pp. 73–91.
- Westerfield, M. (2000). The zebrafish book. A guide for the laboratory use of zebrafish (*Danio rerio*). 4th ed., Univ. of Oregon Press, Eugene.
- Wiesner, C. (2020): Analysis of junctional and F-actin dynamics during blood vessel morphogenesis. Doctoral Thesis, Faculty of Science, University of Basel
- Whitman, Malcolm; Kaplan, David R.; Schaffhausen, Brian; Cantley, Lewis; Roberts, Thomas M. (1985): Association of phosphatidylinositol kinase activity with polyoma middle-T competent for transformation. In *Nature* 315.
- Wild, Raphael; Klems, Alina; Takamiya, Masanari; Hayashi, Yuya; Strähle, Uwe; Ando, Koji et al. (2017): Neuronal sFlt1 and Vegfaa determine venous sprouting and spinal cord vascularization. In *Nature communications* 8, p. 13991. DOI: 10.1038/ncomms13991.
- Wiley, David M.; Kim, Jun-Dae; Hao, Jijun; Hong, Charles C.; Bautch, Victoria L.; Jin, SukWon (2011): Distinct signalling pathways regulate sprouting angiogenesis from the dorsal aorta and the axial vein. In *Nature cell biology* 13 (6), pp. 686–692. DOI: 10.1038/ncb2232.
- Yin, Jianmin; Heutschi, Daniel; Belting, Heinz-Georg; Affolter, Markus (2021): Building the complex architectures of vascular networks: Where to branch, where to connect and where to remodel? In *Current topics in developmental biology* 143, pp. 281–297. DOI: 10.1016/bs.ctdb.2021.01.002.
- Yoshioka, Kazuaki; Yoshida, Kotaro; Cui, Hong; Wakayama, Tomohiko; Takuwa, Noriko; Okamoto, Yasuo et al. (2012): Endothelial PI3K-C2 $\alpha$ , a class II PI3K, has an essential role in angiogenesis and vascular barrier function. In *Nature medicine* 18 (10), pp. 1560–1569. DOI: 10.1038/nm.2928.

Zhang, Yu; Xu, Bing; Chen, Qi; Yan, Yong; Du, Jiulin; Du, Xufei (2018): Apoptosis of Endothelial Cells Contributes to Brain Vessel Pruning of Zebrafish During Development. In *Frontiers in molecular neuroscience* 11, p. 222. DOI: 10.3389/fnmol.2018.00222.

Zhou, Wenping; Ristori, Emma; He, Liqun; Ghersi, Joey J.; Mehta, Sameet; Zhang, Rong et al. (2020): Akt is required for artery formation during embryonic vascular development. In *BioRxiv*. DOI: 10.1101/2020.06.04.134718.

Zimmermann, S.; Moelling, K. (1999): Phosphorylation and regulation of Raf by Akt (protein kinase B). In *Science (New York, N.Y.)* 286 (5445), pp. 1741–1744. DOI: 10.1126/science.286.5445.1741.

## Copyright Information

Licenses for Figure 1, Figure 2 and Figure 3 were kindly provided by Elsevier via RightsLink, and the respective license information is attached in the following.

Figure 8 B was licensed under a “Creative Commons Attribution 4.0. International License, which permits unrestricted use, distribution modification and reproduction in any medium, provided proper acknowledgement is given to the original authors” (Journalpermissions@SpringerNature, 7<sup>th</sup> August, 2023).

Figures designed with BioRender were created under the Basic (Free) Version of BioRender. The BioRender website states that “if your thesis is going to be uploaded to a University database or library we do not consider this as a published thesis. Therefore, you can definitely use our free basic version for this” (BioRender, 16<sup>th</sup> August 2023). Whenever BioRender was used to create a figure, this is indicated in the figure description. Watermarks were kept as requested.

# ELSEVIER LICENSE TERMS AND CONDITIONS

Aug 16, 2023

This Agreement between Biozentrum, Univeristy Basel -- Kathrin Gundel ("You") and Elsevier ("Elsevier") consists of your license details and the terms and conditions provided by Elsevier and Copyright Clearance Center.

License Number	5604271483037
License date	Aug 08, 2023
Licensed Content Publisher	Elsevier
Licensed Content Publication	Elsevier Books
Licensed Content Title	Current Topics in Developmental Biology
Licensed Content Author	Magdalena M. Baer, Helene Chanut-Delalande, Markus Affolter
Licensed Content Date	Jan 1, 2009
Licensed Content Pages	26
Start Page	137
End Page	162
Type of Use	reuse in a thesis/dissertation
Portion	figures/tables/illustrations
Number of figures/tables /illustrations	2
Format	both print and electronic
Are you the author of this Elsevier chapter?	No
Will you be translating?	No
Title	PhD Thesis
Institution name	Biozentrum Basel
Expected presentation date	Sep 2023
Portions	Figures 6.1, 6.2
Requestor Location	Biozentrum, Univeristy Basel Spitalstrasse 41  Basel, 4056 Switzerland Attn: Biozentrum, Univeristy Basel
Publisher Tax ID	GB 494 6272 12
Total	<b>0.00 CHF</b>
Terms and Conditions	

## INTRODUCTION

1. The publisher for this copyrighted material is Elsevier. By clicking "accept" in connection with completing this licensing transaction, you agree that the following terms and conditions apply to this transaction (along with the Billing and Payment terms and conditions established by Copyright Clearance Center, Inc. ("CCC"), at the time that you opened your RightsLink account and that are available at any time at <https://myaccount.copyright.com>).

## GENERAL TERMS

2. Elsevier hereby grants you permission to reproduce the aforementioned material subject to the terms and conditions indicated.

3. **Acknowledgement:** If any part of the material to be used (for example, figures) has appeared in our publication with credit or acknowledgement to another source, permission must also be sought from that source. If such permission is not obtained then that material may not be included in your publication/copies. Suitable acknowledgement to the source must be made, either as a footnote or in a reference list at the end of your publication, as follows:  
"Reprinted from Publication title, Vol /edition number, Author(s), Title of article / title of chapter, Pages No., Copyright (Year), with permission from Elsevier [OR APPLICABLE SOCIETY COPYRIGHT OWNER]." Also Lancet special credit - "Reprinted from The Lancet, Vol. number, Author(s), Title of article, Pages No., Copyright (Year), with permission from Elsevier."
4. **Reproduction of this material is confined to the purpose and/or media for which permission is hereby given.** The material may not be reproduced or used in any other way, including use in combination with an artificial intelligence tool (including to train an algorithm, test, process, analyse, generate output and/or develop any form of artificial intelligence tool), or to create any derivative work and/or service (including resulting from the use of artificial intelligence tools).
5. **Altering/Modifying Material: Not Permitted.** However figures and illustrations may be altered/adapted minimally to serve your work. Any other abbreviations, additions, deletions and/or any other alterations shall be made only with prior written authorization of Elsevier Ltd. (Please contact Elsevier's permissions helpdesk [here](#)). No modifications can be made to any Lancet figures/tables and they must be reproduced in full.
6. **If the permission fee for the requested use of our material is waived in this instance, please be advised that your future requests for Elsevier materials may attract a fee.**
7. **Reservation of Rights:** Publisher reserves all rights not specifically granted in the combination of (i) the license details provided by you and accepted in the course of this licensing transaction, (ii) these terms and conditions and (iii) CCC's Billing and Payment terms and conditions.
8. **License Contingent Upon Payment:** While you may exercise the rights licensed immediately upon issuance of the license at the end of the licensing process for the transaction, provided that you have disclosed complete and accurate details of your proposed use, no license is finally effective unless and until full payment is received from you (either by publisher or by CCC) as provided in CCC's Billing and Payment terms and conditions. If full payment is not received on a timely basis, then any license preliminarily granted shall be deemed automatically revoked and shall be void as if never granted. Further, in the event that you breach any of these terms and conditions or any of CCC's Billing and Payment terms and conditions, the license is automatically revoked and shall be void as if never granted. Use of materials as described in a revoked license, as well as any use of the materials beyond the scope of an unrevoked license, may constitute copyright infringement and publisher reserves the right to take any and all action to protect its copyright in the materials.
9. **Warranties:** Publisher makes no representations or warranties with respect to the licensed material.
10. **Indemnity:** You hereby indemnify and agree to hold harmless publisher and CCC, and their respective officers, directors, employees and agents, from and against any and all claims arising out of your use of the licensed material other than as specifically authorized pursuant to this license.
11. **No Transfer of License:** This license is personal to you and may not be sublicensed, assigned, or transferred by you to any other person without publisher's written permission.
12. **No Amendment Except in Writing:** This license may not be amended except in a writing signed by both parties (or, in the case of publisher, by CCC on publisher's behalf).
13. **Objection to Contrary Terms:** Publisher hereby objects to any terms contained in any purchase order, acknowledgment, check endorsement or other writing prepared by you, which terms are inconsistent with these terms and conditions or CCC's Billing and Payment terms and conditions. These terms and conditions, together with CCC's Billing and Payment terms and conditions (which are incorporated herein), comprise the entire agreement between you and publisher (and CCC) concerning this licensing transaction. In the event of any conflict between your obligations established by these terms and conditions and those established by CCC's Billing and Payment terms and conditions, these terms and conditions shall control.
14. **Revocation:** Elsevier or Copyright Clearance Center may deny the permissions described in this License at their sole discretion, for any reason or no reason, with a full refund payable to you. Notice of such denial will be made using the contact information provided by you. Failure to receive such notice will not alter or invalidate the denial. In no event will Elsevier or Copyright Clearance Center be responsible or liable for any costs, expenses or damage incurred by you as a result of a denial of your permission request, other than a refund of the amount(s) paid by you to Elsevier and/or Copyright Clearance Center for denied permissions.

#### LIMITED LICENSE

The following terms and conditions apply only to specific license types:

15. **Translation:** This permission is granted for non-exclusive world **English** rights only unless your license was granted for translation rights. If you licensed translation rights you may only translate this content into the languages you requested. A professional translator must perform all translations and reproduce the content word for word preserving the integrity of the article.
16. **Posting licensed content on any Website:** The following terms and conditions apply as follows: Licensing material from an Elsevier journal: All content posted to the web site must maintain the copyright information line on the bottom of each image; A hyper-text must be included to the Homepage of the journal from which you are licensing at <http://www.sciencedirect.com/science/journal/xxxxx> or the Elsevier homepage for books at <http://www.elsevier.com>; Central Storage: This license does not include permission for a scanned version of the material to be stored in a central repository such as that provided by Heron/XanEdu.

Licensing material from an Elsevier book: A hyper-text link must be included to the Elsevier homepage at <http://www.elsevier.com>. All content posted to the web site must maintain the copyright information line on the bottom of each image.

**Posting licensed content on Electronic reserve:** In addition to the above the following clauses are applicable: The web site must be password-protected and made available only to bona fide students registered on a relevant course. This permission is granted for 1 year only. You may obtain a new license for future website posting.

17. **For journal authors:** the following clauses are applicable in addition to the above:

**Preprints:**

A preprint is an author's own write-up of research results and analysis, it has not been peer-reviewed, nor has it had any other value added to it by a publisher (such as formatting, copyright, technical enhancement etc.).

Authors can share their preprints anywhere at any time. Preprints should not be added to or enhanced in any way in order to appear more like, or to substitute for, the final versions of articles however authors can update their preprints on arXiv or RePEc with their Accepted Author Manuscript (see below).

If accepted for publication, we encourage authors to link from the preprint to their formal publication via its DOI. Millions of researchers have access to the formal publications on ScienceDirect, and so links will help users to find, access, cite and use the best available version. Please note that Cell Press, The Lancet and some society-owned have different preprint policies.

Information on these policies is available on the journal homepage.

**Accepted Author Manuscripts:** An accepted author manuscript is the manuscript of an article that has been accepted for publication and which typically includes author-incorporated changes suggested during submission, peer review and editor-author communications.

Authors can share their accepted author manuscript:

- immediately
  - via their non-commercial person homepage or blog
  - by updating a preprint in arXiv or RePEc with the accepted manuscript
  - via their research institute or institutional repository for internal institutional uses or as part of an invitation-only research collaboration work-group
  - directly by providing copies to their students or to research collaborators for their personal use
  - for private scholarly sharing as part of an invitation-only work group on commercial sites with which Elsevier has an agreement
- After the embargo period
  - via non-commercial hosting platforms such as their institutional repository
  - via commercial sites with which Elsevier has an agreement

In all cases accepted manuscripts should:

- link to the formal publication via its DOI
- bear a CC-BY-NC-ND license - this is easy to do
- if aggregated with other manuscripts, for example in a repository or other site, be shared in alignment with our hosting policy not be added to or enhanced in any way to appear more like, or to substitute for, the published journal article.

**Published journal article (JPA):** A published journal article (PJA) is the definitive final record of published research that appears or will appear in the journal and embodies all value-adding publishing activities including peer review co-ordination, copy-editing, formatting, (if relevant) pagination and online enrichment.

Policies for sharing publishing journal articles differ for subscription and gold open access articles:

**Subscription Articles:** If you are an author, please share a link to your article rather than the full-text. Millions of researchers have access to the formal publications on ScienceDirect, and so links will help your users to find, access, cite, and use the best available version.

Theses and dissertations which contain embedded PJAs as part of the formal submission can be posted publicly by the awarding institution with DOI links back to the formal publications on ScienceDirect.

If you are affiliated with a library that subscribes to ScienceDirect you have additional private sharing rights for others' research accessed under that agreement. This includes use for classroom teaching and internal training at the institution (including use in course packs and courseware programs), and inclusion of the article for grant funding purposes.

**Gold Open Access Articles:** May be shared according to the author-selected end-user license and should contain a [CrossMark logo](#), the end user license, and a DOI link to the formal publication on ScienceDirect.

Please refer to Elsevier's [posting policy](#) for further information.

18. **For book authors** the following clauses are applicable in addition to the above: Authors are permitted to place a brief summary of their work online only. You are not allowed to download and post the published electronic version of your chapter, nor may you scan the printed edition to create an electronic version. **Posting to a repository:** Authors are permitted to post a summary of their chapter only in their institution's repository.

**19. Thesis/Dissertation:** If your license is for use in a thesis/dissertation your thesis may be submitted to your institution in either print or electronic form. Should your thesis be published commercially, please reapply for permission. These requirements include permission for the Library and Archives of Canada to supply single copies, on demand, of the complete thesis and include permission for Proquest/UMI to supply single copies, on demand, of the complete thesis. Should your thesis be published commercially, please reapply for permission. Theses and dissertations which contain embedded PJAs as part of the formal submission can be posted publicly by the awarding institution with DOI links back to the formal publications on ScienceDirect.

#### **Elsevier Open Access Terms and Conditions**

You can publish open access with Elsevier in hundreds of open access journals or in nearly 2000 established subscription journals that support open access publishing. Permitted third party re-use of these open access articles is defined by the author's choice of Creative Commons user license. See our [open access license policy](#) for more information.

#### **Terms & Conditions applicable to all Open Access articles published with Elsevier:**

Any reuse of the article must not represent the author as endorsing the adaptation of the article nor should the article be modified in such a way as to damage the author's honour or reputation. If any changes have been made, such changes must be clearly indicated.

The author(s) must be appropriately credited and we ask that you include the end user license and a DOI link to the formal publication on ScienceDirect.

If any part of the material to be used (for example, figures) has appeared in our publication with credit or acknowledgement to another source it is the responsibility of the user to ensure their reuse complies with the terms and conditions determined by the rights holder.

#### **Additional Terms & Conditions applicable to each Creative Commons user license:**

**CC BY:** The CC-BY license allows users to copy, to create extracts, abstracts and new works from the Article, to alter and revise the Article and to make commercial use of the Article (including reuse and/or resale of the Article by commercial entities), provided the user gives appropriate credit (with a link to the formal publication through the relevant DOI), provides a link to the license, indicates if changes were made and the licensor is not represented as endorsing the use made of the work. The full details of the license are available at <http://creativecommons.org/licenses/by/4.0>.

**CC BY NC SA:** The CC BY-NC-SA license allows users to copy, to create extracts, abstracts and new works from the Article, to alter and revise the Article, provided this is not done for commercial purposes, and that the user gives appropriate credit (with a link to the formal publication through the relevant DOI), provides a link to the license, indicates if changes were made and the licensor is not represented as endorsing the use made of the work. Further, any new works must be made available on the same conditions. The full details of the license are available at <http://creativecommons.org/licenses/by-nc-sa/4.0>.

**CC BY NC ND:** The CC BY-NC-ND license allows users to copy and distribute the Article, provided this is not done for commercial purposes and further does not permit distribution of the Article if it is changed or edited in any way, and provided the user gives appropriate credit (with a link to the formal publication through the relevant DOI), provides a link to the license, and that the licensor is not represented as endorsing the use made of the work. The full details of the license are available at <http://creativecommons.org/licenses/by-nc-nd/4.0>. Any commercial reuse of Open Access articles published with a CC BY NC SA or CC BY NC ND license requires permission from Elsevier and will be subject to a fee.

Commercial reuse includes:

- Associating advertising with the full text of the Article
- Charging fees for document delivery or access
- Article aggregation
- Systematic distribution via e-mail lists or share buttons

Posting or linking by commercial companies for use by customers of those companies.

#### **20. Other Conditions:**

v1.10

Questions? E-mail us at [customercare@copyright.com](mailto:customercare@copyright.com).

---

---

# ELSEVIER LICENSE TERMS AND CONDITIONS

Aug 16, 2023

This Agreement between Biozentrum, Univeristy Basel -- Kathrin Gundel ("You") and Elsevier ("Elsevier") consists of your license details and the terms and conditions provided by Elsevier and Copyright Clearance Center.

License Number	5604280262097
License date	Aug 08, 2023
Licensed Content Publisher	Elsevier
Licensed Content Publication	Developmental Cell
Licensed Content Title	How to Plumb a Pisces: Understanding Vascular Development and Disease Using Zebrafish Embryos
Licensed Content Author	Benjamin M. Hogan, Stefan Schulte-Merker
Licensed Content Date	Sep 25, 2017
Licensed Content Volume	42
Licensed Content Issue	6
Licensed Content Pages	17
Start Page	567
End Page	583
Type of Use	reuse in a thesis/dissertation
Portion	figures/tables/illustrations
Number of figures/tables /illustrations	1
Format	both print and electronic
Are you the author of this Elsevier article?	No
Will you be translating?	No
Title	PhD Thesis
Institution name	Biozentrum Basel
Expected presentation date	Sep 2023
Portions	Figure 1, (C,F)
Requestor Location	Biozentrum, Univeristy Basel Spitalstrasse 41  Basel, 4056 Switzerland Attn: Biozentrum, Univeristy Basel
Publisher Tax ID	GB 494 6272 12
Total	<b>0.00 USD</b>
Terms and Conditions	

## INTRODUCTION

1. The publisher for this copyrighted material is Elsevier. By clicking "accept" in connection with completing this licensing transaction, you agree that the following terms and conditions apply to this transaction (along with the Billing and Payment terms and conditions established by Copyright Clearance Center, Inc. ("CCC"), at the time that you opened your RightsLink account



and that are available at any time at <https://myaccount.copyright.com>).

### GENERAL TERMS

2. Elsevier hereby grants you permission to reproduce the aforementioned material subject to the terms and conditions indicated.
3. Acknowledgement: If any part of the material to be used (for example, figures) has appeared in our publication with credit or acknowledgement to another source, permission must also be sought from that source. If such permission is not obtained then that material may not be included in your publication/copies. Suitable acknowledgement to the source must be made, either as a footnote or in a reference list at the end of your publication, as follows:  
"Reprinted from Publication title, Vol /edition number, Author(s), Title of article / title of chapter, Pages No., Copyright (Year), with permission from Elsevier [OR APPLICABLE SOCIETY COPYRIGHT OWNER]." Also Lancet special credit - "Reprinted from The Lancet, Vol. number, Author(s), Title of article, Pages No., Copyright (Year), with permission from Elsevier."
4. Reproduction of this material is confined to the purpose and/or media for which permission is hereby given. The material may not be reproduced or used in any other way, including use in combination with an artificial intelligence tool (including to train an algorithm, test, process, analyse, generate output and/or develop any form of artificial intelligence tool), or to create any derivative work and/or service (including resulting from the use of artificial intelligence tools).
5. Altering/Modifying Material: Not Permitted. However figures and illustrations may be altered/adapted minimally to serve your work. Any other abbreviations, additions, deletions and/or any other alterations shall be made only with prior written authorization of Elsevier Ltd. (Please contact Elsevier's permissions helpdesk [here](#)). No modifications can be made to any Lancet figures/tables and they must be reproduced in full.
6. If the permission fee for the requested use of our material is waived in this instance, please be advised that your future requests for Elsevier materials may attract a fee.
7. Reservation of Rights: Publisher reserves all rights not specifically granted in the combination of (i) the license details provided by you and accepted in the course of this licensing transaction, (ii) these terms and conditions and (iii) CCC's Billing and Payment terms and conditions.
8. License Contingent Upon Payment: While you may exercise the rights licensed immediately upon issuance of the license at the end of the licensing process for the transaction, provided that you have disclosed complete and accurate details of your proposed use, no license is finally effective unless and until full payment is received from you (either by publisher or by CCC) as provided in CCC's Billing and Payment terms and conditions. If full payment is not received on a timely basis, then any license preliminarily granted shall be deemed automatically revoked and shall be void as if never granted. Further, in the event that you breach any of these terms and conditions or any of CCC's Billing and Payment terms and conditions, the license is automatically revoked and shall be void as if never granted. Use of materials as described in a revoked license, as well as any use of the materials beyond the scope of an unrevoked license, may constitute copyright infringement and publisher reserves the right to take any and all action to protect its copyright in the materials.
9. Warranties: Publisher makes no representations or warranties with respect to the licensed material.
10. Indemnity: You hereby indemnify and agree to hold harmless publisher and CCC, and their respective officers, directors, employees and agents, from and against any and all claims arising out of your use of the licensed material other than as specifically authorized pursuant to this license.
11. No Transfer of License: This license is personal to you and may not be sublicensed, assigned, or transferred by you to any other person without publisher's written permission.
12. No Amendment Except in Writing: This license may not be amended except in a writing signed by both parties (or, in the case of publisher, by CCC on publisher's behalf).
13. Objection to Contrary Terms: Publisher hereby objects to any terms contained in any purchase order, acknowledgment, check endorsement or other writing prepared by you, which terms are inconsistent with these terms and conditions or CCC's Billing and Payment terms and conditions. These terms and conditions, together with CCC's Billing and Payment terms and conditions (which are incorporated herein), comprise the entire agreement between you and publisher (and CCC) concerning this licensing transaction. In the event of any conflict between your obligations established by these terms and conditions and those established by CCC's Billing and Payment terms and conditions, these terms and conditions shall control.
14. Revocation: Elsevier or Copyright Clearance Center may deny the permissions described in this License at their sole discretion, for any reason or no reason, with a full refund payable to you. Notice of such denial will be made using the contact information provided by you. Failure to receive such notice will not alter or invalidate the denial. In no event will Elsevier or Copyright Clearance Center be responsible or liable for any costs, expenses or damage incurred by you as a result of a denial of your permission request, other than a refund of the amount(s) paid by you to Elsevier and/or Copyright Clearance Center for denied permissions.

### LIMITED LICENSE

The following terms and conditions apply only to specific license types:

15. **Translation:** This permission is granted for non-exclusive world **English** rights only unless your license was granted for translation rights. If you licensed translation rights you may only translate this content into the languages you requested. A professional translator must perform all translations and reproduce the content word for word preserving the integrity of the article.
16. **Posting licensed content on any Website:** The following terms and conditions apply as follows: Licensing material from an Elsevier journal: All content posted to the web site must maintain the copyright information line on the bottom of each image; A

hyper-text must be included to the Homepage of the journal from which you are licensing at <http://www.sciencedirect.com/science/journal/xxxxx> or the Elsevier homepage for books at <http://www.elsevier.com>; Central Storage: This license does not include permission for a scanned version of the material to be stored in a central repository such as that provided by Heron/XanEdu. Licensing material from an Elsevier book: A hyper-text link must be included to the Elsevier homepage at <http://www.elsevier.com>. All content posted to the web site must maintain the copyright information line on the bottom of each image.

**Posting licensed content on Electronic reserve:** In addition to the above the following clauses are applicable: The web site must be password-protected and made available only to bona fide students registered on a relevant course. This permission is granted for 1 year only. You may obtain a new license for future website posting.

17. **For journal authors:** the following clauses are applicable in addition to the above:

**Preprints:**

A preprint is an author's own write-up of research results and analysis, it has not been peer-reviewed, nor has it had any other value added to it by a publisher (such as formatting, copyright, technical enhancement etc.).

Authors can share their preprints anywhere at any time. Preprints should not be added to or enhanced in any way in order to appear more like, or to substitute for, the final versions of articles however authors can update their preprints on arXiv or RePEc with their Accepted Author Manuscript (see below).

If accepted for publication, we encourage authors to link from the preprint to their formal publication via its DOI. Millions of researchers have access to the formal publications on ScienceDirect, and so links will help users to find, access, cite and use the best available version. Please note that Cell Press, The Lancet and some society-owned have different preprint policies. Information on these policies is available on the journal homepage.

**Accepted Author Manuscripts:** An accepted author manuscript is the manuscript of an article that has been accepted for publication and which typically includes author-incorporated changes suggested during submission, peer review and editor-author communications.

Authors can share their accepted author manuscript:

- immediately
  - via their non-commercial person homepage or blog
  - by updating a preprint in arXiv or RePEc with the accepted manuscript
  - via their research institute or institutional repository for internal institutional uses or as part of an invitation-only research collaboration work-group
  - directly by providing copies to their students or to research collaborators for their personal use
  - for private scholarly sharing as part of an invitation-only work group on commercial sites with which Elsevier has an agreement
- After the embargo period
  - via non-commercial hosting platforms such as their institutional repository
  - via commercial sites with which Elsevier has an agreement

In all cases accepted manuscripts should:

- link to the formal publication via its DOI
- bear a CC-BY-NC-ND license - this is easy to do
- if aggregated with other manuscripts, for example in a repository or other site, be shared in alignment with our hosting policy not be added to or enhanced in any way to appear more like, or to substitute for, the published journal article.

**Published journal article (JPA):** A published journal article (PJA) is the definitive final record of published research that appears or will appear in the journal and embodies all value-adding publishing activities including peer review co-ordination, copy-editing, formatting, (if relevant) pagination and online enrichment.

Policies for sharing publishing journal articles differ for subscription and gold open access articles:

**Subscription Articles:** If you are an author, please share a link to your article rather than the full-text. Millions of researchers have access to the formal publications on ScienceDirect, and so links will help your users to find, access, cite, and use the best available version.

Theses and dissertations which contain embedded PJAs as part of the formal submission can be posted publicly by the awarding institution with DOI links back to the formal publications on ScienceDirect.

If you are affiliated with a library that subscribes to ScienceDirect you have additional private sharing rights for others' research accessed under that agreement. This includes use for classroom teaching and internal training at the institution (including use in course packs and courseware programs), and inclusion of the article for grant funding purposes.

**Gold Open Access Articles:** May be shared according to the author-selected end-user license and should contain a [CrossMark logo](#), the end user license, and a DOI link to the formal publication on ScienceDirect.

Please refer to Elsevier's [posting policy](#) for further information.

18. **For book authors** the following clauses are applicable in addition to the above: Authors are permitted to place a brief

summary of their work online only. You are not allowed to download and post the published electronic version of your chapter, nor may you scan the printed edition to create an electronic version. **Posting to a repository:** Authors are permitted to post a summary of their chapter only in their institution's repository.

**19. Thesis/Dissertation:** If your license is for use in a thesis/dissertation your thesis may be submitted to your institution in either print or electronic form. Should your thesis be published commercially, please reapply for permission. These requirements include permission for the Library and Archives of Canada to supply single copies, on demand, of the complete thesis and include permission for Proquest/UMI to supply single copies, on demand, of the complete thesis. Should your thesis be published commercially, please reapply for permission. Theses and dissertations which contain embedded PJAs as part of the formal submission can be posted publicly by the awarding institution with DOI links back to the formal publications on ScienceDirect.

### **Elsevier Open Access Terms and Conditions**

You can publish open access with Elsevier in hundreds of open access journals or in nearly 2000 established subscription journals that support open access publishing. Permitted third party re-use of these open access articles is defined by the author's choice of Creative Commons user license. See our [open access license policy](#) for more information.

#### **Terms & Conditions applicable to all Open Access articles published with Elsevier:**

Any reuse of the article must not represent the author as endorsing the adaptation of the article nor should the article be modified in such a way as to damage the author's honour or reputation. If any changes have been made, such changes must be clearly indicated.

The author(s) must be appropriately credited and we ask that you include the end user license and a DOI link to the formal publication on ScienceDirect.

If any part of the material to be used (for example, figures) has appeared in our publication with credit or acknowledgement to another source it is the responsibility of the user to ensure their reuse complies with the terms and conditions determined by the rights holder.

#### **Additional Terms & Conditions applicable to each Creative Commons user license:**

**CC BY:** The CC-BY license allows users to copy, to create extracts, abstracts and new works from the Article, to alter and revise the Article and to make commercial use of the Article (including reuse and/or resale of the Article by commercial entities), provided the user gives appropriate credit (with a link to the formal publication through the relevant DOI), provides a link to the license, indicates if changes were made and the licensor is not represented as endorsing the use made of the work. The full details of the license are available at <http://creativecommons.org/licenses/by/4.0>.

**CC BY NC SA:** The CC BY-NC-SA license allows users to copy, to create extracts, abstracts and new works from the Article, to alter and revise the Article, provided this is not done for commercial purposes, and that the user gives appropriate credit (with a link to the formal publication through the relevant DOI), provides a link to the license, indicates if changes were made and the licensor is not represented as endorsing the use made of the work. Further, any new works must be made available on the same conditions. The full details of the license are available at <http://creativecommons.org/licenses/by-nc-sa/4.0>.

**CC BY NC ND:** The CC BY-NC-ND license allows users to copy and distribute the Article, provided this is not done for commercial purposes and further does not permit distribution of the Article if it is changed or edited in any way, and provided the user gives appropriate credit (with a link to the formal publication through the relevant DOI), provides a link to the license, and that the licensor is not represented as endorsing the use made of the work. The full details of the license are available at <http://creativecommons.org/licenses/by-nc-nd/4.0>. Any commercial reuse of Open Access articles published with a CC BY NC SA or CC BY NC ND license requires permission from Elsevier and will be subject to a fee.

Commercial reuse includes:

- Associating advertising with the full text of the Article
- Charging fees for document delivery or access
- Article aggregation
- Systematic distribution via e-mail lists or share buttons

Posting or linking by commercial companies for use by customers of those companies.

#### **20. Other Conditions:**

v1.10

Questions? E-mail us at [customercare@copyright.com](mailto:customercare@copyright.com).

# ELSEVIER LICENSE TERMS AND CONDITIONS

Aug 16, 2023

This Agreement between Biozentrum, Univeristy Basel -- Kathrin Gundel ("You") and Elsevier ("Elsevier") consists of your license details and the terms and conditions provided by Elsevier and Copyright Clearance Center.

License Number	5604280423611
License date	Aug 08, 2023
Licensed Content Publisher	Elsevier
Licensed Content Publication	Current Biology
Licensed Content Title	Distinct Cellular Mechanisms of Blood Vessel Fusion in the Zebrafish Embryo
Licensed Content Author	Lukas Herwig, Yannick Blum, Alice Krudewig, Elin Ellertsdottir, Anna Lenard, Heinz-Georg Belting, Markus Affolter
Licensed Content Date	Nov 22, 2011
Licensed Content Volume	21
Licensed Content Issue	22
Licensed Content Pages	7
Start Page	1942
End Page	1948
Type of Use	reuse in a thesis/dissertation
Portion	figures/tables/illustrations
Number of figures/tables /illustrations	1
Format	both print and electronic
Are you the author of this Elsevier article?	No
Will you be translating?	No
Title	PhD Thesis
Institution name	Biozentrum Basel
Expected presentation date	Sep 2023
Portions	Figure 5 (B,C)
Requestor Location	Biozentrum, Univeristy Basel Spitalstrasse 41  Basel, 4056 Switzerland Attn: Biozentrum, Univeristy Basel
Publisher Tax ID	GB 494 6272 12
Total	<b>0.00 CHF</b>
Terms and Conditions	

## INTRODUCTION

1. The publisher for this copyrighted material is Elsevier. By clicking "accept" in connection with completing this licensing transaction, you agree that the following terms and conditions apply to this transaction (along with the Billing and Payment terms and conditions established by Copyright Clearance Center, Inc. ("CCC"), at the time that you opened your RightsLink account

and that are available at any time at <https://myaccount.copyright.com>).

### GENERAL TERMS

2. Elsevier hereby grants you permission to reproduce the aforementioned material subject to the terms and conditions indicated.
3. Acknowledgement: If any part of the material to be used (for example, figures) has appeared in our publication with credit or acknowledgement to another source, permission must also be sought from that source. If such permission is not obtained then that material may not be included in your publication/copies. Suitable acknowledgement to the source must be made, either as a footnote or in a reference list at the end of your publication, as follows:  
"Reprinted from Publication title, Vol /edition number, Author(s), Title of article / title of chapter, Pages No., Copyright (Year), with permission from Elsevier [OR APPLICABLE SOCIETY COPYRIGHT OWNER]." Also Lancet special credit - "Reprinted from The Lancet, Vol. number, Author(s), Title of article, Pages No., Copyright (Year), with permission from Elsevier."
4. Reproduction of this material is confined to the purpose and/or media for which permission is hereby given. The material may not be reproduced or used in any other way, including use in combination with an artificial intelligence tool (including to train an algorithm, test, process, analyse, generate output and/or develop any form of artificial intelligence tool), or to create any derivative work and/or service (including resulting from the use of artificial intelligence tools).
5. Altering/Modifying Material: Not Permitted. However figures and illustrations may be altered/adapted minimally to serve your work. Any other abbreviations, additions, deletions and/or any other alterations shall be made only with prior written authorization of Elsevier Ltd. (Please contact Elsevier's permissions helpdesk [here](#)). No modifications can be made to any Lancet figures/tables and they must be reproduced in full.
6. If the permission fee for the requested use of our material is waived in this instance, please be advised that your future requests for Elsevier materials may attract a fee.
7. Reservation of Rights: Publisher reserves all rights not specifically granted in the combination of (i) the license details provided by you and accepted in the course of this licensing transaction, (ii) these terms and conditions and (iii) CCC's Billing and Payment terms and conditions.
8. License Contingent Upon Payment: While you may exercise the rights licensed immediately upon issuance of the license at the end of the licensing process for the transaction, provided that you have disclosed complete and accurate details of your proposed use, no license is finally effective unless and until full payment is received from you (either by publisher or by CCC) as provided in CCC's Billing and Payment terms and conditions. If full payment is not received on a timely basis, then any license preliminarily granted shall be deemed automatically revoked and shall be void as if never granted. Further, in the event that you breach any of these terms and conditions or any of CCC's Billing and Payment terms and conditions, the license is automatically revoked and shall be void as if never granted. Use of materials as described in a revoked license, as well as any use of the materials beyond the scope of an unrevoked license, may constitute copyright infringement and publisher reserves the right to take any and all action to protect its copyright in the materials.
9. Warranties: Publisher makes no representations or warranties with respect to the licensed material.
10. Indemnity: You hereby indemnify and agree to hold harmless publisher and CCC, and their respective officers, directors, employees and agents, from and against any and all claims arising out of your use of the licensed material other than as specifically authorized pursuant to this license.
11. No Transfer of License: This license is personal to you and may not be sublicensed, assigned, or transferred by you to any other person without publisher's written permission.
12. No Amendment Except in Writing: This license may not be amended except in a writing signed by both parties (or, in the case of publisher, by CCC on publisher's behalf).
13. Objection to Contrary Terms: Publisher hereby objects to any terms contained in any purchase order, acknowledgment, check endorsement or other writing prepared by you, which terms are inconsistent with these terms and conditions or CCC's Billing and Payment terms and conditions. These terms and conditions, together with CCC's Billing and Payment terms and conditions (which are incorporated herein), comprise the entire agreement between you and publisher (and CCC) concerning this licensing transaction. In the event of any conflict between your obligations established by these terms and conditions and those established by CCC's Billing and Payment terms and conditions, these terms and conditions shall control.
14. Revocation: Elsevier or Copyright Clearance Center may deny the permissions described in this License at their sole discretion, for any reason or no reason, with a full refund payable to you. Notice of such denial will be made using the contact information provided by you. Failure to receive such notice will not alter or invalidate the denial. In no event will Elsevier or Copyright Clearance Center be responsible or liable for any costs, expenses or damage incurred by you as a result of a denial of your permission request, other than a refund of the amount(s) paid by you to Elsevier and/or Copyright Clearance Center for denied permissions.

### LIMITED LICENSE

The following terms and conditions apply only to specific license types:

15. **Translation:** This permission is granted for non-exclusive world **English** rights only unless your license was granted for translation rights. If you licensed translation rights you may only translate this content into the languages you requested. A professional translator must perform all translations and reproduce the content word for word preserving the integrity of the article.
16. **Posting licensed content on any Website:** The following terms and conditions apply as follows: Licensing material from an Elsevier journal: All content posted to the web site must maintain the copyright information line on the bottom of each image; A



hyper-text must be included to the Homepage of the journal from which you are licensing at <http://www.sciencedirect.com/science/journal/xxxxx> or the Elsevier homepage for books at <http://www.elsevier.com>; Central Storage: This license does not include permission for a scanned version of the material to be stored in a central repository such as that provided by Heron/XanEdu. Licensing material from an Elsevier book: A hyper-text link must be included to the Elsevier homepage at <http://www.elsevier.com>. All content posted to the web site must maintain the copyright information line on the bottom of each image.

**Posting licensed content on Electronic reserve:** In addition to the above the following clauses are applicable: The web site must be password-protected and made available only to bona fide students registered on a relevant course. This permission is granted for 1 year only. You may obtain a new license for future website posting.

17. **For journal authors:** the following clauses are applicable in addition to the above:

**Preprints:**

A preprint is an author's own write-up of research results and analysis, it has not been peer-reviewed, nor has it had any other value added to it by a publisher (such as formatting, copyright, technical enhancement etc.).

Authors can share their preprints anywhere at any time. Preprints should not be added to or enhanced in any way in order to appear more like, or to substitute for, the final versions of articles however authors can update their preprints on arXiv or RePEc with their Accepted Author Manuscript (see below).

If accepted for publication, we encourage authors to link from the preprint to their formal publication via its DOI. Millions of researchers have access to the formal publications on ScienceDirect, and so links will help users to find, access, cite and use the best available version. Please note that Cell Press, The Lancet and some society-owned have different preprint policies. Information on these policies is available on the journal homepage.

**Accepted Author Manuscripts:** An accepted author manuscript is the manuscript of an article that has been accepted for publication and which typically includes author-incorporated changes suggested during submission, peer review and editor-author communications.

Authors can share their accepted author manuscript:

- immediately
  - via their non-commercial person homepage or blog
  - by updating a preprint in arXiv or RePEc with the accepted manuscript
  - via their research institute or institutional repository for internal institutional uses or as part of an invitation-only research collaboration work-group
  - directly by providing copies to their students or to research collaborators for their personal use
  - for private scholarly sharing as part of an invitation-only work group on commercial sites with which Elsevier has an agreement
- After the embargo period
  - via non-commercial hosting platforms such as their institutional repository
  - via commercial sites with which Elsevier has an agreement

In all cases accepted manuscripts should:

- link to the formal publication via its DOI
- bear a CC-BY-NC-ND license - this is easy to do
- if aggregated with other manuscripts, for example in a repository or other site, be shared in alignment with our hosting policy not be added to or enhanced in any way to appear more like, or to substitute for, the published journal article.

**Published journal article (JPA):** A published journal article (PJA) is the definitive final record of published research that appears or will appear in the journal and embodies all value-adding publishing activities including peer review co-ordination, copy-editing, formatting, (if relevant) pagination and online enrichment.

Policies for sharing publishing journal articles differ for subscription and gold open access articles:

**Subscription Articles:** If you are an author, please share a link to your article rather than the full-text. Millions of researchers have access to the formal publications on ScienceDirect, and so links will help your users to find, access, cite, and use the best available version.

Theses and dissertations which contain embedded PJAs as part of the formal submission can be posted publicly by the awarding institution with DOI links back to the formal publications on ScienceDirect.

If you are affiliated with a library that subscribes to ScienceDirect you have additional private sharing rights for others' research accessed under that agreement. This includes use for classroom teaching and internal training at the institution (including use in course packs and courseware programs), and inclusion of the article for grant funding purposes.

**Gold Open Access Articles:** May be shared according to the author-selected end-user license and should contain a [CrossMark logo](#), the end user license, and a DOI link to the formal publication on ScienceDirect.

Please refer to Elsevier's [posting policy](#) for further information.

18. **For book authors** the following clauses are applicable in addition to the above: Authors are permitted to place a brief

summary of their work online only. You are not allowed to download and post the published electronic version of your chapter, nor may you scan the printed edition to create an electronic version. **Posting to a repository:** Authors are permitted to post a summary of their chapter only in their institution's repository.

**19. Thesis/Dissertation:** If your license is for use in a thesis/dissertation your thesis may be submitted to your institution in either print or electronic form. Should your thesis be published commercially, please reapply for permission. These requirements include permission for the Library and Archives of Canada to supply single copies, on demand, of the complete thesis and include permission for Proquest/UMI to supply single copies, on demand, of the complete thesis. Should your thesis be published commercially, please reapply for permission. Theses and dissertations which contain embedded PJAs as part of the formal submission can be posted publicly by the awarding institution with DOI links back to the formal publications on ScienceDirect.

### **Elsevier Open Access Terms and Conditions**

You can publish open access with Elsevier in hundreds of open access journals or in nearly 2000 established subscription journals that support open access publishing. Permitted third party re-use of these open access articles is defined by the author's choice of Creative Commons user license. See our [open access license policy](#) for more information.

#### **Terms & Conditions applicable to all Open Access articles published with Elsevier:**

Any reuse of the article must not represent the author as endorsing the adaptation of the article nor should the article be modified in such a way as to damage the author's honour or reputation. If any changes have been made, such changes must be clearly indicated.

The author(s) must be appropriately credited and we ask that you include the end user license and a DOI link to the formal publication on ScienceDirect.

If any part of the material to be used (for example, figures) has appeared in our publication with credit or acknowledgement to another source it is the responsibility of the user to ensure their reuse complies with the terms and conditions determined by the rights holder.

#### **Additional Terms & Conditions applicable to each Creative Commons user license:**

**CC BY:** The CC-BY license allows users to copy, to create extracts, abstracts and new works from the Article, to alter and revise the Article and to make commercial use of the Article (including reuse and/or resale of the Article by commercial entities), provided the user gives appropriate credit (with a link to the formal publication through the relevant DOI), provides a link to the license, indicates if changes were made and the licensor is not represented as endorsing the use made of the work. The full details of the license are available at <http://creativecommons.org/licenses/by/4.0>.

**CC BY NC SA:** The CC BY-NC-SA license allows users to copy, to create extracts, abstracts and new works from the Article, to alter and revise the Article, provided this is not done for commercial purposes, and that the user gives appropriate credit (with a link to the formal publication through the relevant DOI), provides a link to the license, indicates if changes were made and the licensor is not represented as endorsing the use made of the work. Further, any new works must be made available on the same conditions. The full details of the license are available at <http://creativecommons.org/licenses/by-nc-sa/4.0>.

**CC BY NC ND:** The CC BY-NC-ND license allows users to copy and distribute the Article, provided this is not done for commercial purposes and further does not permit distribution of the Article if it is changed or edited in any way, and provided the user gives appropriate credit (with a link to the formal publication through the relevant DOI), provides a link to the license, and that the licensor is not represented as endorsing the use made of the work. The full details of the license are available at <http://creativecommons.org/licenses/by-nc-nd/4.0>. Any commercial reuse of Open Access articles published with a CC BY NC SA or CC BY NC ND license requires permission from Elsevier and will be subject to a fee.

Commercial reuse includes:

- Associating advertising with the full text of the Article
- Charging fees for document delivery or access
- Article aggregation
- Systematic distribution via e-mail lists or share buttons

Posting or linking by commercial companies for use by customers of those companies.

#### **20. Other Conditions:**

v1.10

Questions? E-mail us at [customercare@copyright.com](mailto:customercare@copyright.com).





# Acknowledgements

*„But the answers you seek will never be found at home.”*

*-Bronski Beat, “Smalltown Boy”, 1994*

What a journey this has been. Growing up as a smalltown girl, rural and familial. Leaving home and finding my way through three universities, each teaching me more. And now, the grand finale: a PhD thesis.

This journey was made possible only with the support of many people. First and foremost I would like to thank Prof. Markus Affolter for welcoming me in his laboratory and allowing me to pursue this PhD project. I am glad to have had the opportunity to work with him and I always admired the positive atmosphere in the lab which was to a great extent his doing. Markus, I draw my hat to your never ending fascination for science, your genuine attitude and the optimism you create in people.

Secondly, I would like to thank Dr. Heinz-Georg Belting for supervision and guidance throughout my time as a PhD student. I profited immensely from his knowledge and ideas, and although we had some difficult discussions along the way, I genuinely enjoyed learning from you and with you. Henry, you pushed me further than I would have ever dared to go and helped shape the scientist I am now. Thank you.

I want to thank Prof. Susan Mango for being part of my committee and for the most constructive and always helpful input. I also thank Prof. Elke Ober for being the external expert on this PhD thesis and for valuable discussions.

A huge thank you goes to Helen Mawer and Dr. Martin Müller, without whom the lab would probably sometimes drown in chaos. I thank Kumutini Kulendra and Andreas Rodriguez for taking excellent daily care of my fish and for fulfilling my repeated orders of Paramecia culture when I would go crazy again in breeding fish stocks. Because backups of backups are necessary. I think.

I would like to thank the team of the Imaging Facility at the Biozentrum for their high quality support and microscopy services. Especially Dr. Kai Schleicher was an immense help and never grew tired of explaining or troubleshooting during imaging sessions, even when the solution was just an ON-button away.

Every journey needs company, and so did mine. Hence I would like to thank all the former and current members of the Affolter lab: Dr. Shinya Matsuda, Dr. Alessandra Vigano (for discussions about German economy and Italian politics), Dr. Jianmin Yin (who has many cool imaging tricks up his sleeve), Dr. Katarzyna Łepeta, Dr. Maria Paraskevi Kotini, Dr. Daniel Heutschi, Dr. Gustavo Aguilar (who for me defines the image of a born scientist), Dr. Milena Bauer, Dr. Niklas Simon, Cindy Reinger (for being a fellow horse girl), Dr. Sheida Hadji Rasouliha, Basil Willi and Marina Signer.

A special place in my heart goes to my two fellow PhD students, Ludovico Maggi and Sophie Schnider, with whom I became close friends over the last years. You guys cheered me up more than you think and saved my day more than once. Ludo, my dearest partner in crime, and Sophie, my ever-open ear, I am sure your PhD journeys will come to a great end and you will be excellent scientists (if you aren't already). In the meantime, let's go for a coffee and some "fresh" air.

I also would like to thank our former Master student Fabio Tschudin, who contributed a central part of the PI3-Kinase project and cleared the path for key aspects of the work. I sometimes wonder who between the two of us learned more during this time, about the project and about ourselves. Fabio, I wish you all the best and I am most sure that you will be a damn cool teacher.

I thank my family for watching my journey from afar, but supporting me nonetheless. To my father for letting his girl do and become whatever she wanted and to my mother for encouragement when I did not see an end to work. To my siblings, simply for existing. To my grandmother, who I would have loved to see me defending this thesis, although I am sure she is watching now, too.

I thank my friends at the barn for being there for me in my "second life": Isa, Bianca, Annkathrin, Anni and all the daily faces. You backed me up and helped me maintain balance, both mentally and physically.

Last but not least I would like to thank a particularly special person in my life. A man who supported me more than anyone else, endured my ramblings, dried my tears and laughed the stress off with me. My hero, my crutch and my best friend. My home.  
Thank you.

# Kathrin Ingeburg Gundel



Born 10.09.1993 in Lebach/Germany  
Adress Gellertstraße 5  
53123 Bonn, Germany  
E-Mail [kathrin.gundel@ukbonn.de](mailto:kathrin.gundel@ukbonn.de)  
Phone +49 1575/2426578

## Academic Education

---

11/2018 – 09/2023 **University of Basel, Switzerland**  
Graduate Student in Developmental Cell Biology

10/2016 – 10/2018 **Albert-Ludwigs University Freiburg**  
Master Student, Major in Developmental Biology  
and Genetics

10/2012 – 04/2016 **Ruprecht-Karls University Heidelberg**  
Bachelor Student in Biosciences

09/2004 - 06/2012 **Albert Schweitzer-Gymnasium Dillingen**

## Professional Experience

---

11/2023- Today **University Hospital Bonn, Institute for Pathology**  
Postdoctoral Researcher in the group of Prof. Verena Tischler, Department of translational molecular pathology

11/2018 – 09/2023 **Biozentrum, University Basel**  
Doctoral research project on the group of Prof. Markus Affolter, investigating the role of lipid kinases in the development of multicellular blood vessels  
First author publication in preparation  
Supervision of several interns and coaching of a

master student including master thesis

01/2018 – 09/2018

**Centre for translational cell research  
(ZTZ) Freiburg**

Master thesis project in the group of Prof. Ian Frew on genomic instability and accumulation of DNA-damage in clear cell renal cell carcinoma

12/2016 – 12/2017

**Max-Planck Institute for Immunology and  
Epigenetics Freiburg**

Research Assistant in the group of Prof. Ritwick Sawarkar, project on the role of nuclear Hsp90 as a regulator of the cell cycle

Co-Author in

Cell Rep. 2019 Nov 5;29(6):1645-1659.e9.doi:  
10.1016/j.celrep.2019.09.084

04/2016 – 09/2016

**Centre for Organismal Studies Heidelberg**

Research Assistant in the group of Prof. Annika Guse, project work on the establishment of *Symbiodinium spec.* as a model organism in coral symbiosis research

12/2015 – 03/2016

**European Molecular Biology Laboratory  
(EMBL) Heidelberg**

Bachelor project in the group of Prof. Detlev Arendt on the development of the axochord in *Platynereis dumerilii* as homologue of the ancestral chorda dorsalis

09/2014 – 10/2015

**Centre for Organismal Studies Heidelberg**

Research Assistant in the group of Prof. Alexis Maizel, common lab work, e.g. plasmid preparation and sowing and harvest of *Arabidopsis thaliana*